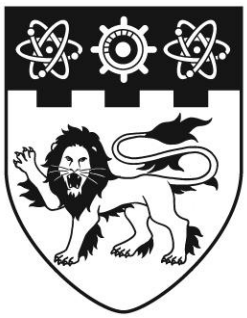

NANYANG TECHNOLOGICAL UNIVERSITY

Synthesis of High Value Chemicals from Biomass Platform Chemicals

KOH PENG FEI JACKSON

SCHOOL OF PHYSICAL AND MATHEMATICAL SCIENCES

2016

SYNTHESIS OF HIGH VALUE CHEMICALS FROM BIOMASS PLATFORM CHEMICALS

KOH PENG FEI JACKSON

2016

Synthesis of High Value Chemicals from Biomass Platform Chemicals

KOH PENG FEI JACKSON

School of Physical and Mathematical Sciences

A thesis submitted to the Nanyang Technological University
in partial fulfillment of the requirement for the degree of
Doctor of Philosophy

2016

ACKNOWLEDGEMENTS

I would like to express my heartfelt gratitude towards my supervisor, Professor Loh Teck Peng, for the wonderful opportunity to work in his research group. His dedication, wisdom and vision have inspired me on numerous occasions in the face of seemingly insurmountable challenges. I am grateful to Dr. Wang Peng for his meticulous guidance which crafted a solid foundation and his encouragements, without which all these would not have been possible.

In addition, special thanks go to Mr. Wong Zhen Zhou, Ms. Cheng Jun Kee, Mr. Shen Liang and Mr. Wang Wee Jian for their selfless assistance rendered both inside and outside of the laboratory. Past and present colleagues such as Dr. Xu Yunhe, Dr. Huang Jingmei, Dr. Chok Yew Keong, Dr. Magesh, Dr. Hu Xuhong, Dr. Zhao Kai, Mr. Ou Yong Chee Wai, Roy as well as the rest of the research group have also assisted me along the course of my projects.

Also, I would like to acknowledge Dr. Ganguly, Dr. Li Yongxin, Ms. Goh Ee Ling, Mr. Ong Yiren Derek, Ms. Zhu Wen Wei, Ms. Pui Pang Yi and Ms. Seow Ai Hua for their instrument expertise and technical assistance. On the administrative front, I am grateful to Ms. Chen Xiaoping, Ms. Florence Ng and Ms. Celine Hum for their timely and valuable advices.

Most importantly, this thesis is dedicated to my supportive family and loving wife as they have been a constant source of support and encouragement. Words cannot begin to describe the sacrifices they have made and I am deeply indebted to them.

TABLE OF CONTENTS

LIST OF ABBREVIATIONS

Ac	Acetyl
ACN	Acetonitrile
Anhyd.	Anhydrous
Aq.	Aqueous
Ar	Aryl
ATR	Attenuated total reflection
Bn	Benzyl
Boc	*tert*-Butyloxycarbonyl
Bpin	Boron pinacol ester
Bz	Benzoyl
Conc.	Concentration
Conv.	Conversion
C_3SO_3Hmim	3-Methyl-1-(3-sulfopropyl)-1*H*-imidazolium
DBU	1,8-Diazabicyclo[5.4.0]undec-7-ene
DCE	1,2-Dichloroethane
DCM	Dichloromethane
DEAD	Diethyl azodicarboxylate
DMF	*N*,*N*-dimethylformamide
DMSO	Dimethyl sulfoxide
ee	Enantiomeric excess

Emim	1-Ethyl-3-methylimidazolium
ESI	Electrospray Ionization
Et	Ethyl
EtOAc/EA	Ethyl acetate
Eq./Equiv.	Equivalent(s)
FTIR	Fourier transform infrared spectroscopy
h	hours
HMF	Hydroxymethylfurfural
HPLC	High Performance Liquid Chromatography
HRMS	High-Resolution Mass Spectrometry
^{i}Pr	Isopropyl
KSA	Ketene silyl acetal
L*	Chiral ligand(s)
LDA	Lithium diisopropylamide
LD_{50}	Median lethal dose
Lit.	Literature
M	Concentration (mol/L)
M^{+}	Parent ion peak (mass spectrum)
*m*CPBA	*meta*-Chloroperoxybenzoic acid
Me	Methyl
Min	Minute(s)
mol%	Mole percent

MOM	Methoxymethyl
Mp	Melting point
MS	Molecular sieves
MsCl	Methanesulfonyl chloride
NBS	*N*-Bromosuccinimide
^{n}BuLi	*n*-Butyllithium
NK_1	Neurokinin-1
NMR	Nuclear Magnetic Resonance
NOE	Nuclear Overhauser Effect
NOESY	Nuclear Overhauser Enhancement Spectroscopy
ORTEP	Oak Ridge Thermal Ellipsoid Plot
PEG	Polyethylene glycol
PET	Polyethylene terephthalate
PG/P	Protecting group
Ph	Phenyl
Phen	Phenanthroline
PMP	*para*-Methoxyphenyl
Ppm	Parts per million
PPTS	Pyridinium *para*-toluenesulfonate
Rac	Racemic
R_f	Retention factor
RT	Room temperature

TBAC	Tetrabutylammonium chloride
TBAF	Tetrabutylammonium fluoride
TBAI	Tetrabutylammonium iodide
TBDPS	*tert*-Butyldiphenylsilyl
TBS	*tert*-Butyldimethylsilyl
^{t}Bu	*tert*-Butyl
Temp.	Temperature
THF	Tetrahydrofuran
THP	Tetrahydropyran
TLC	Thin Layer Chromatography
TMEDA	Tetramethylethylenediamine
TMS	Trimethylsilyl
TMSOTf	Trimethylsilyl triflate
Ts	*para*-Toluenesulfonyl
TsDPEN	Tosylated diphenylethylenediamine
UV	Ultraviolet

SUMMARY

In this thesis, the conversion of biomass to several high value chemicals *via* versatile and synthetically useful platform chemicals were described. These high value chemicals include a common intermediate that allow access to several potent NK_1 receptor antagonists which are associated with the treatment of anxiety and emesis, as well as biologically active natural products aspergillides A and B with cytotoxic activity against mouse lymphocytic leukemia cell (L1210). In particular, the syntheses of aspergillides A and B was achieved such that all of the carbons present are derived from biomass derived platform chemicals. These demonstrate the feasibility of constructing valuable biologically active compounds using biomass as a sustainable chemical feedstock.

Chapter 1

In Chapter 1, the unsustainability of fossil fuels was discussed and biomass was introduced as a potential surrogate feedstock in view of it being a source of renewable carbon-based chemicals as well as other advantages. The concept of a biorefinery was discussed together with the associated conversion processes for an understanding of current industrial developments. Several biomass derived platform chemicals were reviewed in terms of their production, utility and applications to highlight their immense potential and suitability to be considered as starting material in chemical synthesis. The aim of this thesis was also presented in light of the research group's longstanding interest and involvement in the conversion of biomass.

Chapter 2

In Chapter 2, several potent non-peptidic NK_1 receptor antagonists and how they could be accessed *via* a common piperidone intermediate were introduced. Prior syntheses of the protected form of this piperidone intermediate required a minimum of 6 steps, several silica gel chromatography purifications and with less than 40% overall yield. We described a facile synthesis of the common intermediate in 54% overall yield and 97% *ee* over 5 steps from rice straw derived furfural **2** with only a single silica gel chromatography purification. The synthetic utility of this common piperidone intermediate was illustrated with the synthesis of one such NK_1 receptor antagonist.

Chapter 3

In Chapter 3, biologically active natural products aspergillides A and B with cytotoxic activity against mouse lymphocytic leukemia cell (L1210) were introduced and prior total syntheses were discussed. We described the racemic and asymmetric formal syntheses of these biologically active natural products through a series of optimizations and investigations. To the best of our knowledge, this sets a precedent for the construction of biologically active natural products entirely from biomass derived platform chemicals. The key steps include an asymmetric transfer hydrogenation reaction, a novel Achmatowicz rearrangement/triple reduction sequence, the first application of micellar Negishi coupling on an advanced synthetic intermediate as well as enzymatic kinetic resolutions to access both enantiomers of fragment A.

CHAPTER 1

Biomass as a Sustainable and Renewable Feedstock for Chemicals and Fuels

CHAPTER 1 BIOMASS AS A SUSTAINABLE AND RENEWABLE FEEDSTOCK FOR CHEMICALS AND FUELS

1.1 Fossil Fuels – Non-Renewable and Unsustainable

Fossil fuels such as coal, petroleum and natural gas have served as cheap and easily accessible sources of energy and chemical feedstock for several centuries and they account for about 86% of the world's energy usage in 2014[1]. However, after more than 150 years of coal-based chemistry and 50 years of petroleum chemistry[2], the world is now at a major crossroad to decide if it should continue indulging in the short-term riches of fossil fuels by turning a blind eye to the glaring limitations of fossil fuels.

The formation of fossil fuels is an enduring process stretching over millions of years and although they are constantly being formed, albeit at a slow rate, fossil fuels are considered non-renewable from the perspective of the human lifetime time frame. Contrary to the amount of time needed for the regeneration of fossil fuels, the rapid consumption of fossil fuels occurs in a much shorter time frame of hundreds of years. Such a vast disparity between the rate of formation and consumption renders fossil fuels an unsustainable feedstock that is bound to come to a grinding halt once available reservoirs are depleted.

The world is currently experiencing a dramatic increase in population since the 20th century, marked by technological advances that reduces child mortality and raises life expectancy. It is projected that this upward momentum will persist to achieve a

[1] BP Statistical Review of World Energy June 2015. http://www.bp.com/content/dam/bp/pdf/energy-economics/statistical-review-2015/bp-statistical-review-of-world-energy-2015-full-report.pdf (accessed Oct 20, 2015).

[2] Kamm, B. Introduction of Biomass and Biorefineries. In *The Role of Green Chemistry in Biomass Processing and Conversion*; Xie, H.; Gathergood, N., Eds. John Wiley & Sons, Inc.: New Jersey, 2012; pp 1-26.

world population of 9.3 billion in 2050 from the 7 billion in 2011[3]. At the present rate of consumption, it is estimated that larger reserves of coal and petroleum are expected to deplete in less than 140 years and 50 years respectively[4]. The expansion of the world population will inevitably lead to a greater demand for energy and materials as well as accelerating the rate of consumption, resulting in the earlier onset of fossil fuels depletion. Recent attempts to expand the exploration of fossil fuels reservoirs to the Arctic[5] highlight the urgency and desperation for more sources of fossil fuels.

Concomitantly, the alarming rate of use of fossil fuels has also placed much stress upon Earth and its ecosystems. Massive amounts of carbon-rich fossil fuels are extracted from underground, consumed and expelled into the atmosphere in the form of anthropogenic carbon dioxide at an annual rate of 30 million tons worldwide[6]. This increase in carbon dioxide concentration contributes to the "greenhouse effect"[7] which brings about climate changes such as the rise of global temperatures and sea levels. These abrupt changes have directly or indirectly resulted in various natural disasters[8] and loss of biodiversity[9], and could have a more significant impact in the future if the use of fossil fuels is not arrested. In addition, the use of fossil fuels such as coal results in emissions of sulphur oxides, nitrogen oxides and heavy metals, such as mercury and lead, which are detrimental to the well-being of mankind[10].

---

[3] Lee, R. *Science* **2011,** *333*, 569-573.
[4] Gupta, R. B.; Demirbas, A. *Gasoline, Diesel and Ethanol Biofuels from Grasses and Plants*. Cambridge University Press: New York, 2010; pp 1-24.
[5] British Broadcasting Company (BBC) News. http://www.bbc.com/news/business-34377434 (accessed Oct 20, 2015).
[6] Chakar, F. S.; Ragauskas, A. J. *Ind. Crops. Prod.* **2004,** *20*, 131-141.
[7] Mitchell, J. F. B. *Reviews of Geophysics* **1989,** *27*, 115-139.
[8] a) Min, S.-K.; Zhang, X.; Zwiers, F. W.; Hegerl, G. C. *Nature* **2011,** *470*, 378-381; b) Pall, P.; Aina, T.; Stone, D. A.; Stott, P. A.; Nozawa, T.; Hilberts, A. G. J.; Lohmann, D.; Allen, M. R. *Nature* **2011,** *470*, 382-385.
[9] a) Pimm, S. L.; Jenkins, C. N.; Abell, R.; Brooks, T. M.; Gittleman, J. L.; Joppa, L. N.; Raven, P. H.; Roberts, C. M.; Sexton, J. O. *Science* **2014,** *344*; b) McCauley, D. J.; Pinsky, M. L.; Palumbi, S. R.; Estes, J. A.; Joyce, F. H.; Warner, R. R. *Science* **2015,** *347*.
[10] Gupta, R. B.; Demirbas, A. *Gasoline, Diesel and Ethanol Biofuels from Grasses and Plants*.

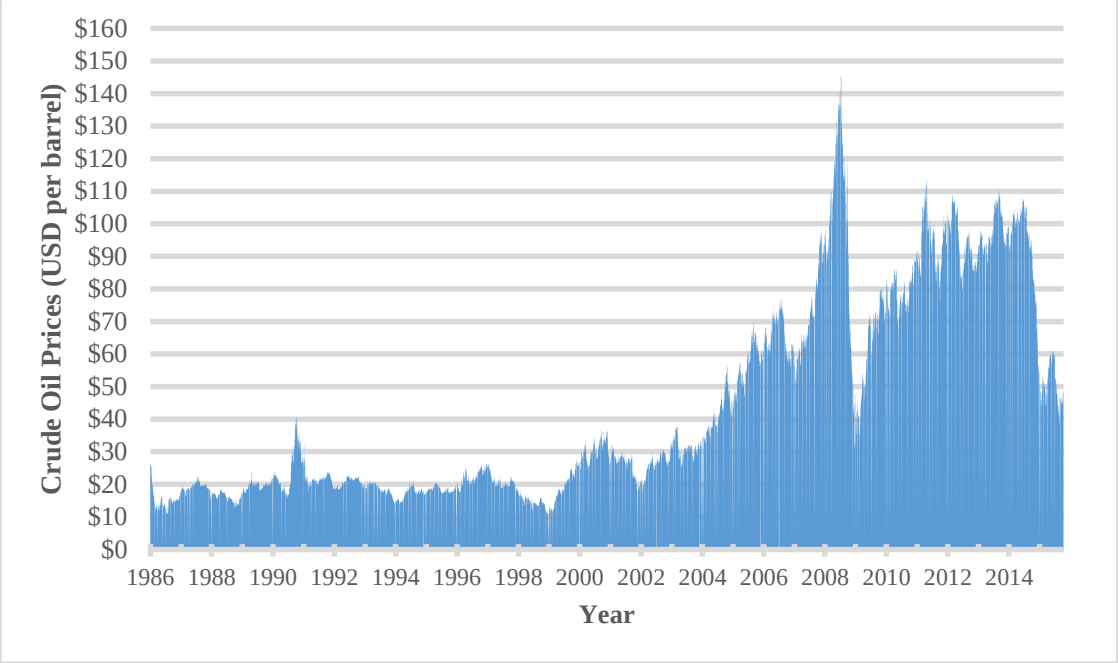

Figure 1: Prices of crude oil of the past 20 years in USD/Barrel

Also, in countries with no natural sources of fossil fuels, the issue of energy security is a major concern, due to the uneven distribution of fossil fuels. Organizations, such as the Organization of Petroleum Exporting Countries (OPEC) consisting of 12 oil-rich nations, dominate the global production of crude oil and have significant control over crude oil prices[4]. The volatility of crude oil prices is characterised by spikes as high as US$140 per barrel in 2008 and crashes to as low as US$11 per barrel[11] (Figure 1). Such dominance result in significant political power as demonstrated by the 1973 oil embargo[4] during the Yom Kippur war, leading to the crippling of global economy and major disruptions in daily lives.

Cambridge University Press: New York, 2010; pp 25-40.

[11] a) U.S. Energy Information Administration (EIA). Spot Prices for Crude Oil and Petroleum Products. http://www.eia.gov/dnav/pet/hist/LeafHandler.ashx?n=PET&s=RWTC&f=D (accessed Oct 20, 2015); b) Murray, J.; King, D. *Nature* **2012,** *481*, 433-435.

The recent shale gas revolution[12] in the United States has seen the United States become the world's largest oil and gas producer[1]. As a result of this change in energy landscape, the price of crude oil dropped 50% to about US$50 per barrel at the time of writing. This is generally attributed to Saudi Arabia's decision to increase oil production beyond market demand in order to lower the oil price and price out competitors who cannot sustain the low profit margins due to the artificially suppressed oil price. Hence, the current perceived low oil price is not a true reflection of market prices and is not expected to persist in the long term. Moreover, the shale gas revolution is fundamentally based on fossil fuels and their extractions have corresponding environmental impacts such as the contamination of groundwater[13].

In view of the severe limitations of fossil fuels as a feedstock for chemicals and energy, significant international attention has been placed on the development of sustainable energy sources[14] to secure new energy sources and chemical feedstocks to alleviate increasing demands and negative impacts of finite fossil fuels. These include solar, hydro, tidal, geothermal, wind, nuclear energy as well as biomass[15]. Among the alternative sources of energy, biomass is the only feedstock that offers a source of renewable carbon-based chemicals and fuels[16]. The potential and importance of biomass as a surrogate feedstock for fossil fuels has been named as "a top priority on the international political agenda"[17]. Various governments such as the United States and European Union have implemented short to mid-term targets to ensure that 20% of

[12] Hughes, J. D. *Nature* **2013,** *494,* 307-308.
[13] a) Jackson, R. B.; Vengosh, A.; Darrah, T. H.; Warner, N. R.; Down, A.; Poreda, R. J.; Osborn, S. G.; Zhao, K.; Karr, J. D. *Proc. Natl. Acad. Sci. U. S. A.* **2013,** *110,* 11250-11255; b) Stokstad, E. *Science* **2014,** *344,* 1468-1471.
[14] Chu, S.; Majumdar, A. *Nature* **2012,** *488,* 294-303.
[15] Gupta, R. B.; Demirbas, A. *Gasoline, Diesel and Ethanol Biofuels from Grasses and Plants*. Cambridge University Press: New York, 2010; pp 41-55.
[16] a) Sheldon, R. A. *Catal. Today* **2011,** *167,* 3-13; b) Vennestrøm, P. N. R.; Osmundsen, C. M.; Christensen, C. H.; Taarning, E. *Angew. Chem. Int. Ed.* **2011,** *50,* 10502-10509; c) He, M.; Sun, Y.; Han, B. *Angew. Chem. Int. Ed.* **2013,** *52,* 9620-9633.
[17] Sheldon, R. A. *Chem. Soc. Rev.* **2012,** *41,* 1437-1451.

transportation fuels are bio-based by 2030 and 2020 respectively. The United States also seeks to have 25% of carbon-based industrial feedstock chemicals to be bio-based by 2030[18].

1.2 Biomass – Introduction and Advantages

Biomass is defined by the United States Department of Energy as "any organic matter that is available on a renewable or recurring basis (excluding old-growth timber), including dedicated energy crops and trees, agricultural food and feed crop residues, aquatic plants, wood and wood residues, animal wastes, and other waste materials"[19]. Beyond the fact that biomass is the only source of renewable carbon-based fuels and chemicals, it also offers several advantages over other forms of renewable energy and conventional fossil fuels[20]. Biomass is an abundant resource and it has been proposed by the U.S. that more than 1.3 billion tons of biomass could be sustainably produced on an annual basis from forestry and agricultural residues[21]. In addition to its abundance, it is also a renewable and easily accessible feedstock as the growing of new biomass can occur in the matter of years and there are no requirements for drilling of oil wells or dangerous mining activities. Biomass can have a relatively stable availability as compared to other renewables which may experience fluctuating availabilities as they are subjected to different weather conditions such as sun, wind and tides. Biomass also offers better geographical distribution compared to fossil fuels where the Middle East, comprising of only 2% of the world population, possess 63%

[18] Kamm, B.; Kamm, M.; Gruber, P. R.; Kromus, S. Biorefinery Systems – An Overview. In *Biorefineries-Industrial Processes and Products*, Kamm, B.; Gruber, P. R.; Kamm, M., Eds.; Wiley-VCH Verlag GmbH & Co. KGaA: Weinheim, 2008; pp 1-40.

[19] Biomass Research and Development, Act of 2000. http://www.biomassboard.gov/ pdfs/biomass_rd_ act_2000.pdf (accessed Oct 22, 2015)

[20] de Jong, W.; van Ommen, J. R. Introduction. In *Biomass as a Sustainable Energy Source for the Future*; de Jong, W.; van Ommen, J. R., Eds. John Wiley & Sons, Inc: New Jersey, 2014; pp 1-35.

[21] Perlack, R. D.; Stokes, B. J. *U.S. Billion-Ton Update: Biomass Supply for a Bioenergy and Bioproducts Industry*; ORNL/TM-2011/224; U.S. Department of Energy: Oak Ridge, TN, 2011.

of the world's petroleum reserves[4]. Finally, the chemical functionalities present in biomass offers a distinct opportunity for functionalizations in the chemical industry compared to the relatively simple hydrocarbons derived from fossil fuels[22].

The first generation of biomass feedstocks used in the production of bioethanol were sugarcane in Brazil and corn in the United States, but there are several disadvantages concerning the use of food-based biomass feedstocks[23]. Firstly, there is a perpetual ethical debate on the issue of food versus fuel as food crops are being used for the production of fuels while malnutrition remains a significant challenge in developing countries. Next, food crops have their inherent value, which would drive up the costs of their development as energy and chemical feedstocks, due to competition with food prices. Last but not least, in order to meet the enormous demand for fuels, vast land areas are required, over and above existing agricultural lands, which may lead to accelerated clearing of rainforests and loss of habitats.

Hence, the use of inedible biomass is the way forward towards sustainable and renewable surrogate for fossil fuels and this has been tipped to have the greatest potential for success[18]. Of particular interest is the valorization of agricultural crop residues such as straw and woody residues from forestry wastes[24]. These byproducts and wastes are currently handled in an inefficient manner whereby agricultural wastes

[22] Tuck, C. O.; Pérez, E.; Horváth, I. T.; Sheldon, R. A.; Poliakoff, M. *Science* **2012,** *337*, 695-699.
[23] a) Fairley, P. *Nature* **2011,** *474*, S2-S5; b) Graham-Rowe, D. *Nature* **2011,** *474*, S6-S8; c) Ragauskas, A. J.; Williams, C. K.; Davison, B. H.; Britovsek, G.; Cairney, J.; Eckert, C. A.; Frederick, W. J.; Hallett, J. P.; Leak, D. J.; Liotta, C. L.; Mielenz, J. R.; Murphy, R.; Templer, R.; Tschaplinski, T. *Science* **2006,** *311*, 484-489; d) Tilman, D.; Socolow, R.; Foley, J. A.; Hill, J.; Larson, E.; Lynd, L.; Pacala, S.; Reilly, J.; Searchinger, T.; Somerville, C.; Williams, R. *Science* **2009,** *325*, 270-271.
[24] a) Christou, M.; Alexopoulou, E. The terrestrial biomass: formation and properties (crops and residual biomass). In *Biorefinery - From Biomass to Chemicals and Fuels*; Aresta, M.; Dibenedetto, A.; Dumeignil, F., Eds. Walter de Gruyter GmbH & Co. KG: Berlin, 2012; pp 49-80; b) Gupta, R. B.; Demirbas, A. *Gasoline, Diesel and Ethanol Biofuels from Grasses and Plants*. Cambridge University Press: New York, 2010; pp 56-72.

are burnt in open fields[25] to prepare for subsequent planting season and causing serious air pollution issues[26]. Other ways of treating these wastes include combusting these low calorie residues for only a small amount of energy and production of low value fiberboards which does not maximize their utility.

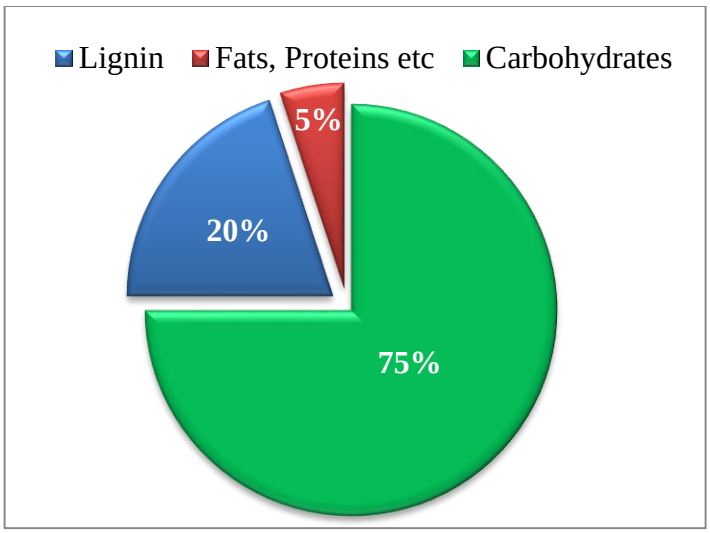

Figure 2: Components of Biomass

Amongst the components of biomass shown in Figure 2, it is evident that carbohydrates form the majority and carbohydrates can be further divided into 3 main classes: cellulose, starch and hemicellulose. Cellulose is the most abundant biopolymer found on Earth with an estimated annual production of 10 x 10^{10} tons and is made up of repeating glucose units linked together by β-(1→4)-glycosidic bonds (Figure 3). Its abundance and the presence of a single repeating monomer has garnered intense research attention towards its degradations and transformations[27]. Another

[25] Sudhakar, S.; Amit, R. P.; Robert, F. B.; Harpreet, S. Energy Harvest: A Possible Solution to the Open Field Stubble Burning in Punjab, India. In *Biomass and biofuels: advanced biorefineries for sustainable production and distribution*; Jose, S.; Bhaskar, T., Eds. CRC Press, Taylor & Francis Group: Florida, 2015; pp 183-198.

[26] Gustafsson, Ö.; Kruså, M.; Zencak, Z.; Sheesley, R. J.; Granat, L.; Engström, E.; Praveen, P. S.; Rao, P. S. P.; Leck, C.; Rodhe, H. *Science* **2009,** *323*, 495-498.

[27] a) Luterbacher, J. S.; Rand, J. M.; Alonso, D. M.; Han, J.; Youngquist, J. T.; Maravelias, C. T.; Pfleger, B. F.; Dumesic, J. A. *Science* **2014,** *343*, 277-280 and references cited therein; b) Krässig, H.; Schurz, J.; Steadman, R. G.; Schliefer, K.; Albrecht, W.; Mohring, M.; Schlosser, H. Cellulose. In

biopolymer made up of repeating glucose units would be starch, where amylose and amylopectin can be found. The difference between cellulose and starch lies in the α-(1→4)-linkages found in the latter while amylopectin differs from amylose by the presence of α-(1→6)-linkages leading to branching compared to the linear amylose[28].

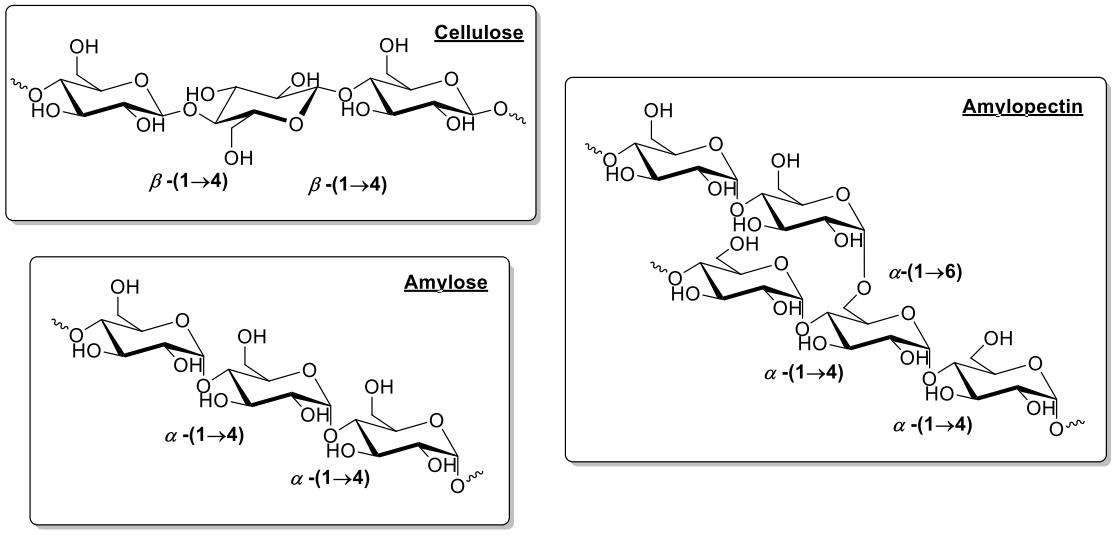

Figure 3: Different linkages found in cellulose and starch

Previously discussed limitations of using food crops, which is rich in starch, hinder the potential of starch as a potential renewable feedstock as compared to cellulose. The highly ordered structure of cellulose results in extensive intra- and intermolecular hydrogen bonding which renders it resistant to depolymerization and results in the recalcitrance of biomass[29]. This is highlighted by the fact that cellulose is 100 times more resistant to hydrolysis than starch[27c]. Only in recent years have

Ullmann's Renewable Resources, Wiley-VCH Verlag GmbH & Co. KGaA: Weinheim, 2013 pp 123-176; c) Hayes, D. J.; Fitzpatrick, S.; Hayes, M. H. B.; Ross, J. R. H. The Biofine Process – Production of Levulinic Acid, Furfural, and Formic Acid from Lignocellulosic Feedstocks. In *Biorefineries-Industrial Processes and Products*, Kamm, B.; Gruber, P. R.; Kamm, M., Eds.; Wiley-VCH Verlag GmbH & Co. KGaA: Weinheim, 2008; pp 139-164.

[28] a) Pérez, S.; Bertoft, E. *Starch - Stärke* **2010,** *62*, 389-420; b) Wertz, J.-L.; Bédué, O. Cellulose, the Predominant Constituent of Biomass. In *Lignocellulosic Biorefineries*; EFPL Press: Lausanne, 2013; pp 123-187.

[29] a) Himmel, M. E.; Ding, S.-Y.; Johnson, D. K.; Adney, W. S.; Nimlos, M. R.; Brady, J. W.; Foust, T. D. *Science* **2007,** *315*, 804-807; b) Sanderson, K. *Nature* **2011,** *474*, S12-S14; c) Jung, S.; Foston, M.; Kalluri, U. C.; Tuskan, G. A.; Ragauskas, A. J. *Angew. Chem. Int. Ed.* **2012,** *51*, 12005-12008.

researchers made progress in the dissolution of cellulose using a NaOH/urea aqueous solution[30].

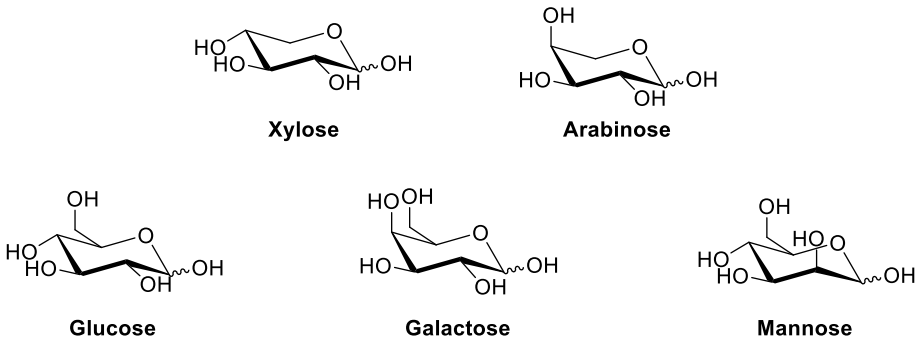

Figure 4: Pentoses and Hexoses found in hemicellulose

Hemicellulose, on the other hand, comprises of a heterogeneous mixture of branched polymers made up of a variety of 5-carbon and 6-carbon monosaccharides[31] (Figure 4). One of these monomers is xylose, which is the second most abundant monosaccharide after glucose and is made up of only 5 carbons. Hemicellulose are more susceptible to reactions than cellulose due to their lower degree of polymerization and hence lower molecular weight. The key role of hemicellulose is to strengthen plant cell walls due to interactions with cellulose and lignin[32].

Last but not least, lignin is a phenolic polymer randomly constructed from 3 different substituted phenols, *p*-coumaryl, coniferyl and sinapyl alcohol[6,33] (Figure 5). The native structure of lignin has not been fully characterized but an array of bonding types has been identified and their relative abundance quantified[34] as shown in Figure

[30] a) Xiong, X.; Duan, J. Dissolution and Application of Cellulose in NaOH/Urea Aqueous Solution. In *The Role of Green Chemistry in Biomass Processing and Conversion*; John Wiley & Sons, Inc.: New Jersey, 2012; pp 205-240; b) Zhou, J.; Zhang, L. *Polym. J.* **2000,** *32*, 866-870.
[31] Wertz, J.-L.; Bédué, O. Hemicelluloses and Lignin, Other Key Constituents of Biomass. In *Lignocellulosic Biorefineries*; EFPL Press: Lausanne, 2013; pp 239-297.
[32] a) Ordaz-Ortiz, J. J.; Marcus, S. E.; Paul Knox, J. *Mol. Plant* **2009,** *2*, 910-921; b) Scheller, H. V.; Ulvskov, P. *Annu. Rev. Plant Biol.* **2010,** *61*, 263-289.
[33] Xu, C.; Arancon, R. A. D.; Labidi, J.; Luque, R. *Chem. Soc. Rev.* **2014,** *43*, 7485-7500.
[34] Zakzeski, J.; Bruijnincx, P. C. A.; Jongerius, A. L.; Weckhuysen, B. M. *Chem. Rev.* **2010,** *110,*

5. The complex nature of lignin renders it resistant to enzymatic degradation and it acts as a "glue" to fill the spaces between cellulose and hemicellulose to impart rigidity and hydrophobicity to cell walls[31,35]. Lignin has garnered less valorization efforts due to its complexities despite being a source of aromatic compounds and high abundance from the delignification process in pulp and paper industries[34,36].

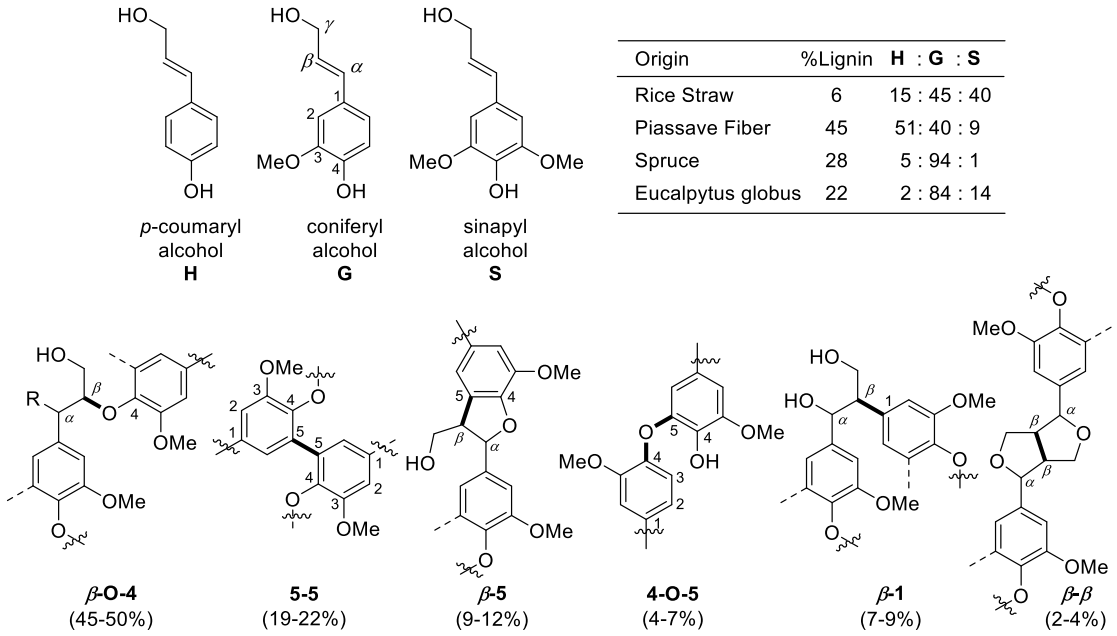

Origin	%Lignin	**H** : **G** : **S**
Rice Straw	6	15 : 45 : 40
Piassave Fiber	45	51: 40 : 9
Spruce	28	5 : 94 : 1
Eucalpytus globus	22	2 : 84 : 14

Figure 5: Complexities of lignin in terms of distribution of monomers and bondings

1.3 Biorefinery – Concepts and Processes

To harness the tremendous potential of biomass as a renewable feedstock for sustainable fuels and chemicals, the concept of a biorefinery was developed[23c] (Figure 6). The biorefinery has been defined as "a facility that integrates biomass-conversion processes and equipment to produce fuels, power, and chemicals from biomass"[37], and

3552-3599.

[35] Saake, B.; Lehnen, R. Lignin. In *Ullmann's Renewable Resources*, Wiley-VCH Verlag GmbH & Co. KGaA: Weinheim, 2013 pp 379-394.

[36] Decina, S.; Crestini, C. Conversion of lignin: chemical technologies and biotechnologies – oxidative strategies in lignin upgrade. In *Biorefinery - From Biomass to Chemicals and Fuels*; Aresta, M.; Dibenedetto, A.; Dumeignil, F., Eds. Walter de Gruyter GmbH & Co. KG: Berlin, 2012; pp 167-206.

[37] de Jong, W. Biorefineries. In *Biomass as a Sustainable Energy Source for the Future*; de Jong, W.;

is analogous to the existing petrochemical refineries. Several strategies have also been developed to ensure that biorefineries have multiple product streams where fuels are classified as low value-high volume products and pharmaceuticals are classified as high value-low volume products[38]. The high oxygen content of biomass feedstocks relative to fossil fuels allows for the opportunity to derive new functionalized chemicals in a manner not easily accessible by fossil fuels and could be deoxygenated[39] to produce existing bulk chemicals which could be "dropped in" into existing pipelines for further upgrading[16b].

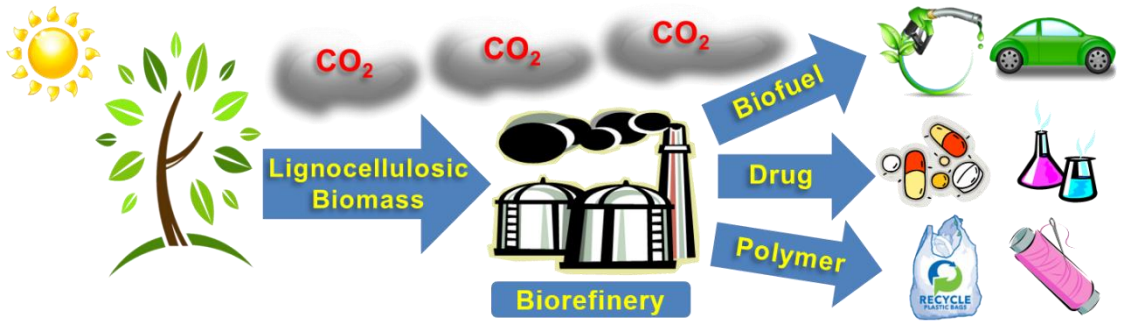

Figure 6: Illustration of the biorefinery concept

The ideal outcome of these biorefineries is to produce a myriad of products economically and upon consumption or end-of-life of the products, the carbon dioxide (CO_2) produced from the use or disposal will be absorbed by new biomass during photosynthesis to complete the carbon-neutral cycle. Various processes have been developed to break down biomass in view of its recalcitrance and the diverse nature of its components so that valuable and useful products can be produced at an industrial scale.

van Ommen, J. R., Eds. John Wiley & Sons, Inc: New Jersey, 2014; pp 469-502.

[38] Bozell, J. J.; Petersen, G. R. *Green Chem.* **2010,** *12*, 539-554.

[39] Nakagawa, Y.; Liu, S.; Tamura, M.; Tomishige, K. *ChemSusChem* **2015,** *8*, 1114-1132.

1.3.1 Pretreatment Methods

The presence of extensive hydrogen bonding, high degree of polymerization and complex crosslinking of the biomass components hinders access of enzymes and chemicals from the exterior and thus making raw biomass resistant to degradation. Pretreatment methods have been developed to modify these lignocellulosic components' structure as so to improve accessibility of chemicals and enzymes to facilitate degradation. These methods are classified based on their modes of action, into physical, chemical, physicochemical and biological methods[40] (Figure 7).

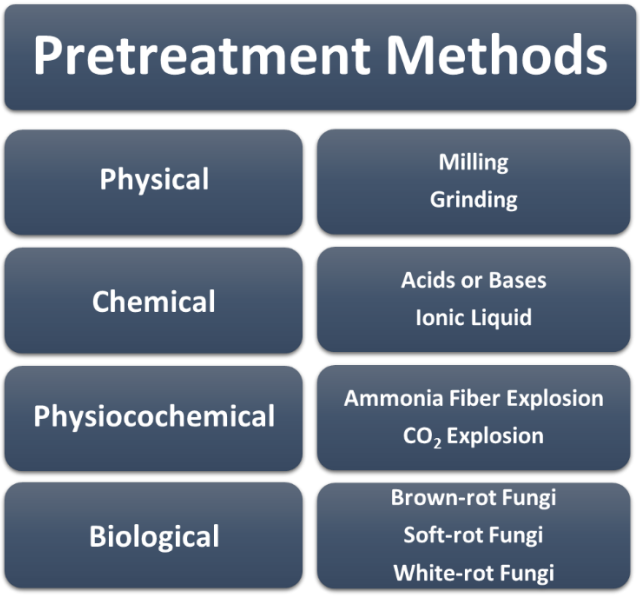

Figure 7: Summary of pretreatment methods

Physical methods such as milling and grinding breaks down biomass feedstock into smaller particle sizes, thereby increasing available surface area and physical

[40] a) Shafiei, M.; Kumar, R.; Karimi, K. Pretreatment of Lignocellulosic Biomass. In *Lignocellulose-Based Bioproducts*; Karimi, K., Ed. Springer International Publishing: Heidelberg, 2015; Vol. 1, pp 85-154; b) Wertz, J.-L.; Bédué, O. Pretreatments of Lignocellulosic Biomass. In *Lignocellulosic Biorefineries*; EFPL Press: Lausanne, 2013; pp 299-350; c) Galletti, A. M. R.; Antonetti, C. Biomass pretreatment: separation of cellulose, hemicellulose, and lignin – existing technologies and perspectives. In *Biorefinery - From Biomass to Chemicals and Fuels*; Aresta, M.; Dibenedetto, A.; Dumeignil, F., Eds. Walter de Gruyter GmbH & Co. KG: Berlin, 2012; pp 101-121; d) Kumar, P.; Barrett, D. M.; Delwiche, M. J.; Stroeve, P. *Ind. Eng. Chem. Res.* **2009,** *48*, 3713-3729.

density[41]. The increase in available surface area increases the rate of subsequent reactions while the increase in physical density aids in transportation and storage of biomass feedstock as in its raw form, it is bulky and inefficient to transport and store compared to fossil fuels. Chemical methods such as treatment with acids or bases and ionic liquids help to effect hydrolysis and solubilize certain components of biomass[42]. The solubilization of lignin and/or hemicellulose allows for the separation of cellulose, with minimal degradation loss, through filtration and the pretreated cellulose can then be subjected to further depolymerization reactions.

Physicochemical methods such as ammonia fiber explosion and CO_2 explosion occur when liquid ammonia or supercritical CO_2 is added to biomass under high pressure and the pressure is quickly released, resulting in an explosive decompression[43]. These explosions disrupt the biomass structures, reduce crystallinity and partial hydrolysis could also be observed due to the mild basic or acidic conditions employed. Biological methods involve the use of fungi such as brown-rot fungus, white-rot fungus and soft-rot fungus to exploit the enzymes present for degradation of biomass components[44]. The enzymes found in white-rot fungus are known for their ability to degrade lignin while preserving cellulose and hemicellulose. Conversely, brown- and soft-rot fungi show selectivity for polysaccharides over lignin thus allowing for separation and breakdown of biomass components in subsequent steps.

[41] Vidal, B., Jr.; Dien, B.; Ting, K. C.; Singh, V. *Appl. Biochem. Biotechnol.* **2011,** *164*, 1405-1421.
[42] Xie, H.; Zhao, Z. K. Selective Breakdown of (Ligno)cellulose in Ionic Liquids. In *Ionic Liquids: Applications and Perspectives*; Kokorin, A., Ed. InTech: Rijeka, 2011; pp 61-80.
[43] a) Mes-Hartree, M.; Dale, B. E.; Craig, W. K. *Appl. Microbiol. Biotechnol.* **1988,** *29*, 462-468; b) Zheng, Y.; Lin, H.-M.; Wen, J.; Cao, N.; Yu, X.; Tsao, G. *Biotechnol. Lett.* **1995,** *17*, 845-850.
[44] Chen, S.; Zhang, X.; Singh, D.; Yu, H.; Yang, X. *Biofuels* **2010,** *1*, 177-199.

1.3.2 Conversion Processes

Among the numerous conversion processes for the valorization of biomass, they can be broadly categorized into 3 main classes, namely thermal conversion, biological conversion and chemical conversion (Figure 8). These processes generate a myriad of products for different purposes and have their corresponding advantages and disadvantages.

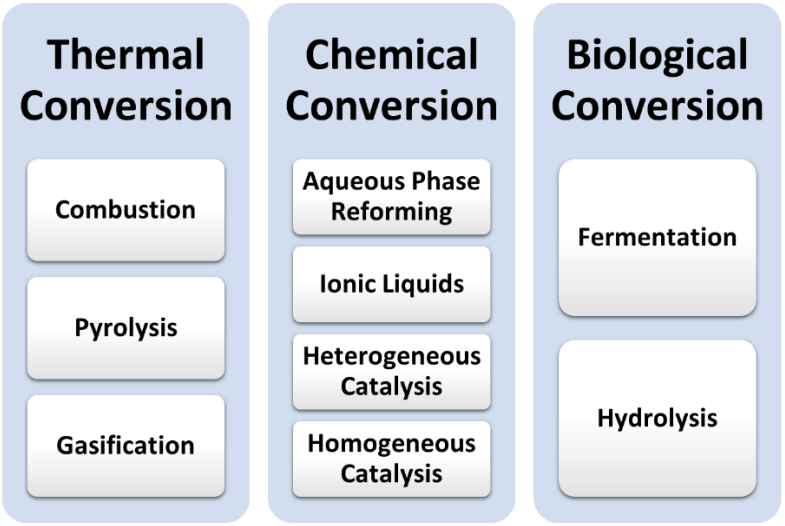

Figure 8: Examples of different conversion processes

Thermal Conversion

The key features of thermal conversion are the short residence time in a continuous process using dry feedstock but with poor selectivity. Combustion, pyrolysis and gasification are 3 types of thermal conversion for the valorization of biomass and they vary in the conditions and the desired products[45] (Figure 9).

[45] a) Thallada, B.; Bhavya, B.; Rawel, S.; Priyanka, O. Thermochemical Biomass Conversion for Rural Biorefinery. In *Biomass and biofuels: advanced biorefineries for sustainable production and distribution*; Jose, S.; Bhaskar, T., Eds. CRC Press, Taylor & Francis Group: Florida, 2015; pp 103-118; b) Wertz, J.-L.; Bédué, O. Thermochemical Conversion of Lignocellulosic Biomass. In *Lignocellulosic Biorefineries*; EFPL Press: Lausanne, 2013; pp 419-474; c) Lappas, A. A.; Iliopoulou, E. F.; Kalogiannis, K.; Stefanidis, S. Conversion of biomass to fuels and chemicals via thermochemical

Combustion of biomass has been carried out ever since humans learned how to make fire to obtain light and heat. It has remained as the most mature and direct method to convert biomass to energy[46]. Combustion of biomass involves the burning of biomass in the presence of oxygen to generate CO_2 and water as the main by-products as well as large amount of energy. The amount of oxides of nitrogen generated from biomass combustion is considerably less than that from fossil fuel combustion and the low sulfur content of biomass further reduces the amount of pollutants formed.

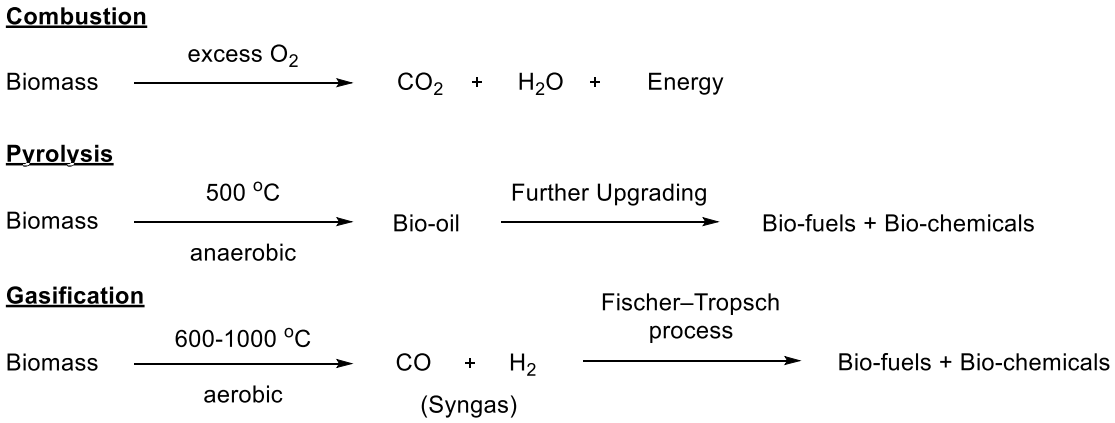

Figure 9: Overview of thermal conversions

Pyrolysis of biomass involves the decomposition of biomass under thermal conditions (500 °C) in the absence of oxygen[47]. This process converts biomass to bio-oil which is a mixture of highly oxygenated organic molecules that has negligible nitrogen and sulfur contents. The high oxygen content in bio-oil causes it to have poor fuel properties and hence bio-oil has to be further upgraded before it can be used as bio-fuels or to generate bio-chemicals[48]. However, the increase in physical density

processes. In *Biorefinery - From Biomass to Chemicals and Fuels*; Aresta, M.; Dibenedetto, A.; Dumeignil, F., Eds. Walter de Gruyter GmbH & Co. KG: Berlin, 2012; pp 33-361.

[46] Tao, K.; Vladimir, S. Combustion of Biomass. In *Biomass Processing Technologies*; Strezov, V.; Evans, T. J., Eds. CRC Press/Taylor & Francis Group: Boca Raton, 2014; pp 53-80.

[47] Cara, J. M.; Les, S.; Vladimir, S. Pyrolysis of Biomass. In *Biomass Processing Technologies*; Strezov, V.; Evans, T. J., Eds. CRC Press/Taylor & Francis Group: Boca Raton, 2014; pp 123-154.

[48] a) Fu, Q.; Xie, H.; Argyropoulos, D. S. Pyrolysis Oils from Biomass and Their Upgrading. In *The*

results in greater efficiency during storage and transportation for further upgrading, as well as higher energy density[49].

Gasification of biomass is conducted at a much higher temperature (1000 ºC) in the presence of limited oxygen to convert biomass into simple gaseous molecules like carbon monoxide and hydrogen[50]. The overarching philosophy of gasification is to convert complex biomass into homogeneous gas products, also known as synthesis gas (syngas), which can be employed in the Fischer-Tropsch process[51] to generate useful liquid hydrocarbons which is familiar to conventional petroleum refineries. Gasification can also be coupled with a fermentation process as the anaerobic bacteria involved are able to convert both carbon monoxide and hydrogen into ethanol[52].

Biological Conversion

Biological conversion of biomass focusses on the use of various enzymes to breakdown the resilient mix of cellulose, hemicellulose and lignin. The processes generally involve an initial hydrolysis as the preparative step to improve accessibility to the sugar monomers that are locked in the polysaccharides[53] (Scheme 1). Pretreatment methods have a significant impact on the yield of the enzymatic hydrolysis as biomass recalcitrance needs to be overcome before enzymes can work

Role of Green Chemistry in Biomass Processing and Conversion; John Wiley & Sons, Inc.: New Jersey, 2012; pp 263-280; b) Annette, E.; Vladimir, S.; Tim, J. E. Bio-Oil Applications and Processing. In *Biomass Processing Technologies*; Strezov, V.; Evans, T. J., Eds. CRC Press/Taylor & Francis Group: Boca Raton, 2014; pp 357-378; c) Venderbosch, R. H. *ChemSusChem* **2015,** *8*, 1306-1316.

[49] Mettler, M. S.; Vlachos, D. G.; Dauenhauer, P. J. *Energy Environ. Sci.* **2012,** *5*, 7797-7809.

[50] Tao, K.; Vladimir, S. Gasification of Biomass. In *Biomass Processing Technologies*; Strezov, V.; Evans, T. J., Eds. CRC Press/Taylor & Francis Group: Boca Raton, 2014; pp 81-122.

[51] Katrin, T.; Vladimir, S. Fischer-Tropsch Synthesis from Biosyngas. In *Biomass Processing Technologies*; Strezov, V.; Evans, T. J., Eds. CRC Press/Taylor & Francis Group: Boca Raton, 2014; pp 309-356.

[52] Köpke, M.; Held, C.; Hujer, S.; Liesegang, H.; Wiezer, A.; Wollherr, A.; Ehrenreich, A.; Liebl, W.; Gottschalk, G.; Dürre, P. *Proc. Natl. Acad. Sci. U. S. A.* **2010,** *107*, 13087-13092.

[53] Wertz, J.-L.; Bédué, O. Biochemical Conversion of Biomass. In *Lignocellulosic Biorefineries*; EFPL Press: Lausanne, 2013; pp 351-418.

effectively on the components of biomass[54]. However, due to the fragile nature of enzymes, the pH of the selected pretreatment methods should not degrade the enzymes and the by-products of pretreatment should not inhibit the desired enzymatic actions[55].

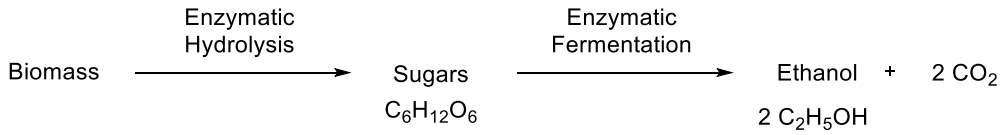

Scheme 1: Overview of biological conversions

The most widely used enzyme for fermentation is s*accharomyces cerevisiae*, also known as 'Baker's yeast', is used for the production of bread, beer and wine *etc*[56]. With a high hydrolysis yield of more than 90% to give a concentrated sugar solution, fermentation enzymes are added to the sugar solution to begin the fermentation process to give a theoretical yield of 2 ethanol molecules per molecule of glucose. Genetic engineering of yeasts have allowed for the fermentation of xylose[57], increased the rate of fermentation, and even to produce biofuels directly[58]. However, high costs of enzymes, remains a challenge to be overcome as it increases the cost price of the products despite utilizing a cheap feedstock.

Chemical Conversion

Chemical conversion of biomass represents a big subclass of conversion

[54] Bornscheuer, U.; Buchholz, K.; Seibel, J. *Angew. Chem. Int. Ed.* **2014,** *53*, 10876–10893.
[55] Eckard, A. Enzymatic Hydrolysis Technologies for the Production of Biofuels. In *Lignocellulose-Based Bioproducts*; Karimi, K., Ed. Springer International Publishing: Heidelberg, 2015; Vol. 1, pp 155-173.
[56] Katrin, T.; Vladimir, S. Fermentation of Biomass. In *Biomass Processing Technologies*; Strezov, V.; Evans, T. J., Eds. CRC Press/Taylor & Francis Group: Boca Raton, 2014; pp 257-308.
[57] Alper, H.; Moxley, J.; Nevoigt, E.; Fink, G. R.; Stephanopoulos, G. *Science* **2006,** *314*, 1565-1568.
[58] Bokinsky, G.; Peralta-Yahya, P. P.; George, A.; Holmes, B. M.; Steen, E. J.; Dietrich, J.; Soon Lee, T.; Tullman-Ercek, D.; Voigt, C. A.; Simmons, B. A.; Keasling, J. D. *Proc. Natl. Acad. Sci. U. S. A.* **2011,** *108*, 19949-19954.

processes[59] due to the rich chemical functionalities present in biomass as compared to fossil fuels, the myriad of derivable products and the seemingly endless list of tunable catalysts to enable such transformations. These conversions are broadly categorized into 4 main categories, namely aqueous phase reforming, ionic liquids, heterogeneous and homogeneous catalysis (Figure 8).

Aqueous phase reforming has its origins from the production of renewable hydrogen from sugars and sugar alcohols, however the technology has been successfully recalibrated to produce light alkanes albeit with low selectivity and modest yields[60]. In order to produce diesel range fuels, the hydrocarbons produced are required to have greater molecular weight, and the classical Aldol reaction was employed.

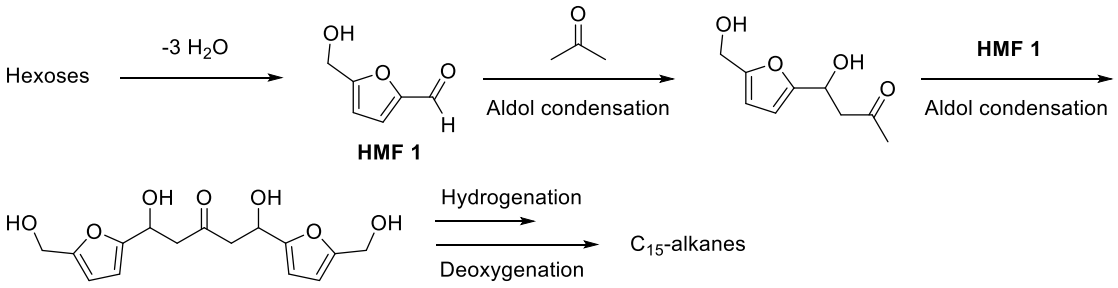

Scheme 2: Generation of diesel range fuels from biomass

Hydroxymethylfurfural (HMF) **1** is a well-studied intermediate derived from biomass and by facilitating Aldol cross-condensation reactions with acetone, a 15-carbon intermediate could be generated before further hydrogenation and deoxygenation to obtain C_{15}-alkanes[61] (Scheme 2). The desired hydrophobic products are expected to separate easily as a distinct layer from the aqueous reaction medium

[59] Chatterjee, C.; Pong, F.; Sen, A. *Green Chem.* **2015,** *17*, 40-71.
[60] Huber, G. W.; Cortright, R. D.; Dumesic, J. A. *Angew. Chem. Int. Ed.* **2004,** *43*, 1549-1551.
[61] a) Huber, G. W.; Chheda, J. N.; Barrett, C. J.; Dumesic, J. A. *Science* **2005,** *308*, 1446-1450; b) Chheda, J. N.; Huber, G. W.; Dumesic, J. A. *Angew. Chem. Int. Ed.* **2007,** *46*, 7164-7183.

thus avoiding distillation and saving costs. The relatively lower temperature used compared to thermal conversions also reduces energy consumption and the hydrogen required could be provided by aqueous phase reforming of sugars and sugar alcohols.

Ionic liquids are salts comprising of an organic cation and an organic or inorganic anion, with a low melting point (< 100 ºC)[62]. As such ionic liquids possess interesting properties and applications which are intensively investigated by researchers internationally[63]. Ionic liquids possess low vapour pressure, making it a safer alternative to traditional organic solvents and they are highly customizable due to the large possibilities of side chains and ionic combinations. In view of their ability to dissolve biomass, ionic liquids have been involved in biomass conversions from pretreatment to hydrolysis processes[64]. For example, the inherent acidity of the ionic liquid [C_3SO_3Hmim][Cl] (Figure 10) is able to hydrolyse cellulose in the presence of water to give a total reducing sugar yield of 62%[65] while [Emim][Cl] (Figure 10) is able to dehydrate glucose to HMF in the presence of catalytic amounts of $CrCl_2$ with a yield of 68%.[66]

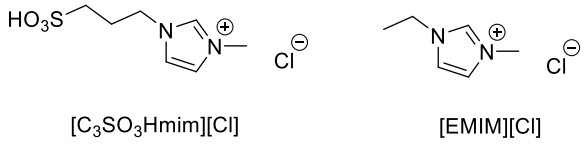

[C_3SO_3Hmim][Cl] [EMIM][Cl]

Figure 10: Examples of ionic liquids used in biomass conversion

[62] Hayes, R.; Warr, G. G.; Atkin, R. *Chem. Rev.* **2015,** *115*, 6357-6426.
[63] Wasserscheid, P.; Keim, W. *Angew. Chem. Int. Ed.* **2000,** *39*, 3772-3789.
[64] a) Brandt, A.; Grasvik, J.; Hallett, J. P.; Welton, T. *Green Chem.* **2013,** *15*, 550-583; b) Xie, H.; Liu, W.; Beadham, I.; Gathergood, N. Biorefinery with Ionic Liquids. In *The Role of Green Chemistry in Biomass Processing and Conversion*; John Wiley & Sons, Inc.: New Jersey, 2012; pp 75-133. c) Wahlstrom, R. M.; Suurnakki, A. *Green Chem.* **2015,** *17*, 694-714.
[65] a) Amarasekara, A. S.; Owereh, O. S. *Ind. Eng. Chem. Res.* **2009,** *48*, 10152-10155; b) da Costa Lopes, A. M.; Bogel-Łukasik, R. *ChemSusChem* **2015**, *8*, 947–965.
[66] Zhao, H.; Holladay, J. E.; Brown, H.; Zhang, Z. C. *Science* **2007,** *316*, 1597-1600.

Heterogeneous catalysis involves the use of catalyst that is in a different phase from the reactants and it offers the distinct advantage of ease of separation and reuse[67]. Some classes of heterogeneous catalysts include zeolites, functionalized silica, and bimetallic catalysts[68]. A wide variety of reactions could be carried out using these catalysts such as reforming, hydrogenation, oxidation, hydrolysis and deoxygenation[39,69]. Of particular interest is the use of supported metal oxide in the dehydration of xylose to furfural **2** in 60% yield which is an important intermediate analogous to the dehydration of glucose to HMF **1**[70] (Figure 11). HMF **1** could be further transformed into dimethylfuran[71], a potential transportation fuel with 40% higher energy density than ethanol, in a reaction involving bimetallic catalyst copper-ruthenium (CuRu) catalyst[72] (Figure 11).

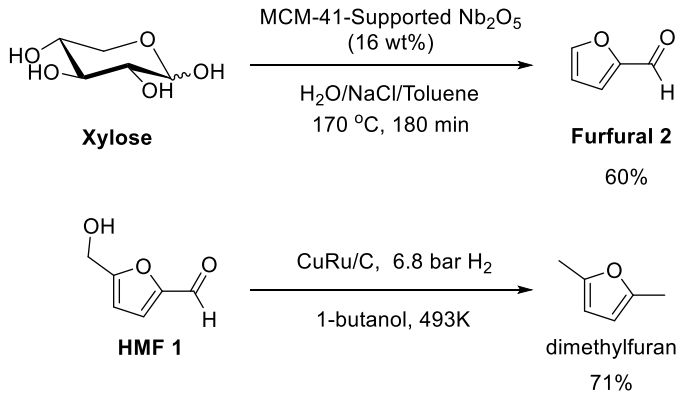

Figure 11: Heterogeneous catalysts used in hydrolysis and hydrogenation reactions

[67] Dibenedetto, A.; Colucci, A.; Pastore, C. Heterogeneous catalysis applied to the conversion of biogenic substances, platform molecules, and oils. In *Biorefinery - From Biomass to Chemicals and Fuels*; Aresta, M.; Dibenedetto, A.; Dumeignil, F., Eds. Walter de Gruyter GmbH & Co. KG: Berlin, 2012; pp 279-296.

[68] a) Vilcocq, L.; Castilho, P. C.; Carvalheiro, F.; Duarte, L. C. *ChemSusChem* **2014**, 7: 1010–1019; b) Huang, Y.-B.; Fu, Y. *Green Chem.* **2013,** *15*, 1095-1111; c) Alonso, D. M.; Wettstein, S. G.; Dumesic, J. A. *Chem. Soc. Rev.* **2012,** *41*, 8075-8098; d) Taarning, E.; Osmundsen, C. M.; Yang, X.; Voss, B.; Andersen, S. I.; Christensen, C. H. *Energy Environ. Sci.* **2011,** *4*, 793-804.

[69] a) Besson, M.; Gallezot, P.; Pinel, C. *Chem. Rev.* **2014,** *114*, 1827-1870; b) Gosselink, R. W.; Stellwagen, D. R.; Bitter, J. H. *Angew. Chem. Int. Ed.* **2013,** *52*, 5089-5092.

[70] García-Sancho, C.; Sádaba, I.; Moreno-Tost, R.; Mérida-Robles, J.; Santamaría-González, J.; López-Granados, M.; Maireles-Torres, P. *ChemSusChem* **2013,** *6*, 635-642.

[71] Saha, B.; Abu-Omar, M. M. *ChemSusChem* **2015,** *8*, 1133-1142.

[72] Roman-Leshkov, Y.; Barrett, C. J.; Liu, Z. Y.; Dumesic, J. A. *Nature* **2007,** *447*, 982-985.

Homogeneous catalysis involves the use of catalyst that is in a same phase from the reactants and it offers the advantage of faster reaction due to homogeneity and tunability of catalyst parameters. Hydrolysis reactions are typically carried out in aqueous acid solutions due to limited solubility of biomass components in organic solvents. Heteropolyacids such as $H_3PW_{12}O_{40}$ are used in the aqueous depolymerization of cellulose to yield glucose[73] while inorganic acids such as H_2SO_4 can be applied to the transformation of glucose to levulinic acid[74] **3** which is a versatile intermediate. There have been also successful attempts to improve the yield of HMF **1** by employing acid-catalyzed dehydration of biomass in a mixture of aqueous and organic medium so that the side reactions can be minimized by partitioning the HMF into the organic phase[75].

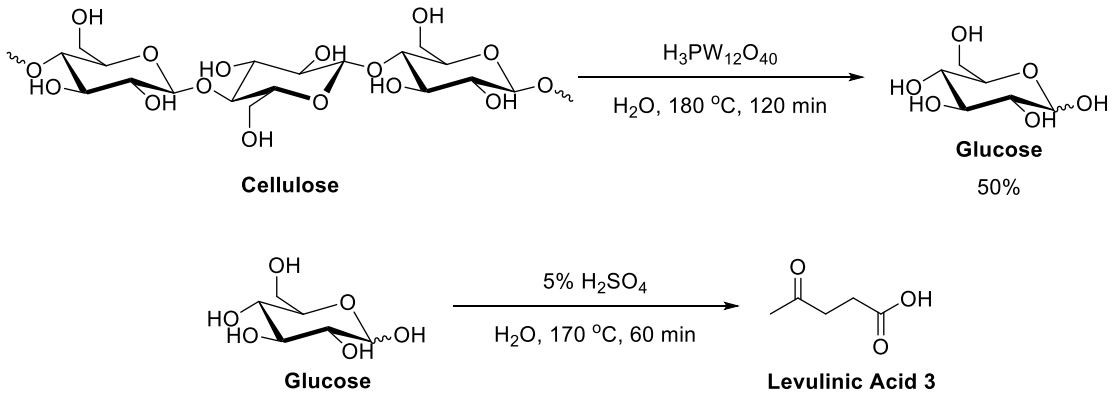

Figure 12: Homogeneous catalysts used in biomass conversions

1.4 Platform Chemicals – Production and Applications

As the only source of renewable carbon, biomass is poised to become the surrogate feedstock for both bulk and fine chemicals in view of its abundance,

[73] Fischmeister, C.; Bruneau, C.; Vigier, K. D. O.; Jérôme, F. Catalytic conversion of biosourced raw materials: homogeneous catalysis. In *Biorefinery - From Biomass to Chemicals and Fuels*; Aresta, M.; Dibenedetto, A.; Dumeignil, F., Eds. Walter de Gruyter GmbH & Co. KG: Berlin, 2012; pp 231-262.
[74] Rackemann, D. W.; Doherty, W. O. S. *Biofuels, Bioprod. Biorefin.* **2011,** *5*, 198-214.
[75] Saha, B.; Abu-Omar, M. M. *Green Chem.* **2014,** *16*, 24-38.

sustainability, cost and chemical functionality. An extensive selection of products can be derived from biomass and only a handful of chemicals were shortlisted by the U.S. Department of Energy as the "top ten chemical opportunities" for targeted development in 2004[76]. This practical list of targeted chemicals was termed "platform chemicals" in view of their ease of access, industrial viability, market size and ability to serve as a platform for further derivatization to other useful compounds. The list was further updated in 2010 by one of the co-authors in the initial report to reflect the spur of development brought about by the research and industrial communities[38] (Figure 13). Of particular significance are HMF **1**, furfural **2**, levulinic acid **3** and ethanol **4**, all of which have been briefly described in the previous sections.

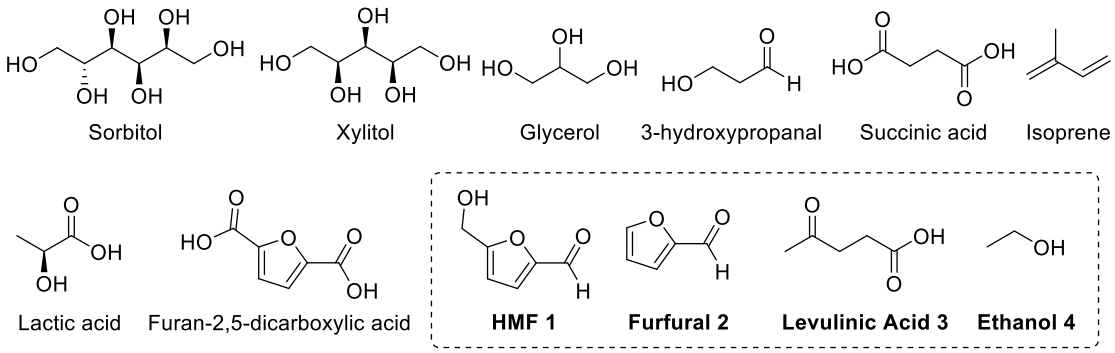

Figure 13: List of top biomass derived platform chemicals

The production of HMF **1** from biomass has been extensively reviewed[77] and common feedstocks include fructose, glucose, cellulose and even raw biomass material. One particular dehydration pathway has been thoroughly investigated and the

[76] Werpy, T.; Petersen, G. *Top Value Added Chemicals from Biomass: Volume I -- Results of Screening for Potential Candidates from Sugars and Synthesis Gas*; DOE/GO-102004-1992; U.S. Department of Energy: Oak Ridge, TN, 2004; pp 1-76.

[77] a) Zakrzewska, M. E.; Bogel-Łukasik, E.; Bogel-Łukasik, R. *Chem. Rev.* **2010,** *111*, 397-417; b) Rosatella, A. A.; Simeonov, S. P.; Frade, R. F. M.; Afonso, C. A. M. *Green Chem.* **2011,** *13*, 754-793; c) van Putten, R.-J.; van der Waal, J. C.; de Jong, E.; Rasrendra, C. B.; Heeres, H. J.; de Vries, J. G. Chem. Rev. 2013, 113, 1499-1597; d) Teong, S. P.; Yi, G.; Zhang, Y. *Green Chem.* **2014,** *16*, 2015-2026; e) Wang, T.; Nolte, M. W.; Shanks, B. H. *Green Chem.* **2014,** *16*, 548-572;

mechanism[78] is proposed to be initiated by the boric acid-promoted isomerization of glucose to fructose before successive dehydrations can occur (Figure 14). The keen interest on HMF **1** stems from its ease of access from abundant cellulose, its rich chemical functionality comprising of an alcohol, aldehyde and furan ring, allowing it to undergo various transformations to yield other high utility chemicals[77b,c,e,79] (Figure 15). The first industrial plant for the production of HMF **1** from biomass had been set up in 2014[80] while a pilot plant has been set up to produce HMF ethers by Avantium Chemicals[81].

[78] a) Ståhlberg, T.; Rodriguez-Rodriguez, S.; Fristrup, P.; Riisager, A. *Chem. Eur. J.* **2011**, *17*, 1456-1464; b) Antal Jr, M. J.; Mok, W. S. L.; Richards, G. N. *Carbohyd. Res.* **1990**, *199*, 91-109.

[79] a) Liu, D.; Chen, E. Y. X. *Green Chem.* **2014,** *16*, 964-981; b) Gallezot, P. *Chem. Soc. Rev.* **2012,** *41*, 1538-1558.

[80] AVA Biochem Press Release. http://www.ava-biochem.com/media/downloads_EN/press_releases/First_Industrial_Production_For_Renewable_5_HMF.pdf (accessed Nov 24, 2015).

[81] a) van Putten, R.-J.; Dias, A. S.; de Jong, E. Furan-Based Building Blocks from Carbohydrates. In *Catalytic Process Development for Renewable Materials*, Imhof, P.; van der Waal, J. C. Eds.; Wiley-VCH Verlag GmbH & Co. KGaA: Weinheim, 2013; pp 81-117.

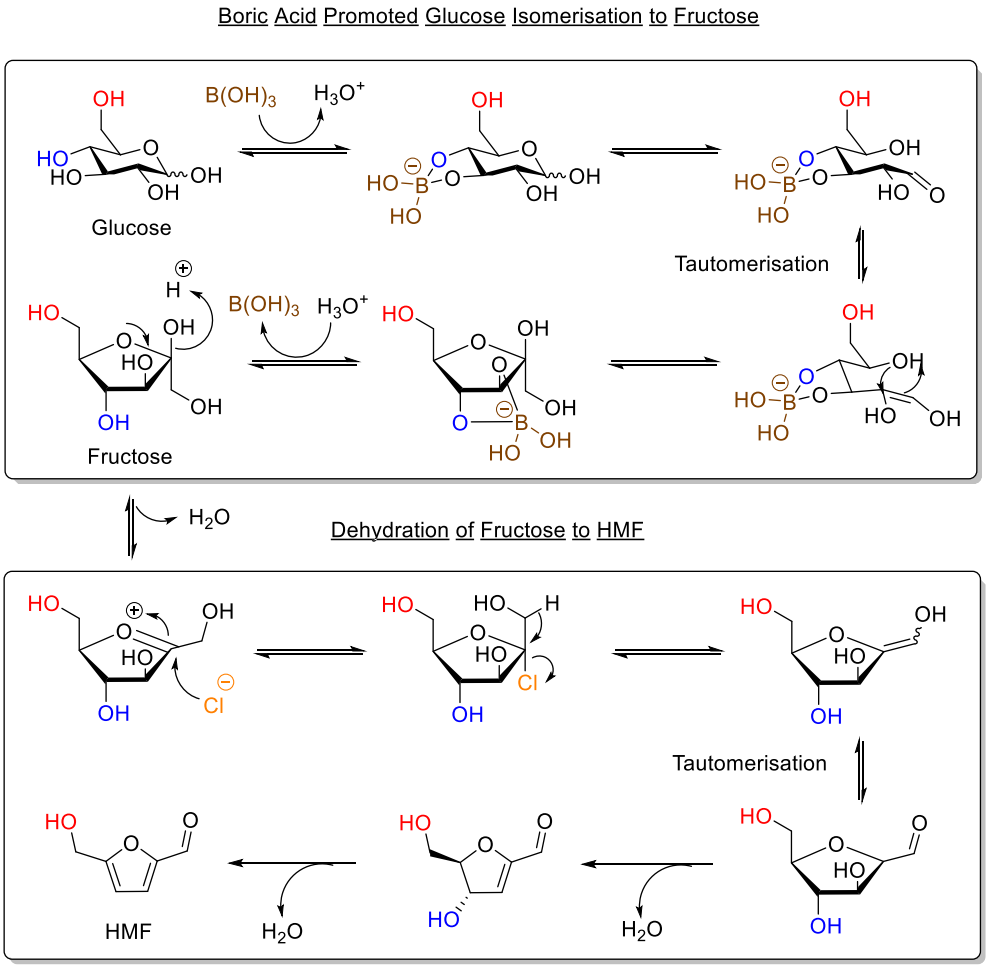

Figure 14: Proposed glucose dehydration pathway promoted by boric acid[78]

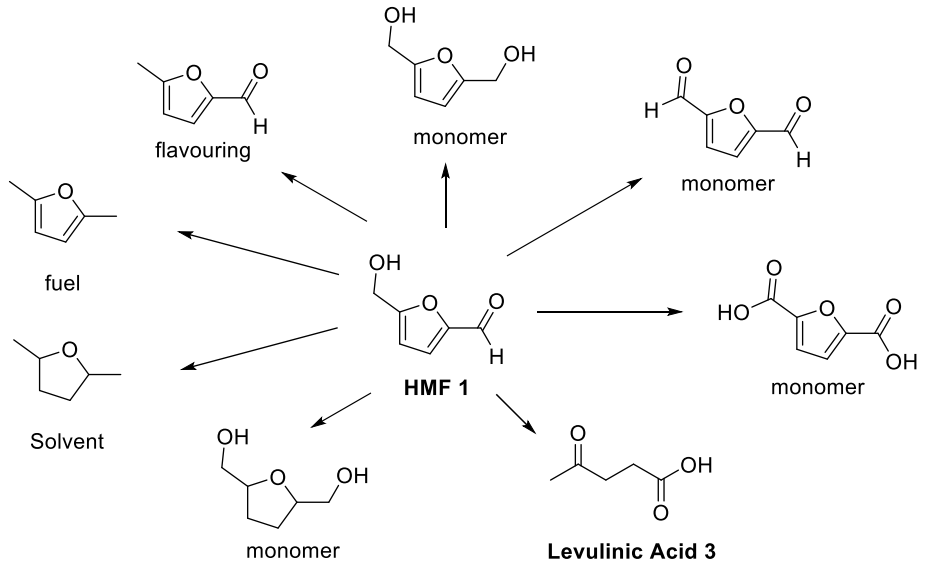

Figure 15: Versatility and utility of the derivatives of HMF **1**

Furfural **2** is derived from the second most abundant sugar, xylose, which is a pentose and hence has one less carbon than its 6-carbon analogue HMF **1**. Industrially, furfural **2** is produced from agricultural raw materials at a rate of 300 000 tons per year[82] and recent developments[83] highlight the possibility of reducing the already relatively low production cost of furfural **2** thus increasing its potential utility. Similarly, furfural **2** and its derivatives possess substantial practical applications such as synthesis of natural products[84], starting material for Nylon 6,6[2], chiral inducers[85], fuels[86], extractant[82a], fungicide, solvents and resins[81,] (Figure 16).

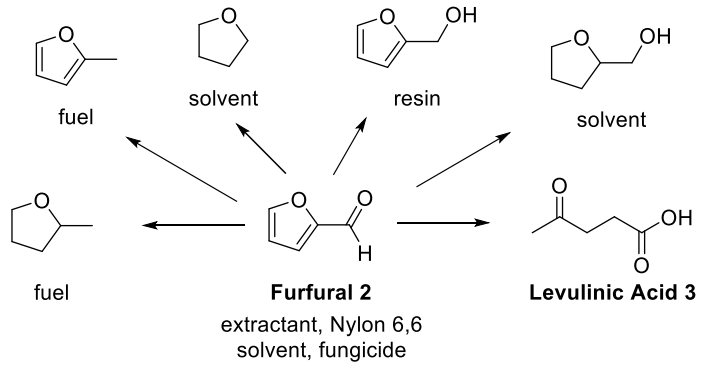

Figure 16: Applications of furfural **2** and its derivatives

Together, HMF **1** and furfural **2**, hold great potential to be exploited for chemical synthesis due to the furan ring present. The interesting reactions of furfuryl alcohols and furanoxonium intermediates have been the center of attention for numerous

[82] a) Zeitsch, K. J. *The Chemistry and Technology of Furfural and its Many By-Products*; Sugar Series, Vol. 13; Elsevier: Amsterdam, 2000; b) Corma, A.; Iborra, S.; Velty, A. *Chem. Rev.* **2007,** *107,* 2411-2502.
[83] Xing, R.; Qi, W.; Huber, G. W. *Energy Environ. Sci.* **2011,** *4,* 2193-2205.
[84] a) Leverett, C. A.; Cassidy, M. P.; Padwa, A. *J. Org. Chem.* **2006,** *71,* 8591-8601; b) Cassidy, M. P.; Padwa, A. *Org. Lett.* **2004,** *6,* 4029-4031; c) Harris, J. M.; Padwa, A. *J. Org. Chem.* **2003,** *68,* 4371-4381; d) Harris, J. M.; Padwa, A. *Org. Lett.* **2002,** *4,* 2029-2031; e) Haukaas, M. H.; O'Doherty, G. A. *Org. Lett.* **2001,** *3,* 401-404.
[85] Kabro, A.; Escudero-Adán, E. C.; Grushin, V. V.; van Leeuwen, P. W. N. M. *Org. Lett.* **2012,** *14,* 4014-4017.
[86] a) Lange, J.-P.; van der Heide, E.; van Buijtenen, J.; Price, R. *ChemSusChem* **2012,** *5,* 150-166; b) Climent, M. J.; Corma, A.; Iborra, S. *Green Chem.* **2014,** *16,* 516-547.

research groups[87] (Figure 17). The Piancatelli reaction[88] involves the generation of a furanoxonium intermediate following the hydrolysis of the furfuryl alcohol **5** and a Nazarov cyclization reaction[89] leading to a 4-hydroxycyclopent-2-enone derivative **6**. Similarly, the furanoxonium intermediate could be trapped by suitable 1,3-dienes in an intermolecular [4+3] cycloaddition reaction[90] to generate 7-membered rings such as **7**, with the furan ring intact for further derivatizations. Alternatively, the furfuryl alcohol **5** could undergo oxidation of the furan ring to initiate the Achmatowicz rearrangement reaction[91] to yield dihydropyranone **8**. The Achmatowicz rearrangement reaction is a powerful tool[92] for the construction of tetrahydropyran cores present in natural products[93] and the nitrogen variant, the aza-Achmatowicz rearrangement reaction involving furfuryl amine, has also been developed and applied extensively[94]. The mechanisms of the Achmatowicz and aza-Achmatowicz rearrangements are illustrated

[87] Palframan, M. J.; Pattenden, G. *Chem. Commun.* **2014,** *50*, 7223-7242.
[88] Piancatelli, G.; Scettri, A.; Barbadoro, S. *Tetrahedron Lett.* **1976,** *17*, 3555-3558.
[89] Nazarov, I. N.; Zaretskaya, I. I. *Bull. Acad. Sci. (USSR)* **1942**, 200-209.
[90] Winne, J. M.; Catak, S.; Waroquier, M.; Van Speybroeck, V. *Angew. Chem. Int. Ed.* **2011,** *50*, 11990-11993.
[91] a) Achmatowicz Jr, O.; Bukowski, P.; Szechner, B.; Zwierzchowska, Z.; Zamojski, A. *Tetrahedron* **1971,** *27*, 1973-1996; b) Achmatowicz Jr, O.; Bielski, R. *Carbohydr. Res.* **1977,** *55*, 165-176.
[92] a) Lefebvre, Y. *Tetrahedron Lett.* **1972,** *13*, 133-136; b) Couladouros, E. A.; Georgiadis, M. P. *J. Org. Chem.* **1986,** *51*, 2725-2727; c) Georgiadis, M. P.; Albizati, K. E.; Georgiadis, T. M. *Org. Prep. Proced. Int.* **1992,** *24*, 95-118; d) Cuccarese, M. F.; O'Doherty, G. A. Application of the Achmatowicz Rearrangement for the Synthesis of Oligosaccharides. In *Asymmetric Synthesis II: More Methods and Applications* Wiley-VCH Verlag GmbH & Co. KGaA: Weinheim, 2012; pp 249-259.
[93] Recent examples of Achmatowicz rearrangement in total syntheses: a) Sridhar, Y.; Srihari, P. *Org. Biomol. Chem.* **2013,** *11*, 4640-4645; b) Sridhar, Y.; Srihari, P. *Eur. J. Org. Chem.* **2013**, 578-587; c) Ghosh, A. K.; Chen, Z.-H. *Org. Lett.* **2013,** *15*, 5088-5091; d) Bhuniya, R.; Nanda, S. *Tetrahedron* **2013,** *69*, 1153-1165; e) Takamura, H.; Tsuda, K.; Kawakubo, Y.; Kadota, I.; Uemura, D. *Tetrahedron Lett.* **2012,** *53*, 4317-4319; f) Srihari, P.; Sridhar, Y. *Eur. J. Org. Chem.* **2011**, 6690-6697; g) Robertson, J.; North, C.; Sadig, J. E. R. *Tetrahedron* **2011,** *67*, 5011-5023; h) Herrmann, A. T.; Martinez, S. R.; Zakarian, A. *Org. Lett.* **2011,** *13*, 3636-3639; i) Gazaille, J. A.; Abramite, J. A.; Sammakia, T. *Org. Lett.* **2011,** *14*, 178-181; j) Nicolaou, K. C.; Baker, T. M.; Nakamura, T. *J. Am. Chem. Soc.* **2010,** *133*, 220-226; k) Ghosh, A. K.; Li, J. *Org. Lett.* **2010,** *13*, 66-69.
[94] a) van der Pijl, F.; van Delft, F. L.; Rutjes, F. P. J. T. *Eur. J. Org. Chem.* **2015,** *2015*, 4811-4829; b) Zhou, W.-S.; Lu, Z.-H.; Xu, Y.-M.; Liao, L.-X.; Wang, Z.-M. *Tetrahedron* **1999,** *55*, 11959-11983; c) Liao, L.-X.; Wang, Z.-M.; Zhang, H.-X.; Zhou, W.-S. *Tetrahedron: Asymmetry* **1999,** *10*, 3649-3657; d) Ciufolini, M. A.; Hermann, C. Y. W.; Dong, Q.; Shimizu, T.; Swaminathan, S.; Xi, N. *Synlett* **1998**, 105-114; e) Zhou, W.-S.; Xie, W.-G.; Lu, Z.-H.; Pan, X.-F. *J. Chem. Soc., Perkin Trans. 1* **1995**, 2599-2604; f) Wei-Shan, Z.; Wen-Ge, X.; Zhi-Hui, L.; Xin-Fu, P. *Tetrahedron Lett.* **1995,** *36*, 1291-1294; g) Hopman, J. C. P.; van den Berg, E.; Ollero, L. O.; Hiemstra, H.; Nico Speckamp, W. *Tetrahedron Lett.* **1995,** *36*, 4315-4318; h) Altenbach, H.-J.; Wischnat, R. *Tetrahedron Lett.* **1995,** *36*, 4983-4984; i) Lu, Z.-H.; Zhou, W.-S. *J. Chem. Soc., Perkin Trans. 1* **1993**, 593-596.

in Figure 18 where the furan ring undergoes oxidative ring opening to afford an unsaturated diketone which is then subjected to nucleophilic ring closing.

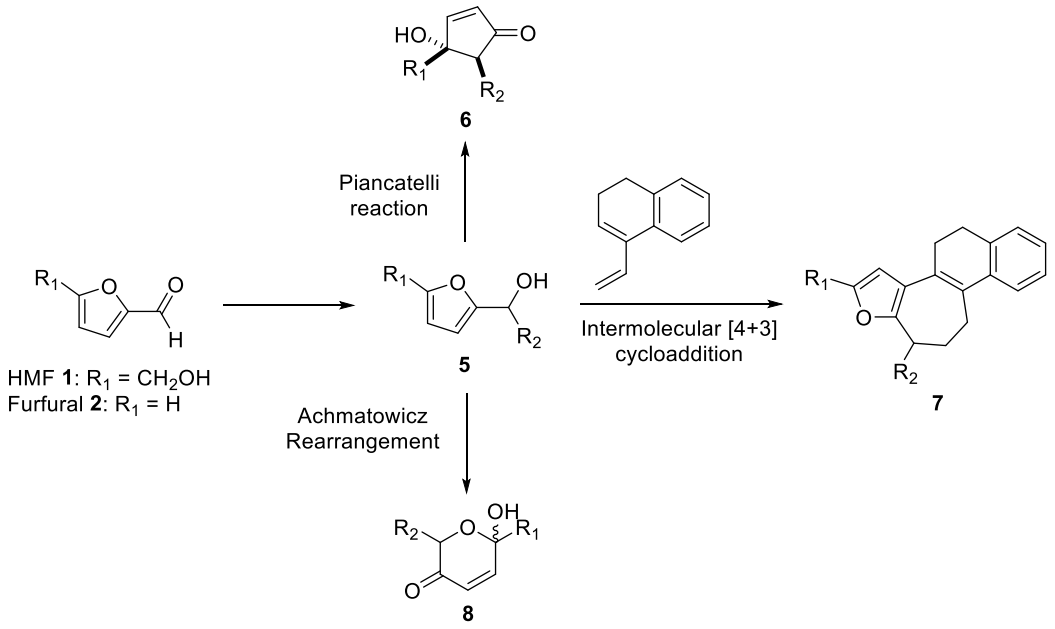

Figure 17: Diversity of reactions of applicable to furan derivatives

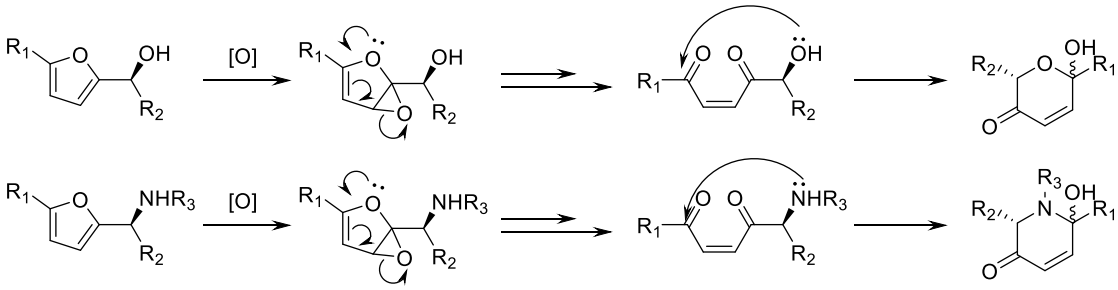

Figure 18: Mechanisms of the Achmatowicz and aza-Achmatowicz rearrangement

Levulinic acid **3**, containing both ketone and carboxylic functional groups, originates from both cellulose and hemicellulose *via* HMF **1** and furfural **2** as intermediates respectively[74]. The production of levulinic acid **3** from HMF **1** releases an equivalent of formic acid, a commodity chemical, as a useful by-product of economic value. Correspondingly, levulinic acid **3** also has a wide range of

applications in the domains of fuel[86b], solvent, resins and flavoring (Figure 19). The production of levulinic acid **3** from biomass has already been commercialized[81,95].

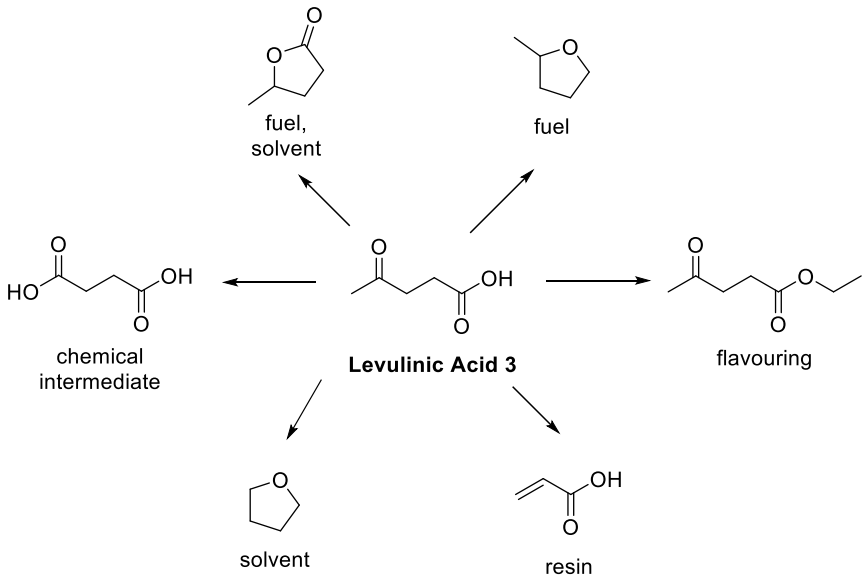

Figure 19: Examples of the utility of levulinic acid **3** and its derivatives

Ethanol **4** production from the fermentation of biomass is arguably the most established process in terms of biomass conversion and it is used in many countries as a fuel directly or as a petrol blend[96]. However, due to the food, energy, environment trilemma[23] discussed previously in section 1.2, the focus of the underlying feedstock is slowly shifting from food-based crops to low-value lignocellulosic biomass components. An interesting application of bioethanol **4** is the production of ethylene glycol from bioethanol. Ethylene glycol is one of the monomer used in the production polyethylene terephthalate (PET), the key polymer used in bottles with an annual production of 60 million tons[97]. A key driver towards sustainable materials in plastic

[95] a) BusinessGreen: Sustainable Thinking. http://www.businessgreen.com/bg/news/2434852/football-star-mathieu-flamini-reveals-secret-biofuel-investments (accessed Nov 23, 2015); b) GFBiochemicals. http://www.gfbiochemicals.com/company/#about-us (accessed Nov 23, 2015)

[96] Gupta, R. B.; Demirbas, A. *Gasoline, Diesel and Ethanol Biofuels from Grasses and Plants*. Cambridge University Press: New York, 2010; pp 84-101.

[97] a) McIntyre, J. E. In *Modern Polyesters: Chemistry and Technology of Polyesters and Copolyesters*; Scheirs, J.; Long, T. E., Eds.; John Wiley & Sons: Chichester, 2003; pp 3-30; b) PCI Xylenes &

packaging is the Coca-Cola Company with their "PlantBottle™" technology[98] which utilizes bioethanol to produce the ethylene glycol used in their bottles and it reported an annual reduction of 30,000 metric tons of carbon dioxide emission[99].

1.5 Thesis Aim

Our group has a longstanding interest in the conversion of lignocellulosic biomass to useful and valuable chemicals. We have developed a methodology involving the Cu-catalyzed amide bond formation of lignin model compounds with secondary amines under aerobic conditions to afford the different phenolic component products in modest to good yields[100] (Scheme 3). Next, we have independently discovered the use of non-toxic arylboronic acids in ionic liquids to convert glucose to HMF **1** and this methodology could be further extended to the direct conversion of cellulose to HMF **1**[101](Scheme 4). This methodology offers the advantages of non-toxicity and catalyst tunability as compared to the use of toxic chromium catalysts[66]. In addition, we have also explored the development of an $InCl_3$-heteropolyacid catalytic system in aqueous medium to convert cellulose to levulinic acid **3** in a green and selective manner[102] (Scheme 5). The catalytic system could also be successfully applied to raw waste biomass material such as rice straw and saw dust from Chinese fir.

Polyesters. The PTA, PET, and Polyester Fibre Market Background; Guildford, 2012.

[98] van Es, D. S.; der Klis, F. v.; Knoop, R. J. I.; Molenveld, K.; Sijtsma, L.; van Haveren, J. Other Polyesters from Biomass Derived Monomers. In *Bio-Based Plastics: Materials and Applications*; Kabasci, S., Ed.; John Wiley & Sons Ltd: Chichester, 2013; pp 241-274.

[99] PlantBottle: Frequently Asked Questions. The Coca-Cola Company. http://www.coca-colacompany.com/stories/plantbottle-frequently-asked-questions/ (accessed Nov 05, 2015).

[100] Zhang, J.; Liu, Y.; Chiba, S.; Loh, T.-P. *Chem. Commun.* **2013**, *49*, 11439-11441.

[101] a) Lukamto, D. H.; Wang, P.; Loh, T.-P. *Asian J. Org. Chem.* **2013**, *2*, 947-951; b) Lukamto, D. H.; Wang, P.; Loh, T. P. U.S. PRV. 61/666,067, **2012**; c) Lukamto, D. H.; Wang, P.; Loh, T. P. PCT/SG2013/000272, **2013**.

[102] Loh, T.-P.; Huang, J.-M.; Luo, Y.; Ou Yong, C.-W. R.; Ng, K. S. L. unpublished results.

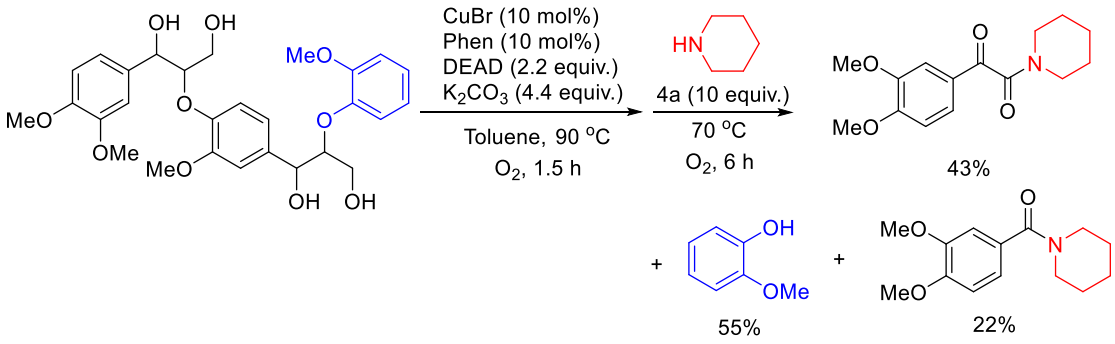

Scheme 3: Conversion of lignin model compounds *via* Cu-catalyzed aerobic amide bond formation

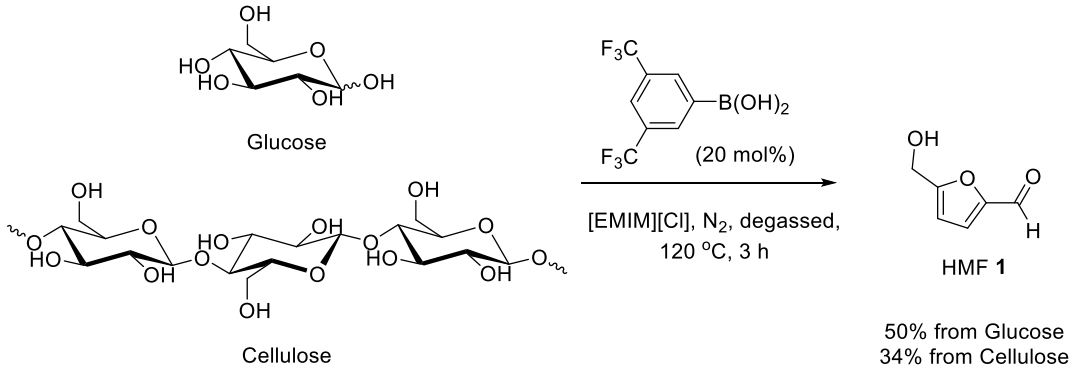

Scheme 4: Catalytic conversion of carbohydrates into platform chemical HMF **1** using arylboronic acids

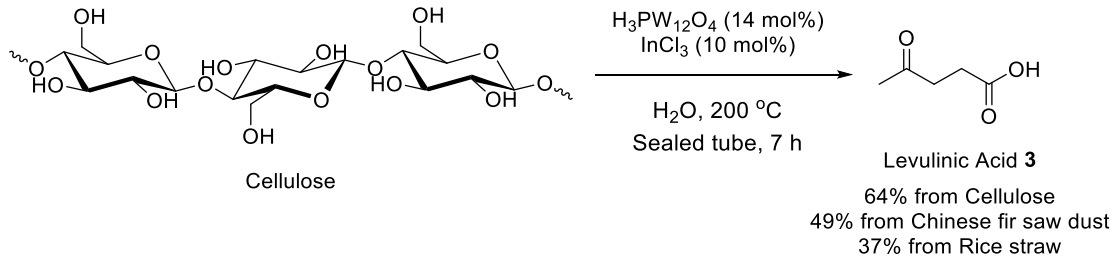

Scheme 5: Green and selective conversion of cellulose to levulinic acid **3** in $InCl_3$-heteropolyacid catalytic system

In view of the vast amount of technologies for the production of biomass derived platform chemicals, biomass derived platform chemicals are well-positioned to be a

cheap, useful and sustainable replacement for the chemicals used in chemical industry which is typically derived from conventional fossil fuels. This thesis aims to explore the development of syntheses of high value chemicals, such as drug intermediates or biologically active natural products, from biomass platform chemicals whereby all or a significant portion of the carbon atoms present are of biomass origins.

CHAPTER 2

Biomass Derived Furfural-Based Facile Synthesis of Protected (2S)-Phenyl-3-Piperidone, a Common Intermediate for Many Drugs

CHAPTER 2 BIOMASS DERIVED FURFURAL-BASED FACILE SYNTHESIS OF PROTECTED (2*S*)-PHENYL-3-PIPERIDONE, A COMMON INTERMEDIATE FOR MANY DRUGS

2.1 Introduction

Substance P is an 11-amino acid neuropeptide discovered in 1931 and the most abundant neurokinin found in the central nervous system of mammals[103]. The amino acid sequence of Substance P was only unveiled in 1971[104] and its corresponding receptor was identified as the neurokinin-1 (NK_1) receptor[105]. The association of Substance P with the regulation of anxiety, depression, stress and emesis led to strong interests in the development of suitable small molecule NK_1 receptor antagonists[106]. Initial attempts focused on peptide derivatives of Substance P but faced several limitations in terms of bioavailability and potency.

It was only until the year 1991 when 3 different pharmaceutical companies announced the first examples of non-peptidic NK_1 receptor antagonists[107] and a whole host of such NK_1 receptor antagonists were introduced for testing[108] (Figure 20). A common feature of these potent NK_1 receptor antagonists developed by 4 different pharmaceutical companies is the presence of the central (2*S*)-phenyl-3-piperidone core. The construction of this common intermediate would allow easy access to a variety of

---

[103] v. Euler, U. S.; Gaddum, J. H. *J. Physiol. (Lond.)* **1931,** *72*, 74-87.
[104] a) Chang, M. M.; Leeman, S. E.; Niall, H. D. *Nat. New Biol.* **1971,** *232*, 86-87; b) Tregear, G. W.; Niall, H. D.; Potts, J. T.; Leeman, S. E.; Chang, M. M. *Nat. New Biol.* **1971,** *232*, 87-89.
[105] Fong, T. M.; Anderson, S. A.; Yu, H.; Huang, R. R.; Strader, C. D. *Mol. Pharmacol.* **1992,** *41*, 24-30.
[106] a) Hesketh, P. *Support Care Cancer* **2001,** *9*, 350-354; b) Ebner, K.; Singewald, N. *Amino Acids* **2006,** *31*, 251-272.
[107] a) Snider, R.; Constantine, J.; Lowe, J.; Longo, K.; Lebel, W.; Woody, H.; Drozda, S.; Desai, M.; Vinick, F.; Spencer, R.; et, al. *Science* **1991,** *251*, 435-437; b) Garret, C.; Carruette, A.; Fardin, V.; Moussaoui, S.; Peyronel, J. F.; Blanchard, J. C.; Laduron, P. M. *Proc. Natl. Acad. Sci. U. S. A.* **1991,** *88*, 10208-10212; c) Marisa Rosso; Muñoz, M.; Berger, M. *Scientific World Journal* **2012,** *2012*, 21.
[108] Huang, S.-C.; Korlipara, V. L. *Expert Opin. Ther. Pat.* **2010,** *20*, 1019-1045.

potent NK_1 receptor antagonists *via* subsequent decorations of the remaining substituents around the piperidone core.

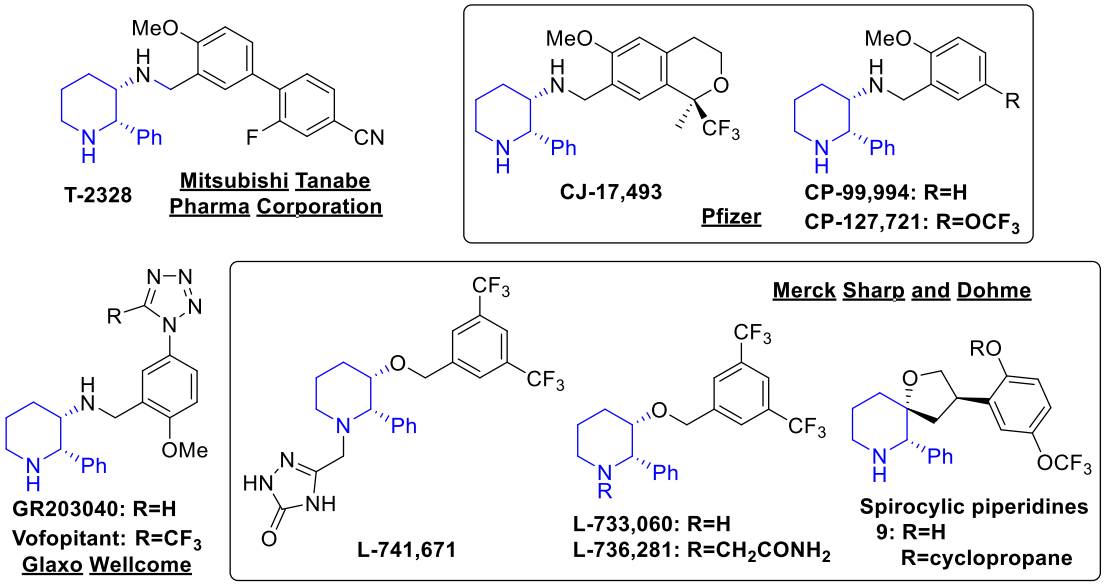

Figure 20: Examples of NK_1 receptor antagonists with common piperidone core

Given the attractiveness of this versatile piperidone core, there have been a considerable amount of effort put into its synthesis in various protected forms, usually as an intermediate towards one of the many NK_1 receptor antagonists[109,110]. 3 of these syntheses by Merck[109a], Aggarwal[109b] and Ollivier[109c] are briefly described. Merck's synthesis[109a] began with the chain elongation of phenylacetylene **10** and *cis*-reduction of the alkyne moiety to generate *cis*-styrene **11** which was then subjected to Jacobsen's epoxidation conditions to afford the desired epoxide with 62% yield and 92%

[109] a) Lee, J.; Hoang, T.; Lewis, S.; Weissman, S. A.; Askin, D.; Volante, R. P.; Reider, P. J. *Tetrahedron Lett.* **2001,** *42*, 6223-6225; b) Kokotos, C. G.; Aggarwal, V. K. *Chem. Commun.* **2006**, 2156-2158; c) Gaucher, X.; Jida, M.; Ollivier, J. *Synlett* **2009**, 3320-3322.

[110] a) Calvez, O.; Langlois, N. *Tetrahedron Lett.* **1999,** *40*, 7099-7100; b) Williams, B. J.; Cascieri, M. A.; Chicchi, G. G.; Harrison, T.; Owens, A. P.; Owen, S. N.; Rupniak, N. M. J.; Tattersall, D. F.; Williams, A.; Swain, C. J. *Bioorg. Med. Chem. Lett.* **2002,** *12*, 2719-2722; c) Huang, P.-Q.; Liu, L.-X.; Wei, B.-G.; Ruan, Y.-P. *Org. Lett.* **2003,** *5*, 1927-1929; d) Atobe, M.; Yamazaki, N.; Kibayashi, C. *J. Org. Chem.* **2004,** *69*, 5595-5607; e) Liu, L.-X.; Ruan, Y.-P.; Guo, Z.-Q.; Huang, P.-Q. *J. Org. Chem.* **2004,** *69*, 6001-6009; f) Takahashi, K.; Nakano, H.; Fujita, R. *Tetrahedron Lett.* **2005,** *46*, 8927-8930; g) Garrido, N. M.; García, M.; Sánchez, M. R.; Díez, D.; Urones, J. G. *Synlett* **2010**, 387-390; h) Pansare, S. V.; Paul, E. K. *Org. Biomol. Chem.* **2012,** *10*, 2119-2125.

enantioselectivity (Scheme 6). Refluxing **12** with benzylamine resulted in nucleophilic substitution at the epoxide and the alkyl chloride to give pyrrolidinol **13**. Activation of the alcohol function group in **13** with methanesulfonyl chloride (MsCl) set the stage for the ring expansion when the acetate anion is introduced to trap the resulting bicyclic aziridinium intermediate and yield the desired acetoxy-piperidine **14**. A change of protecting group on the *N* atom from benzyl (Bn) to *tert*-butyloxycarbonyl (Boc) gave **15** whose acetate group was then cleaved under basic conditions and oxidised to the desired Boc-protected (2*S*)-phenyl-3-piperidone core **16** with an overall yield of 18% from phenylacetylene **10**.

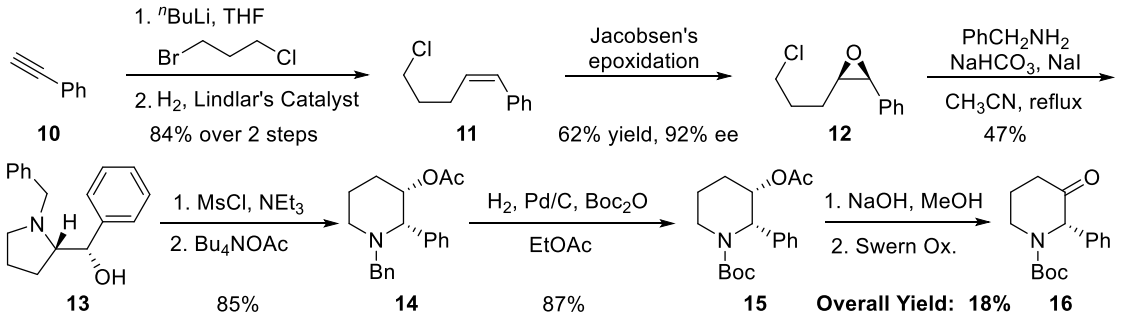

Scheme 6: Merck's synthesis of Boc-protected (2*S*)-phenyl-3-piperidone core **16**

Aggarwal's approach[109b] commenced with the tosylation of pyrrolidine **17** and an electrochemical oxidation of at 2-position to produce aminal **18** which was converted to hemiaminal **19** under acidic conditions (Scheme 7). **19** was subjected to a chiral sulfur ylide, generated from a chiral sulfonium salt **S** and a base, which then yielded chiral epoxide **20** in 94% enantiomeric excess (*ee*). Subsequent treatment with trimethylsilyl triflate (TMSOTf) afforded pyrrolidinol **21** which was then oxidized to the desired tosyl-protected (2*R*)-phenyl-3-piperidone core **22** with an overall yield of 33% from pyrrolidine **17**.

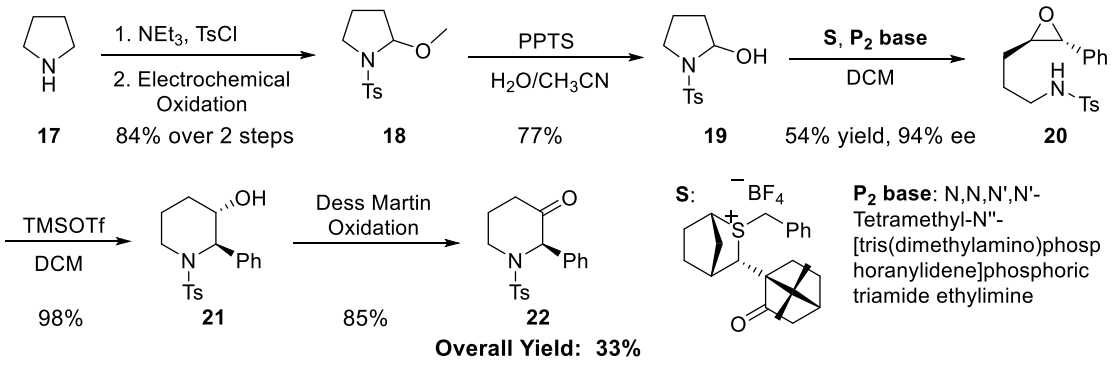

Scheme 7: Aggarwal's synthesis of tosyl-protected (2*R*)-phenyl-3-piperidone core **22**

Ollivier initiated the synthesis[109c] from phenylglycine **23** with an allylation and toyslation on the amine moiety to give phenylglycine derivative **25** (Scheme 8). **25** then underwent an intramolecular Kulinkovich cyclopropanation between the terminal alkene and the ester moiety to yield a disastereomeric mixture of azabicyclo[3.1.0]hexanols **26**. The cyclopropanol moiety then underwent a Saegusa oxidation to generate dihydropyridinone **27** which was then reduced to furnish the desired tosyl-protected (2*S*)-phenyl-3-piperidone core **28** with an overall yield of 37% from phenylglycine **23**.

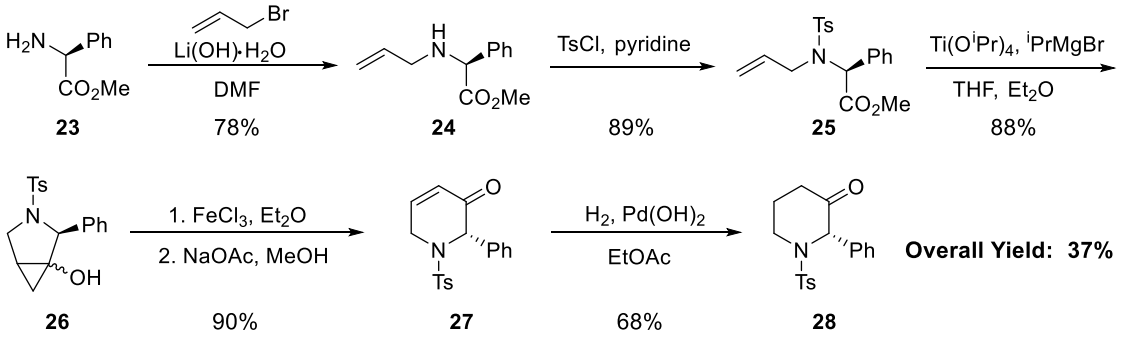

Scheme 8: Ollivier's synthesis of tosyl-protected (2*S*)-phenyl-3-piperidone core **28**

Among these syntheses, all of them require a minimum of 6 steps and lengthy silica gel chromatography purifications to arrive at the desired protected piperidone

core with less than 40% yield. Hence, it remains a challenge to develop a facile synthesis of the common piperidone core using renewable biomass derived platform chemicals, with minimal silica gel chromatography, high yield and enantioselectivity. Moreover, it has been reported that the piperidine core is the most common nitrogen heterocycle found in all the U.S. FDA approved small molecule pharmaceuticals[111] and is hence a synthetically useful scaffold for drug development.

We envisaged that the desired tosyl-protected (2*S*)-phenyl-3-piperidone core **28**, could be accessed from hemiaminal **29** by reducing the conjugated alkene as well as the hemiaminal moiety and **29** would be easily derived from an aza-achmatowicz rearrangement reaction of enantioenriched furfuryl amine **30** (Scheme 9). Construction of the stereocenter would rely on a rhodium-catalyzed asymmetric arylation methodology from furfuryl imine **31** which could be synthesized from furfural **2**.

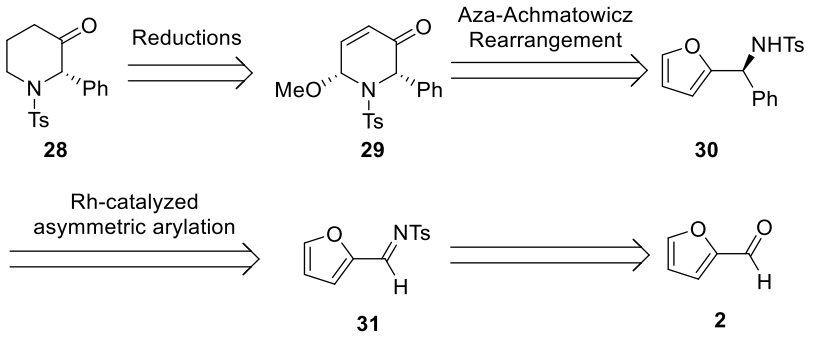

Scheme 9: Retrosynthetic analysis of tosyl-protected (2*S*)-phenyl-3-piperidone core

As previously discussed in Chapter 1, furfural **2** can be derived from biomass as a platform chemical and we seek to utilize furfural **2** directly from biomass raw material such as rice straw. Rice straw is an inevitable agricultural waste of an important staple

[111] Vitaku, E.; Smith, D. T.; Njardarson, J. T. *J. Med. Chem.* **2014,** *57*, 10257-10274.

food, rice. 500 million tons of rice is produced annually[112a] and this leads to the generation of enormous amounts of rice straw in rice producing countries in Asia such as: Philippines (11 million tons/year), Thailand (22 million tons/year), India (97 million tons/year) and China (110 million tons/year)[112b,c]. After harvesting the desired rice grains, these rice straws are left uncollected in open fields and are often burnt as a quick and cheap way to clear the fields for a new planting season, leading to serious air pollutions that are detrimental to the health of general public[25,112]. Therefore, we seek to utilize rice straw as a starting point of the synthesis towards **28** which is a common intermediate for many potent NK_1 receptor antagonists (Figure 21).

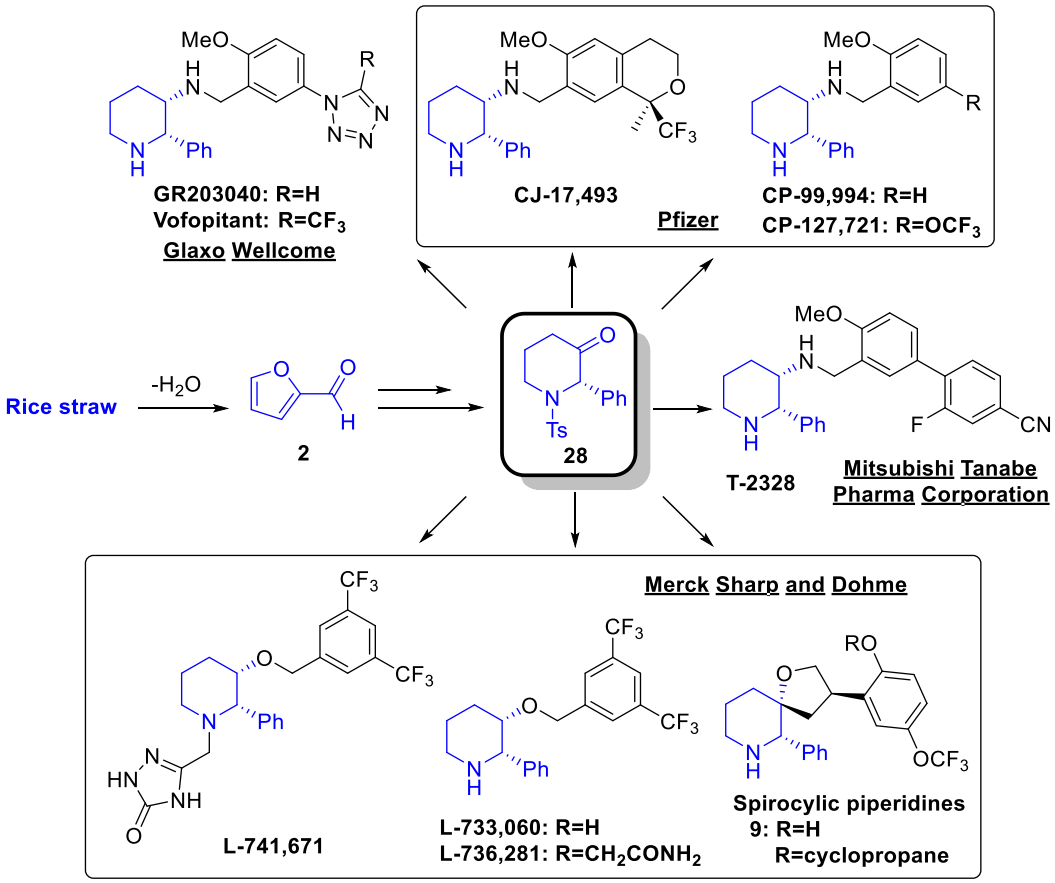

Figure 21: Rice straw as a starting material to access various NK_1 receptor antagonists

[112] a) Kadam, K. L.; Forrest, L. H.; Jacobson, W. A. *Biomass Bioenergy* **2000,** *18*, 369-389; b) Li, Q.; Hu, S.; Chen, D.; Zhu, B. *Biomass Bioenergy* **2012,** *47*, 277-288; c) Gadde, B.; Menke, C.; Wassmann, R. *Biomass Bioenergy* **2009,** *33*, 1532-1546.

2.2 Results and Discussions

2.2.1 Racemic synthesis of tosyl-protected 2-phenyl-3-piperidone ***rac*-28**

We began the conversion of rice straw to furfural **2** by modifying a previously reported procedure which employed corn cobs[113] as the raw biomass material. The rice straw was obtained directly from a rice farm in China and sun-dried as an initial step to reduce the water content present. Subsequently, the rice straw was subjected to further drying in a vacuum oven at 80 ^{o}C to remove moisture and prevent decomposition during prolonged storage. Prior to the reaction, the rice straw was cut into smaller pieces of 2-3 cm in length to increase surface area and facilitate stirring during the reaction.

Subjecting the dried and cut rice straw to acidic reflux conditions, equipped with a Dean-Stark apparatus, promoted the formation of furfural **2**. It is essential to reduce the exposure of furfural **2** to the acidic environment to minimize decompositions and this could be achieved by using biphasic systems[114] or in this case, furfural **2** would form an azeotrope with water which would distill into the Dean-Stark apparatus. The distillate containing furfural **2** and water will come into contact with a denser organic phase which would result in the partitioning of furfural **2** from the aqueous phase into the organic phase. The denser organic phase is then removed hourly from the Dean-Stark apparatus *via* a stopcock at the bottom to monitor the reaction progress. Washing the combined organic phase with aqueous solutions and removal of solvents gave crude furfural **2** in a yield of 8.1 wt% with respect to the mass of rice straw used (Scheme 10).

---

[113] Adams, R.; Voorhees, V. *Org. Synth.* **1921**, *1*, 49
[114] Amiri, H.; Karimi, K.; Roodpeyma, S. *Carbohydr. Res.* **2010,** *345*, 2133-2138.

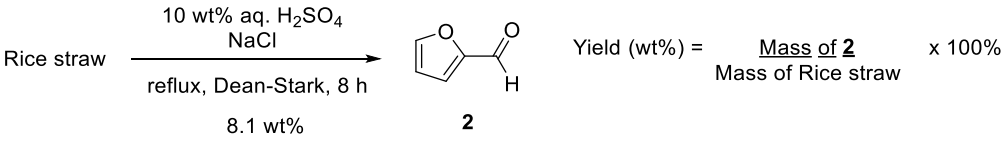

Scheme 10: Modified synthesis of furfural **2** from rice straw

The crude furfural **2** obtained was sufficiently pure and could be directly employed in the following step. Imine formation from furfural **2** under Dean-Stark conditions led to the formation of furfuryl imine **31** which could be purified *via* recrystallization with a yield of 75% (Scheme 11). In the racemic attempt, the phenyl moiety could be conveniently installed using Grignard reaction[115] which furnished furfuryl amine ***rac*-30** after recrystallization in 76% yield.

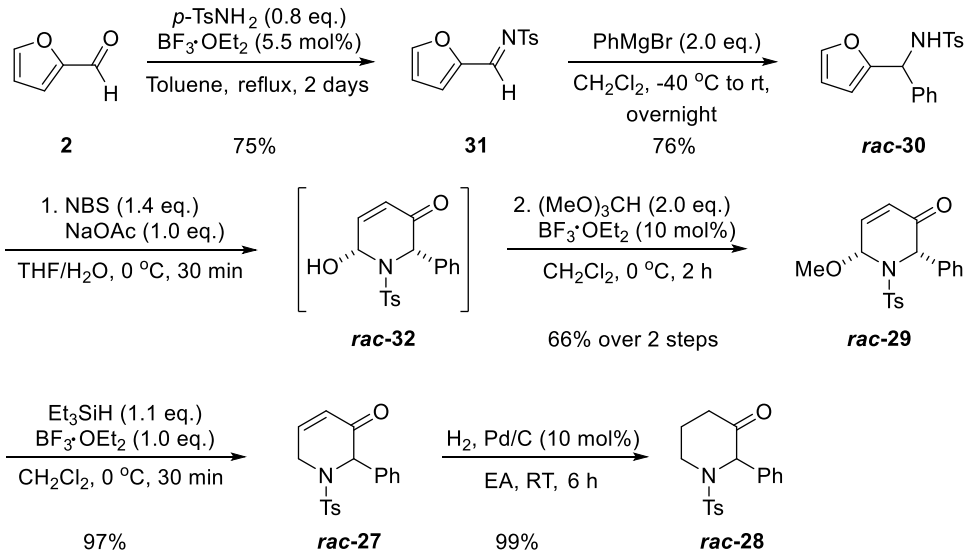

Scheme 11: Synthetic route of tosyl-protected 2-phenyl-3-piperidone ***rac*-28**

Furfuryl amine ***rac*-30** was then subjected to the aza-Achmatowicz rearrangement[91,92] reaction[116] to give hemiaminal ***rac*-32** as a single diastereomer.

[115] Grignard, V. C. R. *Acad. Sci.* **1900**, *130*, 1322.
[116] Use of Lefebvre's condition for oxidation resulted in low yield due over-oxidation of the hemiaminal product to give a diketone ***rac*-32'** (see experimental section for X-ray structure)

However, as hemiaminal ***rac*-32** was not stable to silica gel chromatography[117], isolation, characterization and determination of relative stereochemistry proved to be a challenge until we could obtain crystals directly from the crude mixture. Fortunately, we were able to obtain suitable crystals for single-crystal X-ray crystallography analysis[118] to assign the *cis* relative stereochemistry in of hemiaminal ***rac*-32** (Figure 22). Interestingly, the high diastereoselectivity of the reaction was accompanied by both the hydroxyl and phenyl substituents being oriented in a pseudoaxial manner. These observations were attributed to the anomeric effect present in the hemiaminal as well as the minimizing of $A^{1,3}$-strain[119] with the bulky tosyl protecting group.

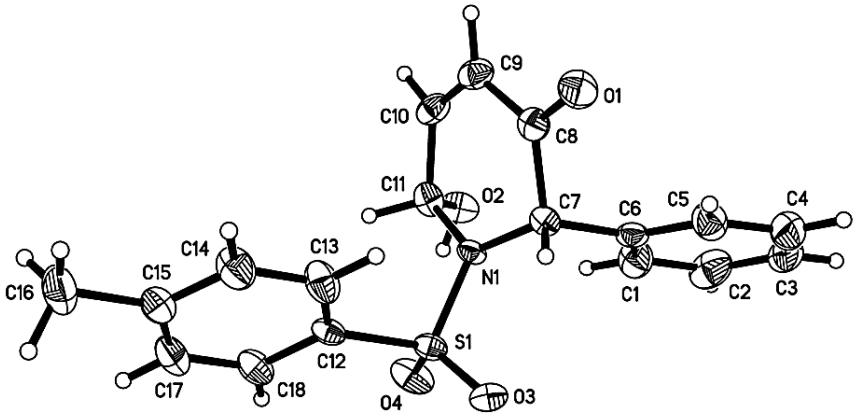

Figure 22: ORTEP drawing of hemiaminal ***rac*-32**

In view of the difficulty of isolating ***rac*-32**, subsequent attempts employed the crude mixture, containing ***rac*-32**, of the aza-Achmatowicz rearrangement reaction and converted it to the more stable aminal ***rac*-29** as a single diastereomer with 66% yield over the 2 steps. The relative stereochemistry of aminal ***rac*-29** was once again assigned unequivocally by single-crystal X-ray crystallography analysis[118] to reveal a

[117] Hodgson, R.; Kennedy, A.; Nelson, A.; Perry, A. *Synlett* **2007**, 1043.
[118] CCDC Deposition Numbers of the crystalline compounds are provided in the Experimental Section.
[119] a) Brown, J. D.; Foley, M. A.; Comins, D. L. *J. Am. Chem. Soc.* **1988,** *110*, 7445-7447; b) Yoo, S.-e.; Lee, S. H. *J. Org. Chem.* **1994,** *59*, 6968-6972.

cis pseudoaxial relationship between the methoxy and phenyl substituent (Figure 23).

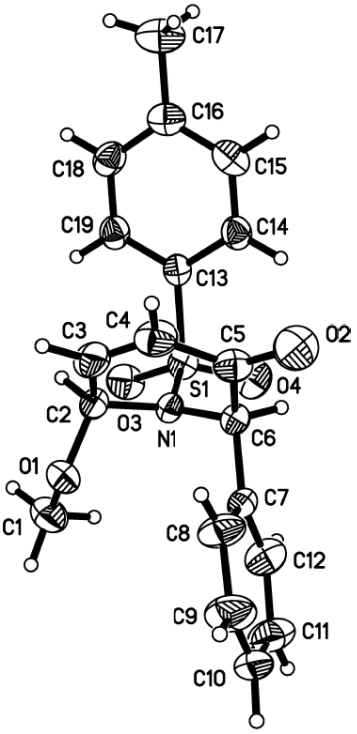

Figure 23: ORTEP drawing of aminal ***rac*-29**

Next, aminal ***rac*-29** was successfully reduced[120] to the dihydropyridinone ***rac*-27** with an excellent yield of 97% and then converted to the desired tosyl-protected 2-phenyl-3-piperidone ***rac*-28** with palladium-catalyzed hydrogenation of the alkene moiety. The hydrogenation proceeded smoothly and a simple filtration of the heterogeneous catalyst was sufficient to yield pure piperidone ***rac*-28** in an almost quantitative manner.

2.2.2 Asymmetric synthesis of tosyl-protected (2*S*)-phenyl-3-piperidone ***rac*-28**

[120] a) Kursanov, D. N.; Parnes, Z. N.; Loim, N. M. *Synthesis* **1974**, 633-651; b) Lewis, M. D.; Cha, J. K.; Kishi, Y. *J. Am. Chem. Soc.* **1982,** *104*, 4976-4978; c) Um, J. M.; Houk, K. N.; Phillips, A. J. *Org. Lett.* **2008,** *10*, 3769-3772.

Encouraged by the promising results of the racemic synthesis, we embarked on the asymmetric synthesis of enantioenriched tosyl-protected (2*S*)-phenyl-3-piperidone ***rac*-28**. Using the furfuryl imine **31** synthesized from the rice straw derived furfural, we attempted a rhodium-catalyzed asymmetric arylation methodology[121] developed by Hayashi's group[121a] to install the critical stereocenter present in the enantioenriched furfuryl amine **30**. The use of the commercially available 2,5-diphenyl -(1*R*,4*R*)-bicyclo[2.2.2]octadiene **L*** afforded the furfuryl amine **30** in 97% yield and 99% *ee* with the desired *S* absolute configuration as reported (Scheme 12). In view of the excellent efficiency of this step, there was no need for purification using silica gel chromatography and the crude product **30** from the asymmetric arylation reaction could be immediately subjected to the aza-Achmatowicz rearrangement reaction to generate the *cis* hemiaminal **32**.

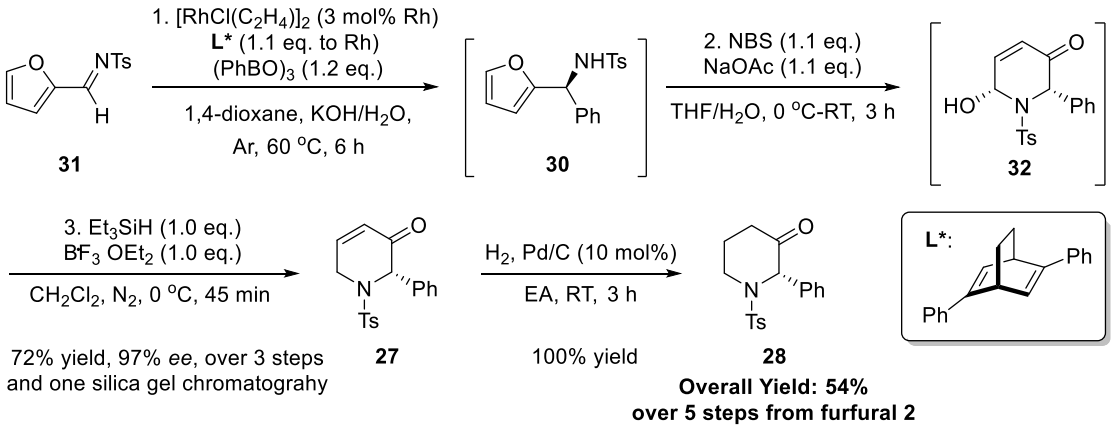

Scheme 12: Synthetic route of tosyl-protected (2*S*)-phenyl-3-piperidone **28**

Similarly, there was no need for purification of hemiaminal **32** using silica gel

[121] a) Tokunaga, N.; Otomaru, Y.; Okamoto, K.; Ueyama, K.; Shintani, R.; Hayashi, T. *J. Am. Chem. Soc*. **2004,** *126*, 13584-13585; b) Review: Tian, P.; Dong, H.-Q.; Lin, G.-Q. *ACS Catal.* **2012,** *2*, 95-119.

chromatography and the crude mixture was found to be able to undergo the Lewis acid promoted reduction directly to yield dihydropyridinone **27**, without having to go through the intermediate aminal **29**. At the end of these 3 steps and only one silica gel chromatography, dihydropyridinone **27** was obtained in 72% yield from furfuryl imine **31**. Finally, dihydropyridinone **27** was readily reduced to the desired tosyl-protected (2*S*)-phenyl-3-piperidone **28** in a quantitative manner, again without the need for silica gel chromatography.

However, a precautionary check on the enantiomeric excess of dihydropyridinone **27** revealed a slight deterioration of *ee* value to 97% *ee* and upon investigation, this was attributed to the lability of the α-hydrogen at the stereocenter which result in racemization when exposed to the inherent acidity of silica gel. This issue can be minimized by performing a quick column chromatography, using greater eluent polarity and flow rate, to reduce the exposure to silica gel and a high enantiomeric excess of 97% can be maintained.

In Ollivier's synthesis[109c], an optical rotation value of $[\alpha]^{20}_{D}$ = -145 (c = 0.3, CH_2Cl_2) for dihydropyridinone **27** was reported while in Aggarwal's synthesis[109b], the optical rotation value of the enantiomer **22** was not reported. However, the optical rotation value that we obtained was $[\alpha]^{21}_{D}$ = +123 (c = 1.32, CH_2Cl_2) for 97% *ee* which was similar in magnitude but opposite in sign to the former report. Similarly, Ollivier reported an optical rotation value of $[\alpha]^{20}_{D}$ = +5 (c = 0.2, CH_2Cl_2) for tosyl-protected **(2*S*)**-phenyl-3-piperidone **28** while the optical rotation value that we obtained was $[\alpha]^{23}_{D}$ = -10 (c = 1.01, CH_2Cl_2) for 97% *ee*. These contrasting values came as a surprise as we believed that we had the correct *S* absolute configuration of the stereocenter by employing the right enantiomer of Hayashi's chiral diene ligand.

Hence, in order to confirm the absolute configuration of the synthesized dihydropyridinone **27**, we managed to obtain suitable crystals for single-crystal X-ray crystallography analysis[118] with the sulfur atom present in the tosyl group as the heavy atom. The analysis showed that we have indeed obtained the desired *S* absolute configuration in dihydropyridinone **27** (Figure 24). In addition, we recovered the actual crystal used for X-ray analysis and analyzed it using High Performance Liquid Chromatography (HPLC) on chiral column to confirm that the time of elution is same as the major peak in the synthesized dihydropyridinone **27**. Subjecting the same batch of crystals to the same HPLC analysis yielded the same result, thereby confirming that the absolute configuration obtained from the X-ray analysis can be attributed to the major enantiomer of the synthesized dihydropyridinone **27**. By extension, the *S* absolute configuration could also be assigned to the tosyl-protected (2*S*)-phenyl-3-piperidone **28**.

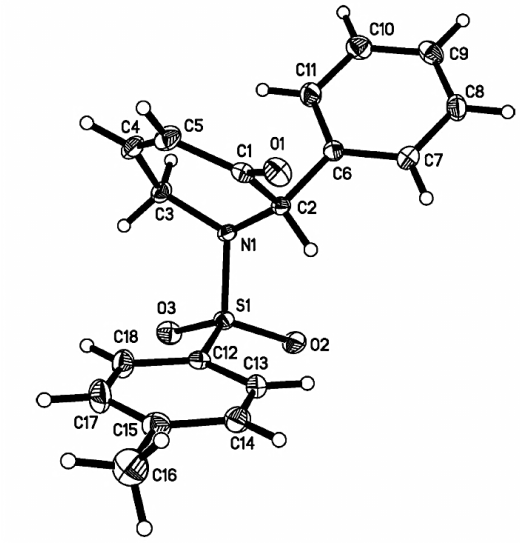

Figure 24: ORTEP drawing of enantioenriched dihydropyridinone **27**

2.2.3 Application of common intermediate for the synthesis of NK_1 receptor antagonist

The synthetic utility of the piperidone core as a common intermediate was illustrated with the synthesis of the more complex NK_1 receptor antagonist shown in Figure 21 due to the necessity to construct the spirocycle and another 2 stereocenters in **9**[122]. The formation of an allenyl alcohol ***rac*-33** was necessary as a precursor to construct the spirocycle and hence we attempted the allenylation of ***rac*-28** using a zinc-catalyzed methodology developed by Fandrick in 2011[123].

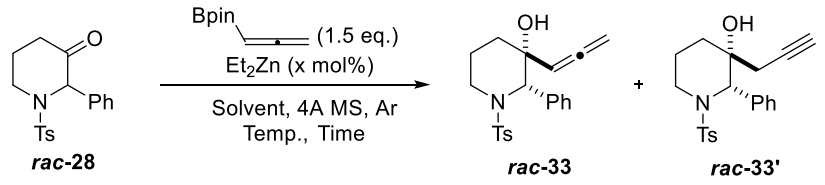

Entry	x	Solvent (Anhyd.)	Conc. (mmol/mL)	Time	Temp.	Conv.[1]	*rac*-33 : *rac*-33'[1]
1	5%	Toluene	0.045	26 h	0 °C to RT	35%	93 : 7
2	10%	Toluene	0.028	48 h	RT	35%	95 : 5
3	5%	DCM	0.125	2.5 h	0 °C	100%	19 : 81
4	5%	DCM/Tol.[2]	0.080	3 h	RT	100%	17 : 83
5	20%	THF	0.063	48 h	RT	10%	36 : 64

[1] Analyzed using ^{1}H-NMR
[2] DCM: Toluene = 1:5

Table 1: Attempts to install the allenyl moiety direct

Initial attempt following reported procedures proceeded sluggishly with low conversion due to low temperature poor substrate solubility and good allene/alkyne selectivity (Table 1, Entry 1). Increasing the reaction temperature and amount of zinc catalyst used did not aid the conversion of the reaction (Table 1, Entry 2). Switching the solvent from toluene to a more polar solvent dicholoromethane (DCM) allowed for

[122] a) Wallace, D. J.; Goodman, J. M.; Kennedy, D. J.; Davies, A. J.; Cowden, C. J.; Ashwood, M. S.; Cottrell, I. F.; Dolling, U.-H.; Reider, P. J. *Org. Lett.* **2001,** *3*, 671-674; b) Kulagowski, J. J.; Curtis, N. R.; Swain, C. J.; Williams, B. J. *Org. Lett.* **2001,** *3*, 667-670; c) Maligres, P. E.; Waters, M. M.; Lee, J.; Reamer, R. A.; Askin, D.; Ashwood, M. S.; Cameron, M. *J. Org. Chem.* **2002,** *67*, 1093-1101.
[123] Fandrick, D. R.; Saha, J.; Fandrick, K. R.; Sanyal, S.; Ogikubo, J.; Lee, H.; Roschangar, F.; Song, J. J.; Senanayake, C. H. *Org. Lett.* **2011,** *13*, 5616-5619.

complete conversion even at low temperature but poor product selectivity (Table 1, Entry 3). Using a mixture of DCM and toluene gave full conversion but poor product selectivity (Table 1, Entry 4). Employing tetrahydrofuran (THF) as the solvent also could not afford desirable results (Table 1, Entry 5).

Consequently, we decided to construct the allenyl alcohol ***rac*-33** from another approach. ***rac*-28** was treated with (trimethylsilyl)methylmagnesium bromide in a Grignard reaction to generate the crude trimethylsilyl substituted propargyl alcohol which could be deprotected under basic conditions to afford propargyl alcohol ***rac*-34** as a single diastereomer (Scheme 13). Crude propargyl alcohol ***rac*-34** underwent a Searles-Crabbé homologation[124] to give the desired allenyl alcohol ***rac*-33** with a yield of 69% over 3 steps from ***rac*-28**. Investigations into the relative stereochemistry by single-crystal X-ray crystallography analysis[118] confirmed that Grignard reaction on the desired face of ketone had taken place (Figure 25). The approach of the Grignard regent *trans* the phenyl substituent can be rationalized by the steric hindrance imposed by the bulky phenyl substituent in the pseudoaxial position.

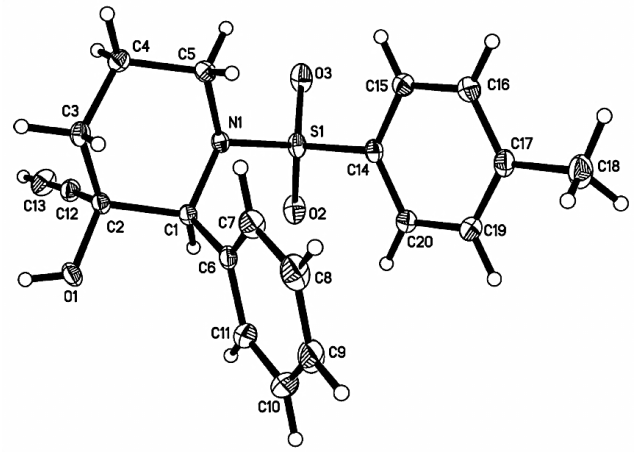

[124] a) Searles, S.; Li, Y.; Nassim, B.; Lopes, M.-T. R.; Tran, P. T.; Crabbé, P. *J. Chem. Soc., Perkin Trans. 1* **1984**, 747-751; b) Bates, R. W.; Lu, Y. *Org. Lett.* **2010,** *12*, 3938-3941; c) Luo, H.; Ma, S. *Eur. J. Org. Chem.* **2013,** *2013*, 3041-3048.

Figure 25: ORTEP drawing of propargyl alcohol ***rac*-34**

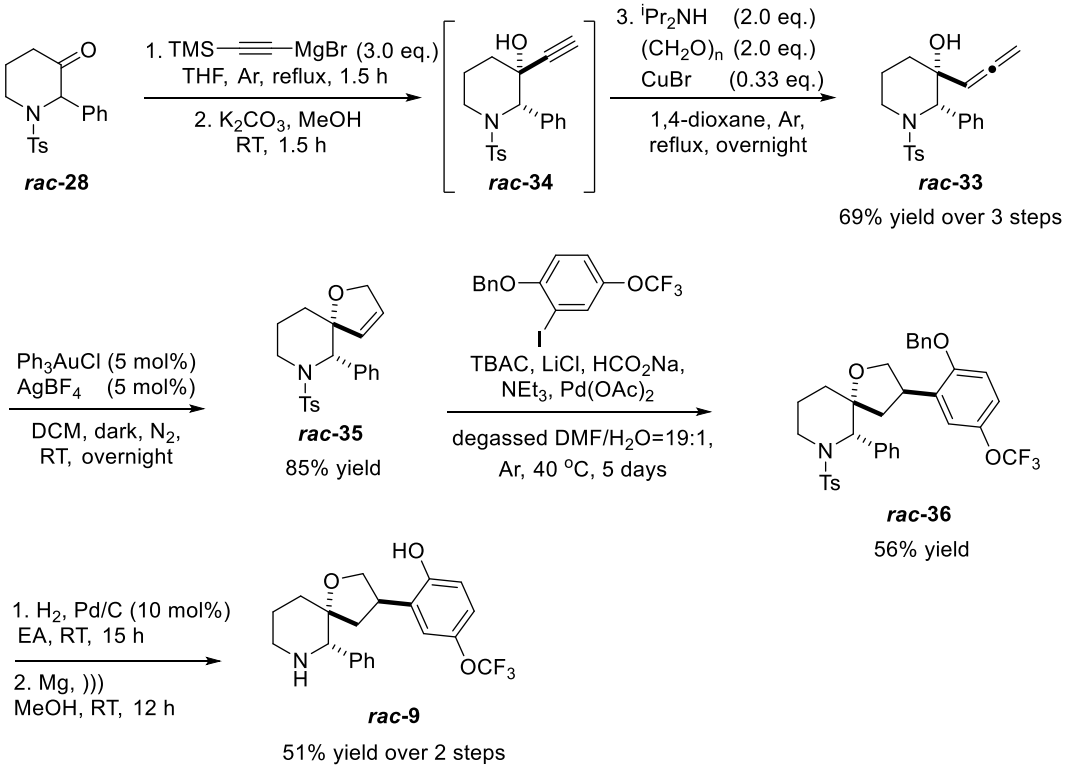

Scheme 13: Application of common intermediate for the synthesis of spirocyclic NK_1 receptor antagonist ***rac*-9**

With the allenyl alcohol ***rac*-33** in hand, the *β*-hydroxyallene moiety could undergo a gold-catalyzed cycloisomerization[125] to produce spirocyclic dihydropyran ***rac*-35** in a good yield of 85%. Analysis of spirocyclic dihydropyran ***rac*-35** using single-crystal X-ray crystallography[118] confirms the structure of the product (Figure 26). The final key step involves a regio- and stereoselective reductive Heck reaction[122b]. Due to steric considerations[126] the arylpalladium species approaches the spirocyclic dihydropyran ***rac*-35** from the less hindered face to generate the intermediate ***rac*-35'** which could be reduced by sodium formate as a hydride source to furnish ***rac*-36**

[125] Gockel, B.; Krause, N. *Org. Lett.* **2006,** *8*, 4485-4488.
[126] Heck, R. F. Palladium-Catalyzed Vinylation of Organic Halides. In *Organic Reactions*; Dauben, W. G., Ed.; John Wiley & Sons Inc: New York, 1982; Vol. 27, p 345.

(Scheme 14). Nuclear Overhauser effect (NOE) analysis confirmed the correlations between the two benzylic protons, in agreement with reported results[122b].

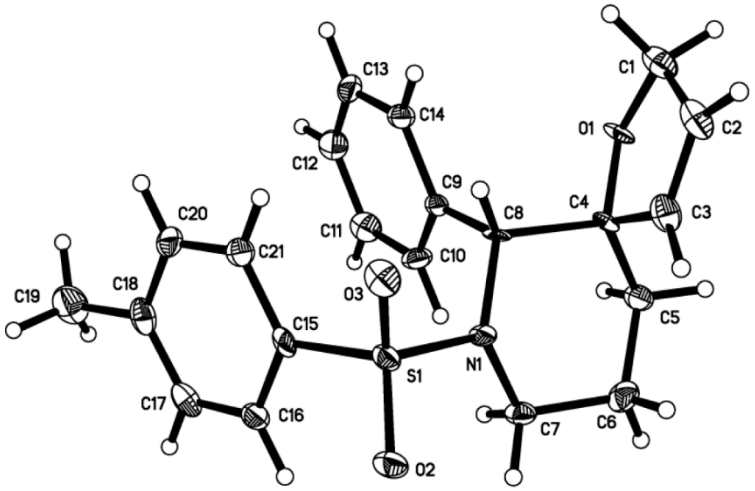

Figure 26: ORTEP drawing of spirocyclic dihydropyran ***rac*-35**

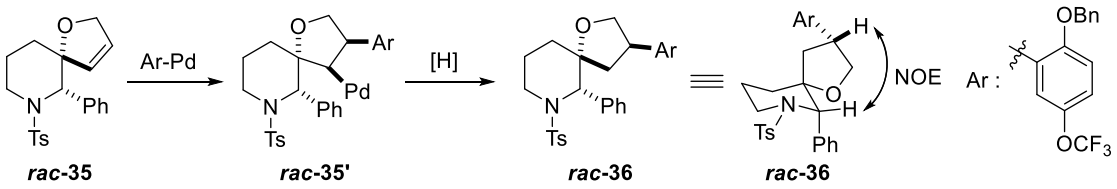

Scheme 14: Formation of ***rac*-36** *via* a reductive Heck reaction and NOE analysis

A succession of palladium-catalyzed debenzylation and magnesium promoted detosylation under sonication conditions unveiled NK_1 receptor antagonist ***rac*-9** in 51% yield over 2 steps. Interestingly, NK_1 receptor antagonist ***rac*-9** was isolated as a white solid in contrast to the yellow oil reported[122b] for the enantiopure form, and could produce suitable crystals for single-crystal X-ray crystallography analysis[118] (Figure 27). In the absence of the tosyl protecting group, the phenyl substituent is observed to occupy the pseudoequatorial position to minimize 1,3-diaxial interactions.

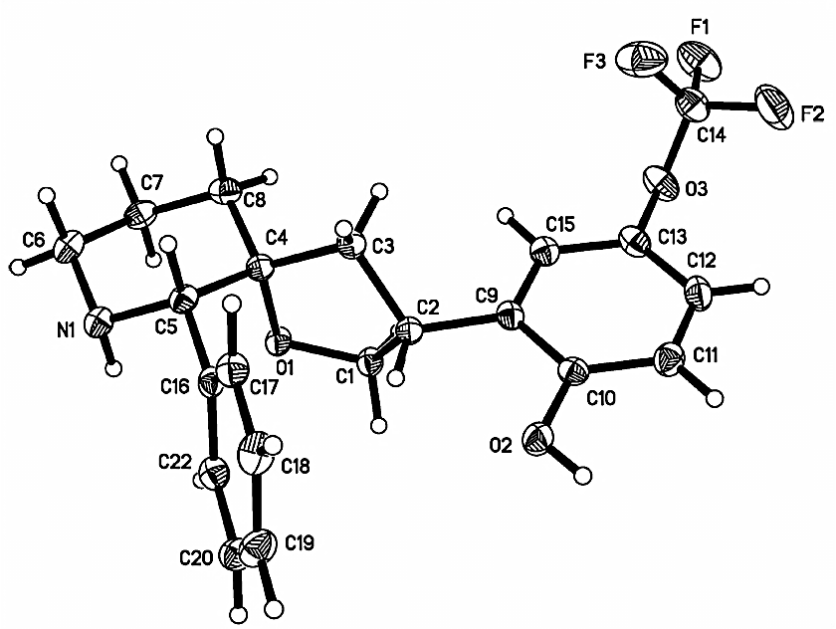

Figure 27: ORTEP drawing of NK_1 receptor antagonist ***rac*-9**

2.3 Conclusions

In conclusion, we have achieved an efficient and facile synthesis of tosyl-protected **(**2*S*)-phenyl-3-piperidone **28**, which is a common intermediate for many NK_1 receptor antagonists, in 54% overall yield and 97% *ee* over 5 steps from rice straw derived furfural **2** with only a single silica gel chromatography purification [127]. The absolute configuration of dihydropyridinone **27** was also conclusively verified to be the desired *S* configuration using single-crystal X-ray crystallography and HPLC analysis despite the disagreement of reported optical rotation values. The synthetic utility of the common intermediate was also showcased with the synthesis of a potent spirocyclic NK_1 receptor antagonist with a series of X-ray structures documenting the synthetic intermediates and the final target molecule.

[127] a) Koh, P.-F.; Wang, P.; Huang, J.-M.; Loh, T.-P. *Chem. Commun.* **2014,** *50*, 8324-8327; b) Loh, T.-P.; Wang, P.; Huang, J.-M.; Koh, P.-F. 3-Piperidone Compounds and Their Use as Neurokinin-1 (NK1) Receptor Antagonists. WO 2014/142761 A1, September 18, 2014.

2.4 Experimentals

2.4.1 General Methods

All reagents were commercially purchased and were used as received for the reactions. All reactions were carried out in oven-dried glassware while THF was freshly distilled from Na/Benzophenone ketyl and DCM was freshly distilled from Calcium Hydride. Rice straw used was collected from a rice straw farm in Jiangxi Province Fengcheng Area, China after being sun-dried. Upon receiving the rice straw, it was further dried in a vacuum oven at 80 ºC for 6 h and stored in an air-tight container. The rice straw is cut into small pieces of about 2-3 cm in length before being used for reaction. Thin-layer chromatography (TLC) was conducted with Merck 60 F254 precoated silica gel plate (0.2 mm thickness) and visualized under UV, by potassium permanganate or ceric ammonium molybdate stain. Flash chromatography was performed using Merck silica gel 60 with distilled solvents. ^{1}H-NMR spectra were performed on a Bruker Avance 300, Bruker Avance 400 or Bruker Avance 500 NMR spectrometer and are reported in ppm downfield from $SiMe_4$ (δ 0.0), relative to the signal of chloroform-d (δ = 7.26, singlet) or methanol-d_4 (δ = 3.31, quintet). Data reported as: s = singlet, d = doublet, t = triplet, q = quartet, m = multiplet, b = broad; coupling constant(s) in Hz; integration. Proton-decoupled ^{13}C-NMR spectra were recorded on Bruker Avance 300 (75 MHz) or 400 (100MHz) or 500 (125 MHz) spectrometer and are reported in ppm using solvent as an internal standard ($CDCl_3$ at 77.16 ppm, CD_3OD at 49.15 ppm). IR spectra were recorded using nujol mull technique on NaCl plates on a Shimadzu IRPrestige-21 FT-IR Spectrophotometer or under attenuated total reflection (ATR) conditions on a PerkinElmer Spectrum 100 FT-IR Spectrometer and were reported in frequency of absorption (cm^{-1}).

High-resolution mass spectral analysis (HRMS) was performed on Q-Tof Premier mass spectrometer (Waters Corporation).

2.4.2 Synthesis and characterization of compounds

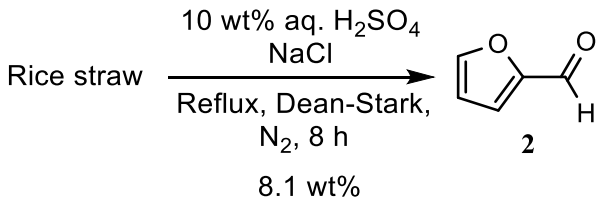

Furan-2-carbaldehyde (2)

To a 250 mL round-bottom flask equipped with a stir bar was added rice straw (10.5 g, 2-3 cm length), NaCl (14.0 g) and 10 wt% aqueous H_2SO_4 (70 mL). The round-bottom flask was then fitted with a Dean-Stark trap with a stopcock at the bottom of the trap and then fitted with water condenser. DCM (10 mL) was added into the Dean Stark trap initially and the reaction mixture was heated to reflux at 150 ^oC. After 1 h, the DCM in the Dean Stark trap was collected *via* the stopcock and fresh DCM (10 mL) was added into the Dean Stark trap through the top of the water condenser. This process was repeated hourly for a total of 8 h and the combined organic layers were washed with saturated aqueous $NaHCO_3$ solution (40 mL) and brine (10 mL) before drying over anhydrous magnesium sulphate, filtered and concentrated under reduced pressure to give **2** as a pale yellow oil (851 mg, 8.86 mmol, 8.1 wt%) ^1H NMR (500 MHz, $CDCl_3$) δ (ppm): 9.68 (s, 1H), 7.70 (t, J = 0.8 Hz, 1H), 7.26 (dd, J = 3.6 Hz, 0.5 Hz 1H), 6.61 (dd, J = 3.6 Hz, 1.7 Hz, 1H); ^{13}C NMR (100 MHz, $CDCl_3$) δ (ppm): 177.9, 152.9, 148.1, 121.2, 112.6; Other characterization data are similar to the authentic sample.

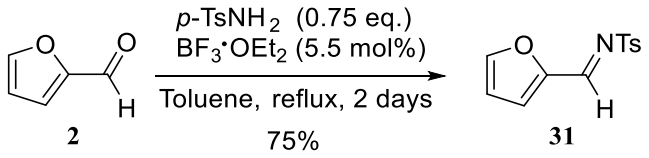

***N*-(furan-2-ylmethylene)-4-methylbenzenesulfonamide (31)**

2 (14.0 g, 146 mmol, 1.0 equiv.), 4-methylbenzenesulfonamide (18.8 g, 110 mmol, 0.75 equiv.), boron trifluoride etherate (1.0 mL, 1.15 g, 8.1 mmol, 5.5 mol%) and toluene (150 mL) were added into a round-bottom flask fitted with a Dean Stark trap. The mixture was heated at reflux for 2 days and activated charcoal was added and stirred for 1 h. The mixture was filtered and the filtrate concentrated under reduced pressure to give a brown solid. Recrystallization from benzene gave *N*-(furan-2-ylmethylene)- 4-methylbenzenesulfonamide **31** as brown crystals (20.5 g, 82.5 mmol, 75%). mp = 100-101 °C (Lit.[84e]: 100-101 °C); TLC (Hexane/Ethyl Acetate = 2:1): R_f = 0.32; ^{1}H NMR (300 MHz, $CDCl_3$) δ (ppm): 8.81 (s, 1H), 7.87 (d, *J* = 8.3 Hz, 2H), 7.74 (d, *J* = 1.6 Hz, 1H), 7.34-7.31 (m, 3H), 6.65 (dd, *J* = 3.6 Hz, 1.7 Hz, 1H), 2.43 (s, 3H); ^{13}C NMR (100 MHz, $CDCl_3$) δ (ppm): 155.7, 149.8, 149.1, 144.6, 135.2, 129.8, 128.1, 124.7, 113.7, 21.7; FTIR (Nujol, NaCl, cm^{-1}): 1607, 1315, 1155, 932; HRMS (ESI) *m/z* Calculated for $C_{12}H_{12}NO_3S$ $[M+H]^+$: 250.0538; found: 250.0541.

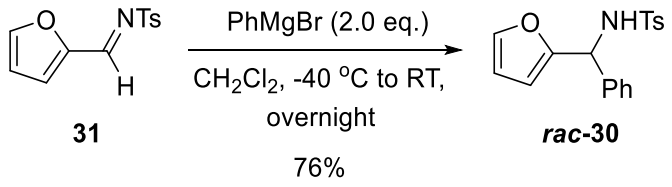

***rac*-*N*-(furan-2-yl(phenyl)methyl)-4-methylbenzenesulfonamide (*rac*-30)**

N-(furan-2-ylmethylene)-4-methylbenzenesulfonamide **31** (2.49 g, 10.0 mmol,

1.0 equiv.) was dissolved in anhydrous THF (40 mL) under N_2 protection and cooled down to -40 ºC. Phenylmagnesium bromide (20 mL of a 1.0 M THF solution, 20.0 mmol, 2.0 equiv.) was added dropwise to the mixture and stirred at -40 ºC for 6 h before allowing it to warm to room temperature. After stirring overnight, the reaction was quenched with saturated aqueous $NaHCO_3$ (40 mL) and the layers were separated. The aqueous phase was extracted with ether (3 x 40 mL) and the combined organic phases were washed with brine (40 mL), dried over anhydrous magnesium sulphate and filtered. Concentration under reduced pressure and recrystallization from Toluene/Hexane gave *rac*-*N*-(furan-2-yl(phenyl)methyl)-4-methylbenzenesulfonamide ***rac*-30** as pale brown crystals (2.50 g, 7.6 mmol, 76%). For full characterization data, refer to experimental details for **(*S*)-*N*-(furan-2-yl(phenyl)methyl)-4 -methylbenzenesulfonamide (30)** below in the asymmetric synthesis.

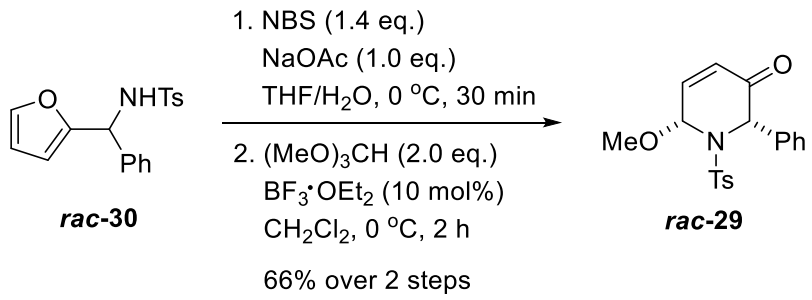

***rac*-30** **rac-29**

rac-6-hydroxy-2-phenyl-1-tosyl-1,6-dihydropyridin-3(2*H*)-one (*rac*-32)

rac-N-(furan-2-yl(phenyl)methyl)-4-methylbenzenesulfonamide ***rac*-30** (981 mg, 3.0 mmol, 1.0 equiv.) was dissolved in a mixture of THF (30 mL) and H_2O (10 mL) at 0 °C. Sodium acetate (246 mg, 3.0 mmol, 1.0 equiv.) was added before *N*-Bromosuccinimide (748 mg, 4.2 mmol, 1.4 equiv.) was slowly added in portions. The mixture was stirred for 1 h at 0 °C before saturated aqueous $Na_2S_2O_3$ solution (50 mL) was added. Ether (100 mL) was added and the layers were separated. The aqueous phase was extracted with Ether (3 x 50 mL) and the combined organic layers were washed with brine (100 mL), dried over anhydrous magnesium sulphate, filtered and concentrated under reduced pressure. The crude product is immediately subjected to the next step without any further purification.

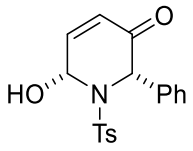

***rac*-32**

Characterization data for ***rac*-32** (recrystallized in CH_2Cl_2 from crude product as pale yellow crystals): mp = 122-123 °C (Decomposed); TLC (Hexane/Ethyl Acetate = 2:1): R_f = 0.26; ^{1}H NMR (300 MHz, $CDCl_3$) δ (ppm): 7.64 (d, *J* = 8.3 Hz, 2H), 7.56-7.53 (m, 2H), 7.33-7.24 (m, 5H), 6.86 (dd, *J* = 10.4 Hz, 4.1 Hz, 1H), 6.11 (dd, *J* = 10.4 Hz,

1.4 Hz, 1H), 5.99-5.96 (m, 1H), 5.47 (s, 1H), 3.48-3.46 (m, 1H), 2.40 (s, 3H); ^{13}C NMR (125 MHz, $CDCl_3$) δ (ppm): 191.2, 144.6, 143.7, 136.8, 136.3, 130.3, 128.8, 128.4, 127.8, 127.6, 127.0, 73.6, 64.2, 21.7; FTIR (Nujol, NaCl, cm^{-1}): 3480, 1682, 1649, 1597, 1321, 1155; HRMS (ESI) *m/z* Calculated for $C_{18}H_{18}NO_4S$ $[M+H]^+$: 344.0957; found: 344.0970.

rac-6-methoxy-2-phenyl-1-tosyl-1,6-dihydropyridin-3(2*H*)-one (_rac_-29)

The crude rearrangement product was dissolved in anhydrous CH_2Cl_2 (60 mL) and cooled down to 0 ºC under N_2 protection. Trimethyl orthoformate (0.65 mL, 0.656 g, 6.0 mmol, 2.0 equiv.) was added followed by boron trifluoride etherate (37 μL, 43 mg, 0.3 mmol, 10 mol%). The reaction was stirred at 0 ºC for 2 h before being quenched with saturated aqueous $NaHCO_3$ solution (30 mL). The layers were separated and the aqueous phase extracted with CH_2Cl_2 (3 x 30 mL). The combined organic layers were washed with brine (50 mL), dried over anhydrous magnesium sulphate and filtered. Concentration under reduced pressure and purification using silica gel chromatography (Eluent: Hexane/THF = 4:1) gave 6-methoxy-2-phenyl-1-tosyl-1,6-dihydropyridin-3(2H)-one ***rac*-29** as a white solid (710 mg, 1.99 mmol, 66% over 2 steps). mp = 117-118 ºC; TLC (Hexane/Ethyl Acetate = 2:1): R_f = 0.43; ^{1}H-NMR (500 MHz, $CDCl_3$) δ (ppm): 7.61 (d, *J* = 8.3 Hz, 2H), 7.36 (d, *J* = 7.2 Hz, 2H), 7.31-7.25 (m, 5H), 6.83 (dd, *J* = 10.3 Hz, 4.5 Hz, 1H), 6.02 (dd, *J* = 10.4 Hz, 1H), 5.59 (dd, *J* = 4.4 Hz, 1H), 5.49 (s, 1H), 3.25 (s, 3H), 2.40 (s, 3H); ^{13}C-NMR (125 MHz, $CDCl_3$) δ (ppm): 192.8, 144.4, 143.1, 137.0, 136.3, 130.2, 128.5, 128.2, 128.2, 127.9, 127.1, 80.9, 63.3, 56.0, 21.7; FTIR (Nujol, NaCl, cm^{-1}): 1694, 1632, 1348, 1165, 1125, 754, 710, 602, 542, 496; HRMS (ESI) *m/z* Calculated for $C_{19}H_{20}NO_4S$ $[M+H]^+$: 358.1113; found: 358.1112.

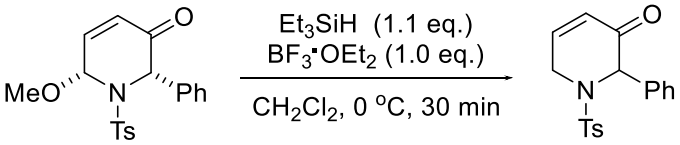

***rac*-29** 97% ***rac*-27**

rac-2-phenyl-1-tosyl-1,2-dihydropyridin-3(6*H*)-one (_rac_-27)

rac-6-methoxy-2-phenyl-1-tosyl-1,6-dihydropyridin-3(2H)-one ***rac*-29** (250 mg, 0.70 mmol, 1.0 equiv.) and triethylsilane (123 μL, 89 mg, 0.77, 1.1 equiv.) were dissolved in anhydrous CH_2Cl_2 (7.5 mL) and cooled down to 0 °C. Boron trifluoride etherate (86 μL, 100 mg, 0.70 mmol, 1.0 equiv.) was added to the mixture and the reaction was stirred for 30 min before being quenched by addition of saturated aqueous $NaHCO_3$ solution (10 mL) and CH_2Cl_2 (5 mL). The layers were separated and the aqueous phase extracted with CH_2Cl_2 (3 x 10 mL). The combined organic layers were washed with brine (15 mL), dried over anhydrous magnesium sulphate and filtered. Concentration under reduced pressure gave *rac*-2-phenyl-1-tosyl-1,2-dihydropyridin-3(6*H*)-one ***rac*-27** as a brown solid (223 mg, 0.69 mmol, 97%). For full characterization data, refer to experimental details for **(*S*)-2-phenyl-1-tosyl-1,6-dihydropyridin-3(2*H*)-one (27)** below in the asymmetric synthesis.

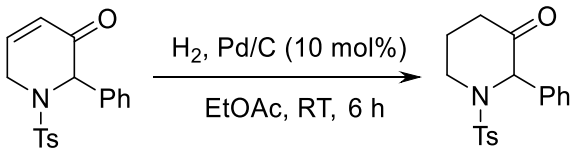

***rac*-27** 99% ***rac*-28**

rac-2-phenyl-1-tosylpiperidin-3-one (_rac_-28)

rac-2-phenyl-1-tosyl-1,2-dihydropyridin-3(6H)-one ***rac*-27** (160 mg, 0.49 mmol, 1.0 equiv.) was dissolved in EtOAc (10 mL) and palladium on activated charcoal (10 wt%, 53 mg, 0.05 mmol, 10 mol%) was added. The round bottom flask was evacuated and refilled with H_2 thrice before H_2 (1 atm) was allowed to bubble through the solution. The reaction was stirred overnight before being filtered through a pad of celite. Concentration under reduced pressure gave *rac*-2-phenyl-1-tosylpiperidin-3-one ***rac*-28** as a pale yellow solid (159 mg, 0.48 mmol, 99%). For full characterization data, refer to experimental details for **(*S*)-2-phenyl-1-tosylpiperidin-3-one (28)** below in the asymmetric synthesis.

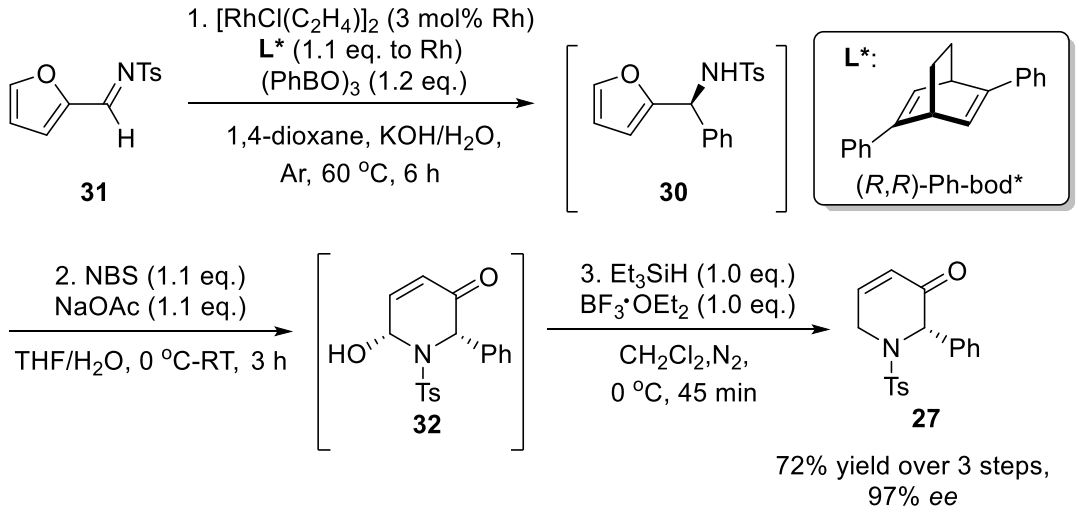

(*S*)-*N*-(furan-2-yl(phenyl)methyl)-4-methylbenzenesulfonamide (30)

To the solution of $[RhCl(C_2H_4)_2)]_2$ (5.8 mg, 0.015 mmol, 3 mol% Rh) and (*R*,*R*)-Ph-bod* (8.5 mg, 0.033 mmol, 1.1 equiv. to Rh) in anhydrous 1,4-dioxane (2.5 mL) was added aqueous KOH (65.0 μL, 3.1 M, 20 mol% KOH, H_2O: 1 equiv. to boron) at room temperature and stirred for 15 min. This solution containing the catalyst was added to the solution of imine **31** (249 mg, 1.0 mmol, 1.0 equiv.) and 2,4,6-triphenylboroxine (374 mg, 1.2 mmol, 1.2 equiv.) in anhydrous 1,4-dioxane (4.0 mL) at the same temperature. After 6 h stirring at 60 °C, the mixture was passed through a short silica gel column (pre-treated with methanol, eluent: ethyl acetate) to give **30** as the crude product and was immediately subjected to the next step without any further purification.

Characterization data for **30** after purification using silica gel chromatography (Eluent: Hexane/Ethyl Acetate = 5:1) to give (*S*)-*N*-(furan-2-yl(phenyl)methyl)-4-methyl-benzenesulfonamide **30** as a pale yellow solid in 97% yield, *ee* = 99%. The *ee* was determined on Chiralcel OD-H column with hexane/2-propanol = 90:10, flow = 0.5 mL/min, wavelength = 220 nm. Retention times: 20.5 min [(*S*)-enantiomer],

22.0 min [(*R*)-enantiomer]. mp = 129-130 ºC; TLC (Hexane/Ethyl Acetate = 2:1): R_f = 0.53; $[\alpha]^{22}_D$ = -18.1 (c = 1.03, $CHCl_3$) for 99% *ee* (Lit.[121a]: $[\alpha]^{20}_D$ = -21.6 (c = 1.03, $CHCl_3$) for 99% *ee*.); ^{1}H NMR (300 MHz, $CDCl_3$) δ (ppm): 7.58 (d, *J* = 8.3 Hz, 2H), 7.26-7.22 (m, 4H), 7.19-7.14 (m, 4H), 6.19 (dd, *J* = 3.2 Hz, 1.9 Hz, 1H), 5.99 (d, *J* = 3.2 Hz, 1H), 5.61 (d, *J* = 7.7 Hz, 1H), 5.23 (d, *J* = 7.6 Hz, 1H), 2.38 (s, 3H); ^{13}C NMR (125 MHz, $CDCl_3$) δ (ppm): 152.3, 143.3, 142.7, 138.4, 137.5, 129.5, 128.7, 128.1, 127.3, 127.2, 110.3, 108.5, 55.6, 21.6; FTIR (Nujol, NaCl, cm^{-1}): 3265, 1597, 1319, 1159, 928; HRMS (ESI) *m/z* Calculated for $C_{18}H_{18}NO_3S$ $[M+H]^+$: 328.1007; found: 328.0992.

Crude **30** from the previous step was dissolved in a mixture of THF (10.0 mL) and H_2O (3.3 mL) at 0 ºC. Sodium acetate (90 mg, 1.1 mmol, 1.1 equiv.) was added before *N*-bromosuccinimide (196 mg, 1.1 mmol, 1.1 equiv.) was slowly added in portions at 0 ºC over 15 min. The mixture was stirred for 3 h at room temperature after the addition of *N*-bromosuccinimide before solid $Na_2S_2O_3$ and brine (7 mL) was added. The mixture was extracted with ethyl acetate (3 x 20 mL) and the combined organic layers were washed with brine (25 mL), dried over anhydrous magnesium sulphate, filtered and concentrated under reduced pressure to give **32** as the crude product and **32** was immediately subjected to the next step without any further purification.

***(S)*-2-phenyl-1-tosyl-1,6-dihydropyridin-3(2*H*)-one (27)**

The crude rearrangement product **32** was dissolved in anhydrous CH_2Cl_2 (9.0 mL) and cooled down to 0 ºC under N_2 protection. Triethylsilane (159 μL, 116 mg, 1.0 mmol, 1.0 equiv.) was added followed by boron trifluoride etherate (123 μL, 142 mg, 1.0 mmol, 1.0 equiv.) and the mixture was allowed to stirred at 0 ºC for 45 min before H_2O (10 mL) was added to quench the reaction. The mixture was extracted with

CH_2Cl_2 (3 x 20 mL). The combined organic layers were washed with brine (25 mL), dried over anhydrous magnesium sulphate and filtered. Concentration under reduced pressure and purification using silica gel chromatography (Eluent: Hexane/Ethyl acetate = 4:1) gave (*S*)-2-phenyl-1-tosyl-1,6-dihydropyridin-3(2*H*)-one **27** as a brown solid (234 mg, 0.72 mmol, 72% over 3 steps), *ee* = 97%. The *ee* was determined on Chiralcel OD-H column with hexane/2-propanol = 90:10, flow = 0.5 mL/min, wavelength = 220 nm. Retention times: 29.7 min [(*R*)-enantiomer], 34.0 min [(*S*)-enantiomer]. mp = 131-132 ºC (Lit.[109c]: yellow oil); TLC (Hexane/Ethyl Acetate = 2:1): R_f = 0.42; $[\alpha]^{21}_D$ = +123 (c = 1.32, CH_2Cl_2) for 97% *ee*. (Lit.[109c]: $[\alpha]^{20}_D$ = -145 (c = 0.3, CH_2Cl_2); ^{1}H NMR (500 MHz, $CDCl_3$) δ (ppm): 7.62 (d, *J* = 8.3 Hz, 2H), 7.35-7.29 (m, 5H), 7.25 (d, *J* = 8.0 Hz, 2H), 6.69 (ddd, *J* = 10.4 Hz, 4.9 Hz, 1.9 Hz, 1H), 5.94 (ddd, *J* = 10.4 Hz, 2.4 Hz, 1.6 Hz, 1H), 5.62 (s, 1H), 4.46 (ddd, *J* = 20.9 Hz, 4.8 Hz, 1.4 Hz, 1H), 3.84 (dt, *J* = 20.9 Hz, 2.4 Hz, 1.6 Hz, 1H), 2.40 (s, 3H); ^{13}C NMR (125 MHz, $CDCl_3$) δ (ppm): 192.3, 144.6, 144.2, 136.5, 133.2, 130.1, 129.1, 128.7, 127.8, 127.2, 127.0, 64.1, 41.8, 21.7; FTIR (Nujol, NaCl, cm^{-1}): 1688, 1628, 1597, 1341, 1159; HRMS (ESI) *m/z* Calculated for $C_{18}H_{18}NO_3S$ $[M+H]^+$: 328.1007; found: 328.1020.

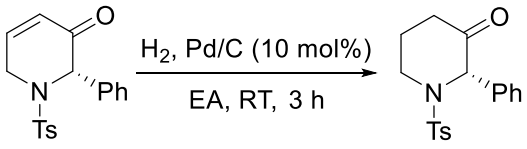

27 100% **28**

(*S*)-2-phenyl-1-tosylpiperidin-3-one (28)

(*S*)-2-phenyl-1-tosyl-1,6-dihydropyridin-3(2H)-one **28** (151 mg, 0.462 mmol, 1.0 equiv.) was dissolved in ethyl acetate (10 mL) and palladium on activated charcoal (10 wt%, 49 mg, 0.046 mmol, 10 mol%) was added. The round bottom flask was evacuated and refilled with H_2 thrice using a H_2 balloon. The reaction was stirred for 3 h at room temperature before being filtered through a pad of celite. Concentration under reduced pressure gave (*S*)-2-phenyl-1-tosylpiperidin-3-one **28** as a pale yellow solid (152 mg, 0.462 mmol, 100%), *ee* = 97%. The *ee* was determined on Chiralcel OD-H column with hexane/2-propanol = 90:10, flow = 0.5 mL/min, wavelength = 220 nm. Retention times: 19.7 min [(*R*)-enantiomer], 23.0 min [(*S*)-enantiomer]. mp = 152-153 °C (Lit.[109c]: deliquescent solid, Lit.[109b]: 152-154 °C); TLC (Hexane/Ethyl Acetate = 2:1): R_f = 0.50; $[\alpha]^{23}_D$ = -10.0 (c = 1.01, CH_2Cl_2) for 97% *ee* (Lit.[109b]: $[\alpha]^{20}_D$ = +5 (c = 0.2, CH_2Cl_2)); ^{1}H NMR (300 MHz, $CDCl_3$) δ (ppm): 7.71 (d, *J* = 8.3 Hz, 2H), 7.36-7.26 (m, 7H), 5.57 (s, 1H), 3.86 (dt, *J* = 14.0 Hz, 5.0 Hz, 1H), 3.44 (ddd, *J* = 14.0 Hz, 9.6 Hz, 4.3 Hz, 1H), 2.43 (s, 3H), 2.40-2.31 (m, 1H), 2.17 (dt, *J* = 16.0 Hz, 5.3 Hz, 1H), 1.79-1.61 (m, 2H); ^{13}C NMR (125 MHz, $CDCl_3$) δ (ppm): 204.6, 144.0, 137.3, 134.0, 130.1, 129.3, 128.3, 127.2, 125.9, 66.9, 41.3, 36.9, 23.6, 21.7; FTIR (Nujol, NaCl, cm^{-1}): 1721, 1595, 1342, 1157; HRMS (ESI) *m/z* Calculated for $C_{18}H_{20}NO_3S$ $[M+H]^+$: 330.1164; found: 330.1166.

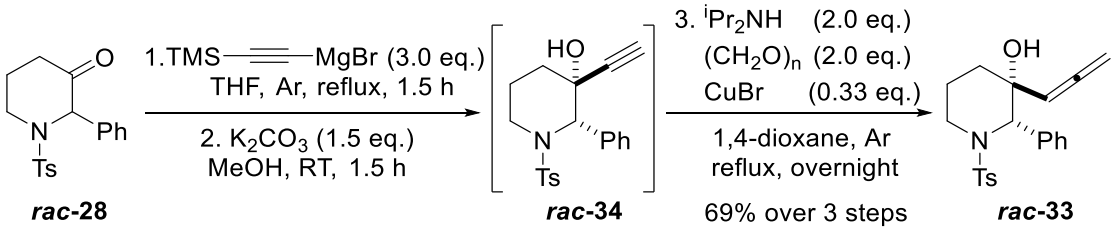

***rac*-3-ethynyl-2-phenyl-1-tosylpiperidin-3-ol (*rac*-34)**

An oven-dried 50 mL two-neck round bottom flask equipped with a stir bar and a reflux condenser was cooled under vacuum and back-filled with Ar thrice before being charged with methylmagnesium bromide (2.0 mL of a 3.0 M solution in ether, 6.0 mmol, 3.0 equiv.), anhydrous THF (2.7 mL) and trimethylsilylacetylene (1.3 mL, 882 mg, 9.0 mmol, 4.5 equiv.). The mixture was heated at reflux for 1.5 h before ***rac*-28** (658 mg, 2.0 mmol, 1.0 equiv.) in anhydrous THF (16.0 mL) was added and the mixture was allowed to stir at reflux for 1.5 h before saturated aqueous NH_4Cl solution (10 mL) was added to quench the reaction. The layers were separated and the aqueous phase extracted with ethyl acetate (3 x 15 mL). The combined organic extracts were washed with saturated aqueous $NaHCO_3$ solution (30 mL), brine (30 mL), dried over anhydrous magnesium sulphate and filtered. Concentration under reduced pressure gave the crude product which was used immediately in the next step without further purification.

The crude product from the Grignard reaction was dissolved in MeOH (20 mL) and solid K_2CO_3 (414 mg, 3.0 mmol, 1.5 equiv.) was added and the mixture was allowed to stir at room temperature for 1.5 h. The solvent was removed under reduced pressure and saturated aqueous NH_4Cl solution (10 mL) and EA (20 mL) were added and the layers were separated. The aqueous phase was extracted with ethyl acetate (3 x 10 mL). The combined organic extracts were washed with saturated aqueous $NaHCO_3$ solution

(20 mL), brine (20 mL), dried over anhydrous magnesium sulphate and filtered. Concentration under reduced pressure gave ***rac*-34** as the crude product which was used immediately in the next step without further purification.

Characterization data for ***rac*-34** after purification using silica gel chromatography (Eluent: Hexane/Ethyl Acetate = 2:1) to give *rac*-3-ethynyl-2-phenyl-1-tosylpiperidin -3-ol ***rac*-34** as a white solid. mp = 169-170 °C; TLC (Hexane/Ethyl Acetate = 2:1): R_f = 0.34; ^{1}H NMR (300 MHz, $CDCl_3$) δ (ppm): 7.41 (d, *J* = 8.3 Hz, 2H), 7.34-7.32 (m, 2H), 7.26-7.22 (m, 3H), 7.06 (d, *J* = 8.1 Hz, 2H), 5.31 (s, 1H), 3.82 (dd, *J* = 13.8 Hz, 4.1 Hz, 1H), 3.39-3.29 (m, 1H), 2.53 (s, 1H), 2.34 (s, 3H), 2.02-1.98 (m, 2H), 1.94 (s, 1H), 1.87-1.83 (m, 2H); ^{13}C NMR (75 MHz, $CDCl_3$) δ (ppm): 143.0, 136.9, 136.2, 129.7, 129.2, 128.4, 128.3, 127.4, 86.1, 73.6, 69.0, 65.6, 41.2, 32.5, 22.0, 21.6; FTIR (ATR, cm^{-1}): 3469, 3297, 3067, 3032, 1597, 1324, 1161; HRMS (ESI) *m/z* Calculated for $C_{20}H_{22}NO_3S$ $[M+H]^+$: 356.1320; found: 356.1311.

***rac*-2-phenyl-3-(propa-1,2-dien-1-yl)-1-tosylpiperidin-3-ol (*rac*-33)**

Isopropylamine (560 μL, 404 mg, 4.0 mmol, 2.0 equiv.) was added to a suspension of crude ***rac*-34**, paraformaldehyde (120 mg, 4.0 mmol, 2.0 equiv.) and CuBr (95 mg, 0.67 mg, 33 mol%) in anhydrous 1,4-dioxane (16.0 mL). The reaction was refluxed overnight and then cooled to room temperature before being filtered through a pad of celite. Concentration under reduced pressure and purification using silica gel chromatography (Eluent: Hexane/Ethyl Acetate = 5:1) gave *rac*-2-phenyl-3-(propa-1,2-dien-1-yl)-1-tosylpiperidin-3-ol ***rac*-33** as a yellow solid (510 mg, 1.38 mmol, 69%) over 3 steps. mp = 96-97 °C; TLC (Hexane/Ethyl Acetate = 2:1): R_f = 0.38; ^{1}H NMR (400 MHz, $CDCl_3$) δ (ppm): 7.30 (d, *J* = 8.2 Hz, 2H), 7.25-7.16 (m, 5H), 7.02 (d, *J* = 8.0 Hz, 2H), 5.52 (t, *J* = 6.7 Hz, 1H), 5.01 (s, 1H), 4.99-4.92 (m, 2H), 3.80 (dd, *J* =

13.1 Hz, 4.5 Hz, 1H), 3.38 (td, *J* = 12.1 Hz, 4.3 Hz, 1H), 2.32 (s, 3H), 1.97-1.91 (m, 2H), 1.82-1.79 (m, 1H), 1.73-1.67 (m, 1H), 1.63 (s, 1H); ^{13}C NMR (100 MHz, $CDCl_3$) δ (ppm): 206.7, 142.8, 136.8, 129.7, 129.2, 128.2 x 2, 128.0, 127.2, 98.1, 80.1, 71.3, 65.6, 41.2, 32.1, 21.5 x 2; FTIR (Nujol, NaCl, cm^{-1}): 3532, 1960, 1597, 1329, 1153; HRMS (ESI) *m/z* Calculated for $C_{21}H_{24}NO_3S$ $[M+H]^+$: 370.1477; found: 370.1461.

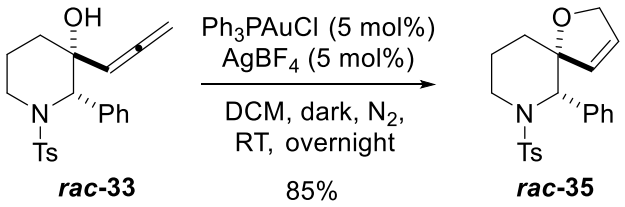

rac-6-phenyl-7-tosyl-1-oxa-7-azaspiro[4.5]dec-3-ene (_rac_-35)

α-Allenic alcohol ***rac*-33** (200 mg, 0.54 mmol, 1.0 equiv.), chloro(triphenylphosphine)gold (I) (13 mg, 0.027 mmol, 5 mol%) and silver tetrafluoroborate (5 mg, 0.027 mmol, 5 mol%) were dissolved in anhydrous CH_2Cl_2 (2.0 mL) under N_2 and in the dark. The mixture was allowed to stir at room temperature in the dark overnight. The mixture was then filtered through a pad of celite and concentrated under reduced pressure. Purification using silica gel chromatography (Eluent: Hexane/Ethyl Acetate = 7:1) gave *rac*-6-phenyl-7-tosyl-1-oxa-7-azaspiro[4.5]dec-3-ene ***rac*-35** as a pale yellow solid (170 mg, 0.46 mmol, 85%). mp = 105-106 ºC; TLC (Hexane/Ethyl Acetate = 2:1): R_f = 0.60; ^{1}H NMR (300 MHz, $CDCl_3$) δ (ppm): 7.39 (d, *J* = 8.3 Hz, 2H), 7.26-7.24 (m, 2H), 7.17-7.13 (m, 3H), 7.07 (d, *J* = 8.1 Hz, 2H), 6.07 (dt, *J* = 6.7 Hz, 2.5 Hz, 1H), 5.87 (d, *J* = 6.2 Hz, 1H), 4.96 (s, 1H), 4.55 (dt, *J* = 13.2 Hz, 2.0 Hz, 1H), 4.29 (dd, *J* = 13.1 Hz, 2.0 Hz, 1H), 3.87-3.81 (m, 1H), 3.35 (ddd, *J* = 13.2 Hz, 11.1 Hz, 5.1 Hz, 1H), 2.35 (s, 3H), 1.95-1.82 (m, 3H), 1.70-1.65 (m, 1H); ^{13}C NMR (100 MHz, $CDCl_3$) δ (ppm): 142.8, 137.8, 137.5, 132.1,

129.3, 129.3, 127.7, 127.6, 127.2 x 2, 90.4, 75.4, 64.7, 41.3, 30.9, 22.5, 21.6; FTIR (Nujol, NaCl, cm^{-1}): 1651, 1599, 1331, 1171; HRMS (ESI) *m/z* Calculated for $C_{21}H_{24}NO_3S$ $[M+H]^+$: 370.1477; found: 370.1480.

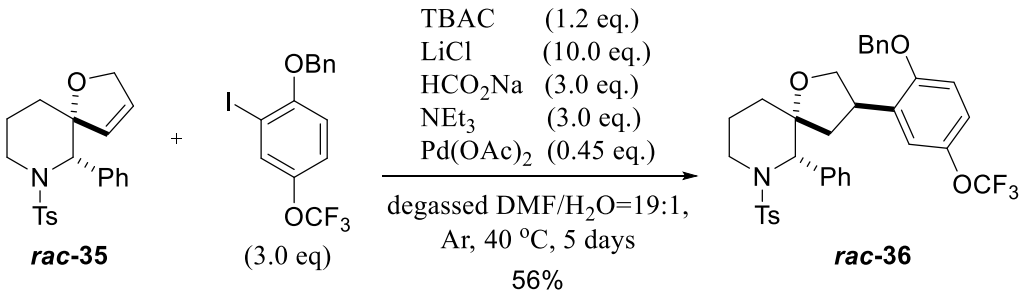

***rac*-3-(2-(benzyloxy)-5-(trifluoromethoxy)phenyl)-6-phenyl-7-tosyl-1-oxa-7-azaspiro[4.5]decane (*rac*-35)**

An oven-dried 10 mL Schlenk tube equipped with a stir bar was charged with spirocycle ***rac*-35** (243 mg, 0.66 mmol, 1.0 equiv.), 1-(benzyloxy)-2-iodo-4-(trifluoromethoxy)benzene (779 mg, 1.98 mmol, 1.98 mmol, 3.0 equiv.), tetrabutylammonium chloride (220 mg, 0.79 mmol, 1.2 equiv.), lithium chloride (279 mg, 6.6 mmol, 10.0 equiv.), sodium formate (134 mg, 1.98 mmol, 3.0 equiv.), triethylamine (275 μL, 200 mg, 1.98 mmol, 3.0 equiv.) and a solution of DMF/H_2O = 19:1 (2.5 mL) under Ar. The mixture was degassed in liquid N_2, allowed to warm to room temperature and backfilled with Ar. The degassing procedure was repeated thrice before palladium (II) acetate (66 mg, 0.30 mmol, 0.45 equiv.) was added and the mixture was degassed again before being heated to 40 °C and stirred for 5 days under Ar. The mixture was filtered through a pad of celite, concentrated under reduced pressure and purified using silica gel chromatography (Eluent: Hexane/Ethyl Acetate = 10:1 to 6:1) to give *rac*-3-(2-(benzyloxy)-5-(trifluoromethoxy)phenyl)-6-phenyl-7-tosyl-1-oxa-7-azaspiro[4.5]decane ***rac*-35** as a pale brown oil (235 mg, 0.37 mmol,

56%). TLC (Hexane/Ethyl Acetate = 2:1): R_f = 0.68; ^{1}H NMR (300 MHz, $CDCl_3$) δ (ppm): 7.45-7.35 (m, 5H), 7.28-7.21 (m, 4H), 7.18-7.12 (m, 4H), 7.05 (d, *J* = 9.2 Hz, 1H), 6.97 (d, *J* = 8.1 Hz, 2H), 6.89 (d, *J* = 8.9 Hz, 1H), 5.13 (d, *J* = 11.8 Hz, 1H), 5.08 (d, *J* = 11.9 Hz, 1H), 5.02 (s, 1H), 4.20 (t, *J* = 7.7 Hz, 1H), 3.98-3.87 (m, 1H), 3.81-3.76 (m, 2H), 3.18 (dt, *J* = 12.2 Hz, 4.5 Hz, 1H), 2.74 (dd, *J* = 12.6 Hz, 7.7 Hz, 1H), 2.29 (s, 3H), 2.07-2.00 (m, 2H), 1.84-1.81 (m, 2H), 1.60-1.55 (m, 1H); ^{13}C NMR (125 MHz, $CDCl_3$) δ (ppm): 155.2, 142.9, 142.7, 137.7, 136.7, 136.6, 131.9, 129.5, 129.1, 128.9, 128.3, 128.0, 127.5, 127.4, 127.1, 121.0, 120.7 (q, *J* = 254.6 Hz), 120.2, 112.6, 83.6, 72.4, 70.8, 64.2, 43.0, 41.5, 39.1, 31.6, 23.4, 21.5; FTIR (ATR, cm^{-1}): 3064, 3033, 1599, 1334, 1152; HRMS (ESI) *m/z* Calculated for $C_{35}H_{35}F_3NO_5S$ $[M+H]^+$: 638.2188; found: 638.2167.

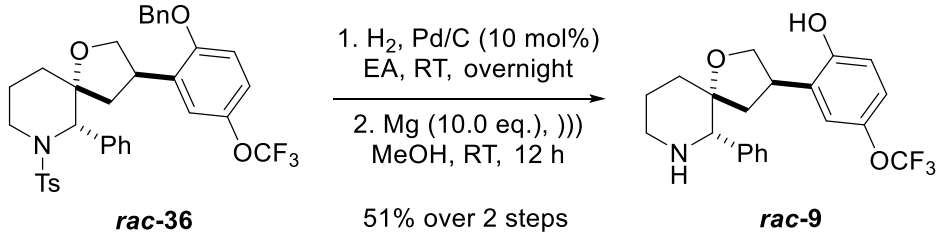

***rac*-36** **rac-9**

(*rac*-9)

***rac*-2-(6-phenyl-1-oxa-7-azaspiro[4.5]decan-3-yl)-4-(trifluoromethoxy)phenol**

The reductive Heck reaction product ***rac*-36** (126 mg, 0.20 mmol, 1.0 equiv.) was dissolved in ethyl acetate (2.0 mL) before palladium on activated charcoal (10 wt%, 21 mg, 0.02 mmol, 10 mol%) was added. The round bottom flask was evacuated and refilled with H_2 thrice using a H_2 balloon. The reaction was stirred overnight at room temperature before being filtered through a pad of celite. Concentration under reduced pressure gave the crude product which was used in the next step without further purification.

The crude hydrogenation product was dissolved in anhydrous MeOH (3 mL) and magnesium powder (48 mg, 2.0 mmol, 10.0 equiv.) was added. The suspension was sonicated overnight and 15% aqueous HCl solution (1.0 mL) was added and the mixture allowed to stir for an additional 15 min before saturated aqueous $NaHCO_3$ solution was added to neutralise the mixture. Ethyl acetate (30 mL) was added and the layers separated. The aqueous phase was extracted with ethyl acetate (3 x 30 mL) and the combined organic extracts were washed with brine (50 mL), dried over anhydrous magnesium sulphate and filtered. Concentration under reduced pressure and purification using silica gel chromatography (Eluent: Hexane/Ethyl Acetate = 2:1 to Ethyl Acetate/Methanol = 2:1) to give *rac*-2-(6-phenyl-1-oxa-7-azaspiro[4.5]decan-3-yl)- 4-(trifluoromethoxy)phenol ***rac*-9** (40 mg, 0.102 mmol, 51% over 2 steps) as a pale yellow solid. mp = 203-204 ºC (decomposed) (Lit.[122a]: yellow oil); TLC (Ethyl Acetate/ Methanol = 2:1): R_f = 0.32; ^{1}H NMR (300 MHz, CD_3OD) δ (ppm): 7.48 (dd, *J* = 7.8 Hz, 1.6 Hz, 2H), 7.38-7.31 (m, 3H), 6.84 (dd, *J* = 8.7 Hz, 2.0 Hz, 1H), 6.75 (d, *J* = 2.6 Hz, 1H), 6.64 (d, *J* = 8.7 Hz, 1H), 3.96 (t, *J* = 7.5 Hz, 1H), 3.65 (dd, *J* = 9.9 Hz, 8.0 Hz, 1H), 3.58 (s, 1H), 3.14-3.09 (m, 1H), 2.73 (dd, *J* = 12.7 Hz, 2.9 Hz, 1H), 2.28-2.14 (m, 2H), 2.05-1.97 (m, 2H), 1.80-1.70 (m, 2H), 1.60 (d, *J* = 11.9 Hz, 1H); ^{13}C NMR (100 MHz, CD_3OD) δ (ppm): 156.0, 142.9, 141.8, 130.4, 129.8, 129.2, 128.8, 122.2 (q, *J* = 252.7 Hz), 121.7, 121.1, 116.6, 83.6, 72.9, 70.1, 47.7, 42.8, 40.4, 38.7, 24.6; FTIR (ATR, cm^{-1}): 3290, 3062, 3032, 1607, 1510, 1494; HRMS (ESI) *m/z* Calculated for $C_{21}H_{23}F_3NO_3$ $[M+H]^+$: 394.1630; found: 394.1611.

2.4.3 Determination of enantiomeric excess by HPLC for 30:

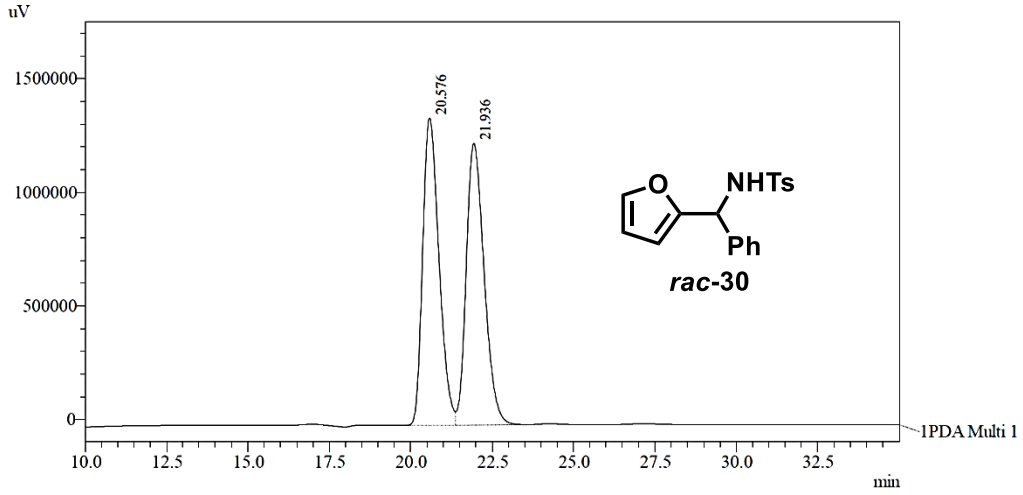

PDA Ch1 220nm 4nm

Peak#	Ret. Time	Area	Height	Area %	Height %
1	20.576	47118803	1351718	49.814	52.162
2	21.936	47470292	1239669	50.186	47.838
Total		94589095	2591387	100.000	100.000

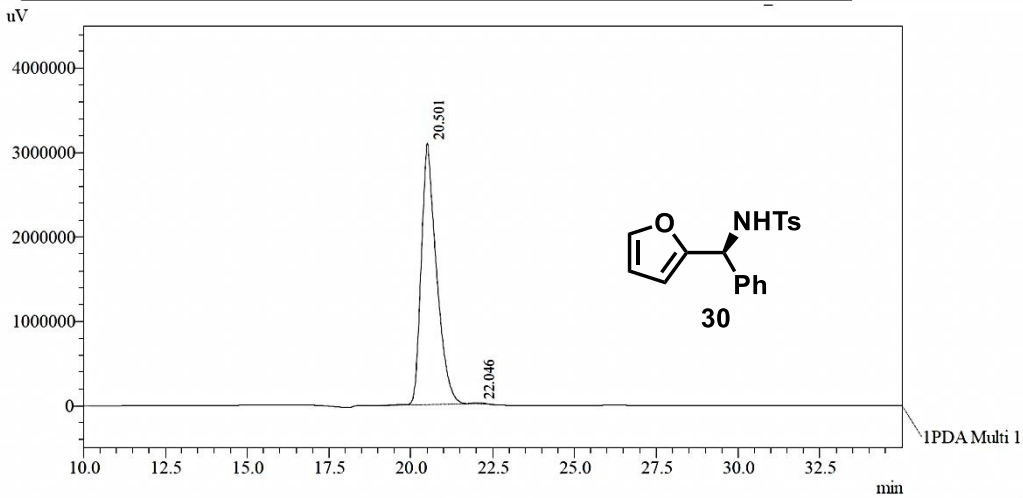

PeakTable

PDA Ch1 220nm 4nm

Peak#	Ret. Time	Area	Height	Area %	Height %
1	20.501	99918858	3095665	99.650	99.526
2	22.046	351238	14730	0.350	0.474
Total		100270096	3110395	100.000	100.000

HPLC trace of **30** (Chiralpak OD-H, Hexanes:i-PrOH = 90:10, 0.5 mL/min, 220 nm)

2.4.4 Determination of enantiomeric excess by HPLC for 27:

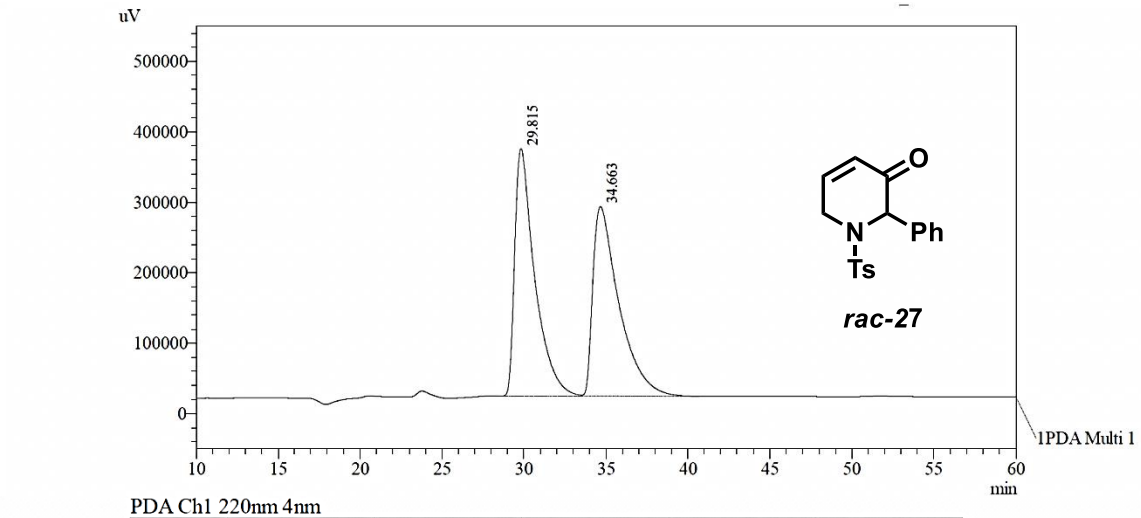

PDA Ch1 220nm 4nm

Peak#	Ret. Time	Area	Height	Area %	Height %
1	29.815	29804785	351211	49.930	56.633
2	34.663	29888398	268941	50.070	43.367
Total		59693183	620152	100.000	100.000

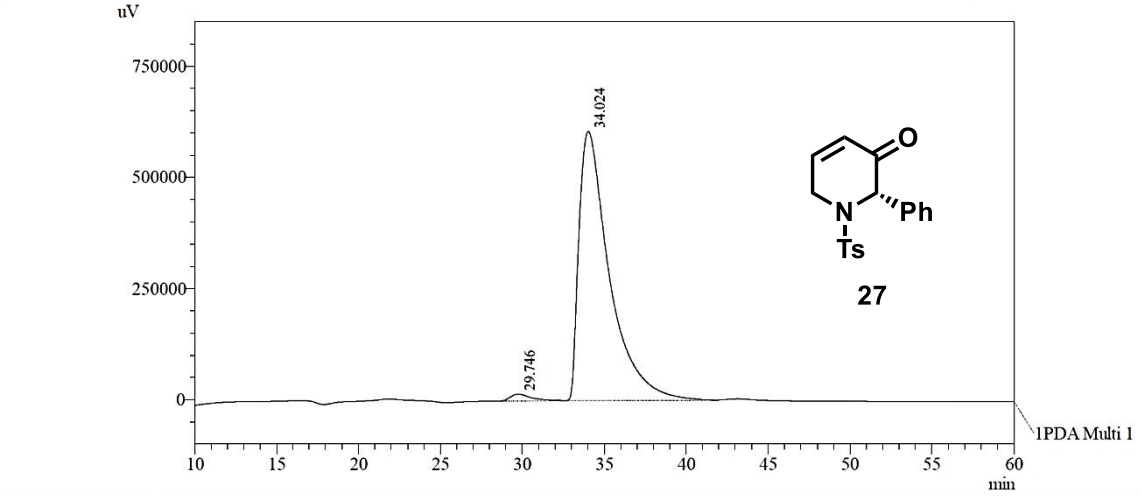

PDA Ch1 220nm 4nm

Peak#	Ret. Time	Area	Height	Area %	Height %
1	29.746	1324658	15138	1.665	2.442
2	34.024	78252880	604692	98.335	97.558
Total		79577538	619830	100.000	100.000

HPLC trace of **27** (Chiralpak OD-H, Hexanes:i-PrOH = 90:10, 0.5 mL/min, 220 nm)

2.4.5 Determination of enantiomeric excess by HPLC for 27 after single-crystal X-ray crystallography:

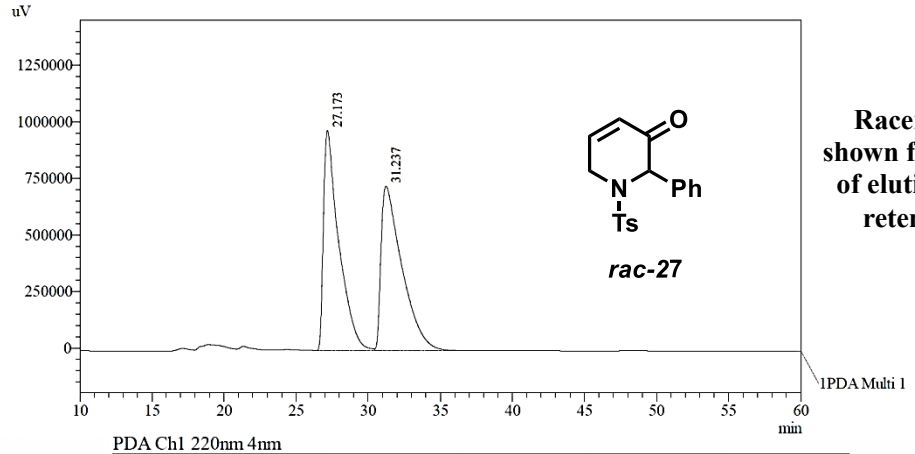

Racemic mixture shown for comparison of elution order and retention times.

PDA Ch1 220nm 4nm

Peak#	Ret. Time	Area	Height	Area %	Height %
1	27.173	72385288	974821	49.624	57.266
2	31.237	73481504	727457	50.376	42.734
Total		145866793	1702278	100.000	100.000

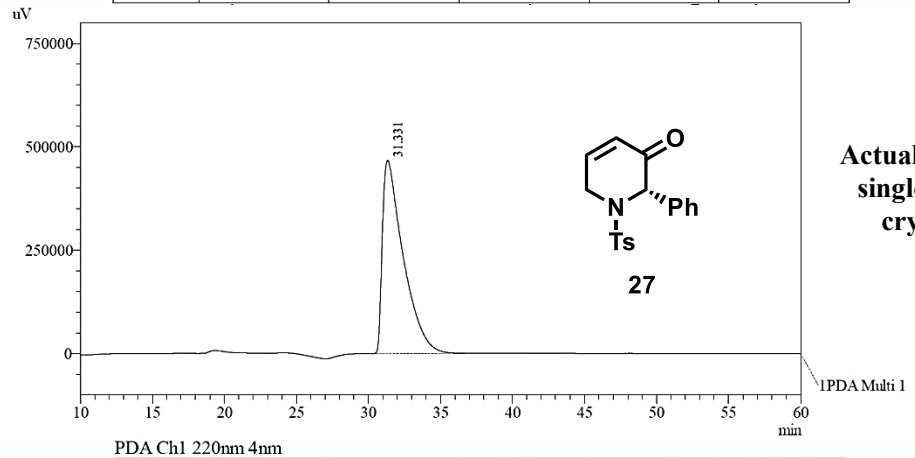

Actual crystal used for single-crystal X-ray crystallography

PDA Ch1 220nm 4nm

Peak#	Ret. Time	Area	Height	Area %	Height %
1	31.331	46998573	466616	100.000	100.000
Total		46998573	466616	100.000	100.000

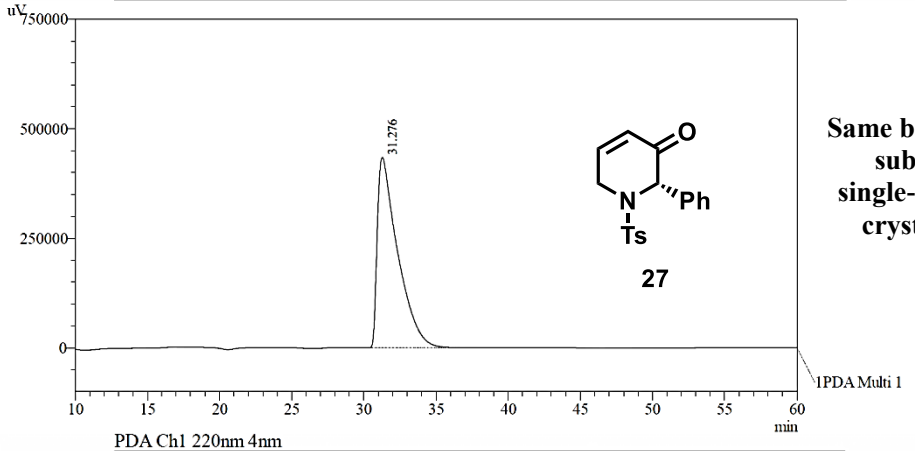

Same batch of crystal submitted for single-crystal X-ray crystallography

PDA Ch1 220nm 4nm

Peak#	Ret. Time	Area	Height	Area %	Height %
1	31.276	42637428	433836	100.000	100.000
Total		42637428	433836	100.000	100.000

HPLC trace of **27** after X-ray (Chiralpak OD-H, Hexanes:i-PrOH = 90:10, 0.5 mL/min, 220 nm)

2.4.6 Determination of enantiomeric excess by HPLC for 28:

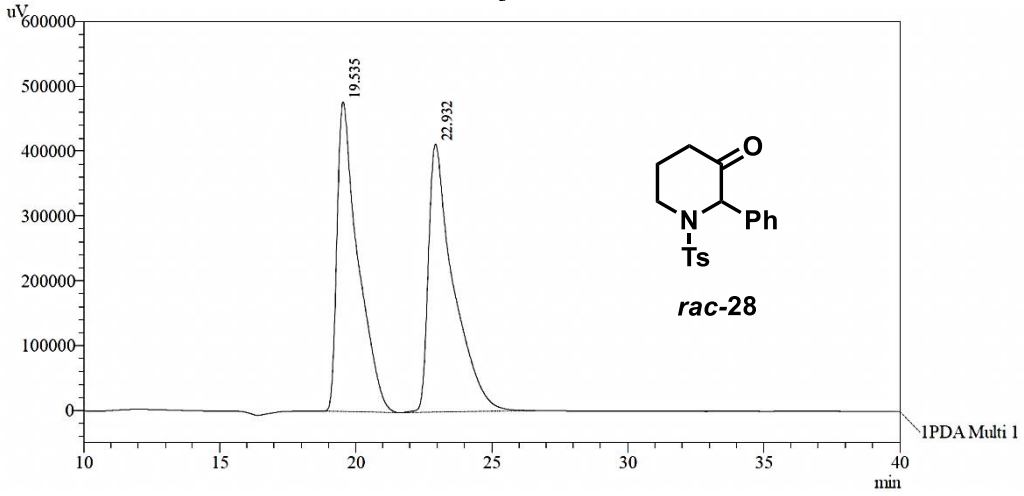

PDA Ch1 220nm 4nm

Peak#	Ret. Time	Area	Height	Area %	Height %
1	19.535	25536746	478258	49.108	53.620
2	22.932	26464316	413679	50.892	46.380
Total		52001062	891937	100.000	100.000

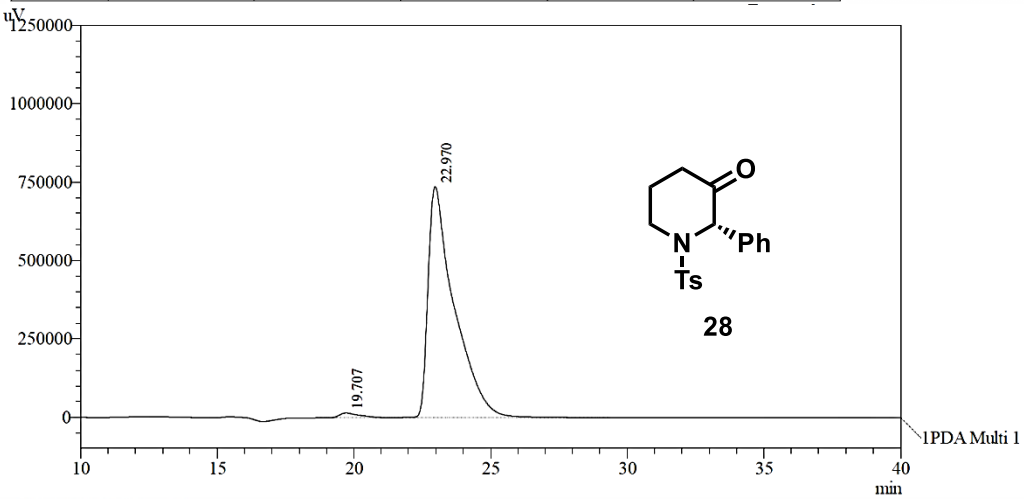

PDA Ch1 220nm 4nm

Peak#	Ret. Time	Area	Height	Area %	Height %
1	19.707	854017	15977	1.697	2.121
2	22.970	49485143	737184	98.303	97.879
Total		50339160	753161	100.000	100.000

HPLC trace of **28** (Chiralpak OD-H, Hexanes:i-PrOH = 90:10, 0.5 mL/min, 220 nm)

2.4.7 Data and CCDC numbers for X-Ray Structures

Cambridge Crystallographic Data Centre Deposition Number: 1436780

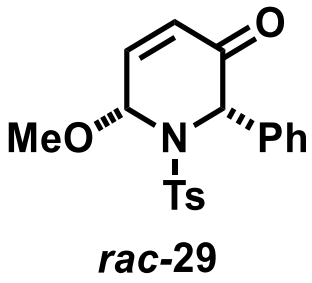

rac-29

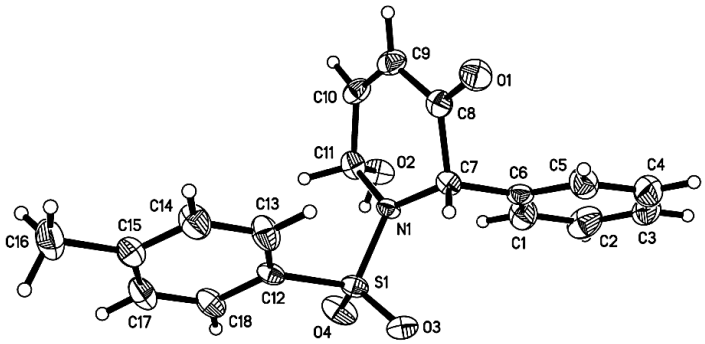

Empirical formula	C19 H19 N O4 S
Formula weight	357.41
Temperature	296(2) K
Wavelength	0.71073 Å
Crystal system	Triclinic
Space group	P-1
Unit cell dimensions	a = 8.176(5) Å a= 108.708(15)°. b = 9.024(5) Å b= 93.459(16)°. c = 12.929(8) Å g = 90.727(17)°.
Volume	901.3(9) $Å^3$
Z	2
Density (calculated)	1.317 Mg/m^3
Absorption coefficient	0.202 mm^{-1}
F(000)	376
Crystal size	0.40 x 0.38 x 0.30 mm^3
Theta range for data collection	1.67 to 30.48°.
Index ranges	-11<=h<=11, -12<=k<=12, -18<=l<=18
Reflections collected	14227
Independent reflections	5416 [R(int) = 0.0359]
Completeness to theta = 30.48°	98.4 %
Absorption correction	Semi-empirical from equivalents
Max. and min. transmission	0.9418 and 0.9234
Refinement method	Full-matrix least-squares on F^2
Data / restraints / parameters	5416 / 225 / 284
Goodness-of-fit on F^2	0.981
Final R indices [I>2sigma(I)]	R1 = 0.0549, wR2 = 0.1442
R indices (all data)	R1 = 0.1048, wR2 = 0.1765
Extinction coefficient	0.071(7)
Largest diff. peak and hole	0.269 and -0.260 $e.Å^{-3}$

Cambridge Crystallographic Data Centre Deposition Number: 1436779

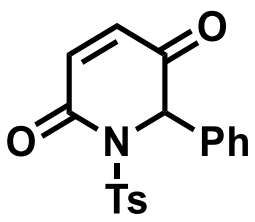

rac-32'

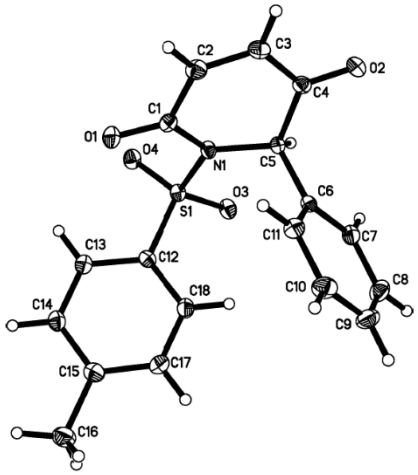

Empirical formula	C18 H15 N O4 S	
Formula weight	341.37	
Temperature	103(2) K	
Wavelength	0.71073 Å	
Crystal system	Triclinic	
Space group	P-1	
Unit cell dimensions	a = 8.7740(3) Å	a= 108.136(2)°.
	b = 10.1670(4) Å	b= 105.082(2)°.
	c = 10.7296(6) Å	g = 108.1140(10)°.
Volume	794.12(6) $Å^3$	
Z	2	
Density (calculated)	1.428 Mg/m^3	
Absorption coefficient	0.226 mm^{-1}	
F(000)	356	
Crystal size	0.40 x 0.34 x 0.32 mm^3	
Theta range for data collection	2.66 to 28.29°.	
Index ranges	-11<=h<=11, -13<=k<=13, -14<=l<=14	
Reflections collected	13412	
Independent reflections	3930 [R(int) = 0.0255]	
Completeness to theta = 28.29°	99.4 %	
Absorption correction	Semi-empirical from equivalents	
Max. and min. transmission	0.9311 and 0.9150	
Refinement method	Full-matrix least-squares on F^2	
Data / restraints / parameters	3930 / 0 / 218	
Goodness-of-fit on F^2	1.084	
Final R indices [I>2sigma(I)]	R1 = 0.0349, wR2 = 0.1007	
R indices (all data)	R1 = 0.0386, wR2 = 0.1034	
Largest diff. peak and hole	0.382 and -0.472 $e.Å^{-3}$	

Cambridge Crystallographic Data Centre Deposition Number: 917487

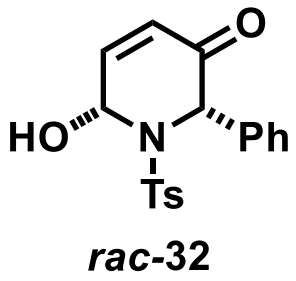

rac-32

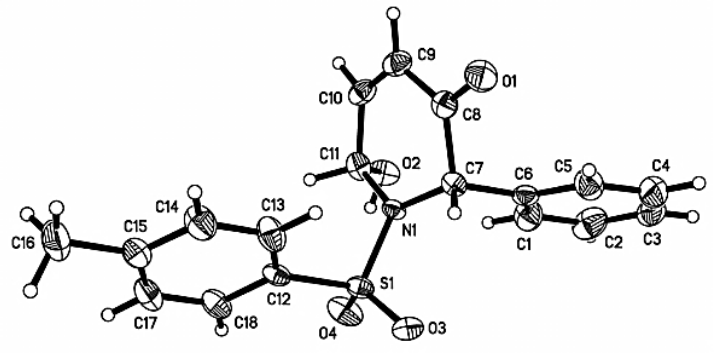

Empirical formula	C18 H17 N O4 S
Formula weight	343.39
Temperature	103(2) K
Wavelength	0.71073 Å
Crystal system	Monoclinic
Space group	P2(1)/n
Unit cell dimensions	a = 8.3044(14) Å a= 90°. b = 10.7213(19) Å b= 91.819(5)°. c = 17.956(3) Å g = 90°.
Volume	1597.9(5) $Å^3$
Z	4
Density (calculated)	1.427 Mg/m^3
Absorption coefficient	0.225 mm^{-1}
F(000)	720
Crystal size	0.24 x 0.22 x 0.04 mm^3
Theta range for data collection	2.21 to 25.01°.
Index ranges	-8<=h<=9, -12<=k<=12, -18<=l<=21
Reflections collected	6904
Independent reflections	2732 [R(int) = 0.0714]
Completeness to theta = 25.01°	97.2 %
Absorption correction	Semi-empirical from equivalents
Max. and min. transmission	0.9911 and 0.9480
Refinement method	Full-matrix least-squares on F^2
Data / restraints / parameters	2732 / 0 / 219
Goodness-of-fit on F^2	1.024
Final R indices [I>2sigma(I)]	R1 = 0.0610, wR2 = 0.1512
R indices (all data)	R1 = 0.0967, wR2 = 0.1963
Largest diff. peak and hole	0.477 and -0.434 $e.Å^{-3}$

Cambridge Crystallographic Data Centre Deposition Number: 917485

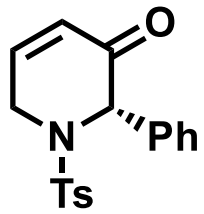

27

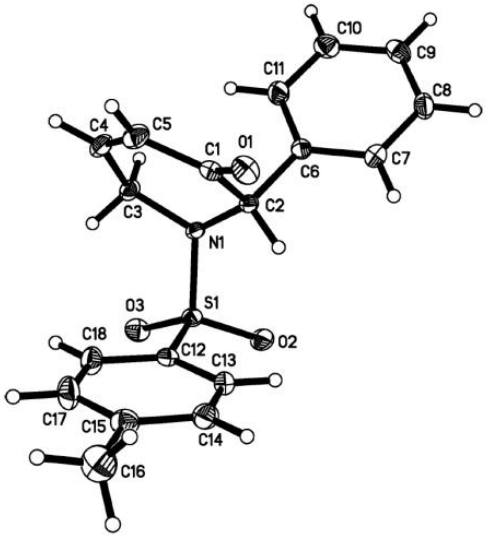

Empirical formula	C18 H17 N O3 S	
Formula weight	327.39	
Temperature	103(2) K	
Wavelength	0.71073 Å	
Crystal system	Monoclinic	
Space group	P2(1)	
Unit cell dimensions	a = 9.9921(7) Å	a= 90°.
	b = 8.0950(6) Å	b= 107.490(2)°.
	c = 10.5243(9) Å	g = 90°.
Volume	811.91(11) $Å^3$	
Z	2	
Density (calculated)	1.339 Mg/m^3	
Absorption coefficient	0.213 mm^{-1}	
F(000)	344	
Crystal size	0.40 x 0.28 x 0.24 mm^3	
Theta range for data collection	2.14 to 28.57°.	
Index ranges	-13<=h<=12, -10<=k<=10, 0<=l<=14	
Reflections collected	3983	
Independent reflections	3983 [R(int) = 0.0000]	
Completeness to theta = 28.57°	98.5 %	
Absorption correction	Semi-empirical from equivalents	
Max. and min. transmission	0.9505 and 0.9195	
Refinement method	Full-matrix least-squares on F^2	
Data / restraints / parameters	3983 / 1 / 209	
Goodness-of-fit on F^2	1.063	
Final R indices [I>2sigma(I)]	R1 = 0.0342, wR2 = 0.0824	
R indices (all data)	R1 = 0.0369, wR2 = 0.0855	
Absolute structure parameter	-0.05(6)	
Largest diff. peak and hole	0.443 and -0.337 $e.Å^{-3}$	

Cambridge Crystallographic Data Centre Deposition Number: 917488

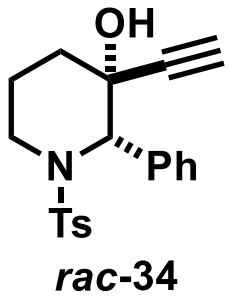

rac-34

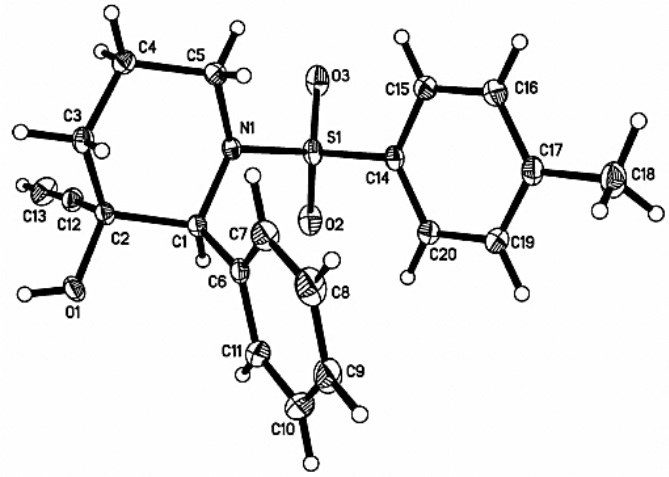

Empirical formula	C20 H21 N O3 S
Formula weight	355.44
Temperature	103(2) K
Wavelength	0.71073 Å
Crystal system	Monoclinic
Space group	P2(1)/n
Unit cell dimensions	a = 10.5854(6) Å a= 90°. b = 16.1439(9) Å b= 113.4850(10)°. c = 11.1053(6) Å g = 90°.
Volume	1740.58(17) $Å^3$
Z	4
Density (calculated)	1.356 Mg/m^3
Absorption coefficient	0.205 mm^{-1}
F(000)	752
Crystal size	0.40 x 0.38 x 0.38 mm^3
Theta range for data collection	3.22 to 31.10°.
Index ranges	-13<=h<=15, -20<=k<=23, -16<=l<=14
Reflections collected	21129
Independent reflections	5563 [R(int) = 0.0333]
Completeness to theta = 31.10°	99.4 %
Absorption correction	Semi-empirical from equivalents
Max. and min. transmission	0.9262 and 0.9225
Refinement method	Full-matrix least-squares on F^2
Data / restraints / parameters	5563 / 0 / 228
Goodness-of-fit on F^2	1.044
Final R indices [I>2sigma(I)]	R1 = 0.0368, wR2 = 0.0958
R indices (all data)	R1 = 0.0439, wR2 = 0.1004
Largest diff. peak and hole	0.471 and -0.476 $e.Å^{-3}$

Cambridge Crystallographic Data Centre Deposition Number: 917489

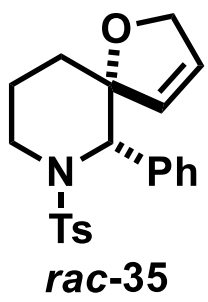

rac-35

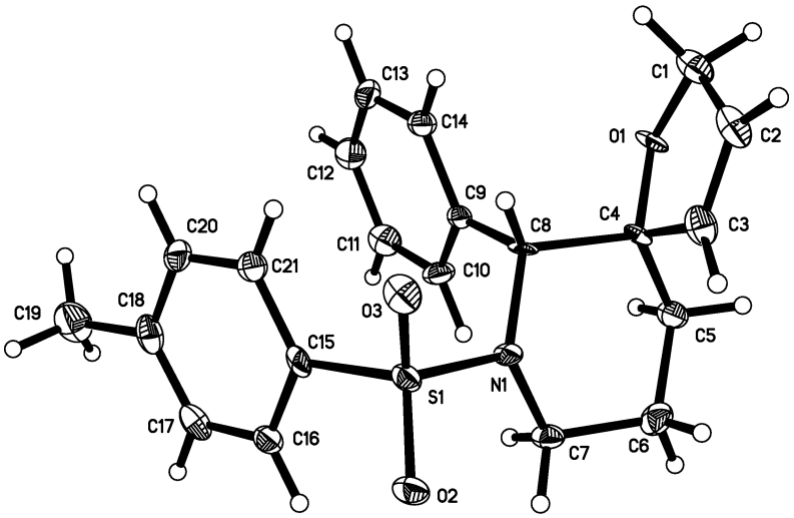

Empirical formula	C21 H23 N O3 S	
Formula weight	369.46	
Temperature	103(2) K	
Wavelength	0.71073 Å	
Crystal system	Monoclinic	
Space group	P2(1)	
Unit cell dimensions	a = 9.789(3) Å	a= 90°.
	b = 9.327(3) Å	b= 114.811(7)°.
	c = 11.044(3) Å	g = 90°.
Volume	915.3(5) Å^3	
Z	2	
Density (calculated)	1.341 Mg/m^3	
Absorption coefficient	0.198 mm^{-1}	
F(000)	392	
Crystal size	0.30 x 0.26 x 0.10 mm^3	
Theta range for data collection	2.03 to 26.89°.	
Index ranges	-12<=h<=12, -11<=k<=10, -13<=l<=13	
Reflections collected	3585	
Independent reflections	3585 [R(int) = 0.0000]	
Completeness to theta = 26.89°	98.5 %	
Absorption correction	Semi-empirical from equivalents	
Max. and min. transmission	0.9805 and 0.9431	
Refinement method	Full-matrix least-squares on F^2	
Data / restraints / parameters	3585 / 1 / 236	
Goodness-of-fit on F^2	1.066	
Final R indices [I>2sigma(I)]	R1 = 0.0583, wR2 = 0.1394	
R indices (all data)	R1 = 0.0757, wR2 = 0.1581	
Absolute structure parameter	0.20(12)	
Largest diff. peak and hole	0.443 and -0.591 e.Å^{-3}	

Cambridge Crystallographic Data Centre Deposition Number: 917486

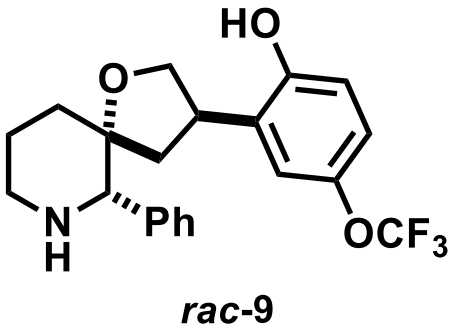

rac-9

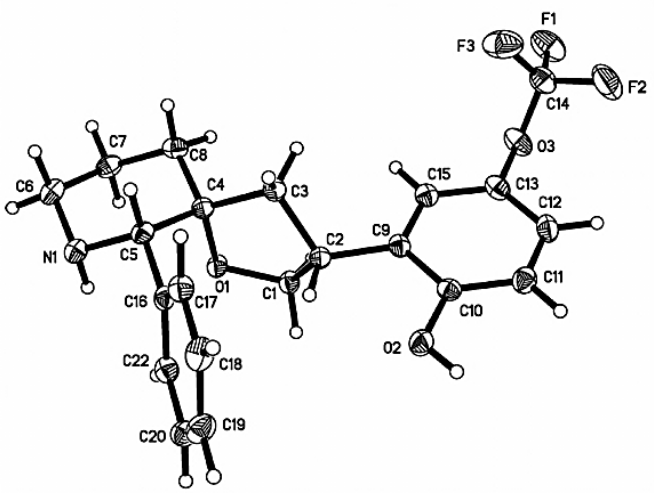

Empirical formula	C46 H52 F6 N2 O8	
Formula weight	874.90	
Temperature	103(2) K	
Wavelength	0.71073 Å	
Crystal system	Triclinic	
Space group	P-1	
Unit cell dimensions	a = 12.6844(10) Å	a= 83.347(3)°.
	b = 13.0079(9) Å	b= 80.714(2)°.
	c = 13.5817(10) Å	g = 83.780(2)°.
Volume	2187.5(3) $Å^3$	
Z	2	
Density (calculated)	1.328 Mg/m^3	
Absorption coefficient	0.107 mm^{-1}	
F(000)	920	
Crystal size	0.40 x 0.24 x 0.18 mm^3	
Theta range for data collection	1.53 to 28.37°.	
Index ranges	-16<=h<=16, -9<=k<=17, -17<=l<=18	
Reflections collected	32539	
Independent reflections	10671 [R(int) = 0.0519]	
Completeness to theta = 25.00°	97.8 %	
Absorption correction	Semi-empirical from equivalents	
Max. and min. transmission	0.9810 and 0.9585	
Refinement method	Full-matrix least-squares on F^2	
Data / restraints / parameters	10671 / 0 / 568	
Goodness-of-fit on F^2	1.031	
Final R indices [I>2sigma(I)]	R1 = 0.0515, wR2 = 0.1386	
R indices (all data)	R1 = 0.0857, wR2 = 0.1710	
Largest diff. peak and hole	0.454 and -0.452 $e.Å^{-3}$	

CHAPTER 3

Synthesis of Biologically Active Natural Products, Aspergillides A and B, Entirely from Biomass Derived Platform Chemicals

CHAPTER 3 SYNTHESIS OF BIOLOGICALLY ACTIVE NATURAL PRODUCTS, ASPERGILLIDES A AND B, ENTIRELY FROM BIOMASS DERIVED PLATFORM CHEMICALS

3.1 Introduction

Marine organisms harbor a treasure trove of diversified biologically active compounds with the potential to serve as drugs and pharmaceutical leads[128]. The potencies and structural complexities of these marine derived natural products have served as a source of inspiration and challenge to organic chemists throughout history[129]. Most metabolites are produced from the *Aspergillus* genus[128a] and aspergillides A, B and C are examples of metabolites originating from marine fungus *Aspergillus ostianus* strain 01F313. These cytotoxic natural products were isolated by Kusumi's group in 2008[130] and after extensive characterizations and elucidations, the structures of aspergillides A, B and C were proposed to be as shown in Figure 28.

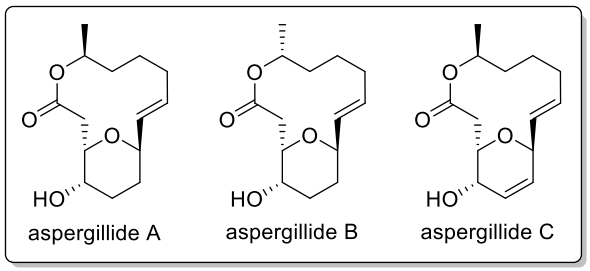

Figure 28: Proposed structures of aspergillides A, B and C

The reported unique architecture of 2,6-*trans*-substituted dihydro- or tetrahydropyran ring present in these 14-membered macrolides, coupled with their

[128] a) Bugni, T. S.; Ireland, C. M. *Nat. Prod. Rep.* **2004,** *21*, 143-163; b) Blunt, J. W.; Copp, B. R.; Keyzers, R. A.; Munro, M. H. G.; Prinsep, M. R. *Nat. Prod. Rep.* **2015,** *32*, 116-211; c) Ng, T. B.; Cheung, R. C.; Wong, J. H.; Bekhit, A. A.; Bekhit, A. E.-D. *Appl. Microbiol. Biotechnol.* **2015,** *99*, 4145-4173.

[129] a) Nicolaou, K. C.; Vourloumis, D.; Winssinger, N.; Baran, P. S. *Angew. Chem. Int. Ed.* **2000,** *39*, 44-122; b) Mohr, J. T.; Krout, M. R.; Stoltz, B. M. *Nature* **2008,** *455*, 323-332.

[130] Kito, K.; Ookura, R.; Yoshida, S.; Namikoshi, M.; Ooi, T.; Kusumi, T. *Org. Lett.* **2008,** *10*, 225-228.

potent cytotoxic activity against mouse lymphocytic leukemia cell (L1210) with median lethal dose (LD_{50}) values of 2.1 μg/mL (aspergillide A), 71.0 μg/mL (aspergillide B) and 2.0 μg/mL (aspergillide C), made these natural products attractive synthetic targets to researchers worldwide[131]. A total of 4 total syntheses and 5 formal syntheses had been reported[132] for aspergillide A and during the initial synthesis of aspergillide B, structural misassignments were discovered and then corrected[133] (Figure 29). This was further supported by analysis of single-crystal X-ray crystallography analysis[134] of the *meta*-bromobenzoate derivatives of aspergillide A **37** and aspergillide B **38** (Figure 30).

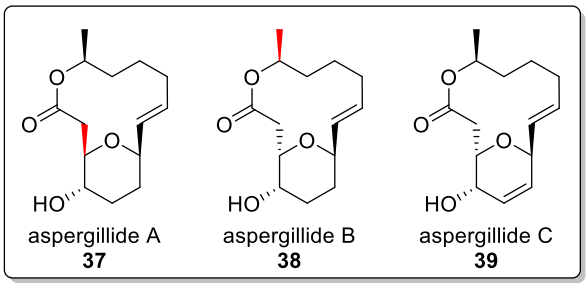

Figure 29: Revised structures of aspergillides A, B and C

[131] Review: Nagasawa, T.; Kuwahara, S. *Heterocycles* **2012,** *85*, 587-613.
[132] a) Nagasawa, T.; Kuwahara, S. *Tetrahedron Lett.* **2010,** *51*, 875-877; b) Nagasawa, T.; Nukada, T.; Kuwahara, S. *Tetrahedron* **2011,** *67*, 2882-2888; c) Díaz-Oltra, S.; Angulo-Pachón, C. A.; Murga, J.; Carda, M.; Marco, J. A. *J. Org. Chem.* **2010,** *75*, 1775-1778; d) Díaz-Oltra, S.; Angulo-Pachón, C. A.; Murga, J.; Falomir, E.; Carda, M.; Marco, J. A. *Chem. Eur. J.* **2011,** *17*, 675-688; e) Fuwa, H.; Yamaguchi, H.; Sasaki, M. *Org. Lett.* **2010,** *12*, 1848-1851; f) Fuwa, H.; Yamaguchi, H.; Sasaki, M. *Tetrahedron* **2010,** *66*, 7492-7503; g) Sabitha, G.; Vasudeva Reddy, D.; Senkara Rao, A.; Yadav, J. S. *Tetrahedron Lett.* **2010,** *51*, 4195-4198; h) Izuchi, Y.; Kanomata, N.; Koshino, H.; Hongo, Y.; Nakata, T.; Takahashi, S. *Tetrahedron: Asymmetry* **2011,** *22*, 246-251; i) Kanematsu, M.; Yoshida, M.; Shishido, K. *Angew. Chem. Int. Ed.* **2011,** *50*, 2618-2620; j) Kanematsu, M.; Shishido, K. *J. Synth. Org. Chem. Jpn.* **2012,** *70*, 1196-1205; k) Zúñiga, A.; Pérez, M.; González, M.; Gómez, G.; Fall, Y. *Synthesis* **2011,** 3301-3306; l) Sharma, G. V. M.; Manohar, V. *Tetrahedron: Asymmetry* **2012,** *23*, 252-263; m) Zeng, J.; Ma, J.; Xiang, S.; Cai, S.; Liu, X.-W. *Angew. Chem. Int. Ed.* **2013,** *52*, 5134-5137.
[133] Hande, S. M.; Uenishi, J. i. *Tetrahedron Lett.* **2009,** *50*, 189-192.
[134] Ookura, R.; Kito, K.; Saito, Y.; Kusumi, T.; Ooi, T. *Chem. Lett.* **2009,** *38*, 384.

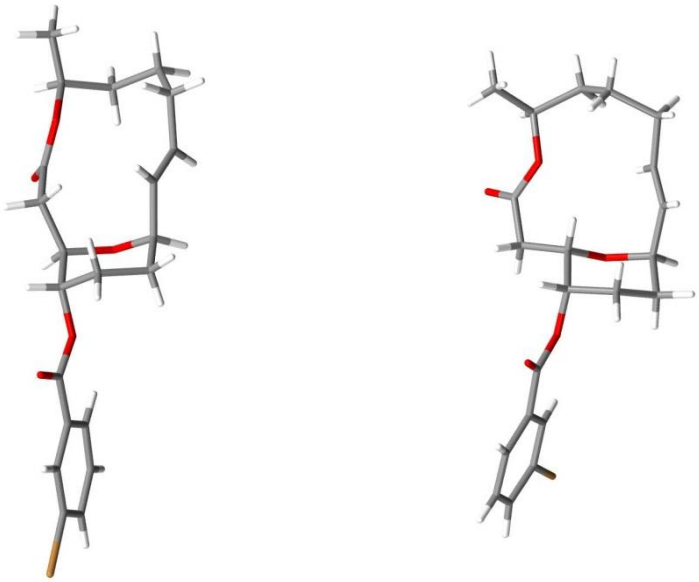

meta-bromobenzoate of **37** *meta*-bromobenzoate of **38**

Figure 30: X-ray structures of *meta*-bromobenzoates derivatives of **37** and **38**

It was observed that in the *meta*-bromobenzoate derivative of aspergillide A **37**, the substituents on the tetrahydropyran (THP) ring are orientated pseudoaxially due to the ring size and double bond geometry as opposed to the observed mixture of pseudoequatorial and pseudoaxial orientations of the substituents of the *meta*-bromobenzoate derivative of aspergillide B **38**. This unfavorable and high energy conformation of **37** resulted in difficulties in the ring-closing reactions and had been exploited for the isomerization of aspergillide A **37** to aspergillide B **38**, which will be further discussed subsequently.

Interestingly, a recent report from Qi's group[135] suggested the isolation of a new 16-membered macrolide named aspergillide D and possessed a proposed structure which is distinctly different from the rest of the reported aspergillides (Figure 31). To the best of our knowledge, there has yet to be any independent synthesis to confirm the elucidated structure of aspergillide D and in the initial report of its isolation, it was

[135] Bao, J.; Xu, X. Y.; Zhang, X. Y.; Qi, S. H. *Nat. Prod. Commun.* **2013,** *8*, 1127-1128.

found to have no antibacterial activity against both and *Staphylococcus aureus* and *Escherichia coli*.

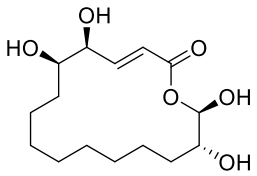

aspergillide D

Figure 31: Proposed structure of aspergillide D

A summary of the 4 total syntheses and 5 formal syntheses of aspergillide A is succinctly shown in Figure 32. Yields shown do not consider yields based on recovered starting material while (T) indicates a total synthesis and (F) indicates a formal synthesis. Values in parenthesis represent the number of steps and yields after considering uncompleted steps for formal syntheses. From the 4 reported total syntheses, the construction of the macrocycle can be broadly classified into 3 main strategies, namely macrolactonization by Kuwahara[132a,b] and Fuwa[132e,f], ring-closing metathesis/photoisomerization by Marco[132c,d] and transannular oxa-conjugate addition by Shishido[132j,k].

Kuwahara[132a,b] and Fuwa[132e,f] attempted the macrolactonizations of seco acids **40** and **41** respectively using a variety of macrolactonization methodologies[136] but their best results only afforded the desired monomeric macrocycles **42** and **43** respectively in 20-30% yield using Yamaguchi macrolactonization[137] after optimization of reaction parameters. The low yields were due to the formation of undesired dimeric products which could be rationalized to be due to the high energy barrier present for the all

[136] Reviews: a) Parenty, A.; Moreau, X.; Campagne, J. M. *Chem. Rev.* **2006,** *106*, 911-939; b) Parenty, A.; Moreau, X.; Niel, G.; Campagne, J. M. *Chem. Rev.* **2012,** *113*, PR1-PR40.
[137] Inanaga, J.; Hirata, K.; Saeki, H.; Katsuki, T.; Yamaguchi, M. *Bull. Chem. Soc. Jpn.* **1979,** *52*, 1989-1993.

pseudoequatorial substituents in seco acids **40** and **41** to flip to an all pseudoaxial conformation in order to bring the two reacting functionality within reaction proximity. This is hard to achieve and hence significant amounts of dimerization occurs despite the high dilution and slow addition reaction conditions employed.

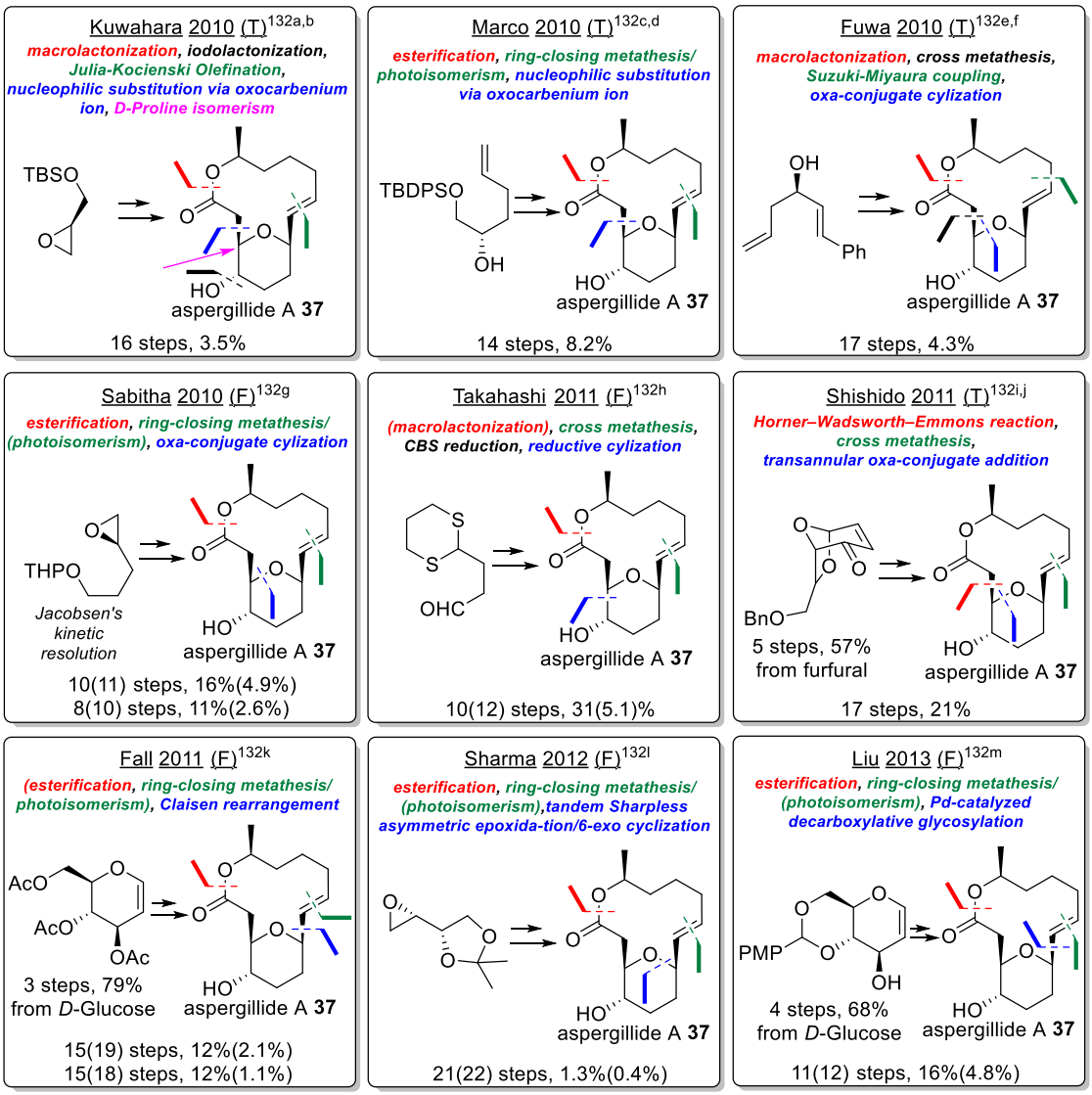

Figure 32: Summary of prior syntheses of aspergillide A

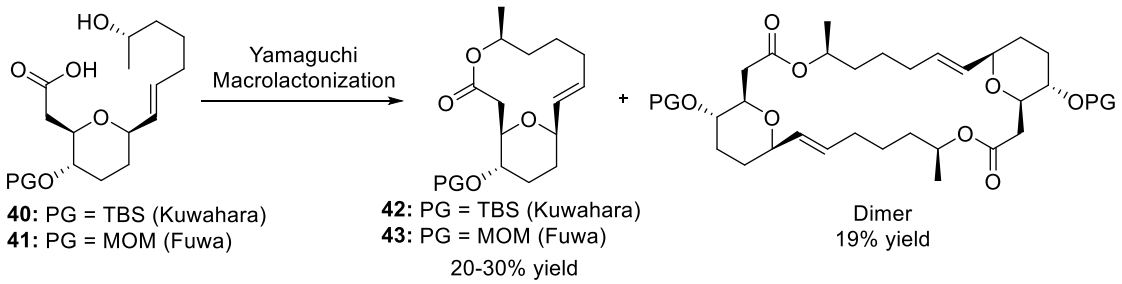

Scheme 15: Extensive dimerization during macrolactonization attempts

Marco[132c,d] circumvented the issue of the high energy conformation required by the macrolactonization by choosing a ring-closing metathesis strategy for the macrocyclization. However, the undesired *Z*-isomer was obtained in excellent yield and deprotection of the benzyl (Bn) protecting group was carried out with high yield (Scheme 16). In order to access the desired *E* double bond geometry present in aspergillide A **37**, a photoisomerization step was employed but it suffered from low conversion and hence low yield due to stability offered by the *Z* double bond which allows the substituents in the THP ring to remain in the pseudoequatorial orientation in contrast to the pseudoaxial orientation when *E* double bond is present.

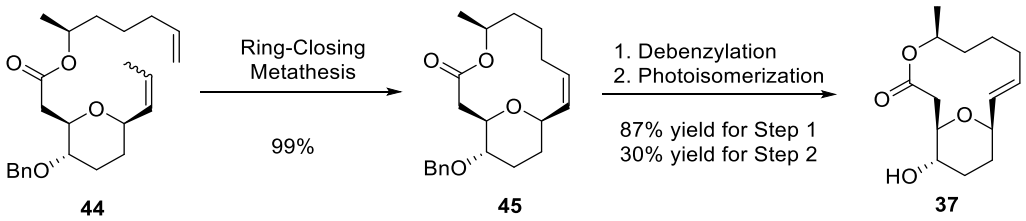

Scheme 16: Poor yield and conversion for photoisomerization step

Shishido[132j,k] developed an elegant strategy involving the use of a transannular oxa-conjugate addition to synthesize the THP ring with the desired *cis* diastereoselectivity in quantitative yield (Scheme 17). They explained the phenomenon using a lithium-chelated transition state which brings the two oxygen atoms together in

the correct orientation to form the desired diastereomer. In addition, they were able to vary the reaction conditions to obtain the *trans* isomer, necessary for the synthesis of aspergillide B **38**, in near quantitative yield, thus establishing a divergent synthesis from the same intermediate **46**. Finally, a thorough investigation also revealed that aspergillide A **37** was able to be isomerized to the more stable aspergillide B **38** under their developed reaction conditions (Scheme 18). Hence, aspergillide A **37** could serve as a synthetic intermediate to access aspergillide B **38** using Shishido's conditions.

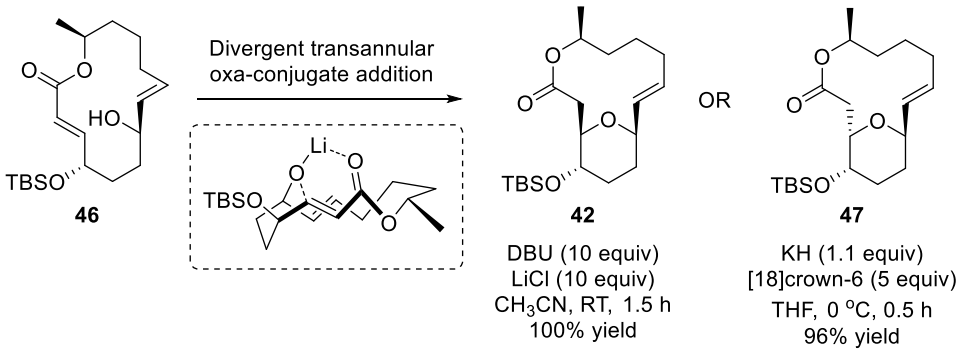

Scheme 17: Divergent transannular oxa-conjugate addition developed by Shishido

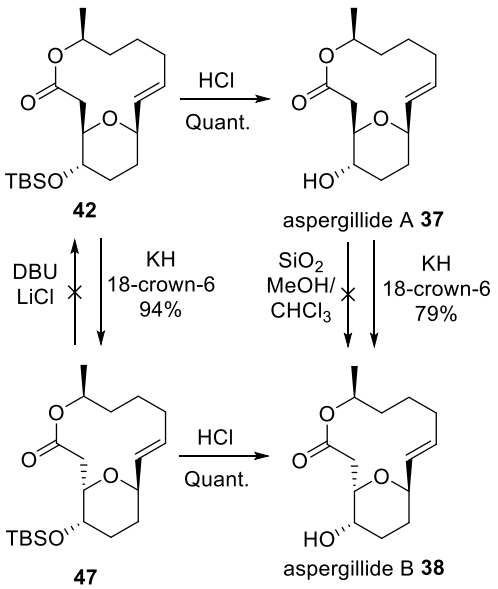

Scheme 18: Isomerization of aspergillide A **37** to aspergillide B **38**

We envisaged that aspergillide A **37**, and hence aspergillide B **38**, could be constructed entirely from biomass derived platform chemicals, whereby all of the carbon present in these biologically active natural products would originate from biomass, *via* the following disconnections shown in Figure 33. Using Negishi coupling[138] and Yamaguchi macrolactonization[137] would allow for the construction of the macrocycle from fragment A and fragment B. Fragment A would originate from levulinic acid **3** *via* several transformations including an enzymatic kinetic resolution[139]. On the other hand, fragment B could be disconnected using Takai iodoolefination [140], Achmatowicz rearrangement reaction[91] and an asymmetric Mukaiyama Aldol reaction[141,142] to originate from biomass derived platform chemical HMF **1**.

[138] a) Negishi, E.-i.; Hu, Q.; Huang, Z.; Qian, M.; Wang, G. *Aldrichim. Acta* **2005,** *38*, 77-90; b) Jana, R.; Pathak, T. P.; Sigman, M. S. *Chem. Rev.* **2011,** *111*, 1417-1492; c) Krasovskiy, A.; Duplais, C.; Lipshutz, B. H. *Org. Lett.* **2010,** *12*, 4742-4744; d) Lipshutz, B. H.; Ghorai, S.; Abela, A. R.; Moser, R.; Nishikata, T.; Duplais, C.; Krasovskiy, A.; Gaston, R. D.; Gadwood, R. C. *J. Org. Chem.* **2011,** *76*, 4379-4391.

[139] a) Review: Ghanem, A. *Tetrahedron* **2007,** *63*, 1721-1754; b) Felluga, F.; Forzato, C.; Ghelfi, F.; Nitti, P.; Pitacco, G.; Pagnoni, U. M.; Roncaglia, F. *Tetrahedron: Asymmetry* **2007,** *18*, 527-536.

[140] Takai, K.; Nitta, K.; Utimoto, K. *J. Am. Chem. Soc.* **1986,** *108*, 7408-7410.

[141] Reviews: a) Mlynarski, J.; Bas, S. *Chem. Soc. Rev.* **2014,** *43*, 577-587; b) Matsuo, J.-i.; Murakami, M. *Angew. Chem. Int. Ed.* **2013,** *52*, 9109-9118; c) Beutner, G. L.; Denmark, S. E. *Angew. Chem. Int. Ed.* **2013,** *52*, 9086-9096.

[142] a) Fu, F.; Teo, Y.-C.; Loh, T.-P. *Tetrahedron Lett.* **2006,** *47*, 4267-4269; b) Zhao, J.-F.; Tan, B.-H.; Loh, T.-P. *Chem. Sci.* **2011,** *2*, 349-352; c) Ollevier, T.; Plancq, B. *Chem. Commun.* **2012,** *48*, 2289-2291; d) Kitanosono, T.; Ollevier, T.; Kobayashi, S. *Chem. Asian J.* **2013,** *8*, 3051-3062; e) Denmark, S. E.; Wynn, T.; Beutner, G. L. *J. Am. Chem. Soc.* **2002,** *124*, 13405-13407.

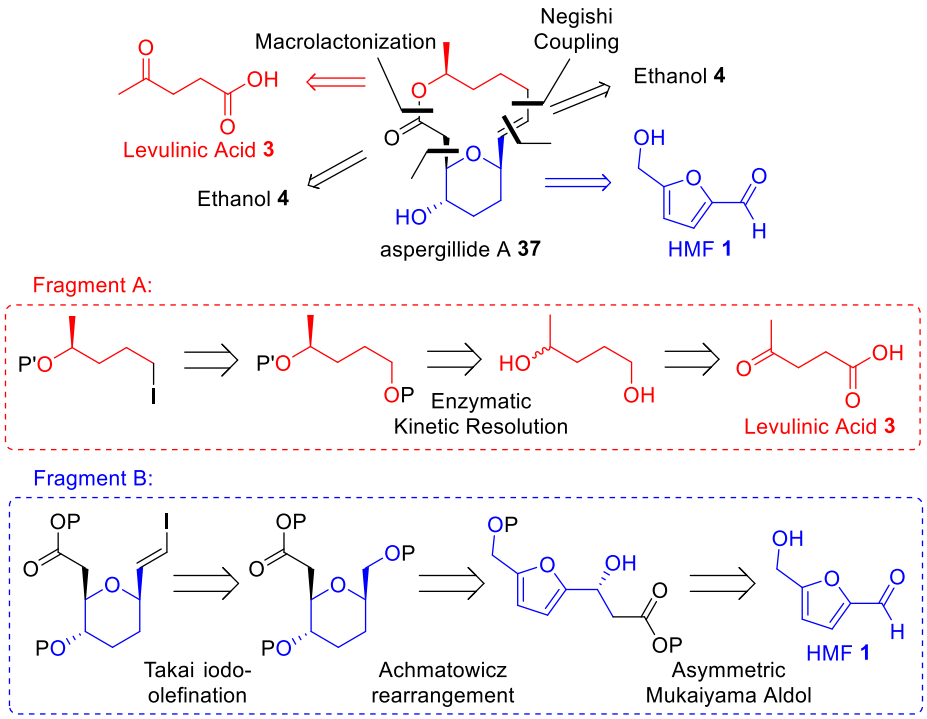

Figure 33: Proposed synthesis of aspergillide A **37**

3.2 Results and Discussions

3.2.1 Synthesis of racemic fragment A

We began the synthesis towards aspergillides A **37** and B **38** by attempting the racemic synthesis of fragment A from biomass derived platform chemical levulinic acid **3**. Levulinic acid **3** was converted to ethyl levulinate **48** in 85% yield in an esterification reaction and then the ketone moiety in **48** was chemoselectively reduced to give racemic *γ*-hydroxyester ***rac*-49** with an excellent yield of 98% (Scheme 19). It is expected that ***rac*-49** would undergo an enzymatic kinetic resolution to obtain the enantioenriched *γ*-hydroxyester **49**. ***rac*-49** was then efficiently protected with the *tert*-butyldiphenylsilyl (TBDPS) protecting group to yield ***rac*-50** before the ester moiety in ***rac*-50** was completely reduced to produce a primary alcohol ***rac*-51** in the presence of excess diisobutylaluminium hydride (DIBAL-H) with a high yield of 90%.

Finally, primary alcohol ***rac*-51** could be transformed into the desired alkyl iodide *rac*-fragment A ***rac*-52** in an iodination reaction with 98% yield. In view of the high yields and efficiencies of the reactions, we were able to use the crude mixtures of each step immediately in the subsequent step for 5 steps to obtain more than 12 g of *rac*-fragment A ***rac*-52** with 60% yield over 5 steps and only one column chromatography from levulinic acid **3**.

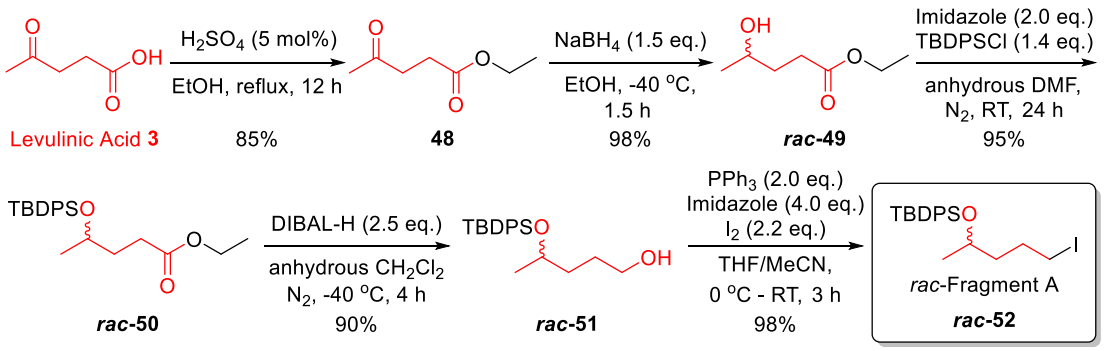

Scheme 19: Synthetic route of *rac*-fragment A from levulinic acid **3**

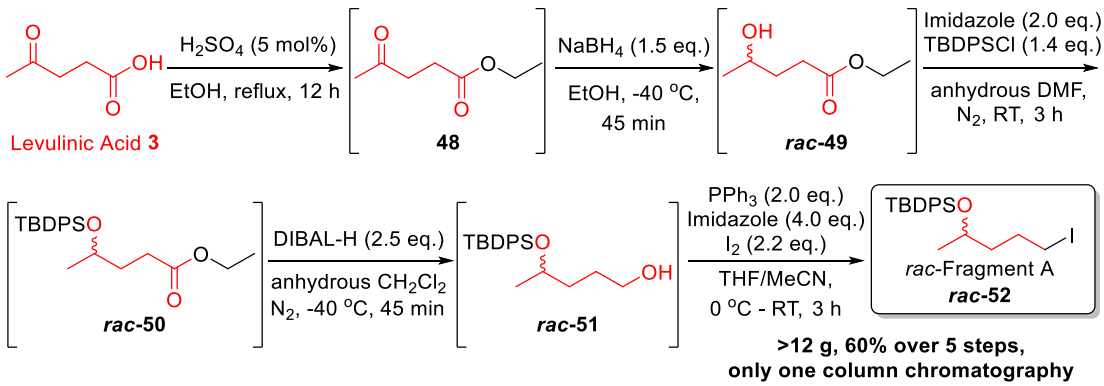

Scheme 20: Large scale synthesis of *rac*-fragment A with only one column chromatography

3.2.2 Synthesis of racemic fragment B

With sufficient quantities of *rac*-fragment A ***rac*-52** in hand, we focused on the synthesis of racemic fragment B from biomass derived platform chemical HMF **1**. We

initiated the synthesis with a benzyl protection[143] of the free alcohol present in HMF **1** in the absence of light to furnish benzylated HMF **53** in 91% yield (Scheme 21). We expect that **53** would undergo an asymmetric Mukaiyama Aldol reaction[141,142] to generate the required stereocenter. Meanwhile subjecting **53** to a racemic cross-Aldol reaction with *tert*-butylacetate generated furfuryl alcohol ***rac*-54** in an almost quantitative yield of 97%.

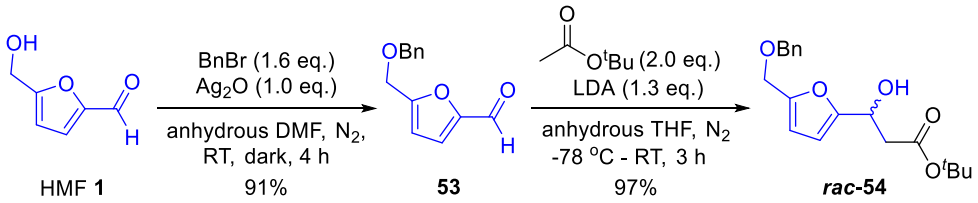

Scheme 21: Benzylation followed by cross-Aldol reaction of HMF **1**

Furfuryl alcohol ***rac*-54** was allowed to undergo the Achmatowicz rearrangement reaction under oxidative conditions to afford hemiacetal ***rac*-55** in a disastereomeric ratio of 87:13 (Scheme 22). This is in contrast to the single diastereomer obtained in the aza-Achmatowicz rearrangement reaction discussed in Chapter 2, probably due to the absence of the bulky tosyl protecting group. The major isomer is presumed to be the one with the hydroxyl orientated in the pseudoaxial position due additional stability offered by the anomeric effect. Subjecting the crude hemiacetal ***rac*-55** to reduction conditions[120] gave dihydropyranone ***rac*-56** as a single diastereomer with 61% unoptimized yield over 2 steps. Inspection of the NMR of the crude reaction mixture showed approximately 5% of unknown side products which were not identified. NOE analysis of the relative stereochemistry of the dihydropyran core in ***rac*-56** was not possible due to overlapping signals but we were confident of the *cis* relative stereochemistry from the results obtained in Chapter 2.

[143] Cottier, L.; Descotes, G.; Eymard, L.; Rapp, K. *Synthesis* **1995**, 303-306.

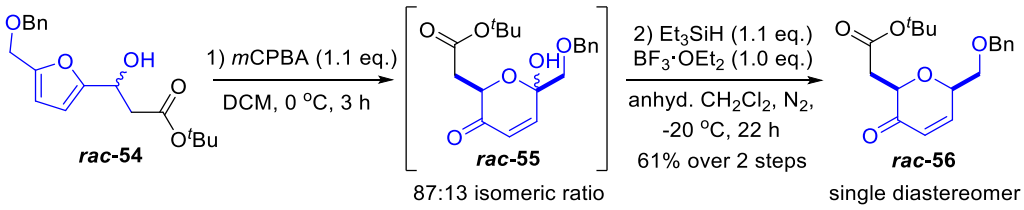

Scheme 22: Achmatowicz rearrangement followed by diastereoselective reduction

The moderate yield of the reactions prompted an optimization of the Achmatowicz rearrangement reaction by varying the oxidant loading, temperature, duration, and a high NMR yield of 89% could be obtained after the optimizations (Table 2, Entry 7). With a high yield for the hemiacetal ***rac*-55**, we hypothesized that further reductions of the dihydropyranone ***rac*-56** could be achieved in the presence of excess Lewis acid and silane *via* a 1,4-reduction of the *α,β*-unsaturated ketone moiety to tetrahydropyranone ***rac*-57** followed by a 1,2-reduction to tetrahydropyranol ***rac*-58** (Scheme 23). This Achmatowicz rearrangement/triple reduction sequence would avoid the need to perform hydrogenation of the double bond in dihydropyranone ***rac*-56** as well as a subsequent hydride reduction to access tetrahydropyranol ***rac*-58**.

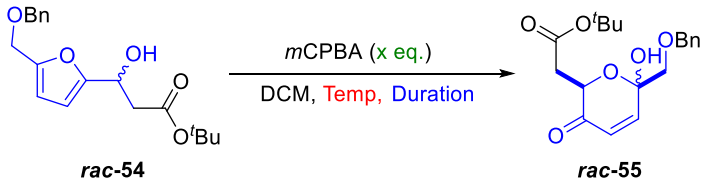

Entry	x	Temp	Duration	NMR Yield[1]
1	1.1	RT	1 h	69%
2	1.1	RT	2.5 h	73%
3	1.1	0 °C	2.5 h	71%
4	1.1	Reflux	24 h	72%
5	1.1	RT	24 h	78%
6	1.0	RT	10 h	83%
7	1.0	RT	24 h	89%

[1]Using nitrobenzene as internal standard

Table 2: Optimization of Achmatowicz rearrangement

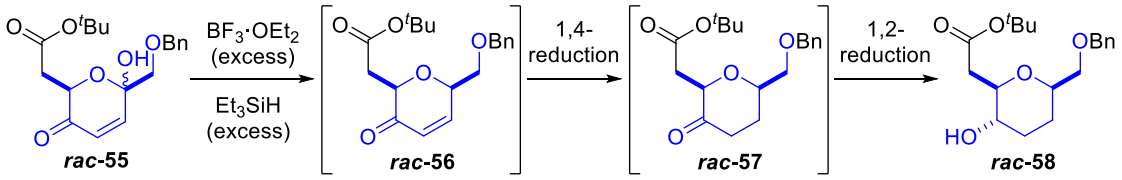

Scheme 23: Achmatowicz rearrangement/ triple reduction hypothesis

Hence, we embarked on the testing of this hypothesis by employing excess Lewis acid and silane, and we were delighted to obtain a combined yield of 47% over 2 steps from furfuryl alcohol ***rac*-54**, comprising of 41% of tetrahydropyranol ***rac*-58** and 6% of dihydropyranol ***rac*-59** (Table 3, Entry 1). The formation of dihydropyranol ***rac*-59** could be explained by a competing 1,2-reduction of dihydropyranone ***rac*-56** instead of the desired 1,4-reduction as hypothesized. However, dihydropyranol ***rac*-59** could also be a viable intermediate in this synthesis as subsequent debenzylation under hydrogenative conditions would remove the unnecessary unsaturation in dihydropyranol ***rac*-59** and result in the same product. Varying the amount of Lewis acid, silane, temperature, duration allowed for the overall yield over 2 steps to increase to 75% (Table 3, Entry 5).

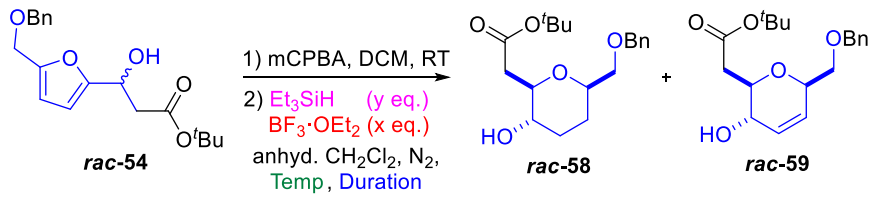

Entry	x	y	Conc.	Temp	Duration	Yield[1] of ***rac*-58**	Yield[1] of ***rac*-59**
1	3.0	6.0	0.2 M	-20 °C	43 h	41%	6%
2	4.0	6.0	1.0 M	-20 °C	20 h	31%	5%
3	4.0	6.0	1.0 M	-78 -> -40 °C	70 h	50%	5%
4	4.0	6.0	0.2 M	-40 °C	36 h	62%	2%
5	6.0	10.0	0.2 M	-40 °C	15 h	69%	6%

[1] Isolated yield over 2 steps

Table 3: Optimization of the Achmatowicz rearrangement/triple reduction sequence

With the investigation of the relative stereochemistry of dihydropyranol ***rac*-59** using NOE, it was revealed that the 2,6-substituents are indeed *cis* to each other resulting in NOE correlations between H_a and H_b, while the NOE correlation between H_b and H_c was still inconclusive at this point of time (Figure 34, Left). Using a mixture of tetrahydropyranol ***rac*-58** and dihydropyranol ***rac*-59**, the free alcohol was protected using the *tert*-butyldimethylsilyl (TBS) protecting group to yield a mixture of tetrahydropyran ***rac*-60** and dihydropyran ***rac*-61** (Scheme 24). NOE analysis of tetrahydropyran ***rac*-60** showed no NOE correlations between H_b and H_c, thereby confirming the relative stereochemistry of the secondary alcohol (Figure 34, Right). Next, debenzylation under hydrogenative conditions resulted in the convergence of intermediates ***rac*-60** and ***rac*-61** into a single product ***rac*-62** (Scheme 24).

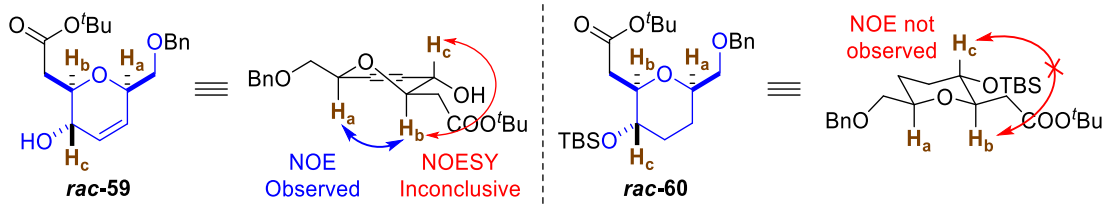

Figure 34: NOE analysis of intermediates ***rac*-59** and ***rac*-60**

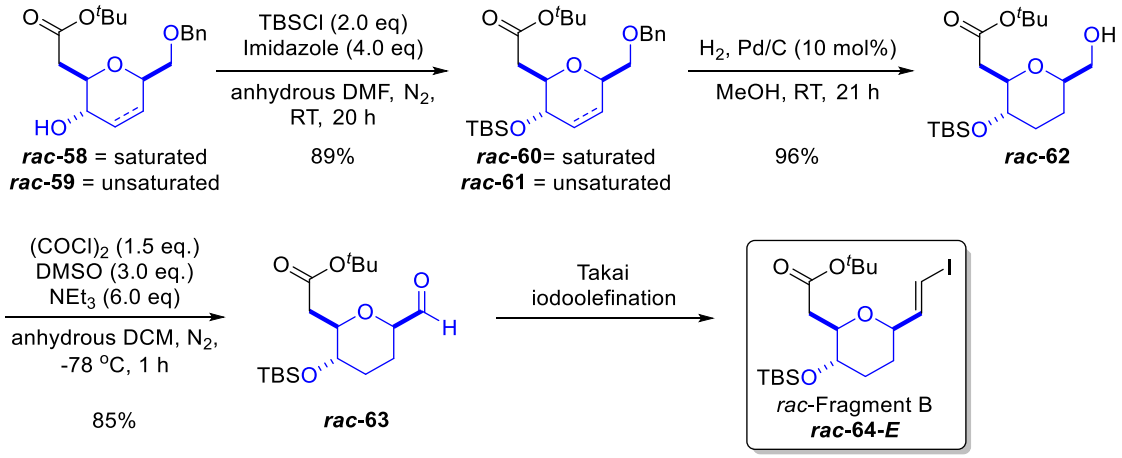

Scheme 24: Completion of the racemic synthesis of fragment B

Swern oxidation[144] of primary alcohol ***rac*-62** produced aldehyde ***rac*-63** with a good yield of 85% which had to be used immediately due to slight instability. The remaining Takai iodoolefination[140] step was subjected to temperature and solvent optimizations as it has been previously reported that a mixed solvent system could afford better *E*/*Z* selectivity[145]. The first 2 attempts revealed that a lower temperature required a long reaction duration due to lower conversion but resulted in slightly higher *E*/*Z* selectivity (Table 4, Entries 1 and 2). Employing a mixed solvent system of anhydrous dioxane and THF at both room temperature and 0 °C resulted in better *E*/*Z* selectivity but at the expense of isolated yields due to slower conversion (Table 4, Entries 3 and 4). Increasing the scale of the optimized conditions furnished racemic *E*-vinyl iodide fragment B ***rac*-64-*E*** and *Z*-vinyl iodide ***rac*-64-*Z*** in 82% yield and 81:19 *E*/*Z* selectivity (Table 4, Entry 5), and these two geometric isomers could be carefully separated using silica gel chromatography. With that, the racemic synthesis of fragment B from HMF **1** was completed.

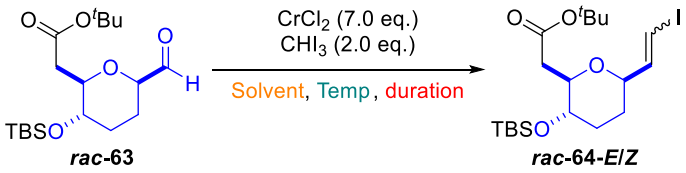

rac*-63** ***rac*-64-*E*/*Z

Entry	Solvent[1]	Temp	Duration	Yield[2]	SM[3]	*E*/*Z*[3]
1	THF	RT	1 h	77%	-	82:18
2	THF	0 °C	3 h	67%	5%	86:14
3	Dioxane/THF=6:1	RT	3 h	63%	1%	88:12
4	Dioxane/THF=6:1	0 °C	21 h	64%	-	89:11
5[4]	THF	RT	1 h	82%	-	81:19

[1] Anhydrous solvents [2] Isolated yields [3] Determined from crude NMR
[4] 2 mmol scale

Table 4: Optimization of Takai iodoolefination using $CrCl_2$

[144] a) Mancuso, A. J.; Huang, S.-L.; Swern, D. *J. Org. Chem.* **1978,** *43*, 2480-2482; b) Omura, K.; Swern, D. *Tetrahedron* **1978,** *34*, 1651-1660; c) Mancuso, A. J.; Brownfain, D. S.; Swern, D. *J. Org. Chem.* **1979,** *44*, 4148-4150.
[145] Evans, D. A.; Black, W. C. *J. Am. Chem. Soc.* **1993,** *115*, 4497-4513.

Surprisingly, racemic *E*-vinyl iodide fragment B ***rac*-64-*E*** was formed as a pale yellow solid and suitable crystals could be grown for single-crystal X-ray crystallography analysis[118]. The structure obtained confirmed the relative stereochemistry which we have attempted to prove using NOE and it is important to note that the substituents on the tetrahydropyran ring of ***rac*-64-*E*** are oriented pseudoequatorially to minimize 1,3-diaxial interactions (Figure 35).

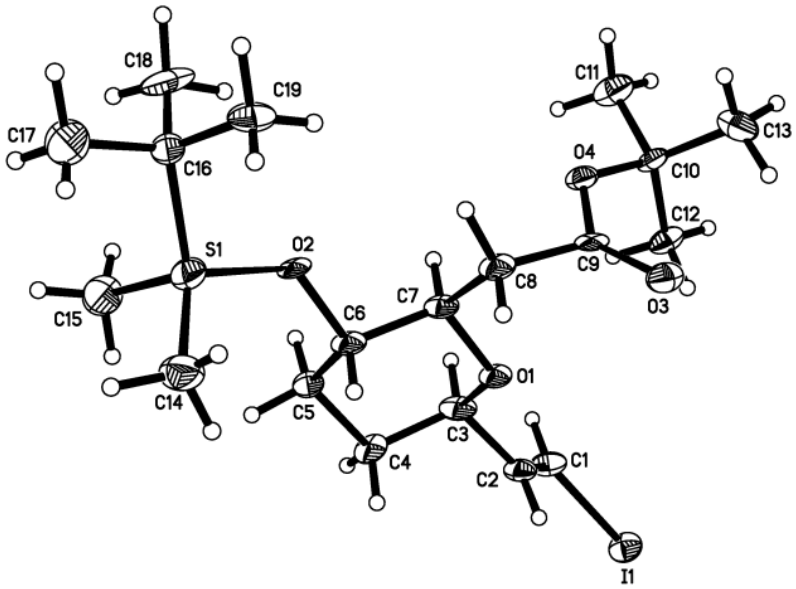

Figure 35: ORTEP drawing of racemic fragment B *E*-vinyl iodide ***rac*-64-*E***

3.2.3 Negishi coupling optimizations and completion of racemic synthesis

Completing the racemic syntheses of both fragments A and B set the stage for Negishi coupling[138] to form the carbon-carbon bond required to connect both fragments. Traditional Negishi coupling is performed anhydrous solvents and the use of highly pyrophoric *tert*-butyllithium is commonly associated with alkyl halide coupling partners. In addition, pre-formation of moisture sensitive organozinc coupling partner is required for efficient transmetallation to occur. In 2010, Lipshutz's group developed a novel methodology to conduct Negishi coupling in aqueous

solutions by utilizing micellar technology with the use of their designer surfactant PTS, which is a diester made from PEG-600, *α*-Tocopherol, Sebacic acid[138c]. This methodology avoids the use of organic solvent and dangerous *tert*-butyllithium as well as the pre-formation of sensitive organozinc compounds, making the reaction greener. In 2011, an improved surfactant "TPGS-750-M"[138d] was developed as well and together, the use of these designer surfactants in micellar catalysis have been widely applied to an extensive array of reactions in recent years[146].

In view of the advantages of such an approach, we decide to subject alkyl iodide *rac*-fragment A ***rac*-52** and *E*-vinyl iodide *rac*-fragment B ***rac*-64-*E*** to a series of optimizations (Table 5). Initial attempts gave very low yield due to low conversion and trace amount of the deiodinated vinyl iodide ***rac*-64-*H*** was observed (Table 5, Entry 1). We suspected that the insolubility of the solid *E*-vinyl iodide ***rac*-64-*E*** in the aqueous medium might be the cause of the low conversion and hence we attempted to dissolve the solid *E*-vinyl iodide ***rac*-64-*E*** in small amount of organic solvents such as ether and THF and gratifying the yield and conversion improved but they remained unsatisfactory (Table 5, Entries 2 and 3). To test if the use of organic solvent was hampering the reaction, we decided to dissolve the solid *E*-vinyl iodide ***rac*-64-*E*** in one of the reagents, tetramethylethylenediamine (TMEDA) and similar results were obtained (Table 5, Entry 4). A control reaction was conducted by using unactivated zinc dust and no product was detected with recovery of the starting material (Table 5, Entry 5).

---

[146] a) Klumphu, P.; Lipshutz, B. H. *J. Org. Chem.* **2014,** *79*, 888-900; b) Kelly, S. M.; Lipshutz, B. H. *Org. Lett.* **2013,** *16*, 98-101; c) Fennewald, J. C.; Lipshutz, B. H. *Green Chem.* **2014,** *16*, 1097-1100; d) Handa, S.; Fennewald, J. C.; Lipshutz, B. H. *Angew. Chem. Int. Ed.* **2014,** *53*, 3432-3435; e) Isley, N. A.; Dobarco, S.; Lipshutz, B. H. *Green Chem.* **2014,** *16*, 1480-1488; f) Minkler, S. R. K.; Isley, N. A.; Lippincott, D. J.; Krause, N.; Lipshutz, B. H. *Org. Lett.* **2014,** *16*, 724-726; g) Linstadt, R. T. H.; Peterson, C. A.; Lippincott, D. J.; Jette, C. I.; Lipshutz, B. H. *Angew. Chem. Int. Ed.* **2014**, *53*, 4159–4163.

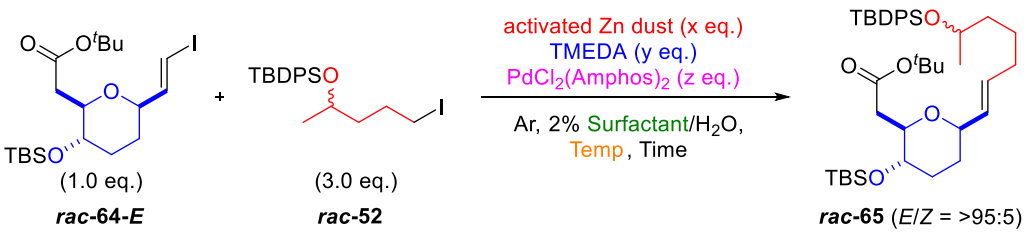

Entry	*rac*-64-*E*	x	y	z	Surfactant	Temp	Time	Yield[1] of *rac*-65 (%SM recovered)	Yield[2] of *rac*-64-*H*
1	Solid	6.0	2.0	0.10	PTS	RT	72 h	10% (58%)	1%
2	In Ether	6.0	2.0	0.10	PTS	RT	24 h	34% (19%)	2%
3	In THF	6.0	2.0	0.10	PTS	RT	72 h	31% (38%)	1%
4[4]	In TMEDA	6.0	4.0	0.10	PTS	RT	24 h	34% (30%)	6%
5	In TMEDA	6.0[3]	4.0	0.10	PTS	RT	72 h	0% (85%)	0%
6	Solid	6.0	4.0	0.10	PTS	40 °C	24 h	41% (27%)	4%
7[4]	Solid	6.0	4.0	0.10	PTS	40 °C	24 h	50% (11%)	17%
8	Solid	6.0	4.0	0.15	PTS	40 °C	24 h	60% (trace)	6%
9	Solid	6.0	4.0	0.15	TPGS-750-M	40 °C	24 h	62% (trace)	6%
10	Solid	6.0	5.0	0.05	TPGS-750-M	40 °C	24 h	68% (trace)	6%

[1]Isolated yields [2]Determined from crude NMR [3]unactivated Zn dust [4] ***rac*-64-*E*** added before ***rac*-52**

Table 5: Optimization of micellar Negishi coupling in water

We turned towards increasing the reaction temperature and we found an improved yield was achieved even with the use of the solid form of *E*-vinyl iodide ***rac*-64-*E*** (Table 5, Entry 6). Reversing the order of addition of the coupling partners resulted in formation of increased amount of side product ***rac*-64-*H*** while increasing the catalyst loading had positive effects on the conversion and yield (Table 5, Entries 7 and 8). Testing the reaction conditions with the improved surfactant "TPGS-750-M" gave a slightly better outcome and further optimization allowed for the lowering of catalyst loading to 5 mol% to give an optimized yield of 68% (Table 5, Entries 9 and 10). To the best of our knowledge, this is the first application of Lipshutz's micellar Negishi coupling protocol to an advanced synthetic intermediate with good yield and excellent selectivity.

Having obtained a satisfactory yield for the Negishi coupling, we proceeded to

carry out the selective deprotection of the TBS protecting group over the TBDPS protecting group [147] to yield secondary alcohol ***rac*-66** before employing the methoxymethyl (MOM) protecting group to produce ***rac*-67** in an almost quantitative manner (Scheme 25). Base hydrolysis of ***rac*-67** unveils the seco acid ***rac*-41** in 90% yield and since seco acid ***rac*-41** has already been reported as an intermediate[132e] to furnish aspergillide A **37** while the isomerization of aspergillide A **37** to aspergillide B **38** has been achieved by Shishido[132i], this completes the formal syntheses of racemic aspergillide A and B.

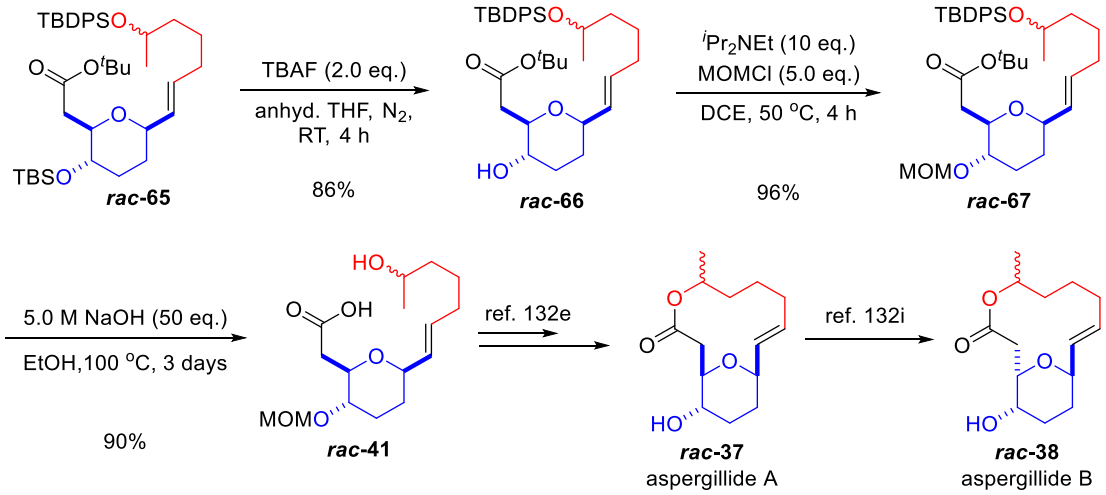

Scheme 25: Completion of the formal syntheses of racemic aspergillide A and B

3.2.4 Synthesis of enantioenriched fragment A

We shifted our attention to the generation of enantioenriched fragment A by subjecting *γ*-hydroxyester ***rac*-49** to the enzymatic kinetic resolution protocol[139] but low yields were obtained due self-lactonization[148]. As such we were compelled to alter our synthetic route for fragment A **52** and a new route was proposed (Scheme 26). The proposed route consisting of a complete reduction of levulinic acid **3**, enzymatic

[147] Crouch, R. D. *Tetrahedron* **2013,** *69*, 2383-2417.
[148] Pàmies, O.; Bäckvall, J.-E. *J. Org. Chem.* **2002,** *67*, 1261-1265.

kinetic resolution, protection, hydrolysis and an iodination reaction.

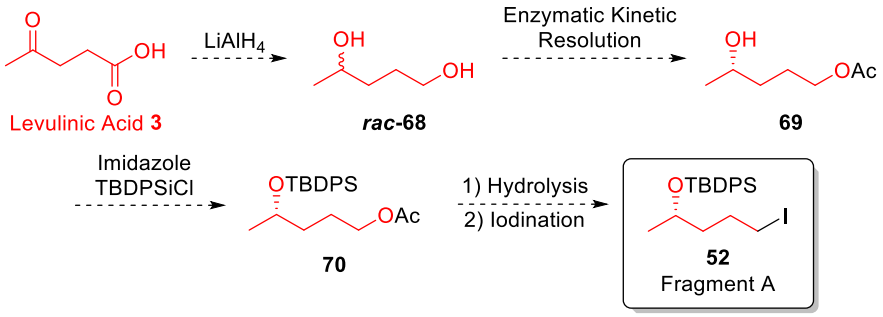

Scheme 26: Proposed alternative synthetic route to fragment A **52**

Thus, levulinic acid **3** was completely reduced to afford diol ***rac*-68** with a good yield of 88% (Scheme 27). It was expected that during the enzymatic kinetic resolution, the primary alcohol would be acetylated first to give secondary alcohol **69** before the kinetic resolution occurs at the more sterically hindered secondary alcohol to yield diacetate **71** (Table 6). The enzymatic kinetic resolution of diol ***rac*-68** was optimized under varying conditions and initial attempt for 5 hours resulted in 62% conversion to diacetate **71**. The *ee* of the reaction could only be determined by chiral HPLC after the installation of an UV-active protecting group such as TBDPS and this conversion for secondary alcohol **69** resulted in an isolated yield of 29% for **70** over two steps with >99% *ee* for the enzymatic kinetic resolution step (Table 6, Entry 1). The absolution configuration of the stereocenter was determined by comparison of optical rotation values of subsequent intermediates with known compounds.

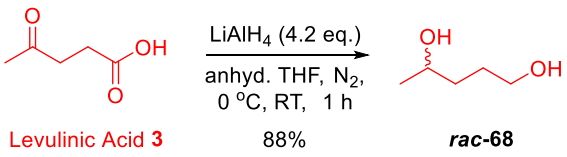

Scheme 27: Complete reduction of levulinic acid **3** to diol ***rac*-68**

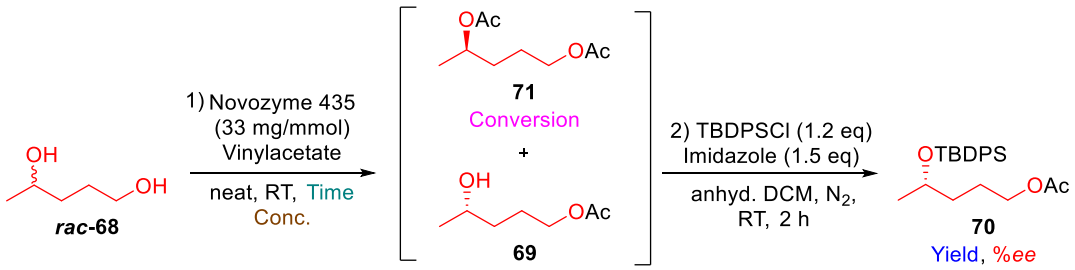

Entry	Conc.	Time	Conv.[1]	Yield[2]	%*ee*
1	3.3 M	5 h	62%	29%[3]	>99%
2	1.0 M	3 h	50%	46%	95%
3	3.3 M	3 h	50%	45%	94%
4	3.3 M	3.5 h	54%	42%	>99%
5	3.3 M	4 h	54%	43%	>99%
6[4]	3.3 M	3.5 h	57%	40%	>99%

[1] Determined using NMR based on ratio of products
[2] Isolated yield over 2 steps [3] With isolation of **69**
[4] 5 mmol scale

Table 6: Optimization of enzymatic kinetic resolution of diol ***rac*-68**

Reducing the reaction concentration and duration helped to reduce the rate of reaction, leading to a decrease of conversion to 50% but at the expense of *ee* of product obtained (Table 6, Entries 2 and 3). Hence, we decided to allow for slightly higher conversion (Table 6, Entries 4 and 5) in order to secure the accompanying excellent stereoselectivity and gratifyingly, we were able to furnish enantioenriched **70** in 40% yield out of the theoretical maximum of 50% over 2 steps with excellent *ee* of >99% (Table 6, Entry 6). All that remains now would be the hydrolysis of the primary acetate moiety in **70** with an almost quantitative yield to afford enantioenriched primary alcohol **51** which was then efficiently converted to the desired alkyl iodide **52** in a similar fashion as the racemic synthesis (Scheme 28). This completes the synthesis of enantioenriched fragment A **52** which could be later employed in the micellar Negishi coupling under the previously optimized reaction conditions.

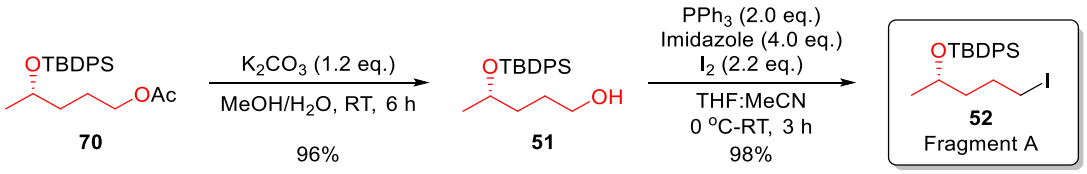

Scheme 28: Completion of the synthesis of enantioenriched fragment A **52**

At the same time we were interested in accessing **71** in high yield and enantioselectivity so that the corresponding enantiomer of fragment A could be obtained if necessary. Since **71** is the product of the more reactive enantiomer of **69**, we decided to investigate the dynamic enzymatic kinetic resolution[149] of ***rac*-68**. The use of a ruthenium racemization catalyst would racemize the less reactive **69** during the reaction so that the theoretical yield of the reaction is increased to 100% instead of being restricted to only 50% in the enzymatic kinetic resolution.

Initial attempts using conditions similar to reported conditions[149] gave the desired diacetate **71** with moderate conversion but low *ee* (Table 7, Entry 1). Enantiomeric excess was determined by chiral HPLC after deprotecting a small sample of diacetate **71** to give enantioenriched diol **68** and then reprotected with UV-active benzoyl (Bz) protecting groups. Increasing the reaction temperature helped to improve conversion but *ee* remained poor and increasing catalyst loading only improved *ee* slightly (Table 7, Entries 2 and 3). Slight amounts of ketone **72** were also detected as a by-product and its occurrence could probably to the reaction of ruthenium-hydride intermediate with acetone which originates from acetylation partner, isopropenyl acetate.

Fortunately, by decreasing the amount of enzymes employed, the enantioselectivity improved significantly to 91% with high conversion (Table 7,

[149] a) Kim, N.; Ko, S.-B.; Kwon, M.-S.; Kim, M.-J.; Park, J. *Org. Lett.*, **2005**, *7*, 4523-4526; b) Hoyos, P.; Pace, V.; Alcántara, A. R. *Adv. Synth. Catal.* **2012,** *354*, 2585-2611; c) Verho, O.; Bäckvall, J.-E. *J. Am. Chem. Soc.* **2015,** *137*, 3996-4009.

Entry 4). The optimal result was obtained by lowering the enzyme loading to 0.5 mg/mmol of substrate (Table 7, Entry 5) and **71** could be generated in 91% NMR yield, 85% isolated yield and 93% *ee*. Further reduction of enzyme loading led to poorer results (Table 7, Entry 6).

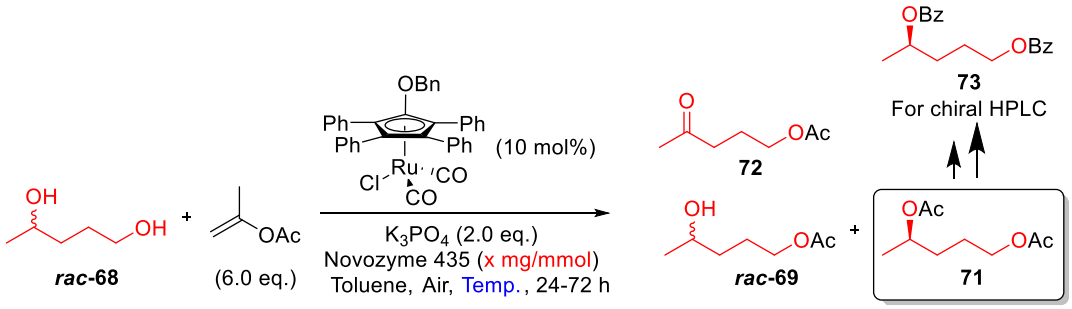

Entry	x	Temp.	Yield[1] of ***rac*-69**	Yield[1] of ***rac*-71**	*ee* of ***rac*-71**	Yield[1] of **72**
1	4	RT	(24%)	(75%)	35%	trace
2	4	50 °C	(5%)	(90%)	33%	(5%)
3[2]	4	50 °C	(5%)	(90%)	37%	(5%)
4	1	50 °C	(4%)	(90%)	91%	(4%)
5	0.5	50 °C	(0%)	(91%)[3]	93%	(9%)
6	0.2	50 °C	(5%)	(76%)	88%	(19%)

[1]NMR yields determined with nitrobenzene as internal standard and are shown in parenthesis
[2]15 mol% catalyst was used
[3]Isolated yield: 85%

Table 7: Optimization of dynamic enzymatic kinetic resolution to access enantiomer

In summary, enantioenriched alkyl iodide fragment A **52** could be synthesized from biomass derived platform chemical levulinic acid **3** *via* a complete reduction, enzymatic kinetic resolution, TBDPS protection, hydrolysis and iodination (Scheme 29). The optimization of the dynamic enzymatic kinetic resolution of ***rac*-68** to access **71** in high yield and enantioselectivity was also carried out to facilitate access to the other enantiomer of fragment A.

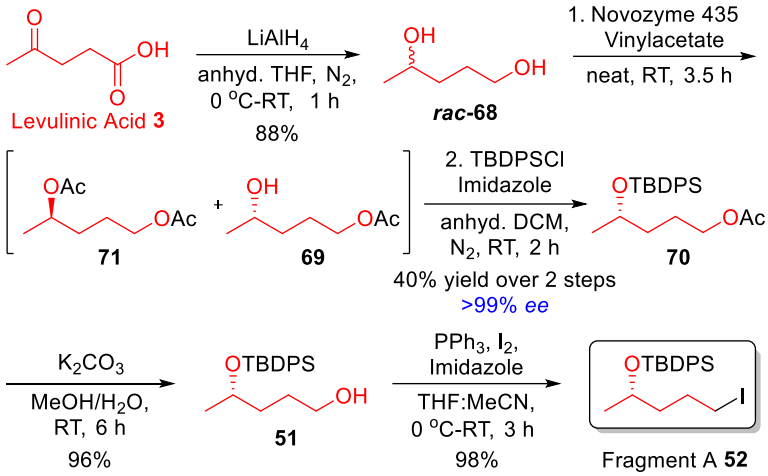

Scheme 29: Overview of the synthesis of enantioenriched fragment A **52**

3.2.5 Synthesis of enantioenriched fragment B

Benzylated HMF **53** was subjected to several Mukaiyama Aldol methodologies that our group has developed previously[142a,b]. Using several types of chiral PyBOX ligands together with the TBS ketene silyl acetal (KSA), low conversion of less than 50% was observed together with 2 other side products (Table 8, Entries 1, 2 and 3). While **74** was the expected product of the reaction, **75** and **76** were probably formed from the hydrolysis of the *tert*-butyl ester and TBS protecting group. Due to the poor product selectivity and yields, the enantioselectivity of the products were not determined. Another condition involved the use of $InBr_3$ as Lewis acid and $AgSbF_6$ as additive but under these reaction conditions trace or no products were detected and the starting material could be recovered (Table 8, Entries 4, 5 and 6). Several attempts involving iron catalysis and chiral Bolm's ligand[142c,d] in aqueous media were also investigated but no products were could be detected.

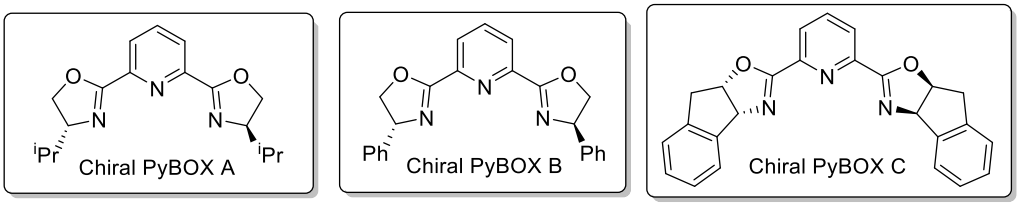

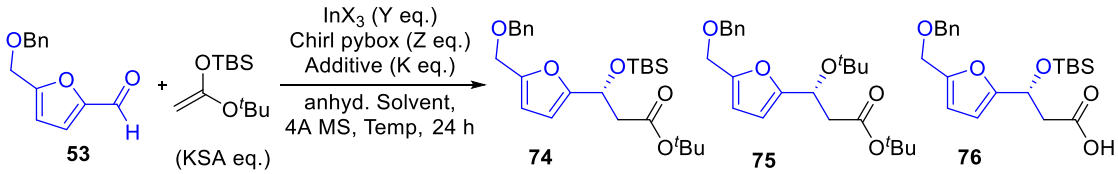

Entry	KSA	InX_3	Y eq.	PyBOX	Z eq.	Additive	K eq.	Solvent	Temp	SM[1]	**74**[1]	**75**[1]	**76**[1]
1	1.2	$In(OTf)_3$	0.20	A	0.22	-	-	DCM	-40 °C	40%	25%	6%	15%
2	1.2	$In(OTf)_3$	0.20	B	0.22	-	-	DCM	-40 °C	37%	30%	7%	16%
3	1.2	$In(OTf)_3$	0.20	C	0.22	-	-	DCM	-40 °C	48%	23%	6%	14%
4	1.5	$InBr_3$	0.05	A	0.06	$AgSbF_6$	0.05	MeCN	-20 °C	87%	1%	-	-
5	1.5	$InBr_3$	0.05	B	0.06	$AgSbF_6$	0.05	MeCN	-20 °C	100%	-	-	-
6	1.5	$InBr_3$	0.05	C	0.06	$AgSbF_6$	0.05	MeCN	-20 °C	90%	-	-	-

[1] Isolated yields

Table 8: Asymmetric Mukaiyama Aldol reaction using Indium-PyBOX systems

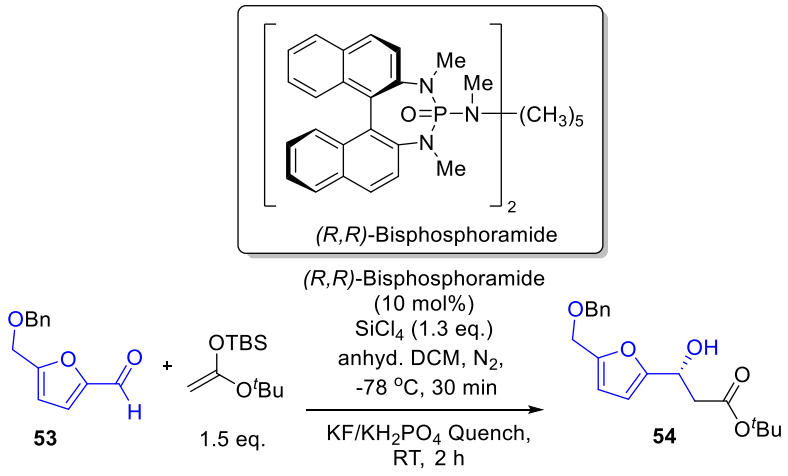

Entry	change from above	SM[1]	Yield[2]	%*ee*
1	as shown above	none	67%	71%
2	O-TMS KSA	none	84%	59%
3	with TBAI (20 mol%)	4%	67%	73%
4	anhyd. THF	6%	76%	22%
5	anhyd. ether	25%	58%	22%

[1]NMR yield based on internal standard [2]Isolated yield

Table 9: Asymmetric Mukaiyama Aldol reaction using chiral bisphosphoramide

Employing Denmark's chiral Lewis base activation of Lewis acid[142e] for the asymmetric Mukaiyama Aldol reaction offered an initial promising result of 67% yield and 71%*ee* (Table 9, Entry 1). However, subsequent attempts at optimization did not lead to any significant improvement of the results (Table 9, Entries 2-5) and we had to alter our approach to the construction of the desired stereocenter.

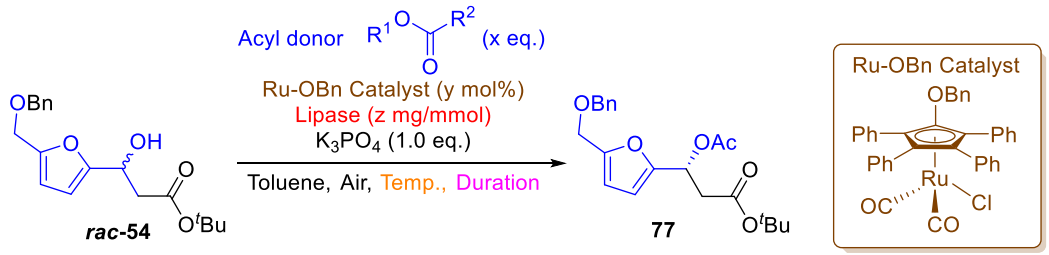

Entry	Acyl donor (x)	(y)	Lipase (z)	Temp.	Duration	Pdt Yield[1]	Pdt %*ee*	SM Yield[1]
1	IPA (1.5)	4	N435 (8)	RT	109 h	(2%)	N.D.[4]	(95%)
2	IPA (1.5)	4	CAL-B (8)	RT	109 h	(3%)	N.D.[4]	(97%)
3	IPA (1.5)	4	N435 (32)	RT	109 h	(6%)	N.D.[4]	(94%)
4	IPA (1.5)	4	CAL-B (32)	RT	109 h	(8%)	N.D.[4]	(92%)
5	IPA (1.5)	-[2]	N435 (8)	RT	72 h	(1%)	N.D.[4]	(99%)
6	IPA (1.5)	-[2]	CAL-B (8)	RT	72 h	(1%)	N.D.[4]	(99%)
7	IPA (1.5)	4	N435 (200)	RT	69 h	7%	40%	86%
8	IPA (1.5)	4	CAL-B(200)	RT	69 h	10%	40%	81%
9	IPA (1.5)	4	N435 (200)	60 °C	69 h	30%	36%	59%
10	IPA (1.5)	4	CAL-B(200)	60 °C	69 h	27%	36%	58%
11	VB (1.5)	4	N435 (200)	RT	120 h	(1%)	N.D.[4]	(97%)
12	VA (1.5)	4	N435 (200)	RT	120 h	(1%)	N.D.[4]	(97%)
13	VB (5.0)	4	N435 (200)	RT	120 h	(1%)	N.D.[4]	(98%)
14	VB (1.5)	4[3]	N435 (200)	RT	120 h	(1%)	N.D.[4]	(97%)
15	VB (1.5)	15	N435 (200)	RT	120 h	(1%)	N.D.[4]	(96%)
16	VA (1.5)	4	Lipase PS (200)	RT	70 h	(5%)	36%	(95%)
17	IPA (1.5)	4	Lipase PS (200)	RT	70 h	(7%)	N.D.[4]	(93%)
18	VB (5.0)	4	Lipase PS (200)	RT	70 h	(3%)	N.D.[4]	(97%)
19	VB (1.5)	4	Lipase PS (200)	70 °C	70 h	(15%)	N.D.[4]	(79%)

[1] Isolated Yields, NMR Yields shown in parenthesis using nitrobenzene as internal standard
[2] No Ru catalyst and K_3PO_4, reaction in TBME [3] 2.0 eq. of K_3PO_4 used [4] Not determined

Vinyl Acetate (VA): R^1 = Vinyl, R^2 = Me
Isopropenyl Acetate (IPA): R^1 = Isopropenyl, R^2 = Me
Vinyl Butyrate (VB): R^1 = Vinyl, R^2 = ^{n}Pr

N435: Novozyme 435
CAL-B: Lipase from Candida antarctica immobilised on acrylic resin
Lipase PS: Lipase from Pseudomonas Cepacia

Table 10: Dynamic enzymatic kinetic resolution optimizations of ***rac*-54**

In view of the relative success of the dynamic enzymatic kinetic resolution of secondary alcohol ***rac*-68**, we decided to explore the same reaction for secondary alcohol ***rac*-54** in an attempt to access enantioenriched **54**. Preliminary results for the reaction were not encouraging as varying amounts of enzymes and racemization catalyst did not result in more than 10% conversion even after extended durations (Table 10, Entries 1-6). Significant increase in enzyme loading and temperature were required for noticeable improvement in conversion but both yield and enantioselectivity were still poor (Table 10, Entries 7-10). Changing to other acyl donors like vinyl acetate and vinyl butyrate did not offer appreciable conversion as well (Table 10, Entries 10-15). Finally, another source of lipase was employed and poor conversion continued to plague the reaction (Table 10, Entries 16-19). We speculate that the sluggish conversion of the secondary alcohol ***rac*-54** to be due to the bulky substituents which may not offer a good fit into the active site of the lipases.

Eventually, we decided to oxidize the secondary alcohol ***rac*-54** to the corresponding *β*-ketoester **78** and a good yield of 86% was obtained (Scheme 30). It was observed that **78** exists as a mixture of keto and enol forms in the ratio 93:7. Next, we employed Noyori's asymmetric transfer hydrogenation[150] to *β*-ketoester **78** and we were heartened to obtain excellent results in terms of both yields and enantioselectivities (Table 11). Acetonitrile (ACN) exhibited better performance than DCM and an excellent yield of 99% and 98% *ee* was achieved (Table 11, Entries 1 and 2). Increasing reaction temperature as well as conducting the reaction under inert conditions did not generate better results (Table 11, Entries 3-5).

[150] a) Fujii, A.; Hashiguchi, S.; Uematsu, N.; Ikariya, T.; Noyori, R. *J. Am. Chem. Soc.* **1996,** *118*, 2521-2522; b) Noyori, R.; Hashiguchi, S. *Acc. Chem. Res.* **1997,** *30*, 97-102; c) Tietze, Lutz F.; Zhou, Y.; Töpken, E. *Eur. J. Org. Chem.* **2000**, 2247-2252; d) Everaere, K.; Mortreux, A.; Carpentier, J.-F. *Adv. Synth. Catal.* **2003,** *345*, 67-77; e) Liu, P. N.; Gu, P. M.; Wang, F.; Tu, Y. Q. *Org. Lett.* **2003,** *6*, 169-172; f) Ishikawa, S.; Hamada, T.; Manabe, K.; Kobayashi, S. *Synthesis* **2005**, 2176-2182; g) Gladiali, S.; Alberico, E. *Chem. Soc. Rev.* **2006,** *35*, 226-236.

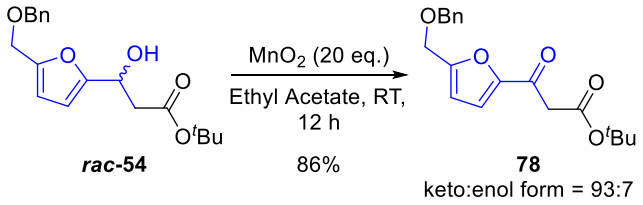

Scheme 30: Oxidation of secondary alcohol ***rac*-54**

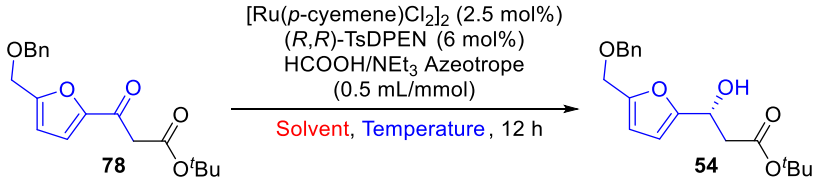

Entry	Solvent	Temperature	Yield[1]	%*ee*
1	DCM	RT	89%[2]	97%
2	ACN	RT	99%	98%
3	DCM	40 °C	99%	94%
4	ACN	40 °C	98%	96%
5[3]	ACN	RT	98%	98%

[1] Isolated Yields [2] 10% SM remaining [3] Inert conditions

Table 11: Optimization of Noyori's asymmetric transfer hydrogenation

We also investigated the asymmetric transfer hydrogenation in aqueous media[151] and the reaction at room temperature was found to be slower, affording 87% yield after 17 hours and a lower enantioselectivity of 91% (Table 12, Entry 1). Increasing the reaction temperature increased the rate and yield of the reaction but at the expense of lower enantioselectivity (Table 12, Entry 2). Switching the rhodium catalyst afforded better yield and enantioselectivity but the results were unable to match those conducted in acetonitrile (Table 12, Entry 3).

[151] a) Wu, X.; Li, X.; Hems, W.; King, F.; Xiao, J. *Org. Biomol. Chem.* **2004,** *2*, 1818-1821; b) Wu, X.; Li, X.; Zanotti-Gerosa, A.; Pettman, A.; Liu, J.; Mills, A. J.; Xiao, J. *Chem. Eur. J.* **2008,** *14*, 2209-2222.

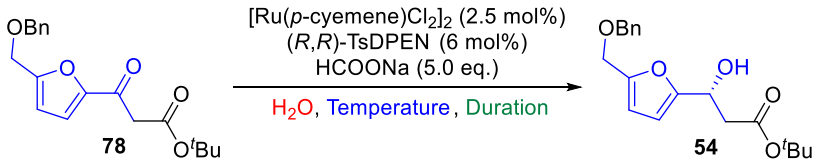

Entry	Temperature	Duration	Yield[1]	%*ee*
1	RT	17 h	87%	91%
2	40 °C	5 h	92%	89%
3[2]	40 °C	2 h	97%	93%

[1] Isolated Yields. [2] [Cp*RhCl$_2$]$_2$ was used instead.

Table 12: Optimization of asymmetric transfer hydrogenation in aqueous media

With the completion of the synthesis of enantioenriched furfuryl alcohol **54**, **54** was carried through the synthetic route devised in the racemic synthesis without any complications. Achmatowicz rearrangement reaction/triple reduction sequence followed by protection, hydrogenation, Swern oxidation and Takai iodoolefination furnished enantioenriched *E*-vinyl iodide fragment B **64-*E*** (Scheme 31).

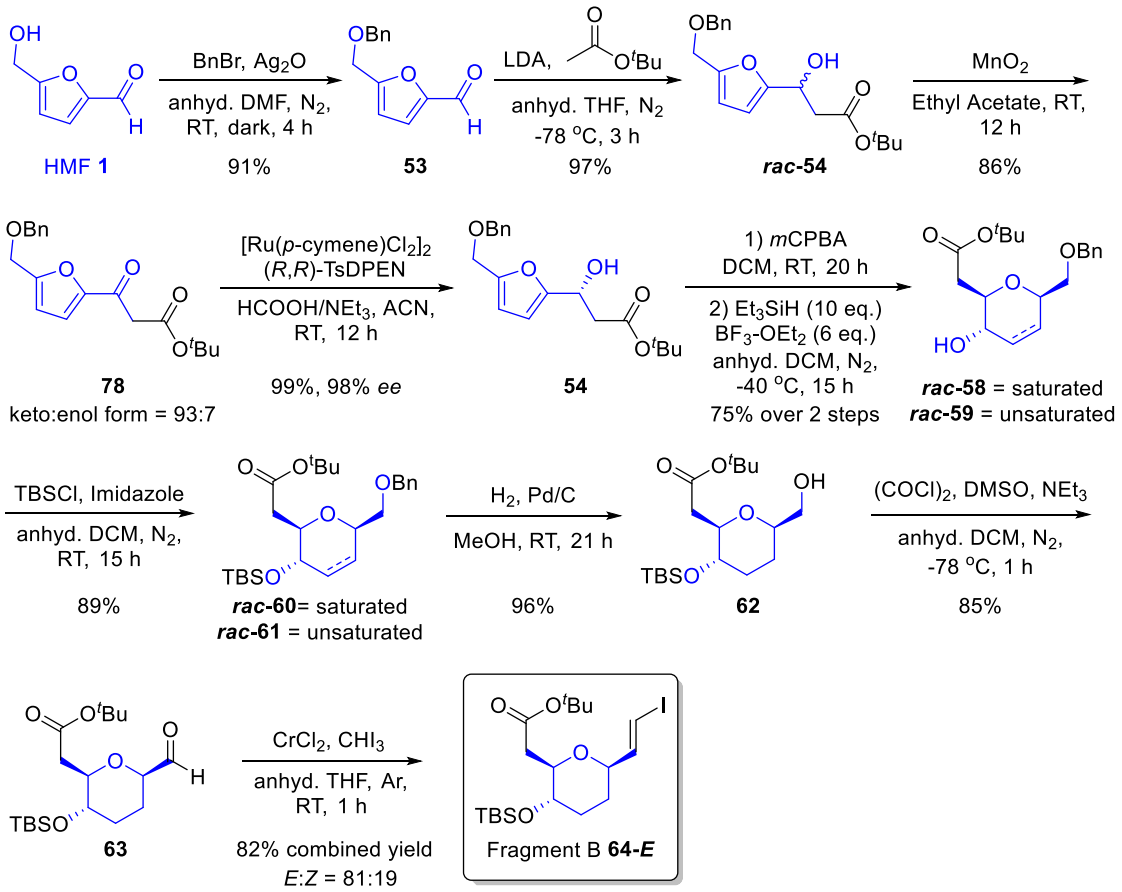

Scheme 31: Overview of the synthesis of enantioenriched fragment B **64-*E***

3.2.6 Completion of enantioenriched synthesis

Subjecting enantioenriched fragment A **52** and fragment B **64-*E*** to Lipshutz's micellar Negishi coupling afforded enantioenriched coupling product **65** (Scheme 32). TBS deprotection using tetrabutylammonium fluoride (TBAF) and MOM protection gave **67** which could be hydrolyzed under basic condition to furnish enantioenriched seco acid **41**. As seco acid **41** has been reported as a synthetic intermediate to access both aspergillides A **37** and B **38**, this completes the formal synthesis of these 2 biologically active natural products from biomass derived platform chemicals.

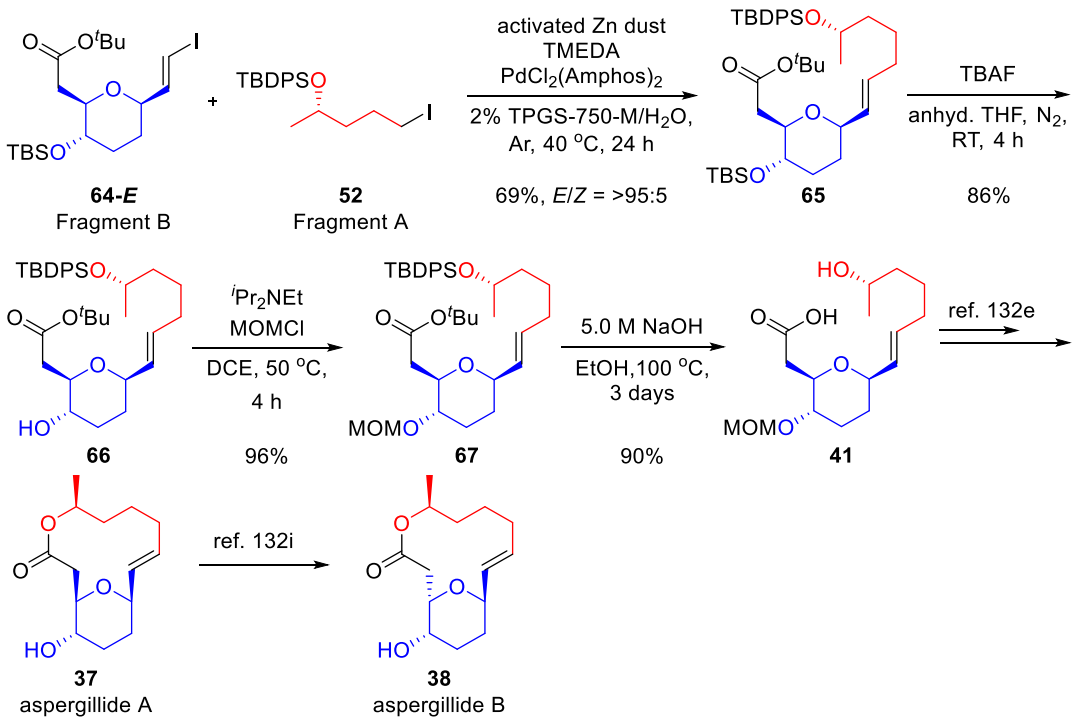

Scheme 32: Formal synthesis of enantioenriched aspergillide A **37** and B **38**

3.3 Conclusions

In conclusion, we achieved the formal synthesis of biologically active natural products aspergillides A and B using biomass derived platform chemicals[152]. The synthesis was planned and executed such that all the carbon atoms present in aspergillides A and B originated from biomass derived platform chemicals. Various optimizations were discussed and several adjustments were made to the original proposed route to complete this synthesis. The key steps include an asymmetric transfer hydrogenation reaction, a novel Achmatowicz rearrangement/triple reduction sequence, application of micellar Negishi coupling on an advanced synthetic intermediate for the first time as well as enzymatic kinetic resolutions to access both enantiomers of fragment A. The long linear sequence involved a total of 14 steps and the reported pre-cursor **41** to aspergillides A and B could be obtained in 14% yield

[152] Koh, P.-F.; Loh, T.-P. *Green Chem.* **2015,** *17*, 3746-3750.

from biomass platform chemicals HMF and levulinic acid. Together, this synthesis sets a precedent for the construction of biologically active natural products entirely from biomass platform chemicals.

3.4 Experimentals

3.4.1 General Methods

All reagents were commercially purchased and were used as received for the reactions. All reactions were carried out in oven-dried glassware while THF was freshly distilled from Na/Benzophenone ketyl and DCM was freshly distilled from Calcium Hydride. Thin-layer chromatography (TLC) was conducted with Merck 60 F254 precoated silica gel plate (0.2 mm thickness) and visualized under UV, by potassium permanganate or ceric ammonium molybdate stain. Flash chromatography was performed using Merck silica gel 60 with distilled solvents. ^{1}H-NMR spectra were performed on a Bruker Avance 300, Bruker Avance 400 or Bruker Avance 500 NMR spectrometer and are reported in ppm downfield from $SiMe_4$ (δ 0.0), relative to the signal of chloroform-d (δ = 7.26, singlet) or methanol-d_4 (δ = 3.31, quintet). Data reported as: s = singlet, d = doublet, t = triplet, q = quartet, m = multiplet, b = broad; coupling constant(s) in Hz; integration. Proton-decoupled ^{13}C-NMR spectra were recorded on Bruker Avance 300 (75 MHz) or Bruker Avance 400 (100MHz) or Bruker Avance 500 (125 MHz) spectrometer and are reported in ppm using solvent as an internal standard ($CDCl_3$ at 77.16 ppm or CD_2Cl_2 at 53.84 ppm). IR spectra were recorded using nujol mull technique for solids and recorded neat (or a concentrated solution of $CHCl_3$) for liquids on NaCl plates on a Shimadzu IRPrestige-21 FT-IR Spectrophotometer were reported in frequency of absorption (cm^{-1}). High-resolution

mass spectral analysis (HRMS) was performed on Q-Tof Premier mass spectrometer (Waters Corporation).

3.4.2 Synthesis and characterization of compounds

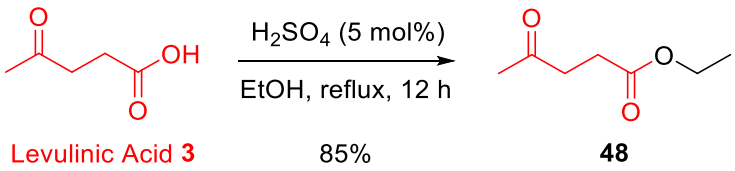

Ethyl 4-oxopentanoate (48)

To an oven-dried 250 mL round-bottomed flask was added a stir bar, levulinic acid **3** (1.00 g, 8.6 mmol, 1.0 equiv.) and ethanol (88 mL). 98% sulfuric acid (23 μL, 42.3 mg, 0.43 mmol, 5 mol%) was added and the mixture was refluxed for 12 h. The mixture was cooled to room temperature, quenched with saturated aqueous $NaHCO_3$ solution (3 mL), diluted with H_2O (10 mL), and concentrated under reduced pressure. The residual crude was extracted with diethyl ether, washed with brine, dried over anhydrous $MgSO_4$, filtered and concentrated under reduced pressure to afford **48** as a pale yellow oil (1.05 g, 7.3 mmol, 85%). TLC (hexanes/ethyl acetate = 4:1): R_f = 0.38; ^{1}H NMR (300 MHz, $CDCl_3$) δ (ppm): 4.13 (q, J = 7.2 Hz, 2H), 2.75 (t, J = 6.5 Hz, 2H), 2.57 (t, J = 6.5 Hz, 2H), 2.20 (s, 3H), 1.26 (t, J = 7.1 Hz, 3H); ^{13}C NMR (75 MHz, $CDCl_3$) δ (ppm): 206.8, 172.9, 60.7, 38.1, 30.0, 28.1, 14.3; FTIR (neat, NaCl, cm^{-1}): 2984, 1732, 1715; HRMS (ESI) *m/z* Calculated for $C_7H_{12}O_3Na$ $[M+Na]^+$: 167.0684; found: 167.0690.

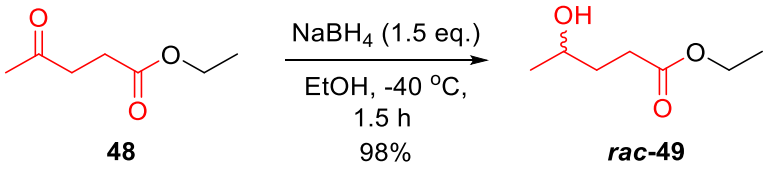

Ethyl 4-hydroxypentanoatee (*rac*-49)

An oven-dried 250 mL round bottom flask equipped with a stir bar was charged with **48** (2.48 g, 17.2 mmol, 1.0 equiv.) and ethanol (85 mL) before cooling down to -40 °C. $NaBH_4$ (976 mg, 25.8 mmol, 1.5 equiv.) was added portionwise under N_2 and the mixture was allowed to stir at -40 °C under N_2 for 1.5 h. The reaction was quenched with the addition of aqueous saturated NH_4Cl (20 mL) and the mixture concentrated under reduced pressure before water (50 mL) and EA (100 mL) were added. The mixture was extracted with EA (30 mL x 3), washed with brine (30 mL) and dried over anhydrous $MgSO_4$. Filtration and concentration under reduced pressure gave the crude product which was purified using silica gel chromatography (Hex/EA = 2:1) to give ***rac*-49** as a pale yellow oil (2.47 g, 16.9 mmol, 98%). TLC (Hexane/Ethyl Acetate = 2:1): R_f = 0.33; ^1H NMR (400 MHz, $CDCl_3$) δ (ppm): 4.14 (q, *J* = 7.1 Hz, 2H), 3.88-3.81 (m, 1H), 2.44 (t, *J* = 7.3 Hz, 2H), 1.86-1.69 (m, 3H), 1.26 (t, *J* = 7.1 Hz, 3H), 1.22 (d, *J* = 6.2 Hz, 3H); ^{13}C NMR (125 MHz, $CDCl_3$) δ (ppm): 174.3, 67.5, 60.6, 34.0, 30.9, 23.6, 14.3; FTIR (DCM, NaCl, cm^{-1}): 3402, 2970, 1732; HRMS (ESI) *m/z* Calculated for $C_7H_{14}O_3Na$ $[M+Na]^+$: 169.0841, found: 169.0840.

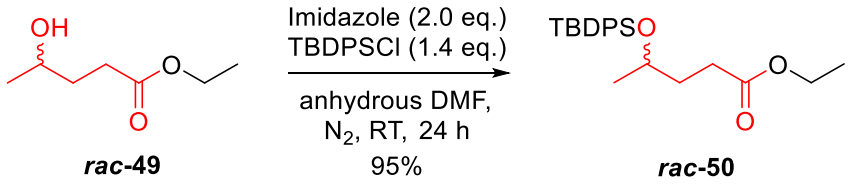

Ethyl 4-((tert-butyldiphenylsilyl)oxy)pentanoate (*rac*-50)

An oven-dried 25 mL round bottom flask equipped with a stir bar was charged with ***rac*-49** (1.00 g, 6.86 mmol, 1.0 equiv.) and anhydrous DMF (7.0 mL) before imidazole (933 mg, 13.7 mmol, 2.0 equiv.) and TBDPSCl (2.5 mL, 2.64 g, 9.60 mmol, 1.4 equiv.) was added sequentially with stirring. The mixture was allowed to stir at room temperature under N_2 for 24 h before quenching with aqueous saturated NH_4Cl (10 mL). The mixture was extracted with ether (25 mL x 3), washed with water (25 mL x 5), brine (25 mL) and dried over anhydrous $MgSO_4$. Filtration and concentration under reduced pressure gave the crude product which was purified using silica gel chromatography (Hex/EA = 50:1 to 10:1) to give ***rac*-50** as a pale yellow oil (2.51 g, 6.54 mmol, 95%). TLC (Hexane/Ethyl Acetate = 10:1): R_f = 0.46; ^{1}H NMR (400 MHz, $CDCl_3$) δ (ppm): 7.68-7.66 (m, 4H), 7.43-7.35 (m, 6H), 4.08 (q, J = 7.1 Hz, 2H), 3.93-3.89 (m, 1H), 2.44-2.31 (m, 2H), 1.81-1.76 (m, 2H), 1.23 (t, J = 7.1 Hz, 3H), 1.05 (s, 9H), 1.03 (d, J = 6.2 Hz, 3H); ^{13}C NMR (100 MHz, $CDCl_3$) δ (ppm): 174.0, 136.0, 136.0, 134.8, 134.3, 129.7, 129.6, 127.7, 127.6, 68.8, 60.4, 34.3, 30.2, 27.2, 23.2, 19.4, 14.4; FTIR (DCM, NaCl, cm^{-1}): 3071, 2965, 1962, 1890, 1825, 1732, 1589; HRMS (ESI) *m/z* Calculated for $C_{23}H_{33}O_3Si$ $[M+H]^+$: 385.2199, found: 385.2183.

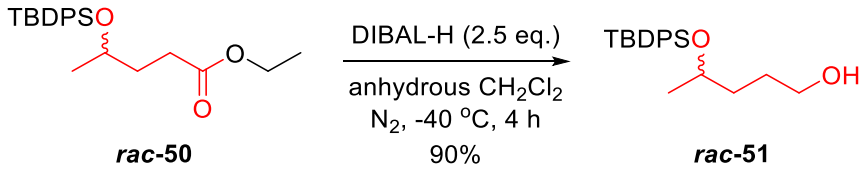

4-((Tert-butyldiphenylsilyl)oxy)pentan-1-ol (*rac*-51)

An oven-dried 50 mL round bottom flask equipped with a stir bar was charged with ***rac*-50** (1.98 g, 5.15 mmol, 1.0 equiv.) and anhydrous DCM (17 mL) before cooling down to -40 °C. DIBAL-H (13 mL, 1.0 M solution in heptane, 12.9 mmol, 2.5 equiv.) was added dropwise under N_2 and the mixture was allowed to stir at -40 °C under N_2 for 1 h. The reaction was quenched with the addition of aqueous saturated potassium sodium tartrate solution (10 mL) and water (10 mL), and the mixture stirred at RT for 1 h before the layers were separated. The aqueous layer was extracted with DCM (20 mL x 3), washed with saturated NH_4Cl solution (15 mL), brine (15 mL) and dried over anhydrous $MgSO_4$. Filtration and concentration under reduced pressure gave the crude product which was purified using silica gel chromatography (Hex/EA = 4:1) to give ***rac*-51** as a pale yellow oil (1.59 g, 4.65 mmol, 90%). TLC (Hexane/Ethyl Acetate = 2:1): R_f = 0.59; ^{1}H NMR (500 MHz, $CDCl_3$) δ (ppm): 7.68-7.67 (m, 4H), 7.42-7.41 (m, 2H), 7.38-7.35 (m, 4H), 3.91 (dq, J = 11.6 Hz, 6.0 Hz, 1H), 3.55-3.53 (m, 2H), 1.60-1.56 (m, 3H), 1.52-1.50 (m, 2H), 1.07 (d, J = 6.5 Hz, 3H), 1.05 (s, 9H); ^{13}C NMR (100 MHz, $CDCl_3$) δ (ppm): 136.0, 136.0, 134.8, 134.4, 129.7, 129.7, 127.7, 127.6, 69.4, 63.2, 35.7, 28.4, 27.2, 23.0, 19.4; FTIR (DCM, NaCl, cm^{-1}): 3361, 3070, 2932, 1589, 1427, 1367, 1111; HRMS (ESI) *m/z* Calculated for $C_{21}H_{31}O_2Si$ $[M+H]^+$: 343.2093, found: 343.2104.

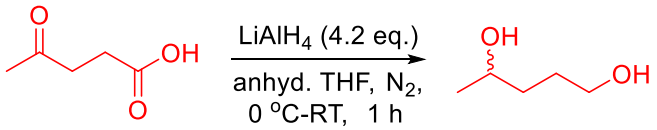

Levulinic Acid **3** 88% ***rac*-68**

Pentane-1,4-diol (*rac*-68)[153]

To an oven-dried, vacuum cooled 250 mL round-bottom flask equipped with a stir bar was added levulinic acid **3** (2.0 mL, 2.29 g, 19.7 mmol, 1.0 equiv.) and anhydrous THF (20 mL) under N_2 atmosphere. The solution was cooled down to 0 °C before $LiAlH_4$ (39.5 mL, 2.0 M solution in THF, 79 mmol, 4.0 equiv.) was slowly added dropwise to give initial effervescence and then a white suspension. After addition, the mixture was allowed to warm to room temperature and allowed to stir at RT for an additional 1 h to give an almost clear solution. The mixture was cooled down to 0 °C and H_2O (3.1 mL) was slowly added dropwise, followed by addition of aqueous NaOH (3.1 mL, 15 wt%, 3.75 M) and finally H_2O (9.2 mL) to give a white suspension after stirring at room temperature for another 1 h. The suspension was filtered through a pad of celite, washed with ethyl acetate and dried over anhydrous $MgSO_4$ before being filtered and concentrated under reduced pressure. Purification using silica gel chromatography (eluent: ethyl acetate) afforded ***rac*-68** as a colourless oil (1.81 g, 17.4 mmol, 88%). TLC (Ethyl Acetate): R_f = 0.23; ^{1}H NMR (400 MHz, $CDCl_3$) δ (ppm): 3.90-3.82 (m, 1H), 3.73-3.63 (m, 2H), 2.48 (bs, 1H), 2.36 (bs, 1H), 1.69-1.47 (m, 4H), 1.22 (d, *J* = 6.2 Hz, 3H); ^{13}C NMR (125 MHz, $CDCl_3$) δ (ppm): 68.1, 63.1, 36.4, 29.3, 23.8; FTIR (neat, NaCl, cm^{-1}): 3306, 2932, 1454, 1373, 1134; HRMS (ESI) *m/z* Calculated for $C_5H_{13}O_2$ $[M+H]^+$: 105.0916; found: 105.0921.

[153] (*R*)-pentan-1,4-diol: Killen, J. C.; Axford, L. C.; Newberry, S. E.; Simpson, T. J.; Willis, C. L. *Org. Lett.* **2012,** *14*, 4194-4197.

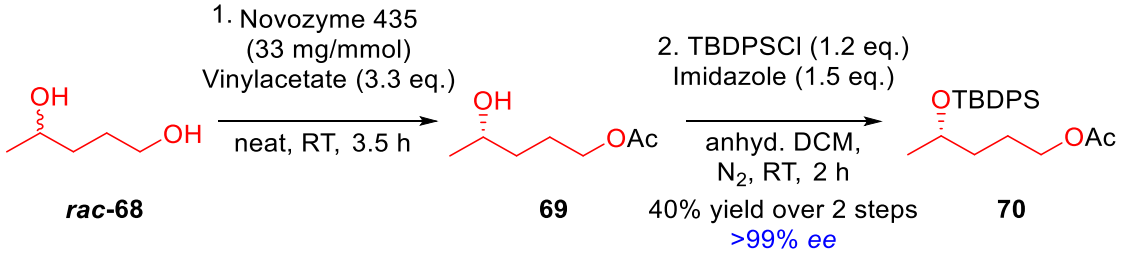

***rac*-68** **69** **70**

(*S*)-4-hydroxypentyl acetate (69)

To a 25 mL round-bottom flask equipped with a stir bar was added pentane-1,4-diol ***rac*-68** (1.80 g, 17.3 mmol, 1.0 equiv.) and vinylacetate (5.3 mL, 4.91 g, 57.1 mmol, 3.3 equiv.) before Novozyme 435 (571 mg, 33 mg/mmol) was added. The suspension was allowed to stir at RT for 3.5 h before filtering through a pad of celite, washed with ethyl acetate and concentrated under reduced pressure to afford a crude mixture which is immediately used in the subsequent step without further purification.

Alternatively the crude mixture can be purified using silica gel chromatography (eluent: hexanes/ethyl acetate = 2:1) to afford **69** as a colourless oil. TLC (hexanes/ethyl acetate = 2:1): R_f = 0.13; $[\alpha]^{23}_D$ = +13.4 (c = 1.49, $CHCl_3$); ^{1}H NMR (400 MHz, $CDCl_3$) δ (ppm): 4.09 (t, *J* = 6.6 Hz, 2H), 3.84 (sextet, *J* = 6.2 Hz, 1H), 2.05 (s, 3H), 1.78-1.67 (m, 3H), 1.54-1.48 (m, 2H), 1.21 (d, *J* = 6.2 Hz, 3H); ^{13}C NMR (100 MHz, $CDCl_3$) δ (ppm): 171.4, 67.5, 64.6, 35.4, 25.0, 23.6, 21.0; FTIR (neat, NaCl, cm^{-1}): 3426, 2967, 1736, 1454, 1368, 1140; HRMS (ESI) *m/z* Calculated for $C_7H_{15}O_3$ $[M+H]^+$: 147.1021; found: 147.1017.

(*S*)-4-((*tert*-butyldiphenylsilyl)oxy)pentyl acetate (70)

To the crude mixture obtained above in a 50 mL round-bottom flask equipped with a stir bar was added anhydrous CH_2Cl_2 (18 mL) under N_2 atmosphere. Imidazole (882 mg, 13.0 mmol, 1.5 equiv. with respect to 50% conversion) was then added at RT and stirred to achieve complete dissolution before *tert*-butyl(chloro)diphenylsilane

(2.7 mL, 2.85 g, 10.4 mmol, 1.2 equiv. with respect to 50% conversion) was added. The mixture was allowed to stir at room temperature for 2 h before saturated aqueous NH_4Cl (10 mL) was added and the layers were separated. The aqueous phase was extracted with CH_2Cl_2 (10 mL x 3) and the combined organic phase washed with brine (10 mL), dried over anhydrous $MgSO_4$ before being filtered and concentrated under reduced pressure. Purification using silica gel chromatography (eluent: hexanes/ethyl acetate = 50:1) to afford **70** as a colourless oil (2.66 g, 6.92 mmol, 40% over 2 steps out the theoretical maximum of 50%), *ee* = >99%. The *ee* was determined on Chiralcel OJ column with hexane/2-propanol = 100:0, flow = 0.5 mL/min, wavelength = 220 nm. Retention times: 10.1 min [(*R*)-enantiomer], 17.4 min [(*S*)-enantiomer]. TLC (hexanes/ethyl acetate = 2:1): R_f = 0.69; $[\alpha]^{21}_D$ = -12.9 (c = 2.11, $CHCl_3$); ^{1}H NMR (400 MHz, $CDCl_3$) δ (ppm): 7.68-7.66 (m, 4H), 7.44-7.35 (m, 6H), 3.96 (t, *J* = 6.6 Hz, 2H), 3.88 (sextet, *J* = 5.9 Hz, 1H), 2.01 (s, 3H), 1.65-1.61 (m, 2H), 1.50-1.46 (m, 2H), 1.06 (d, *J* = 6.2 Hz, 3H), 1.05 (s, 9H); ^{13}C NMR (125 MHz, $CDCl_3$) δ (ppm): 171.3, 136.0, 136.0, 134.9, 134.5, 129.7, 129.6, 127.7, 127.6, 69.2, 64.8, 35.7. 27.2, 24.4, 23.2, 21.1, 19.4; FTIR (neat, NaCl, cm^{-1}): 3071, 2961, 1740, 1589, 1427, 1363, 1111;HRMS (ESI) *m/z* Calculated for $C_{23}H_{32}NaO_3Si$ $[M+Na]^+$: 407.2018; found: 407.2023.

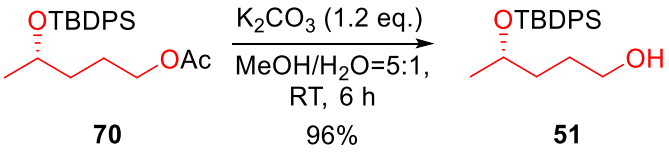

70 **51**

(*S*)-4-((*tert*-butyldiphenylsilyl)oxy)pentan-1-ol (51)[154]

To (*S*)-4-((*tert*-butyldiphenylsilyl)oxy)pentyl acetate **70** (2.60 g, 6.77 mmol, 1.0 equiv.) in a 25 mL round-bottom flask equipped with a stir bar was added MeOH (15 mL) and H_2O (3 mL) before solid K_2CO_3 (1.12 g, 8.12 mmol, 1.2 equiv.) was added in one portion. The mixture was allowed to stir at RT for 6 h before saturated aqueous NH_4Cl (10 mL) and H_2O (10 mL) were added, extracted with ethyl acetate (25 mL x 4), the combined organic phase washed with brine (10 mL), dried over anhydrous $MgSO_4$ before being filtered and concentrated under reduced pressure. Purification using silica gel chromatography (eluent: hexanes/ethyl acetate = 10:1 to 2:1) to afford **51** as a colourless oil (2.22 g, 6.50 mmol, 96%). TLC (hexanes/ ethyl acetate = 2:1): R_f = 0.59; $[\alpha]^{20}_D$ = -9.3 (c = 0.45, MeOH), (Lit.[154]: $[\alpha]_D$ = -50.1 (c = 0.0051, MeOH); $[\alpha]^{21}_D$ = -6.5 (c = 1.00, $CHCl_3$), (Lit.(enantiomer)[155]: $[\alpha]^{22}_D$ = +5.4 (c = 2.10, $CHCl_3$); ^{1}H NMR (500 MHz, $CDCl_3$) δ (ppm): 7.68-7.67 (m, 4H), 7.42-7.41 (m, 2H), 7.41-7.35 (m, 4H), 3.91 (sextet, *J* = 6.0 Hz, 1H), 3.55-3.53 (m, 2H), 1.60-1.56 (m, 3H), 1.52-1.50 (m, 2H), 1.07 (d, *J* = 6.2 Hz, 3H), 1.05 (s, 9H); ^{13}C NMR (100 MHz, $CDCl_3$) δ (ppm): 136.0, 136.0, 134.8, 134.5, 129.7, 129.7, 127.7, 127.6, 69.4, 63.2, 35.7, 28.4, 27.2, 23.0, 19.4; FTIR (neat, NaCl, cm^{-1}): 3361, 3070, 2932, 1589, 1427, 1367, 1111; HRMS (ESI) *m/z* Calculated for $C_{21}H_{31}O_2Si$ $[M+H]^+$: 343.2093; found: 343.2104.

---

[154] Jones, G. B.; Hynd, G.; Wright, J. M.; Sharma, A. *J. Org. Chem.* **1999,** *65*, 263-265.

[155] (*R*)-*tert*-butyl((5-iodopentan-2-yl)oxy)diphenylsilane (enantiomer): Motozaki, T.; Sawamura, K.; Suzuki, A.; Yoshida, K.; Ueki, T.; Ohara, A.; Munakata, R.; Takao, K.-i.; Tadano, K.-i. *Org. Lett.* **2005,** *7*, 2265-2267.

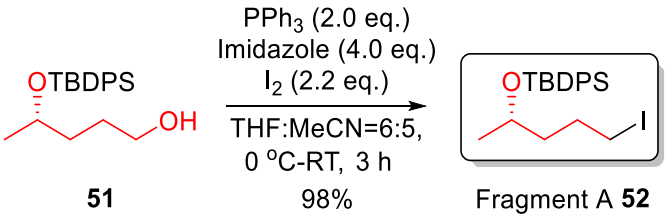

(*S*)-*tert*-butyl((5-iodopentan-2-yl)oxy)diphenylsilane (52)[155]

To a 250 mL round-bottom flask equipped with a stir bar was added PPh_3 (3.13 g, 11.9 mmol, 2.0 equiv.) and imidazole (1.62 g, 23.8 mmol, 4.0 equiv.) before THF/MeCN (6:5) (15 mL) was added and cooled down to 0 °C to give a brown solution. I_2 (3.33 g, 13.1 mmol, 2.2 equiv.) was then added in one portion to the stirring mixture at 0 °C and allowed to stirred at 0 °C for 1 h to give a brown suspension. (*S*)-4-((*tert*-butyldiphenylsilyl)oxy)pentan-1-ol **51** (2.04 g, 5.96 mmol, 1.0 equiv.) dissolved in THF (15 mL) was then added to the suspension was allowed to stir at room temperature for 3 h before saturated aqueous $Na_2S_2O_3$ (10 mL) was added and concentrated under reduced pressure. Ethyl acetate (30 mL) was added to dilute the mixture and the layers were separated, the aqueous phase extracted with EA (30 mL x 3), the combined organic phase washed with brine (10 mL), dried over anhydrous $MgSO_4$ before being filtered and concentrated under reduced pressure. Purification using silica gel chromatography (eluent: hexanes/ethyl acetate = 50:1) to afford **52** as a pale yellow oil (2.63 g, 5.82 mmol, 98%). TLC (hexanes/ethyl acetate = 20:1): R_f = 0.76; $[\alpha]^{20}_D$ = -20.2 (c = 2.17, $CHCl_3$), (Lit.(enantiomer)[155]: $[\alpha]^{22}_D$ = +20.5 (c = 1.93, $CHCl_3$); ^{1}H NMR (500 MHz, $CDCl_3$) δ (ppm): 7.68-7.66 (m, 4H), 7.43-7.35 (m, 6H), 3.87 (sextet, *J* = 5.9 Hz, 1H), 3.11-3.04 (m, 2H), 1.87-1.82 (m, 2H), 1.56-1.49 (m, 2H), 1.06 (d, *J* = 6.2 Hz, 3H), 1.05 (s, 9H); ^{13}C NMR (125 MHz, $CDCl_3$) δ (ppm): 136.0, 136.0, 134.8, 134.4, 129.7, 129.7, 127.7, 127.6, 68.7, 40.3, 29.5, 27.2, 23.4, 19.4, 7.4; FTIR (neat, NaCl, cm^{-1}): 3071, 2961, 1589, 1427, 1377, 1111; HRMS (ESI) *m/z*

Calculated for $C_{21}H_{29}NaOSiI$ $[M+Na]^+$: 475.0930; found: 475.0946.

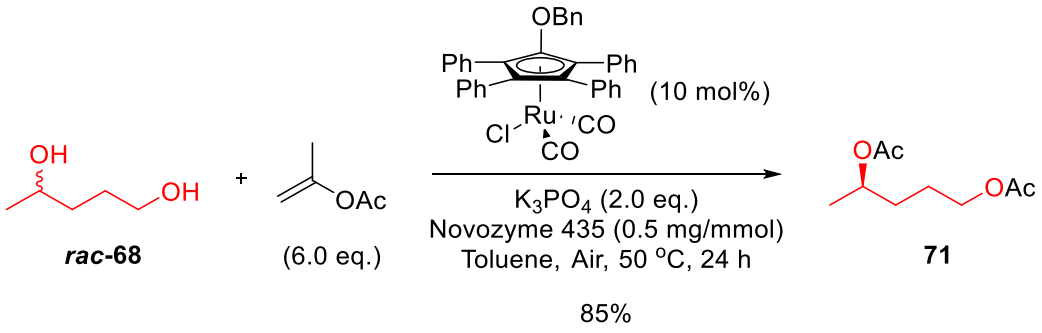

(*R*)-pentane-1,4-diyl diacetate (71)

To an oven-dried 25 mL round-bottomed flask was added a stir bar, ***rac*-68** (208.2 mg, 2.0 mmol, 1.0 equiv.), potassium phosphate (849.2 mg, 4.0 mmol, 2.0 equiv.), (η^5-2,3,4,5-tetraphenyl-1-benzyloxycyclopentadienyl)(chloro)dicarbonylruthenium(II) (133.6 mg, 0.20 mmol, 10 mol%), Novozyme 435 (1.0 mg, 0.5 mg/mmol), isopropenyl acetate (1.2 g, 12.0 mmol, 6.0 equiv.) and toluene (5.4 mL). The mixture was stirred in air at 50 °C for 24 h, then filtered through a short plug of silica gel to obtain the crude product. Purification using silica gel chromatography (eluent: hexanes/ethyl acetate = 20:1 to 4:1) afforded **71** as a pale yellow oil (320 mg, 1.7 mmol, 85%). TLC (hexanes/ethyl acetate = 4:1): R_f = 0.39; $[\alpha]^{23}_D$ = -1.0 (c = 1.63, $CHCl_3$); ^{1}H NMR (400 MHz, $CDCl_3$) δ (ppm): 4.96-4.89 (m, 1H), 4.08-4.05 (m, 2H), 2.05 (s, 3H), 2.03 (s, 3H), 1.67-1.61 (m, 4H), 1.23 (d, *J* = 6.3 Hz, 3H); ^{13}C NMR (100 MHz, $CDCl_3$) δ (ppm): 171.1, 170.7, 70.4, 64.2, 32.4, 24.7, 21.3, 20.9, 20.0; FTIR (neat, NaCl, cm^{-1}): 2976, 2959, 2940, 2876, 1732, 1236; HRMS (ESI) *m/z* Calculated for $C_9H_{17}O_4$ $[M+H]^+$: 189.1127; found: 189.1129.

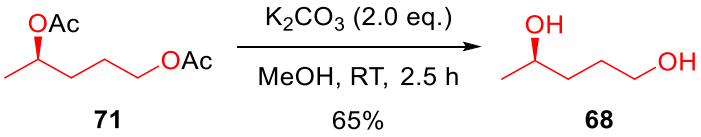

71 **68**

(*R*)-pentane-1,4-diol (68)[153]

To an oven-dried 10 mL round-bottomed flask was added a magnetic stir bar, **71** (50.0 mg, 0.27 mmol, 1.0 equiv.), potassium carbonate (73.4 mg, 0.53 mmol, 2.0 equiv.) and methanol (2.6 mL). The mixture was stirred at room temperature for 2.5 h, then quenched with saturated aqueous ammonium chloride solution (2 mL), followed by addition of H_2O (2 mL). The mixture was extracted with ethyl acetate and the organic phase was washed with brine, dried over anhydrous $MgSO_4$, filtered and concentrated under reduced pressure to afford **68** as a colorless oil (18.2 mg, 0.18 mmol, 65%). TLC (ethyl acetate): R_f = 0.23; $[\alpha]^{22}_D$ = -21.0 (c = 1.34, $CHCl_3$); (Lit.(enantiomer)[153]: $[\alpha]^{24}_D$ = -16.7 (c = 2.4, $CHCl_3$); ^{1}H NMR (400 MHz, $CDCl_3$) δ (ppm): 3.90-3.82 (m, 1H), 3.73-3.63 (m, 2H), 2.48 (bs, 1H), 2.36 (bs, 1H), 1.69-1.47 (m, 4H), 1.22 (d, *J* = 6.2 Hz, 3H); ^{13}C NMR (125 MHz, $CDCl_3$) δ (ppm): 68.1, 63.1, 36.4, 29.3, 23.8; FTIR (neat, NaCl, cm^{-1}): 3306, 2932, 1454, 1373, 1134; HRMS (ESI) *m/z* Calculated for $C_5H_{13}O_2$ $[M+H]^+$: 105.0916; found: 105.0921.

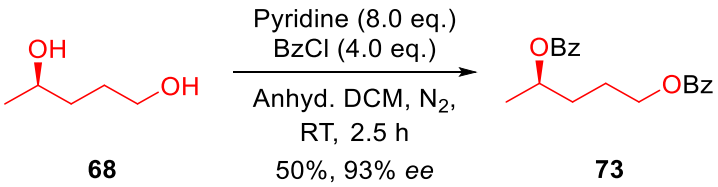

68 **73**

(*R*)-pentane-1,4-diyl dibenzoate (73)

To an oven-dried 5 mL round-bottomed flask was added a stir bar, **68** (10.0 mg, 0.10 mmol, 1.0 equiv.) and anhydrous dichloromethane (0.6 mL). Pyridine (60.8 mg, 0.77 mmol, 8.0 equiv.) and benzoyl chloride (54.0 mg, 0.38 mmol, 4.0 equiv.) were subsequently added and the mixture was stirred at room temperature under a nitrogen atmosphere for 2.5 h, then quenched with saturated aqueous $NaHCO_3$ solution (0.8 mL), followed by addition of H_2O (0.5 mL). The mixture was extracted with dichloromethane and the organic phase was washed with brine, dried over anhydrous $MgSO_4$, filtered and concentrated under reduced pressure. Purification by Preparative Thin Layer Chromatography (eluent: hexanes/ethyl acetate = 30:1) afforded **73** as a pale yellow oil (17.7 mg, 0.057 mmol, 50%), *ee* = 93%. The *ee* was determined on Chiralcel AD-H column with hexanes/2-propanol = 100:0, flow = 1.0 mL/min, wavelength = 230 nm. Retention times: 16.0 min [(*R*)-enantiomer], 19.4 min [(*S*)-enantiomer]. TLC (hexanes/ethyl acetate = 4:1): R_f = 0.57; $[\alpha]^{23}_D$ = -19.8 (c = 0.88, $CHCl_3$); ^{1}H NMR (400 MHz, $CDCl_3$) δ (ppm): 8.05-8.03 (m, 4H), 7.57-7.54 (m, 2H), 7.45-7.42 (m, 4H), 5.28-5.21 (m, 1H), 4.38-4.35 (m, 2H), 1.93-1.82 (m, 4H), 1.39 (d, J = 6.2 Hz, 3H); ^{13}C NMR (100 MHz, $CDCl_3$) δ (ppm): 166.7, 166.2, 133.0, 132.9, 130.8, 130.4, 129.7, 129.6, 128.5, 128.4, 71.2, 64.8, 32.7, 25.0, 20.2; FTIR (neat, NaCl, cm^{-1}): 2974, 2957, 2936, 1715, 1697, 1601; HRMS (ESI) *m/z* Calculated for $C_{19}H_{21}O_4$ $[M+H]^+$: 313.1440; found: 313.1443.

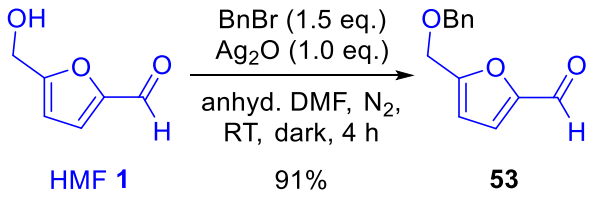

5-((benzyloxy)methyl)furan-2-carbaldehyde (53)[143]

To an oven-dried, vacuum cooled 250 mL round-bottom flask equipped with a stir bar was added 5-(hydroxymethyl)furan-2-carbaldehyde **1** (6.11 g, 48.5 mmol, 1.0 equiv.) and anhydrous DMF (35 mL) under N_2 atmosphere before benzyl bromide (8.6 mL, 12.4 g, 72.7 mmol, 1.5 equiv.) and silver oxide (11.3 g, 48.5 mmol, 1.0 equiv.) were added. The round-bottom flask was covered with aluminium foil to exclude light and the suspension was allowed to stir at room temperature for 4 h. The suspension was diluted with ethyl acetate (30 mL) and filtered through a pad of celite, washed with ethyl acetate and concentrated under reduced pressure. Purification using silica gel chromatography (eluent: hexanes/ethyl acetate = 30:1) to afford **53** as a yellow oil (9.53 g, 44.1 mmol, 91%). TLC (hexanes/ethyl acetate = 2:1): R_f = 0.50; ^{1}H NMR (300 MHz, $CDCl_3$) δ (ppm): 9.63 (s, 1H), 7.36-7.30 (m, 5H), 7.21 (d, J = 3.5 Hz, 1H), 6.54 (d, J = 3.5 Hz, 1H), 4.61 (s, 2H), 4.58 (s, 3H); ^{13}C NMR (75 MHz, $CDCl_3$) δ (ppm): 177.9, 158.6, 152.8, 137.4, 128.7, 128.2, 128.1, 122.0, 111.4, 73.1, 64.3; FTIR (neat, NaCl, cm^{-1}): 3062, 3032, 2859, 1678, 1524, 1454, 1192; HRMS (ESI) *m/z* Calculated for $C_{13}H_{13}O_3$ $[M+H]^+$: 217.0865; found: 217.0863.

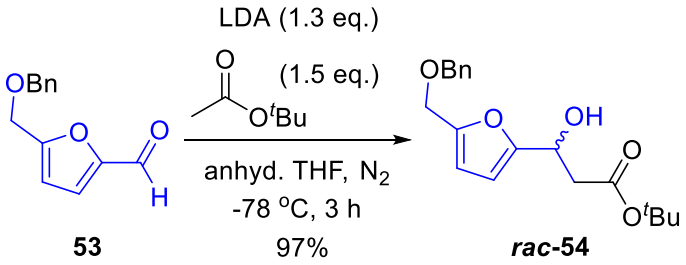

***tert*-butyl 3-(5-((benzyloxy)methyl)furan-2-yl)-3-hydroxypropanoate (*rac*-54)**

To an oven-dried, vacuum cooled 250 mL round-bottom flask equipped with a stir bar was added diisopropylamine (9.2 mL, 6.60 g, 65.4 mmol, 1.5 equiv.) and anhydrous THF (15 mL) under N_2 atmosphere before cooling down to 0 °C. *n*-Butyllithium (35.4 mL, 1.6 m in hexanes, 56.7 mmol, 1.3 equiv.) was slowly added dropwise at 0 °C and stirred for 30 min before cooling down to -78 °C. *tert*-Butyl acetate (8.8 mL, 7.6 g, 65.4 mmol, 1.5 equiv.) dissolved in anhydrous THF (20 mL) was then slowly added dropwise to the mixture at -78 °C and stirred for 30 min. 5-((benzyloxy)methyl)furan-2-carbaldehyde **53** (9.41 g, 43.6 mmol, 1.0 equiv.) dissolved in anhydrous THF (45 mL) was then slowly added dropwise to the mixture at -78 °C and allowed to stir at -78 °C for an additional 3 h. Saturated aqueous NH_4Cl (20 mL) was slowly added to quench the reaction and the mixture was concentrated under reduced pressure before diluting with ethyl acetate (50 mL) and H_2O (50 mL). The layers were separated, the aqueous phase extracted with ethyl acetate (50 mL x 4), the combined organic phase washed with brine (10 mL), dried over anhydrous $MgSO_4$ before being filtered and concentrated under reduced pressure. Purification using silica gel chromatography (eluent: hexanes/ethyl acetate = 6:1 to 2:1) to afford ***rac*-54** as a pale yellow oil (14.0 g, 42.3 mmol, 97%). TLC (hexanes/ethyl acetate = 2:1): R_f = 0.45; ^{1}H NMR (300 MHz, $CDCl_3$) δ (ppm): 7.35-7.30 (m, 5H), 6.27 (d, J = 3.2 Hz, 1H), 6.23 (d, J = 3.1 Hz, 1H), 5.10- 5.04 (m, 1H), 4.54 (s, 2H), 4.45 (s, 2H), 3.38 (d, J

= 5.0 Hz, 1H), 2.82 (dd, *J* = 16.5 Hz, 7.6 Hz, 1H), 2.75 (dd, *J* = 16.4 Hz, 4.8 Hz, 1H), 1.46 (s, 9H); ^{13}C NMR (75 MHz, $CDCl_3$) δ (ppm): 171.5, 155.4, 151.2, 138.0, 128.5, 128.0, 127.9, 110.3, 107.0, 81.8, 72.1, 64.6, 64.1, 40.9, 28.2; FTIR (neat, NaCl, cm^{-1}): 3443, 3060, 2980, 2929.9, 1726, 1454, 1151; HRMS (ESI) *m/z* Calculated for $C_{19}H_{25}O_5$ $[M+H]^+$: 333.1702; found: 333.1691.

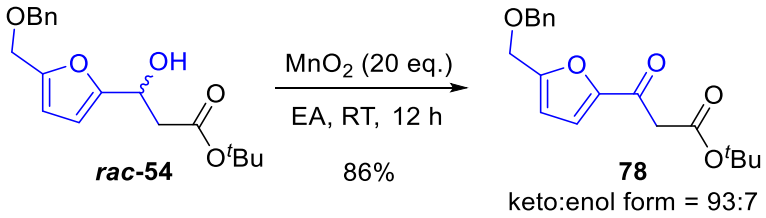

***tert*-butyl 3-(5-((benzyloxy)methyl)furan-2-yl)-3-oxopropanoate (78)**

To *tert*-butyl 3-(5-((benzyloxy)methyl)furan-2-yl)-3-hydroxypropanoate ***rac*-54** (6.66 g, 20.1 mmol, 1.0 equiv.) in a 100 mL round-bottom flask equipped with a stir bar was added ethyl acetate (40 mL) and manganese dioxide (34.9 g, 401 mmol, 20 equiv.). The black suspension was allowed to stir at room temperature for 12 h before being filtered through a pad of celite, washed with ethyl acetate and concentrated under reduced pressure. Purification using silica gel chromatography (eluent: hexanes/ethyl acetate = 10:1 to 2:1) to afford **78** (keto form : enol form = 93:7) as a pale yellow oil which solidified at -30 ºC to give a pale yellow solid (5.69 g, 17.3 mmol, 86%). mp = 53-54 ºC; TLC (hexanes/ethyl acetate = 2:1): R_f = 0.65; ^{1}H NMR (400 MHz, $CDCl_3$) δ (ppm): 7.36-7.30 (m, 5H), 7.21 (d, *J* = 3.6 Hz, 1H, keto), 6.85 (d, *J* = 3.4 Hz, 1H, enol), 6.49 (d, *J* = 3.2 Hz, 1H, keto), 6.41 (d, *J* = 3.4 Hz, 1H, enol), 5.56 (s, 1H, enol), 4.59 (s, 2H, keto), 4.56 (s, 2H, enol), 4.54 (s, 2H, keto), 4.49 (s, 2H, enol), 3.74 (s, 2H), 1.52 (s, 9H, enol), 1.44 (s, 9H, keto); ^{13}C NMR (100 MHz, $CDCl_3$) δ (ppm): 181.6, 166.3, 157.1, 151.9, 137.4, 128.6, 128.1, 128.0, 119.0, 111.6,

82.2, 72.8, 64.2, 46.9, 28.0 (enol peaks not depicted); FTIR (Nujol, NaCl, cm^{-1}): 3117, 2953, 2922, 2852, 1732, 1667, 1454, 1138; HRMS (ESI) *m/z* Calculated for $C_{19}H_{23}O_5$ $[M+H]^+$: 331.1545; found: 333.1547.

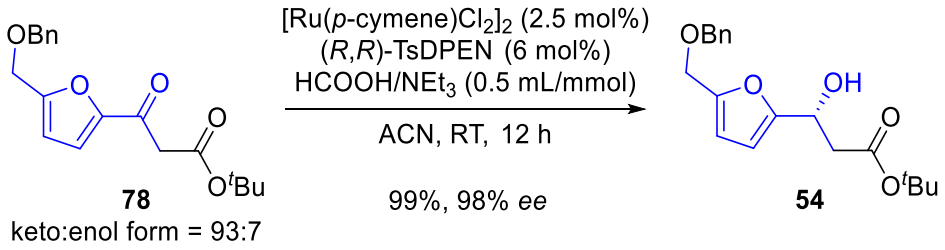

(*R*)-*tert*-butyl 3-(5-((benzyloxy)methyl)furan-2-yl)-3-hydroxypropanoate (54)

To a 50 mL round-bottom flask equipped with a stir bar was added dichloro(*p*-cymene)ruthenium(II) dimer (263 mg, 0.43 mmol, 2.5 mol%), (1*R*,2*R*)-(+)-1,2-diphenylethylenediamine[150c] (376 mg, 1.03 mmol, 6 mol%) and MeCN (34 mL) before triethylamine (356 μL, 260 mg, 2.57 mmol, 15 mol%) was added. The mixture was allowed to stir at room temperature for 1 h to give a dark orange solution before $5HCOOH{\cdot}2NEt_3$ azeotrope (8.6 mL) was added. The mixture was then transferred to another 50 mL round-bottom flask equipped with a stir bar containing *tert*-butyl 3-(5-((benzyloxy)methyl)furan-2-yl)-3-oxopropanoate **78** (5.66 g, 17.2 mmol, 1.0 equiv.) and allowed to stir at room temperature for 12 h. The mixture was concentrated under reduced pressure and purification using silica gel chromatography (eluent: hexanes/ethyl acetate = 4:1) to afford **54** as a pale yellow oil (5.66 g, 17.0 mmol, 99%, *ee* = 98%). The *ee* was determined on Chiralcel OB-H column with hexane/2-propanol = 90:10, flow = 1.0 mL/min, wavelength = 220 nm. Retention times: 10.8 min [(*S*)-enantiomer], 15.4 min [(*R*)-enantiomer]. $[\alpha]^{22}_D$ = +21.9 (c = 2.05, $CHCl_3$).

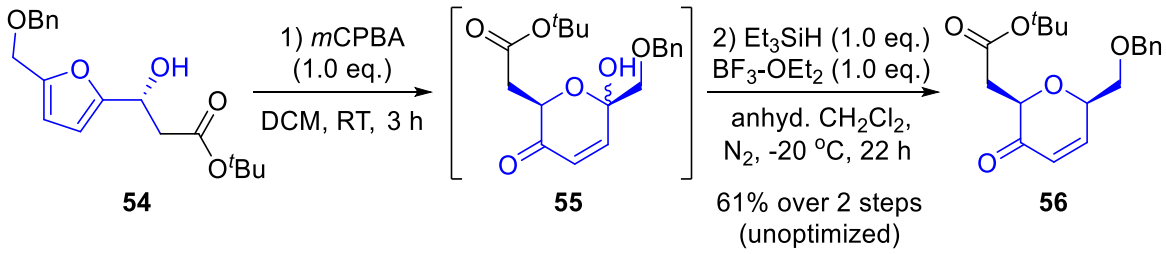

tert-butyl (_R_)-2-(6-((benzyloxy)methyl)-6-hydroxy-3-oxo-3,6-dihydro-2_H_-pyran-2-yl)acetate (55)

To (*R*)-*tert*-butyl 3-(5-((benzyloxy)methyl)furan-2-yl)-3-hydroxypropanoate **54** (445 mg, 1.34 mmol, 1.0 equiv.) in a 25 mL round-bottom flask equipped with a stir bar was added CH_2Cl_2 (4.5 mL) and then *meta*-chloroperoxybenzoic acid (329 mg, ~70 wt. %, 1.34 mmol, 1.0 equiv.) in one portion. The mixture was allowed to stir at room temperature for 3 h to give a white suspension before saturated aqueous $NaHCO_3$ (5 mL) was added. The layers were separated, the aqueous phase extracted with CH_2Cl_2 (5 mL x 3), the combined organic phase washed with water (5 mL), brine (5 mL), dried over anhydrous $MgSO_4$ before being filtered and concentrated under reduced pressure to afford crude **55** as a mixture of isomers (major:minor = 87:13) which is immediately used in the subsequent step without further purification.

Alternatively, the crude mixture can be purified using silica gel chromatography (eluent: hexanes/ethyl acetate = 10:1 to 1:1) to afford **55** as a mixture of isomers (major:minor = 87:13) as a pale yellow oil. TLC (hexanes/ethyl acetate = 2:1): R_f = 0.38; $[\alpha]^{22}_D$ = +41.0 (c = 3.44, $CHCl_3$); ^{1}H NMR (400 MHz, $CDCl_3$) δ (ppm): 7.36-7.32 (m, 5H), 6.89 (d, *J* = 10.4 Hz, 1H, minor), 6.81 (d, *J* = 10.3 Hz, 1H, major), 6.19 (d, *J* = 10.4 Hz, 1H, minor), 6.13 (d, *J* = 10.3 Hz, 1H, major), 4.94 (dd, *J* = 6.9 Hz, 4.4 Hz, 1H), 4.71 (d, *J* = 12.0 Hz, 1H), 4.62 (d, *J* = 12.0 Hz, 1H), 4.43 (bs, 1H, minor),

4.01 (bs, 1H, major), 3.62 (d, *J* = 10.3 Hz, 1H), 3.57 (d, *J* = 10.3 Hz, 1H), 2.88 (dd, *J* = 16.5 Hz, 4.4 Hz, 1H), 2.71 (dd, *J* = 16.5 Hz, 6.9 Hz, 1H), 1.44 (s, 9H, minor), 1.42 (s, 9H, major); ^{13}C NMR (100 MHz, $CDCl_3$) δ (ppm): 195.4, 194.9 (minor), 169.8, 147.5 (minor), 145.2, 137.4, 128.7, 128.2, 128.1, 128.0, 127.9 (minor), 127.9 (minor), 93.9 (minor), 93.2, 81.8 (minor), 81.3, 75.1 (minor), 74.3, 74.1, 74.0 (minor), 73.0 (minor), 71.8, 39.3 (minor), 36.7, 28.2; FTIR (neat, NaCl, cm^{-1}): 3401, 3067, 3030, 2978, 2932, 2868, 1730, 1694, 1632; HRMS (ESI) *m/z* Calculated for $C_{19}H_{25}O_6$ $[M+H]^+$: 349.1651; found: 349.1643.

tert-butyl 2-((2*R*,6*R*)-6-((benzyloxy)methyl)-3-oxo-3,6-dihydro-2*H*-pyran-2-yl) -acetate (56)

To the crude mixture of **55** obtained above in a 25 mL round-bottom flask equipped with a stir bar was added anhydrous CH_2Cl_2 (6.7 mL) under N_2 atmosphere. Triethylsilane (195 μL, 142 mg, 1.34 mmol, 1.0 equiv.) was added and cooled down to -20 ^oC before boron trifluoride diethyl etherate (165 μL, 190 mg, 1.34 mmol, 1.0 equiv.) was slowly added dropwise and stirred at -20 ^oC for another 22 h. The reaction was quenched with saturated aqueous NH_4Cl (5 mL) and H_2O (2 mL) before warming to room temperature. The layers were separated, the aqueous phase extracted with CH_2Cl_2 (5 mL x 4), the combined organic phase washed with water (5 mL), brine (5 mL), dried over anhydrous $MgSO_4$ before being filtered and concentrated under reduced pressure. Purification using silica gel chromatography (eluent: hexanes/ethyl acetate = 10:1 to 2:1) to afford **56** (271 mg, 0.82 mmol, 61% over 2 steps) as a yellow oil. TLC (hexanes/ethyl acetate = 2:1): R_f = 0.50; $[\alpha]^{22}_D$ = +70.4 (c = 2.21, $CHCl_3$); ^{1}H NMR (300 MHz, $CDCl_3$) δ (ppm): 7.36-7.30 (m, 5H), 7.07 (dd, *J* = 10.4 Hz, 1.5 Hz, 1H), 6.18 (dd, *J* = 10.4 Hz, 2.5 Hz, 1H), 4.64-4.56 (m, 3H), 4.45 (ddd, *J* = 7.1 Hz,

4.6 Hz, 2.2 Hz, 1H), 3.71 (dd, *J* = 10.0 Hz, 5.6 Hz, 1H), 3.58 (dd, *J* = 10.0 Hz, 5.9 Hz, 1H), 2.93 (dd, *J* = 16.5 Hz, 4.5 Hz, 1H), 2.62 (dd, *J* = 16.4 Hz, 7.2 Hz, 1H), 1.46 (s, 9H); ^{13}C NMR (100 MHz, $CDCl_3$) δ (ppm): 195.1, 170.0, 148.9, 137.8, 128.6, 128.0, 127.9, 127.4, 81.1, 77.7, 74.0, 73.8, 71.2, 36.8, 28.2; FTIR (neat, NaCl, cm^{-1}): 3057, 3034, 2982, 2934, 2874, 1728, 1628; HRMS (ESI) *m/z* Calculated for $C_{19}H_{25}O_5$ [M+H]$^+$: 333.1702; found: 333.1705.

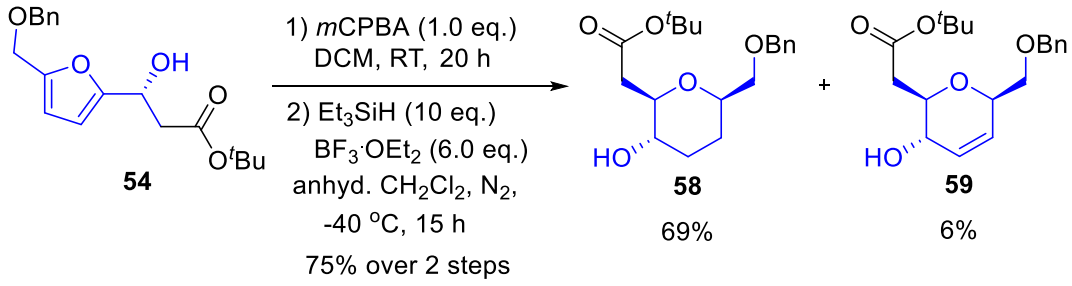

***tert*-butyl 2-((2*R*,3*S*,6*R*)-6-((benzyloxy)methyl)-3-hydroxytetrahydro-2*H*-pyran-2-yl)acetate (58)**

***tert*-butyl 2-((2*R*,3*S*,6*R*)-6-((benzyloxy)methyl)-3-hydroxy-3,6-dihydro-2*H*-pyran-2-yl)acetate (59)**

To (*R*)-*tert*-butyl 3-(5-((benzyloxy)methyl)furan-2-yl)-3-hydroxypropanoate **54** (5.66 g, 17.1 mmol, 1.0 equiv.) in a 100 mL round-bottom flask equipped with a stir bar was added CH_2Cl_2 (40 mL) and then *meta*-chloroperoxybenzoic acid (4.19 g, ~70 wt.%, 17.1 mmol, 1.0 equiv.) in one portion. The mixture was allowed to stir at room temperature for 20 h to give a white suspension before saturated aqueous $NaHCO_3$ (80 mL) was added. The layers were separated, the aqueous phase extracted with CH_2Cl_2 (80 mL x 3), the combined organic phase washed with water (50 mL), brine (10 mL), dried over anhydrous $MgSO_4$ before being filtered and concentrated under reduced pressure to afford crude **55** as a mixture of isomers (major:minor = 91:9)

which is immediately used in the subsequent step without further purification.

To the crude mixture of **55** obtained above in a 100 mL round-bottom flask equipped with a stir bar was added anhydrous CH_2Cl_2 (85 mL) under N_2 atmosphere. Triethylsilane (24.8 mL, 18.1 g, 170 mmol, 10 equiv.) was added and cooled down to -40 ^oC before boron trifluoride diethyl etherate (12.6 mL, 14.5 g, 102 mmol, 6.0 equiv.) was slowly added *via* a syringe pump over 30 min and stirred at -40 ^oC for another 15 h. The reaction was quenched with saturated aqueous NH_4Cl (50 mL) and H_2O (20 mL) before warming to room temperature. The layers were separated, the aqueous phase extracted with CH_2Cl_2 (50 mL x 4), the combined organic phase washed with water (50 mL), brine (10 mL), dried over anhydrous $MgSO_4$ before being filtered and concentrated under reduced pressure. Purification using silica gel chromatography (eluent: hexanes/ethyl acetate = 10:1 to 2:1) to afford **58** (3.96 g, 11.8 mmol, 69% over 2 steps) and **59** (343 mg, 1.03 mmol, 6% over 2 steps) separately as pale yellow oils. Total yield: 75% over 2 steps.

58: TLC (hexanes/ethyl acetate = 2:1): $R_f = 0.23$; $[\alpha]^{23}_D = +24.1$ (c = 2.37, $CHCl_3$); ^1H NMR (500 MHz, $CDCl_3$) δ (ppm): 7.33-1.28 (m, 5H), 4.57 (d, *J* = 12.2 Hz, 1H), 4.53 (d, *J* = 12.2 Hz, 1H), 3.58-3.57 (m, 1H), 3.58-3.57 (m, 1H), 3.53-3.51 (m, 1H), 3.50-3.46 (m, 1H), 3.41 (dd, *J* = 10.1 Hz, 4.4 Hz, 1H), 3.36 (m, 1H), 2.72 (dd, *J* = 15.2 Hz, 5.5 Hz, 1H), 2.50 (dd, *J* = 15.3 Hz, 6.5 Hz, 1H), 2.23 (bs, 1H), 2.14-2.12 (m, 1H), 1.76-1.73 (m, 1H), 1.47 (m, 11H); ^{13}C NMR (75 MHz, $CDCl_3$) δ (ppm): 171.8, 138.5, 128.5, 127.8, 127.7, 81.1, 78.9, 77.0, 73.5, 72.9, 71.0, 40.5, 32.8, 28.2, 28.0; FTIR (neat, NaCl, cm^{-1}): 3443, 3060, 2978, 2934, 2868, 1732, 1603; HRMS (ESI) *m/z* Calculated for $C_{19}H_{29}O_5$ $[M+H]^+$: 337.2015; found: 337.2011.

59: TLC (hexanes/ethyl acetate = 2:1): $R_f = 0.30$; $[\alpha]^{22}_D = +70.1$ (c = 0.72, $CHCl_3$); ^1H

NMR (300 MHz, $CDCl_3$) δ (ppm): 7.34-7.30 (m, 5H), 5.86 (d, *J* = 10.5 Hz, 1H), 5.80 (d, *J* = 10.2 Hz, 1H), 4.57 (s, 2H), 4.34 (m, 1H), 4.05 (m, 1H), 3.71-3.64 (m, 1H), 3.51 (dd, *J* = 10.2 Hz, 6.0 Hz, 1H), 3.46 (dd, *J* = 10.1 Hz, 5.1 Hz, 1H), 2.75 (dd, *J* = 15.5 Hz, 5.7 Hz, 1H), 2.59 (dd, *J* = 15.5 Hz, 6.8 Hz, 1H), 2.37 (bs, 1H), 1.46 (s, 9H); ^{13}C NMR (75 MHz, $CDCl_3$) δ (ppm): 171.6, 138.3, 130.3, 128.8, 128.5, 127.9, 127.8, 81.3, 76.1, 74.7, 73.5, 72.4, 68.2, 40.4, 28.2; FTIR (neat, NaCl, cm^{-1}): 3424, 3060, 2978, 2930, 2868, 1732, 1620; HRMS (ESI) *m/z* Calculated for $C_{19}H_{27}O_5$ $[M+H]^+$: 335.1858; found: 335.1854.

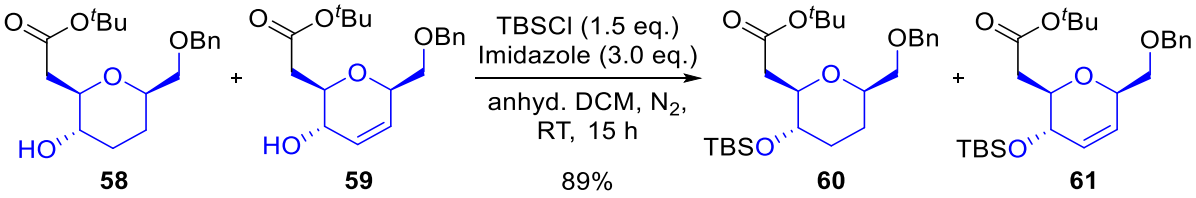

tert-butyl2-((2*R*,3*S*,6*R*)-6-((benzyloxy)methyl)-3-((_tert_-butyldimethylsilyl)oxy)-tetrahydro-2*H*-pyran-2-yl)acetate (58)

tert-butyl2-((2*R*,3*S*,6*R*)-6-((benzyloxy)methyl)-3-((_tert_-butyldimethylsilyl)oxy)-3,6-dihydro-2*H*-pyran-2-yl)acetate (59)

To a mixture of *tert*-butyl 2-((2*R*,3*S*,6*R*)-6-((benzyloxy)methyl)-3-hydroxytetrahydro-2*H*-pyran-2-yl)acetate **58** (3.96 g, 11.8 mmol) and *tert*-butyl 2-((2*R*,3*S*,6*R*)-6-((benzyloxy)methyl)-3-hydroxy-3,6-dihydro-2*H*-pyran-2-yl)acetate **59** (343 mg, 1.03 mmol) in a 50 mL round-bottom flask equipped with a stir bar was added anhydrous CH_2Cl_2 (26 mL) under N_2 atmosphere. Imidazole (2.62 g, 38.5 mmol, 3.0 equiv. w.r.t combined amount of both reactants) was then added at RT and stirred to achieve complete dissolution before *tert*-butyl(chloro)dimethylsilane (2.90 g,

19.2 mmol, 1.5 equiv. w.r.t combined amount of both reactants) was added. The mixture was allowed to stir at room temperature for 15 h before saturated aqueous NH_4Cl (10 mL) and H_2O (5 mL) was added and the layers were separated. The aqueous phase was extracted with CH_2Cl_2 (10 mL x 3) and the combined organic phase washed with H_2O (5 mL) and brine (5 mL), dried over anhydrous $MgSO_4$ before being filtered and concentrated under reduced pressure. Purification using silica gel chromatography (eluent: hexanes/ethyl acetate = 40:1 to 20:1) to afford **60** and **61** as an inseparable mixture (colourless oil) (5.14 g, 11.4 mmol, 89%). TLC (hexanes/ethyl acetate = 10:1): R_f = 0.39; $[\alpha]^{23}_D$ = +48.5 (c = 1.35, $CHCl_3$); ^{1}H NMR (400 MHz, $CDCl_3$) δ (ppm): 7.33-7.27 (m, 5H), 5.76 (m, 2H, **61**), 4.58-4.52 (m, 2H), 4.35 (m, 1H, **61**), 4.08-4.05 (m, 1H, **61**), 3.75 (m, 1H, **61**), 3.59-3.55 (m, 2H), 3.50-3.47 (m, 1H), 3.43-3.32 (m, 2H), 2.78-2.74 (m, 1H), 2.38-2.33 (m, 1H, **61**), 2.24 (dd, *J* = 14.8 Hz, 9.7 Hz, 1H), 2.01 (m, 1H), 1.76-1.73 (m, 1H), 1.44 (m, 11H), 0.06 (s, 6H); ^{13}C NMR (100 MHz, $CDCl_3$) δ (ppm): 171.3, 138.6, 128.4, 127.8, 127.6, 80.4, 79.8, 76.8, 73.4, 72.9, 70.9 , 39.5, 33.2, 28.3, 28.1, 25.9, 18.1, -3.9, -4.6; FTIR (neat, NaCl, cm^{-1}): 3061, 3030, 2953, 2930, 2857, 1732; HRMS (ESI) *m/z* Calculated for $C_{25}H_{43}O_5Si$ $[M+H]^+$: 451.2880; found: 451.2887.

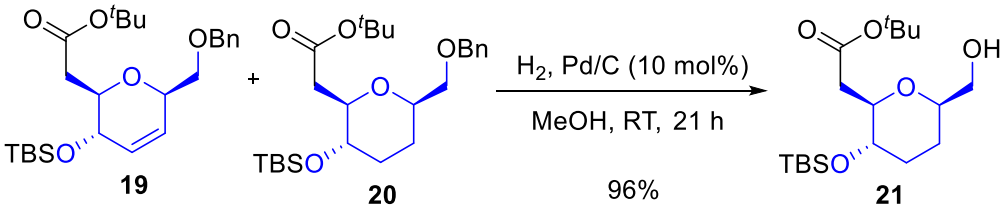

tert-butyl 2-((2*R*,3*S*,6*R*)-3-((_tert_-butyldimethylsilyl)oxy)-6-(hydroxymethyl) -tetrahydro-2*H*-pyran-2-yl)acetate (62)

To a mixture of *tert*-butyl 2-((2*R*,3*S*,6*R*)-6- ((benzyloxy)methyl)-3-((*tert* -butyldimethylsilyl)oxy)tetrahydro-2*H*-pyran-2-yl)acetate **60** and *tert*-butyl 2-((2*R*, 3*S*,6*R*)-6-((benzyloxy)methyl)-3-((*tert*-butyldimethylsilyl)oxy)-3,6-dihydro-2*H*-pyran-2-yl)acetate **61** and (5.00 g, 11.1 mmol, 1.0 equiv.) in a 100 mL round-bottom flask equipped with a stir bar was added MeOH (30 mL) and palladium on carbon (1.18 g, 10 wt. %, 1.11 mmol, 10 mol%). The round-bottom flask was evacuated and backfilled with H_2 (balloon) thrice and allowed to stir at RT for 21 h, filtered through a short plug of silica gel, washed with ethyl acetate and concentrated to afford *tert*-butyl 2-((2*R*,3*S*,6*R*)-3-((*tert*-butyldimethylsilyl)oxy)-6-(hydroxymethyl)tetrahydro-2*H*-pyran -2-yl)acetate **62** as a colourless oil (3.84 g, 10.7 mmol, 96%). TLC (hexanes/ethyl acetate = 2:1): R_f = 0.43; $[\alpha]^{23}_D$ = +42.8 (c = 1.90, $CHCl_3$); ^{1}H NMR (500 MHz, $CDCl_3$) δ (ppm): 3.58-3.54 (m, 2H), 3.48-3.43 (m, 2H), 3.32 (td, *J* = 9.6 Hz, 4.2 Hz, 1H), 2.77 (dd, *J* = 14.8 Hz, 2.8 Hz, 1H), 2.20 (dd, *J* = 14.8 Hz, 9.9 Hz, 1H), 2.02-1.99 (m, 1H), 1.70 (bs, 1H), 1.61-1.48 (m, 3H), 1.45 (s, 9H), 1.42-1.41 (m, 1H), 0.87 (s, 9H), 0.06 (s, 3H), 0.05 (s, 3H); ^{13}C NMR (100 MHz, $CDCl_3$) δ (ppm): 171.2, 80.6, 79.6, 77.8, 70.9, 65.7, 39.6, 32.9, 28.3, 26.8, 25.9, 18.0 , -3.9, -4.6; FTIR (neat, NaCl, cm^{-1}): 3466, 2953, 2930, 2857, 1728; HRMS (ESI) *m/z* Calculated for $C_{18}H_{37}O_5Si$ $[M+H]^+$: 361.2410; found: 361.2417.

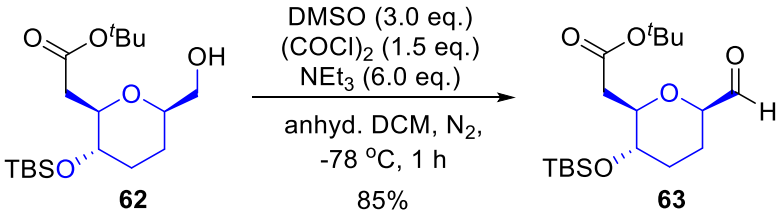

***tert*-butyl 2-((2*R*,3*S*,6*R*)-3-((*tert*-butyldimethylsilyl)oxy)-6-formyltetrahydro-2*H*-pyran-2-yl)acetate (63)**

To an oven-dried, vacuum cooled 250 mL round-bottom flask equipped with a stir bar was added anhydrous DMSO (2.2 mL, 2.40 g, 30.8 mmol, 3.0 equiv.) and anhydrous CH_2Cl_2 (20 mL) under N_2 atmosphere before cooling down to -78 °C. Oxalyl chloride (1.3 mL, 1.95 g, 15.4 mmol, 1.5 equiv.) was slowly added dropwise at -78 °C and stirred for 15 min. *tert*-butyl 2-((2*R*,3*S*,6*R*)-3-((*tert*-butyldimethylsilyl)oxy)-6-(hydroxymethyl)tetrahydro-2*H*-pyran-2-yl) acetate **62** (3.69 g, 10.3 mmol, 1.0 equiv.) dissolved in anhydrous CH_2Cl_2 (50 mL) was then slowly added dropwise to the mixture at -78 °C and stirred for 1 h. Triethylamine (8.5 mL, 6.21 g, 61.5 mmol, 6.0 equiv.) was then added in one portion to the mixture at -78 °C and allowed to stir at -78 °C for an additional 15 min before warming to room temperature and stirred for another 30 min. Saturated aqueous NH_4Cl (20 mL) and H_2O (5 mL) was added to the mixture and the layers were separated, the aqueous phase extracted with CH_2Cl_2 (30 mL x 3), the combined organic phase washed with H_2O (10 mL), brine (10 mL), dried over anhydrous $MgSO_4$ before being filtered and concentrated under reduced pressure. Purification using silica gel chromatography (eluent: hexanes/ethyl acetate = 30:1) to afford **63** as a pale yellow oil (3.12 g, 8.71 mmol, 85%). The aldehyde product is not very stable and should be stored a low temperature or used immediately in the subsequent step. TLC (hexanes/ethyl acetate = 2:1): $R_f = 0.55$; $[\alpha]^{22}_D = +84.4$ (c = 1.72, $CHCl_3$); ^{1}H NMR (500 MHz, $CDCl_3$) δ (ppm): 9.59 (s, 1H), 3.78 (dd, *J* = 11.5 Hz, 2.4

Hz, 1H), 3.64 (td, J = 9.4 Hz, 2.7 Hz, 1H), 3.36 (td, J = 9.6 Hz, 4.2 Hz, 1H), 2.79 (dd, J = 15.1 Hz, 2.8 Hz, 1H), 2.30 (dd, J = 15.2 Hz, 9.6 Hz, 1H), 2.10-2.07 (m, 1H), 1.95-1.92 (m, 1H), 1.57-.50 (m, 2H), 1.46 (s, 9H), 0.87 (s, 9H), 0.06 (s, 6H); ^{13}C NMR (125 MHz, $CDCl_3$) δ (ppm): 201.5, 171.0, 81.1, 80.8, 79.8, 70.2, 39.2, 32.7, 28.3, 26.0, 25.9, 18.0, -3.9, -4.6; FTIR (neat, NaCl, cm^{-1}): 2955, 2930, 2859, 1738, 1732, 1368; HRMS (ESI) *m/z* Calculated for $C_{18}H_{35}O_5Si$ $[M+H]^+$: 359.2254; found: 359.2247.

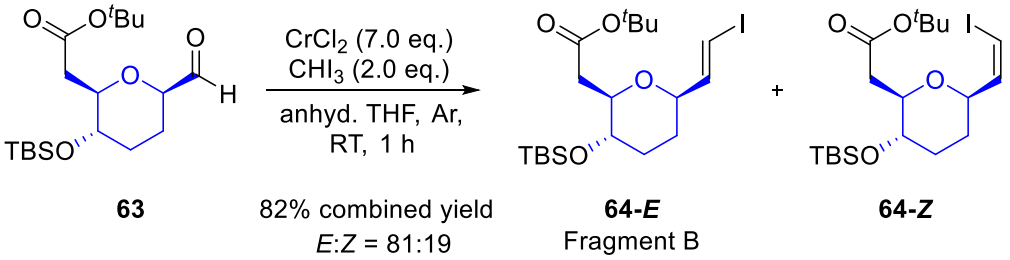

63 | 82% combined yield, *E*:*Z* = 81:19 | **64-*E*** Fragment B | **64-*Z***

tert-butyl 2-((2*R*,3*S*,6*R*)-3-((_tert_-butyldimethylsilyl)oxy)-6-((*E*)-2-iodovinyl) -tetrahydro-2*H*-pyran-2-yl)acetate (64-*E*)

tert-butyl 2-((2*R*,3*S*,6*R*)-3-((_tert_-butyldimethylsilyl)oxy)-6-((*Z*)-2-iodovinyl) -tetrahydro-2*H*-pyran-2-yl)acetate (64-*Z*)

To an oven-dried, vacuum-cooled 100 mL round-bottom flask equipped with a stir bar was added anhydrous chromium(II) chloride (5.39 g, 43.8 mmol, 7.0 equiv.) under Ar atmosphere and cooled down to 0 ºC before anhydrous THF (26 mL) was slowly added at 0 ºC to give a grey suspension. The mixture was allowed to warm to room temperature and a mixture containing *tert*-butyl 2-((2*R*,3*S*,6*R*)-3-((*tert*-butyl -dimethylsilyl)oxy)-6-formyltetrahydro-2*H*-pyran-2-yl)acetate **63** (2.24 g, 6.26 mmol, 1.0 equiv.) and iodoform (4.93 g, 12.5 mmol, 2.0 equiv.) dissolved in anhydrous THF (13 mL) was slowly added dropwise at room temperature to the stirring suspension and allowed to stir for another 1 h to give a brown solution. H_2O (50 mL) and ethyl

acetate (30 mL) was added and the layers were separated. The aqueous phase was extracted with ethyl acetate (50 mL x 3) and the combined organic phase washed with saturated aqueous $NaHCO_3$ (50 mL), saturated aqueous $Na_2S_2O_3$ (50 mL) and brine (30 mL). The organic phase was dried over anhydrous $MgSO_4$, filtered through a pad of silica gel and concentrated under reduced pressure. Purification using silica gel chromatography in the dark (eluent: hexanes/ethyl acetate = 100:1) to afford **64-*E*** as the major product (colourless oil) (1.99 g, 4.13 mmol, 66%) and **64-*Z*** as the minor product (colourless oil) (481 mg, 1.00 mmol, 16%). The products were stored under Ar, in the absence of light at -20 ºC and **64-*E*** was used in the subsequent step within a few days.

64-*E*: TLC (hexanes/ethyl acetate = 10:1): R_f = 0.54; $[\alpha]^{22}_D$ = +47.4 (c = 1.13, $CHCl_3$); ^{1}H NMR (400 MHz, $CDCl_3$) δ (ppm): 6.50 (dd, *J* = 14.5 Hz, 4.6 Hz, 1H), 6.31 (dd, *J* = 14.5 Hz, 1.5 Hz, 1H), 3.83-3.80 (m, 1H), 3.57 (td, *J* = 9.3 Hz, 2.9 Hz, 1H), 3.33 (td, *J* = 9.5 Hz, 4.4 Hz, 1H), 2.73 (dd, *J* = 14.8 Hz, 3.0 Hz, 1H), 2.23 (dd, *J* = 14.8 Hz, 9.7 Hz, 1H), 2.02-1.98 (m, 1H), 1.78-.174 (m, 1H), 1.44 (m, 11H), 0.87 (s, 9H) 0.05 (s, 3H), 0.05 (s,3H); ^{13}C NMR (100 MHz, $CDCl_3$) δ (ppm): 171.2, 145.6, 80.6, 79.8, 78.9, 77.3, 70.5, 39.5, 33.2, 30.8, 28.3, 25.9, 18.1, -3.9, -4.6; FTIR (neat, NaCl, cm^{-1}): 3053, 2953, 2930, 2857, 1730, 1612; HRMS (ESI) *m/z* Calculated for $C_{19}H_{36}IO_4Si$ $[M+H]^+$: 483.1428; found: 483.1425. ***rac*-64-*E***: mp = 53-54 ºC.

64-*Z*: mp = 71-72 ºC; TLC (hexanes/ethyl acetate = 10:1): R_f = 0.46; $[\alpha]^{22}_D$ = +7.8 (c = 1.32, $CHCl_3$); ^{1}H NMR (400 MHz, $CDCl_3$) δ (ppm): 6.27-6.19 (m, 2H), 4.08 (dd, *J* = 8.8 Hz, 8.3 Hz, 1H), 3.60 (td, *J* = 9.3 Hz, 2.5 Hz, 1H), 3.35 (td, *J* = 9.7 Hz, 4.5 Hz, 1H), 2.76-2.71 (m, 1H), 2.19 (dd, *J* = 14.8 Hz, 9.5 Hz, 1H), 2.04-2.00 (m, 1H), 1.84-1.80 (m, 1H), 1.64-1.54 (m, 1H), 1.48-1.38 (m, 10H), 0.87 (s, 9H), 0.05 (s, 3H),

0.04 (s,3H); ^{13}C NMR (100 MHz, CD_2Cl_2) δ (ppm): 171.2, 142.0, 81.9, 80.7, 80.5, 80.0, 70.6, 39.8, 33.5, 29.9, 28.3, 26.0, 18.2, -3.9, -4.6; FTIR (neat, NaCl, cm^{-1}): 3053, 2953, 2930, 2857, 1730, 1620; HRMS (ESI) *m/z* Calculated for $C_{19}H_{36}IO_4Si$ $[M+H]^+$: 483.1428; found: 483.1429. ***rac*-64-*Z***: mp = 71-72 °C.

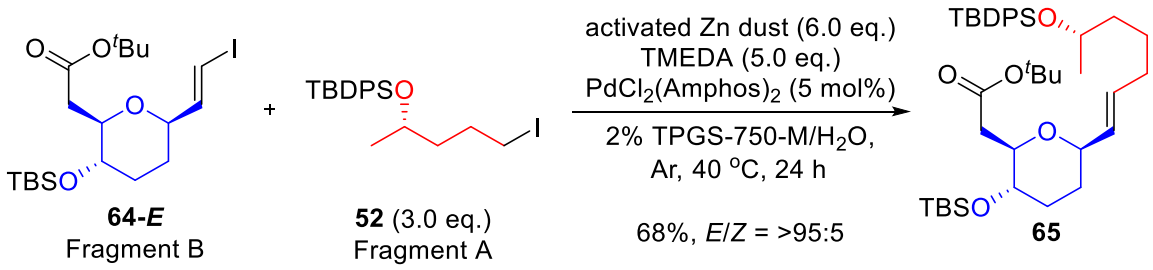

***tert*-butyl 2-((2*R*,3*S*,6*R*)-3-((*tert*-butyldimethylsilyl)oxy)-6-((*S*,*E*)-6-((tert-butyldi-phenyl silyl)oxy)hept-1-en-1-yl)tetrahydro-2*H*-pyran-2-yl)acetate (65)**

To a 4 mL sample vial wrapped in aluminium foil containing *tert*-butyl 2-((2*R*,3*S*,6*R*)-3-((*tert*-butyldimethylsilyl)oxy)-6-((*E*)-2-iodovinyl)tetrahydro-2*H*-pyra n-2-yl)acetate **64-*E*** (300 mg, 0.62 mmol, 1.0 equiv.) and (*S*)-*tert*-butyl((5-iodopentan-2-yl)oxy)diphenylsilane **52** (844 mg, 1.87 mmol, 3.0 equiv.) was added 2% TPGS-750-M solution (1.2 mL) under Ar. Tetramethylethylenediamine (465 μL, 361 mg, 3.11 mmol, 5.0 equiv.) was then added with stirring. $PdCl_2Amphos_2$ (22 mg, 0.031 mmol, 5 mol%) and activated zinc dust[156] (244 mg, 3.73, 6.0 equiv.) were then added together, and the sample vial was sealed under Ar. The mixture was allowed to stir vigorously in the dark, in a pre-heated oil bath at 40 °C for 24 h and allowed to cool to room temperature. The mixture was filtered through a short pad of silica gel (washed with ethyl acetate) and concentrated under reduced pressure.

[156] Activated zinc dust was prepared using a modified procedure from: Yamamura, S.; Toda, M.; Hirata, Y. *Org. Synth.* **1973,** *53*, 86. Zinc dust was stirred in 1M HCl for 30 min, quickly washed with H_2O, filtered and washed with ethanol, acetone, diethyl ether sequentially, dried between filter paper and used immediately.

Purification using silica gel chromatography (eluent: hexanes to hexanes/ethyl acetate = 100:1) followed by Preparative Thin Layer Chromatography (eluent: hexanes/ethyl acetate = 100:1) afforded **65** as a pale yellow oil (286 mg, 0.42 mmol, 68%) as a mixture of *E*/*Z* isomers in the ratio >95/5. TLC (hexanes/ethyl acetate = 20:1): R_f = 0.53; $[\alpha]^{22}_D$ = +18.5 (c = 1.19, $CHCl_3$); ^{1}H NMR (400 MHz, $CDCl_3$) δ (ppm): 7.67 (dd, *J* = 7.9 Hz, 1.4 Hz, 4H), 7.43-7.34 (m, 6H), 5.57 (dt, *J* = 15.5 Hz, 7.2 Hz, 1H), 5.36 (dd, *J* = 15.5 Hz, 5.5 Hz, 1H), 3.84-3.75 (m, 2H), 3.58 (td, *J* = 9.3 Hz, 2.9 Hz, 1H), 3.33 (td, *J* = 9.6 Hz, 4.3 Hz, 1H), 2.74 (dd, *J* = 14.8 Hz, 3.0 Hz, 1H), 2.23 (dd, *J* = 14.8 Hz, 9.7 Hz, 1H), 2.01-1.97 (m, 1H), 1.91-1.86 (m, 2H), 1.71-1.68 (m, 1H), 1.43 (s, 9H), 1.47-1.33 (m, 6H), 1.04 (s, 9H), 1.02 (d, *J* = 6.2 Hz, 3H), 0.88 (s, 9H), 0.06 (s, 3H), 0.05 (s, 3H); ^{13}C NMR (100 MHz, $CDCl_3$) δ (ppm): 171.5, 136.0, 136.0, 135.1, 134.7, 131.8, 130.3, 129.6, 129.5, 127.6, 127.5, 80.3, 79.8, 77.7, 70.9, 69.6, 39.6, 39.1, 33.6, 32.5, 31.5, 28.3, 27.2, 25.9, 24.8, 23.3, 19.4, 18.1, -3.9, -4.6; FTIR (neat, NaCl, cm^{-1}): 3071, 2930, 2867, 1960, 1890, 1825, 1730, 1589; HRMS (ESI) *m/z* Calculated for $C_{40}H_{64}O_5Si_2Na$ $[M+Na]^+$: 703.4190; found: 703.4187.

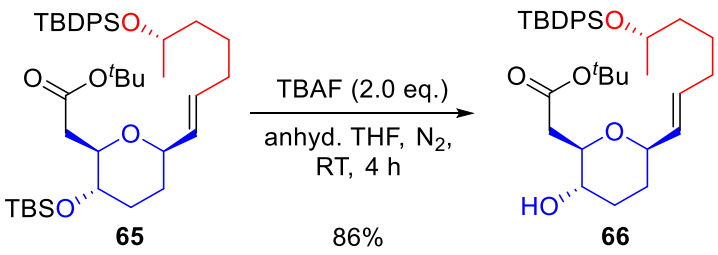

tert-butyl 2-((2*R*,3*S*,6*R*)-6-((*S*,*E*)-6-((_tert_-butyldiphenylsilyl)oxy)hept-1-en-1-yl)-3-hydroxytetrahydro-2*H*-pyran-2-yl)acetate (66)

To _tert_-butyl 2-((2*R*,3*S*,6*R*)-3-((_tert_-butyldimethylsilyl)oxy)-6-((*S*,*E*)-6-((tert-butyl -diphenylsilyl)oxy)hept-1-en-1-yl)tetrahydro-2*H*-pyran-2-yl)acetate **65** (139 mg, 0.205 mmol, 1.0 equiv.) in a 4 mL sample vial equipped with a stir bar, was added anhydrous THF (2.0 mL) before tetrabutylammonium fluoride (0.41 mL, 1.0 M solution in THF, 0.41 mmol, 2.0 equiv.) was added under N_2. The mixture was allowed to stir at RT for 4 h before saturated aqueous NH_4Cl (5 mL) was added to the mixture and the layers were separated, the aqueous phase extracted with EA (10 mL x 3), the combined organic phase washed with, brine (5 mL), dried over anhydrous $MgSO_4$ before being filtered and concentrated under reduced pressure. Purification using silica gel chromatography (eluent: hexanes/ethyl acetate = 5:1) to afford **66** as a pale yellow oil (99.7 mg, 0.176 mmol, 86%). TLC (hexanes/ethyl acetate = 2:1): R_f = 0.48; $[\alpha]^{22}_D$ = +2.5 (c = 0.85, $CHCl_3$); ^{1}H NMR (400 MHz, $CDCl_3$) δ (ppm): 7.68-7.66 (m, 4H), 7.41-7.34 (m, 6H), 5.59 (dt, *J* = 15.5 Hz, 7.2 Hz, 1H), 5.37 (dd, *J* = 15.5 Hz, 5.9 Hz, 1H), 3.85-3.75 (m, 2H), 3.53 (dt, *J* = 9.0 Hz, 6.0 Hz, 1H), 3.39-3.33 (m, 1H), 2.71 (dd, *J* = 15.1 Hz, 5.6 Hz, 1H), 2.49 (dd, *J* = 15.1 Hz, 6.4 Hz, 1H), 2.18 (bs, 1H), 2.16-2.11 (m, 1H), 1.92-1.87 (m, 2H), 1.73-1.70 (m, 1H), 1.45 (s, 9H), 1.45-1.32 (m, 6H), 1.04 (s, 9H), 1.03 (d, *J* = 6.6 Hz, 3H); ^{13}C NMR (100 MHz, $CDCl_3$) δ (ppm): 171.9, 136.0, 136.0, 135.1, 134.7, 132.3, 130.1, 129.6, 129.5, 127.6, 127.5, 81.1, 78.9, 78.0, 71.0,

69.6, 40.5, 39.1, 33.1, 32.4, 31.5, 28.2, 27.2, 24.8, 23.3, 19.4; FTIR (neat, NaCl, cm^{-1}): 3418, 3071, 2932, 2857, 1960, 1892, 1823, 1730, 1589; HRMS (ESI) *m/z* Calculated for $C_{34}H_{50}O_5SiNa$ $[M+Na]^+$: 589.3325; found: 589.3319.

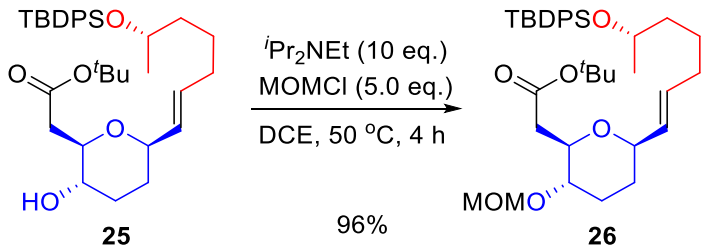

tert-butyl 2-((2*R*,3*S*,6*R*)-6-((*S*,*E*)-6-((*tert*-butyldiphenylsilyl)oxy)hept-1-en-1-yl)-3-(methoxymethoxy)tetrahydro-2*H*-pyran-2-yl)acetate (67)

To *tert*-butyl 2-((2*R*,3*S*,6*R*)-6-((*S*,*E*)-6-((*tert*-butyldiphenylsilyl)oxy)hept-1-en-1-yl)-3-hydroxytetrahydro-2*H*-pyran-2-yl)acetate **66** (96.1 mg, 0.17 mmol, 1.0 equiv.) in a 4 mL sample vial equipped with a stir bar was added 1,2-dichloroethane (1.7 mL) before *N*,*N*-diisopropylethylamine (296 μL, 219 mg, 1.7 mmol, 10 equiv.) was added followed by chloromethyl methyl ether (65 μL, 68.3 mg, 0.85 mmol, 5.0 equiv.). The mixture was allowed to stir at 50 °C for 4 h before being concentrated under reduced pressure. Purification using silica gel chromatography (eluent: hexanes/ethyl acetate = 10:1) to afford **67** as a pale yellow oil (99.6 mg, 0.163 mmol, 96%). TLC (hexanes/ethyl acetate = 2:1): R_f = 0.68; $[\alpha]^{22}_D$ = +15.8 (c = 0.62, CH_2Cl_2); ^{1}H NMR (400 MHz, $CDCl_3$) δ (ppm): 7.67 (dd, *J* = 7.9 Hz, 1.4 Hz, 4H), 7.41-7.34 (m, 6H), 5.58 (dt, *J* = 15.5 Hz, 7.2 Hz, 1H), 5.36 (dd, *J* = 15.5 Hz, 5.7 Hz, 1H), 4.71 (d, *J* = 6.8 Hz, 1H), 4.59 (d, *J* = 6.8 Hz, 1H), 3.84-3.77 (m, 2H), 3.68 (td, *J* = 8.8 Hz, 4.4 Hz, 1H), 3.36 (s, 3H), 3.29 (td, *J* = 9.8 Hz, 4.3 Hz, 1H), 2.71 (dd, *J* = 14.9 Hz, 4.2 Hz, 1H), 2.36 (dd, *J* = 14.9 Hz, 8.2 Hz, 1H), 2.24-2.20 (m, 1H), 1.92-1.86 (m, 2H), 1.74-1.70 (m, 1H), 1.48-1.32 (m, 6H), 1.44 (s, 9H), 1.04 (s, 9H), 1.03 (d, *J* = 7.7 Hz, 3H); ^{13}C NMR

(100 MHz, $CDCl_3$) δ (ppm): 171.0, 136.0, 136.0, 135.1, 134.7, 132.2, 130.2, 129.6, 129.5, 127.6, 127.5, 95.3, 80.4, 77.9, 77.8, 75.6, 69.6, 55.7, 39.9, 39.1, 32.4, 31.2, 30.2, 28.3, 27.2, 24.8, 23.3, 19.4; FTIR (neat, NaCl, cm^{-1}): 3049, 2932, 2857, 1960, 1900, 1827, 1726, 1589; HRMS (ESI) *m/z* Calculated for $C_{36}H_{55}O_6Si$ $[M+H]^+$: 611.3768; found: 611.3776.

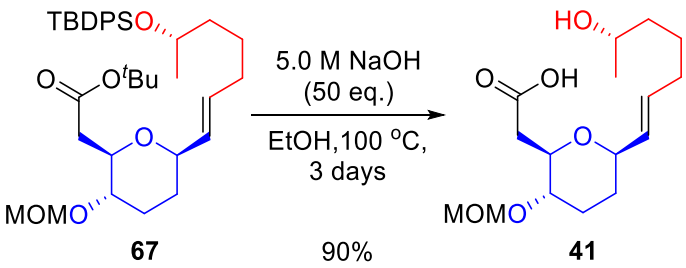

67 90% **41**

2-((2*R*,3*S*,6*R*)-6-((*S*,*E*)-6-hydroxyhept-1-en-1-yl)-3-(methoxymethoxy)tetrahydro-2*H*-pyran-2-yl)acetic acid (41) [132f]

To *tert*-butyl 2-((2*R*,3*S*,6*R*)-6-((*S*,*E*)-6-((*tert*-butyldiphenylsilyl)oxy)hept-1-en-1-yl)-3-(methoxymethoxy)tetrahydro-2*H*-pyran-2-yl)acetate **67** (89.7 mg, 0.147 mmol, 1.0 equiv.) in a 4 mL vial equipped with a stir bar was added ethanol (1.5 mL) before aqueous NaOH (1.5 mL, 5.0 M, 7.5 mmol, 50 equiv.) was added and allowed to stir at 100 °C for 3 days. The mixture was acidified with 3 M HCl (4 mL), extracted with chloroform (12 mL x 4), washed with brine (5 mL), dried over anhydrous $MgSO_4$ before being filtered and concentrated under reduced pressure. Purification using silica gel chromatography (eluent: DCM/MeOH = 20:1 to 10:1) to afford **41** as a colourless oil (41.7 mg, 0.132 mmol, 90%). TLC (DCM/MeOH = 10:1): R_f = 0.27; $[\alpha]^{22}_D$ = +38.9 (c = 0.83, $CHCl_3$). (Lit.[132f]: $[\alpha]^{28}_D$ = +59.8 (c = 1.0, $CHCl_3$); ^1H NMR (400 MHz, $CDCl_3$) δ (ppm): 5.67 (dt, *J* = 15.5 Hz, 7.2 Hz, 1H), 5.45 (dd, *J* = 15.5 Hz, 6.1 Hz, 1H), 4.72 (d, *J* = 6.8 Hz, 1H), 4.60 (d, *J* = 6.8 Hz, 1H), 3.89-3.86 (m, 1H), 3.82-3.76 (m,

1H), 3.70 (td, *J* = 8.6 Hz, 3.4 Hz, 1H), 3.34 (s, 3H), 3.33-3.28 (m, 1H), 2.87 (dd, *J* = 15.5 Hz, 3.2 Hz, 1H), 2.53 (dd, *J* = 15.4 Hz, 8.2 Hz, 1H), 2.26-2.24 (m, 1H), 2.04-2.03 (m, 2H), 1.79-1.76 (m, 1H), 1.58-1.38 (m, 6H), 1.18 (d, *J* = 6.2 Hz, 3H); ^{13}C NMR (100 MHz, $CDCl_3$) δ (ppm): 175.7, 132.6, 130.2, 95.3, 78.2, 77.4, 75.2, 68.2, 55.8, 38.7, 38.2, 32.3, 31.1, 29.9, 25.2, 23.5; FTIR (neat, NaCl, cm^{-1}): 3433, 2936, 1715, 1103, 1036; HRMS (ESI) *m/z* Calculated for $C_{16}H_{28}O_6Na$ $[M+Na]^+$: 339.1784; found: 339.1770.

3.4.3 Determination of enantiomeric excess by HPLC for 70:

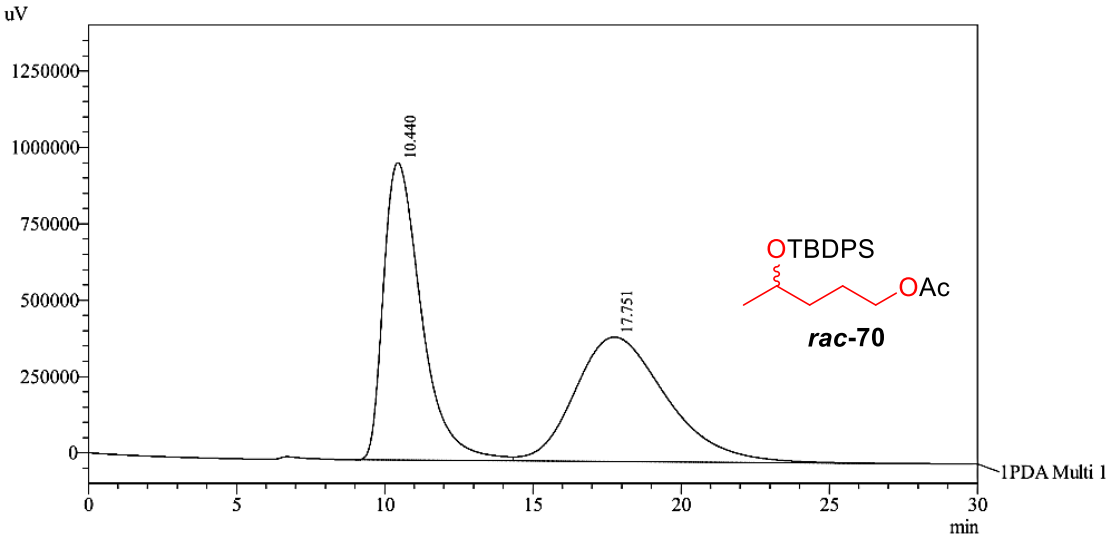

PeakTable

PDA Ch1 220nm 4nm

Peak#	Ret. Time	Area	Height	Area %	Height %
1	10.440	86820408	973805	49.727	70.491
2	17.751	87773940	407648	50.273	29.509
Total		174594348	1381453	100.000	100.000

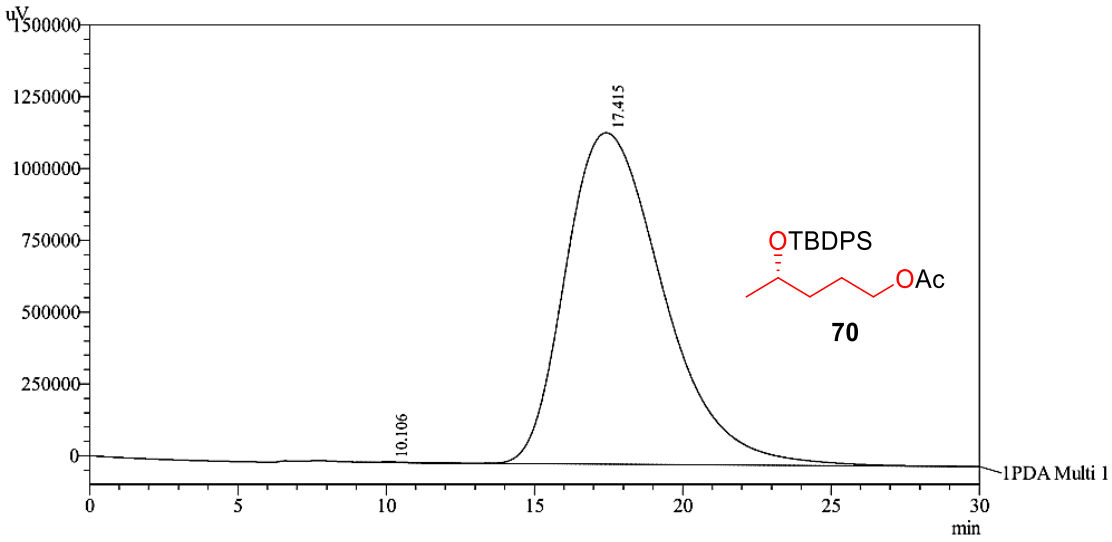

PeakTable

PDA Ch1 220nm 4nm

Peak#	Ret. Time	Area	Height	Area %	Height %
1	10.106	50412	2129	0.019	0.184
2	17.415	265144799	1154354	99.981	99.816
Total		265195211	1156483	100.000	100.000

HPLC trace of **70** (Chiralcel OJ, hexanes/2-propanol = 100:0, 0.5 mL/min, 220 nm)

3.4.4 Determination of enantiomeric excess by HPLC for 73:

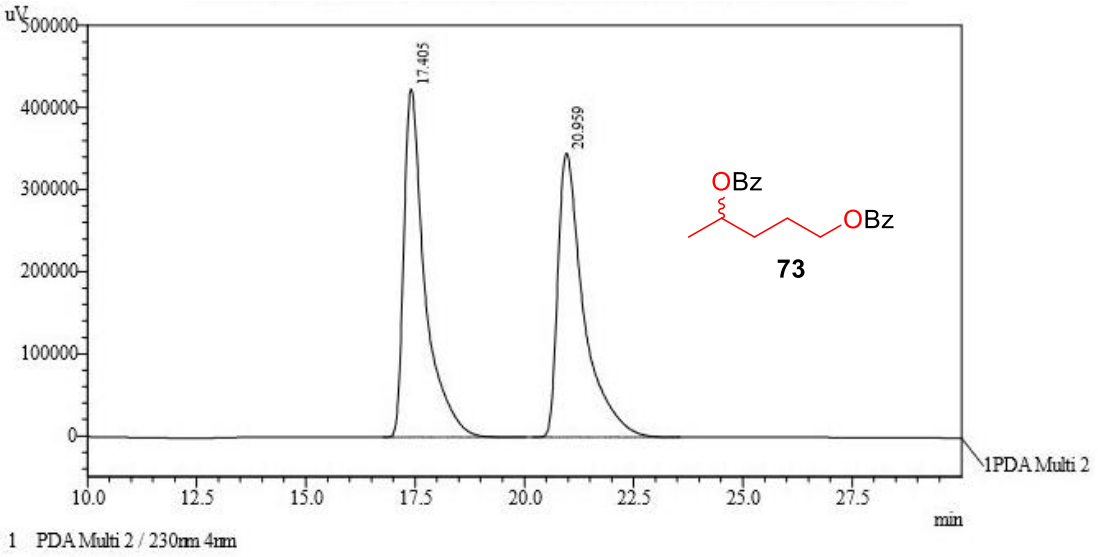

1 PDA Multi 2 / 230nm 4nm

PeakTable

PDA Ch2 230nm 4nm

Peak#	Ret. Time	Area	Height	Area %	Height %
1	17.405	14228671	424111	49.943	55.066
2	20.959	14261095	346070	50.057	44.934
Total		28489766	770181	100.000	100.000

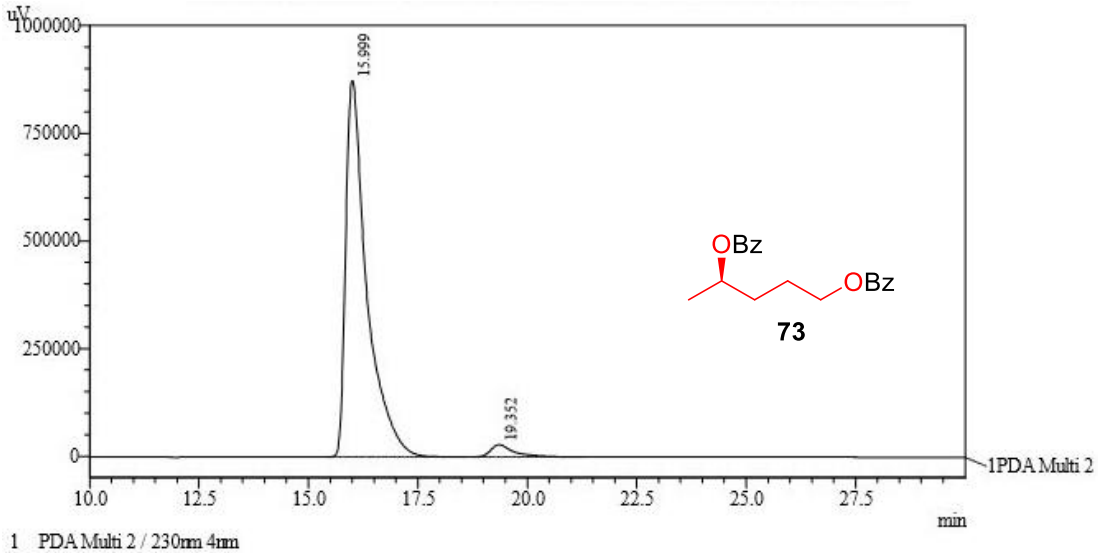

1 PDA Multi 2 / 230nm 4nm

PeakTable

PDA Ch2 230nm 4nm

Peak#	Ret. Time	Area	Height	Area %	Height %
1	15.999	29267370	873448	96.593	96.873
2	19.352	1032407	28198	3.407	3.127
Total		30299777	901646	100.000	100.000

HPLC trace of **73** (Chiralcel AD-H, hexanes/2-propanol = 100:0, 1.0 mL/min, 230 nm)

3.4.5 Determination of enantiomeric excess by HPLC for 54:

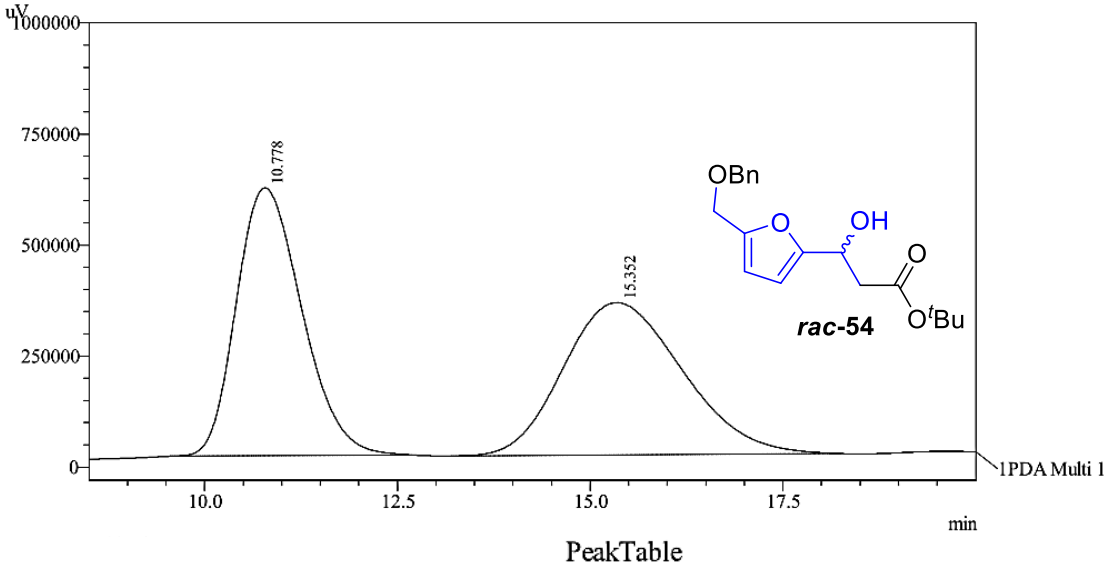

PeakTable

PDA Ch1 220nm 4nm

Peak#	Ret. Time	Area	Height	Area %	Height %
1	10.778	35718382	603334	49.170	63.756
2	15.352	36924915	342977	50.830	36.244
Total		72643297	946311	100.000	100.000

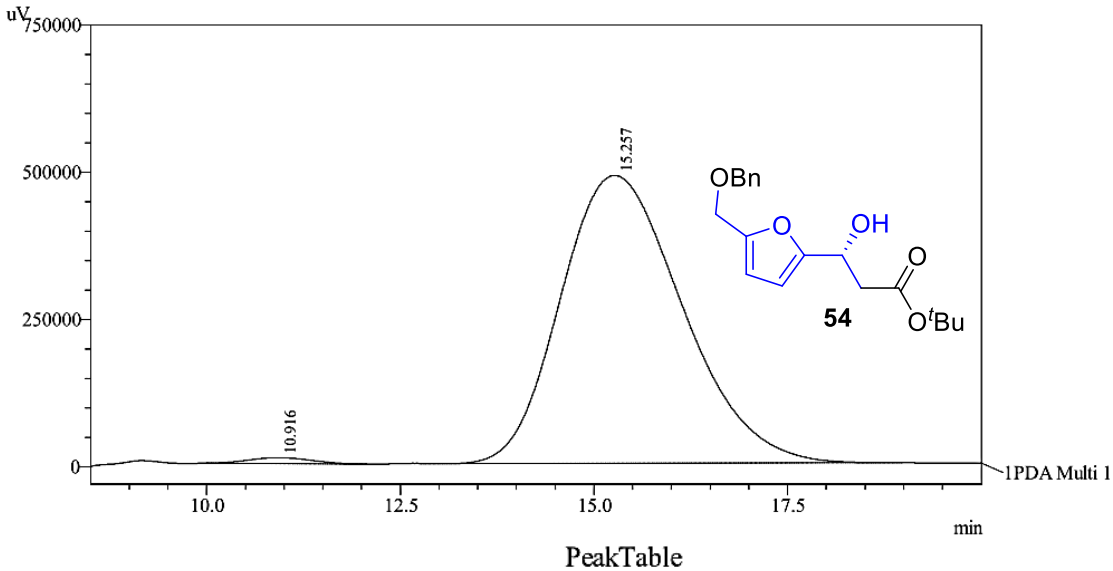

PeakTable

PDA Ch1 220nm 4nm

Peak#	Ret. Time	Area	Height	Area %	Height %
1	10.916	587066	10336	1.086	2.070
2	15.257	53474427	489091	98.914	97.930
Total		54061493	499428	100.000	100.000

HPLC trace of **54** (Chiralcel OB-H, hexanes/2-propanol = 90:10, 1.0 mL/min, 220 nm)

3.4.6 Data and CCDC numbers for X-Ray Structures

Cambridge Crystallographic Data Centre Deposition Number: 1047243

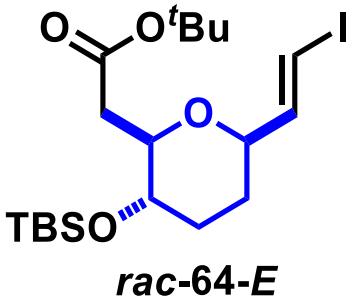

rac-64-*E*

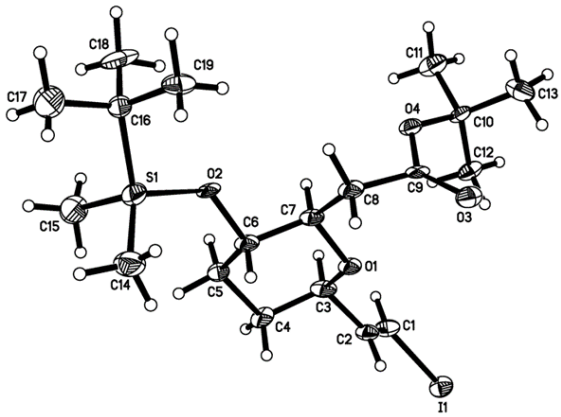

Chemical formula	C19H35IO4S	
Formula weight	486.43	
Temperature	103(2) K	
Wavelength	0.71073 Å	
Crystal size	0.200 x 0.220 x 0.260 mm	
Crystal habit	colorless block	
Crystal system	triclinic	
Space group	P -1	
Unit cell dimensions	a = 10.4883(7) Å	α = 93.874(4)°
	b = 11.9211(7) Å	β = 92.989(4)°
	c = 20.6101(14) Å	γ = 115.747(3)°
Volume	2306.2(3) Å3	
Z	4	
Density (calculated)	1.401 g/cm3	
Absorption coefficient	1.497 mm-1	
F(000)	1000	
Theta range for data collection	1.91 to 26.50°	
Index ranges	-13<=h<=13, -14<=k<=14, -25<=l<=25	
Reflections collected	37880	
Independent reflections	9465 [R(int) = 0.0832]	
Coverage of independent reflections	99.3%	
Absorption correction	multi-scan	
Max. and min. transmission	0.7540 and 0.6970	
Refinement method	Full-matrix least-squares on F2	
Refinement program	SHELXL-2013 (Sheldrick, 2013)	
Function minimized	Σ w(Fo2 - Fc2)2	
Data / restraints / parameters	9465 / 48 / 467	
Goodness-of-fit on F2	1.087	
Final R indices [6267 data; I>2σ(I)]	R1 = 0.0584, wR2 = 0.1277	
R indices all data	R1 = 0.1032, wR2 = 0.1466	
Weighting scheme	w=1/[σ2(Fo2)+(0.0469P)2+8.7339P]	
where P=(Fo2+2Fc2)/3		
Largest diff. peak and hole	0.929 and -1.131 eÅ-3	
R.M.S. deviation from mean	0.141 eÅ-3	

LIST OF PUBLICATIONS

1. Koh, P.-F.; Wang, P.; Huang, J.-M.; Loh, T.-P. *Chem. Commun.* **2014,** *50,* 8324-8327.
2. Loh, T.-P.; Wang, P.; Huang, J.-M.; Koh, P.-F. 3-Piperidone Compounds and Their Use as Neurokinin-1 (NK1) Receptor Antagonists. WO 2014/142761 A1, September 18, 2014.
3. Koh, P.-F.; Loh, T.-P. *Green Chem.* **2015,** *17,* 3746-3750.